

# VIBRATIONAL STUDIES AND PHASE TRANSITION IN DIVALENT METAL PERCHLORATE HEXAHYDRATES

A Thesis Submitted  
in Partial Fulfilment of the Requirements  
for the Degree of  
DOCTOR OF PHILOSOPHY

by  
MITRA BHANU PATEL

*to the*

DEPARTMENT OF PHYSICS  
INDIAN INSTITUTE OF TECHNOLOGY KANPUR  
MAY, 1982

To

My Parents

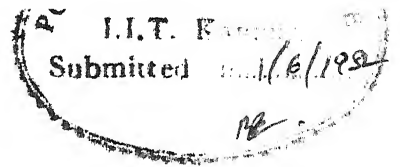
- 6 JUN 1984

CENTRAL LIBRARY

                      
T., Kanpur.

Acc. No. **A.....82827...**

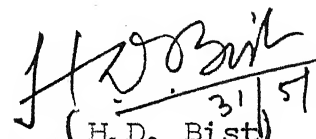
PHY-1982-D-PAT-VIB

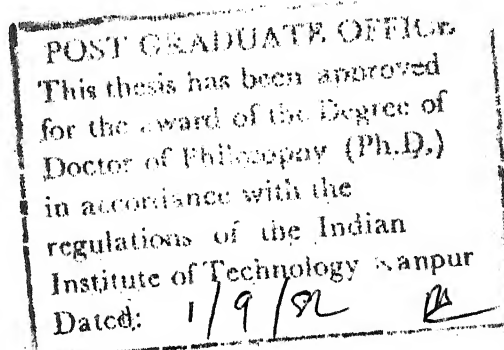


CERTIFICATE

This is to certify that the matter embodied in this thesis entitled, "Vibrational studies and phase transitions in divalent metal perchlorate hexahydrates", submitted for the partial fulfilment of the award of the degree of Doctor of Philosophy in I.I.T. Kanpur, is a record of bonafide research work carried out by Sri Mitra Bhanu Patel under my supervision and guidance. The results embodied in this thesis have not been submitted elsewhere for the award of any degree or diploma.

Dated: May 1982

  
(H.D. Bist)  
Supervisor





### ACKNOWLEDGEMENTS

I feel immense pleasure in thanking Prof. H.D. Bist for suggesting the research problem, constant encouragement inspiring guidance and his forbearance without which this work would have not been possible. He deserves for more than what can be embodied in the words 'thank' and 'gratitude'.

I thank Prof. D.D. Pant, Prof. D.P. Khandelwal, Dr. V.N. Sarin and Dr. V.P. Tayal for the help they rendered during this work.

I greatly appreciate the tremendous help and kind cooperation rendered by all my friends and colleagues.

Thanks are also due to Mr. N. Islam for his meticulous typing, Mr. Lallu Singh and Mr. H.K. Panda for excellent cyclo-styling, Mr. R.K. Bajpai and Mr. A. Bhargava for tracing work, Mr. K. Rajgopalan for recording spectra and all others in the Workshop, Photographic and Xeroxing sections etc. for their timely help.

This column remains incomplete if I forget to express my gratitude to all my family members who showed great patience and gave me help and encouragement during the entire period of research at IIT Kanpur.

*M. B. Patel*  
(M.B. Patel)

## CONTENTS

	Page
Synopsis	i
CHAPTER I	
INTRODUCTION	
1.1.1 General	1
1.1.2 Vibrational and Librational Modes	1
1.1.3 Internal Modes of Water in the Vapour and Condensed Phases	2
1.1.4 Crystal Hydrates	3
1.2.1 Vibrational Spectra of Crystals	4
1.2.2 The Crystal Potential	4
1.3 Isotopic Dilution	6
1.4.1 Structure of Hydrates	8
1.4.2 Symmetry of Water in Crystal Hydrates	9
1.4.3 Structure of Divalent Metal Perchlorate Hexahydrates	10
1.5 Group Theoretical Analysis	14
1.6 Fermi Resonance	15
1.7 Electrical and Mechanical Anharmonicities	17
1.8 Previous Vibrational Studies in IR and Raman	18
1.9.1 Phase Transitions	18
1.9.2 Classification of Phase Transitions	19
1.9.3 Mechanics of Order-Disorder Transitions	22
1.9.4 Experimental Techniques Used for Phase Transitions Studies	25
1.9.5 Previous Studies of Phase Transitions in $M(\text{ClO}_4)_2 \cdot 6\text{H}_2\text{O}$ ( $M = \text{Mg}, \text{Mn}, \text{Co}, \text{Ni}, \text{Zn}, \text{Cd}$ and $\text{Hg}$ )	27
References	28
Tables	38
Figure Captions	45
Figures	46
CHAPTER II	
EXPERIMENTAL TECHNIQUES	48
2.1.1 Infrared Spectra of Solids	48
2.1.2 Factors Affecting IR Spectra of Solids	50
2.2 Raman Spectra of Solids	51
2.3 Infrared Spectrophotometer - P.E.-580	52
2.4 Laser Raman Spectrophotometer Spex-1403	54
2.5 5 Watt Argon Ion Laser	55
2.6.1 Low Temperature Cell	56
2.6.2 The Specac Low Temperature Cell	56
2.7 De-humidifier	57
2.8 Preparation and Purification of Perchlorates	57
2.9 Deuteration of the Samples	58
2.10 Resolution of the Overlapping Bands	59

References	62
Tables	63
Figure Captions	64
Figures	65

## CHAPTER III

VIBRATIONAL STUDIES AND PHASE TRANSITIONS IN  
MAGNESIUM AND NICKEL PERCHLORATE HEXAHYDRATES

Abstract	70
3.1 Introduction	71
3.2 Results and Discussions	72
3.2.1 Internal Vibrations of Water	72
3.2.2 Uncoupled Vibrations of HOD and D <sub>2</sub> O	81
3.2.3 Internal Modes of Perchlorate and Librational and Translation Modes of Water	82
3.2.4 Far-IR	86
3.2.5 Combination Bands in the Region 1700-2350 cm <sup>-1</sup>	86
3.2.6 Phase Transitions	87
References	92
Tables	94
Figure Captions	104
Figures	107

## CHAPTER IV

VIBRATIONAL STUDIES AND PHASE TRANSITIONS  
IN COBALT AND MANGANESE PERCHLORATE HEXAHYDRATES

Abstract	118
4.1 Introduction	119
4.2 Results and Discussions	120
4.2.1 Internal Vibrations of Water	120
4.2.2 Internal Modes of Perchlorate, Librational Modes of Water and Metal-Oxygen Lattice Vibrations	123
4.2.3 Combination Bands	125
4.2.4 Phase Transitions	125
References	129
Tables	130
Figure Captions	134
Figures	135

## CHAPTER V

VIBRATIONAL STUDIES AND PHASE TRANSITIONS  
IN ZINC PERCHLORATE HEXAHYDRATE

Abstract	140
5.1 Introduction	141
5.2 Results and Discussions	142
5.2.1 Internal Modes of H <sub>2</sub> O	142
5.2.2 Perchlorate Vibrations, Librational Modes and Metal-Oxygen Vibrations	145
5.2.3 Phase Transitions	147
5.2.4 Mechanism of Phase Transitions	149

	Page
References	152
Tables	153
Figure Captions	154
Figures	155

## CHAPTER VI

### VIBRATIONAL STUDIES AND PHASE TRANSITIONS IN CADMIUM AND MERCURY PERCHLORATE HEXAHYDRATES

Abstract	162
6.1 Introduction	163
6.2 Results and Discussions	163
6.2.1 Internal Modes of Water	163
6.2.2 Water Librations and Translations	171
6.2.3 Perchlorate Vibrations	175
6.2.4 Conclusion	176
6.2.5 Phase Transitions	177
References	179
Tables	180
Figure Captions	184
Figures	135

## CHAPTER VII

### BACKGROUND AND THE OBJECTIVE

7.1 Background of the Work	194
7.2 Contribution of the Present Work	195
7.3 Suggestions for Future Work	196

## SYNOPSIS

### VIBRATIONAL STUDIES AND PHASE TRANSITIONS IN DIVALENT METAL PERCHLORATE HEXAHYDRATES

We have been interested in the vibrational studies of several hydrates of inorganic salts. The hexahydrated perchlorates of divalent metals, having general formula  $M(\text{ClO}_4)_2 \cdot 6\text{H}_2\text{O}$  (where  $M = \text{Mg, Ni, Co, Mn, Zn, Cd and Hg}$ ) form an interesting series. The Mg, Ni, Co, Mn and Zn salts belong to orthorhombic ( $C_{2v}^7$  space group). The Cd and Hg salts are trigonal ( $C_{3v}^1$  space group) at room temperature (RT). The preliminary infrared data at RT dealing with the internal modes of  $\text{ClO}_4^-$  ion and stretching modes of water are available in literature for few of the above salts. No systematic studies of all the modes belonging to the  $\text{ClO}_4^-$ ,  $\text{H}_2\text{O}$  or  $M-(\text{OH}_2)_6$  (metal-aquo complex) and their temperature dependence are available. Several phase transitions have been observed in these systems on the basis of studies on Mössbauer effect, electron paramagnetic resonance, magnetic susceptibility and anisotropy, specific heat, piezoelectricity, etc. However, the microscopic mechanisms of the transitions in these crystals are not clearly understood. The phase transition in any system is governed by interparticle (atoms and molecules) interactions which can

best be studied by analysing the phonon spectra of the system. With this view point, we have studied the temperature dependence of the phonon spectra of the normal as well as the partially deuterated samples of above mentioned salts. Thus the main attention in the thesis has been to :

- (i) provide a detailed analysis of the vibrational modes of  $M(\text{ClO}_4)_2 \cdot 6\text{H}_2\text{O}$  using IR absorption and Raman scattering techniques and
- (ii) understand the mechanism of the phase transitions exhibited by these systems, utilizing primarily the temperature dependence of thermosensitive infrared bands.

For the sake of brevity, the compounds  $M(\text{ClO}_4)_2 \cdot 6\text{H}_2\text{O}$ , with  $M = \text{Mg, Ni, Co, Mn, Zn, Cd}$  and  $\text{Hg}$  are referred as MPH, NPH, CoPH, MnPH, ZPH, CPH and HPH, in that order.

In Chapter I, a brief review and a critical discussion is presented on the vibrations in molecules and crystals, structure of hydrates, group theoretical analysis, mechanical and electrical anharmonicities, Fermi resonance, types of transformations exhibited by inorganic solids, etc. Various techniques used to investigate phase transitions are also discussed.

Chapter II deals with various experimental aspects needed for the present investigation. A brief description of the techniques used for recording IR and Raman spectra, the IR spectrophotometer P.E.-580, the Ramalog-1403 double monochromator, the 5 watt Argon ion laser, the low temperature cell,

preparation and purification of samples, deuteration of samples, etc., are given in this chapter.

The study of phonons and phase-transitions in MPH and NPH, CoPH and MnPH, ZPH, and CPH and HPH are reported in Chapters III, IV, V and VI, respectively. In each case the IR spectra ( $4000 - 200 \text{ cm}^{-1}$ ) have been recorded at different temperatures while the Raman spectra ( $20 - 4000 \text{ cm}^{-1}$ ) are measured at RT only. From the analysis of these data it is concluded that :

- (i) The RT phases of MPH and NPH are ordered while those of others are disordered.
- (ii) At RT all crystals appear to have only one type of water molecule having nearly  $C_{2v}$  symmetry. At low temperature (LT) the water molecules in MPH and NPH are found to get considerably distorted. In CoPH, MnPH and ZPH they change their site symmetries. In CPH and HPH the water molecules lose their identities and become  $H_3O^+$  and  $OH^-$  ions. Other specific conclusions are summarized chapterwise as follows :

In Chapter III, dealing with the studies of MPH and NPH, it is shown that :

- (a) The uncoupled O-H stretching modes exist in these systems.
- (b) The abnormal intensity ratio of  $\nu_3$  and  $\nu_1$  modes of water is due to the combined effects of (i) the distortion caused by a lowering of  $C_{2v}$  symmetry, (ii) the mechanical anharmonicity and (iii) the electrical anharmonicity.

- (c) The separation between  $\nu_3$  and  $\nu_1$  modes of water is correlated to its net geometry and metal-oxygen ( $M-O_w$ ) coordination in the systems.
- (d) The  $\nu_2$  mode of water in the hydrated crystal is mechanically more harmonic than that of free water.
- (e) A weak resonance interaction exists between the  $2\nu_2$  and  $\nu_1$  modes which increases with increasing hydrogen bond strength.
- (f) A weak intermolecular coupling exists between different water molecules.
- (g) The frequency of the rocking mode of water increases with increasing hydrogen bond strength.
- (h) The frequency of the wagging mode of water increases with increasing  $M-O_w$  coordination.
- (i) The planar rocking mode of water couples with its in-plane bending mode ( $\nu_2$ ) to give a combination mode.
- (j) The distortion in  $H_2O$  structure changes with temperature and shows discontinuities at 225, 193 and 110 K in MPH and at 223 and 180 K in NPH.
- (k) The transitions at 225 and 193 K in MPH and 223 and 180 K in NPH are associated with distortion of water molecules which arises due to tumbling motion of metal-aquo complex.
- (l) The transition at 110 K in MPH is associated with positional ordering of hydrogen atoms.
- (m) The space group below 225 K in MPH (223 K in NPH) is  $C_s^2$ .
- (n) The phase transitions at 335, 370 and 450 K in MPH and 311 and 355 K in NPH arise due to the reorientational motions



of the water molecules and the reorientational potential barrier changes from phase to phase.

Chapter IV on CoPH and MnPH has the following results :

- (a) The phase transitions at 288 and 333 K in CoPH and 248 and 342 K in MnPH arise due to the displacements of the water octahedra to two distinguishable site symmetries.
- (b) The space group  $C_{2v}^7$  changes to  $C_s^1$  in the above transitions.
- (c) In LT phase, CoPH shows a mixture of two types of lattices, i.e. ordered and disordered structure type. The water octahedra occupy crystallographically two different positions; one of them shows spectra similar to those of ordered phases of MPH and NPH and the other exhibits spectra similar to those of disordered phase of ZPH. MnPH also shows a mixture of two types of lattices, both being disordered type.
- (d) The phase transitions at 166 and 160 K in CoPH and MnPH, respectively, arise due to distortion of water molecules.
- (e) The space group below this transition is  $C_1^1$ .

Chapter V covers our detailed studies on ZPH which can be summarized as follows :

- (a) The bending mode of water shows a hypochromic effect which has been observed for the first time.
- (b) The stretching modes of water show bathochromic shifts as well as hypochromic effect.
- (c) A strong resonance interaction is observed between  $2\nu_2$  and  $\nu_1$  of  $H_2O$  at LT.
- (d) The various phase transitions occurring at 284, 256.5 and

233 K are triggered, respectively, by the distortion of the perchlorate ion, the displacement of water octahedra from  $C_s$  to  $C_i$  site symmetry and the ordering of water molecules. (e) The space group  $C_{2v}^7$  at RT changes to  $C_{2h}^5$  at the transition (256.5 K).

Chapter VI pertains to the following results on CPH and HPH :

- (a) The bending mode of water shows hypochromic effect.
- (b) The stretching modes of water show bathochromic shifts without enhancement in intensity.
- (c) Very weak intermolecular coupling is exhibited by the bending mode of water.
- (d) Both the normal hydrates turn out to be pseudohydrates at LT.
- (e) In pseudohydrates the presence of  $H_3O^+$  ion having a pyramidal structure is demonstrated.
- (f) There is a strong resonance interaction between the  $\nu_1$  and  $2\nu_4$  of  $H_3O^+$  ion. The interaction is stronger in HPH than CPH.
- (g) Reconstructive type of phase transition starts to occur at 272 K in both compounds due to thermal contraction of lattice and the rate of reconstruction is very fast at 248 K in CPH and at 243 K in HPH; the normal hydrates turn out to be pseudohydrates (i.e.  $H_2O$  molecules change to  $H_3O^+$  and  $OH^-$  ions). Such a phenomenon has been observed for the first time

in these salts in the field of crystal hydrates.

(h) The phase transitions exhibited after the formation of pseudohydrate (at 120 and 162 K in CPH and 137 K in HPH) arise due to the reorientational motion of  $\text{H}_3\text{O}^+$  ions.

Some correlations and conclusions derived from the present work and suggestions for future investigations are given at the end of the thesis.

## CHAPTER I

### INTRODUCTION

#### 1.1.1 GENERAL

The unusually vast range of variations in the behaviour of water under different ambient conditions and its characterization for important physical, chemical and biological applications have attracted the attention of several spectroscopists. In crystal hydrates the water molecules interact with their surroundings through hydrogen bonding and cation-water coordination. In fact hydrogen bonding is the dominant factor in determining crystal structure and many other important properties not only of solids but also of liquids and gases (1-4).

#### 1.1.2 VIBRATIONAL AND LIBRATIONAL MODES

Vibrational frequencies serve as a sensitive tool to confirm (and determine in some cases) the molecular structure and obtain force fields in and between the molecules. In a large molecule with some identifiable units (triatomic or more), the vibrational frequencies involving internal coordinates pertain to the intra-unit force-fields, but they are also quite sensitive to the environment around the unit. In addition, the unit may have angular motions with respect to rest of the molecules, the internal coordinates

being treated as unaltered. These are called librations and their frequencies depend entirely on the environment. Librational modes, therefore enable us to determine the strength of the crystalline field (from frequency), the symmetry of the environment (from intensities in IR, Raman, etc.), and the relaxation mechanism (from half-width and line shape). The crystalline field directly controls the frequencies, half-widths and intensities of the librational bands, whereas in the internal modes it only introduces modifications. Thus the study of the aforesaid properties of librational modes with their variation with temperature, with isotopic substitution and from one hydrate to another may provide a sensitive means of studying the crystal environment.

### 1.1.3 INTERNAL MODES OF WATER IN VAPOUR AND CONDENSED PHASES

Out of three states of pure water, only the vapour phase vibrational frequencies have been completely characterized (5,6) as summarized in Table 1.1. In liquid water the environment changes continuously with time (7-9) and thus the vibrational frequencies are a superposition of those of a large number of dynamically changing configurations. The vibrational spectra are composed of many unresolved components, broadened into bands, e.g. the  $\nu_1$  and  $\nu_3$  bands

overlap to give a single broad band with shoulders which have some times been resolved into as many as four components. The structure and spectrum of liquid water (4, 7-17) have been discussed by many investigators. The structure has been thought to be composed of ice like conglomerates which continually breakdown and reconstruct over short intervals of time (16, 17); local order exists, but long-range order is absent. In the case of ice spectra (18-20), structural disorder creates difficulty in resolving the OH stretching bands (21).

#### 1.1.4 CRYSTAL HYDRATES

There are a large number of inorganic hydrated crystals containing hydrogen bonded water molecules, and in many of these the hydrogen bond strengths are comparable with those in liquid water and ice. The water molecules in these solid systems are highly interacting and neighbouring vibrations are expected to couple with each other. It is anticipated that studies of water vibrations in hydrogen bonded inorganic hydrates will not only provide information about the force fields in and between the water molecules in these compounds, but also give information about the liquid water and ice systems. The present investigations are concerned with the vibrational and librational studies of water in divalent metal perchlorate hexahydrates.

### 1.2.1 VIBRATIONAL SPECTRA OF CRYSTALS

In order to understand the observed spectrum of a molecular crystal, it is necessary to consider the changes occurring in the spectrum of a molecule when it is transformed from vapour phase to a liquid or a crystal. The theory of crystal vibrations and their selection rules is not reviewed here, since they have been extensively treated in literature (22, 23). However, a few aspects of this theory, to be used later, will be mentioned.

### 1.2.2 THE CRYSTAL POTENTIAL

The potential energy ( $V$ ) associated with a unit cell has been expressed under harmonic approximation in various forms (24,25). Following Tayal et al (26) we shall write it explicitly as :

$$V = \sum_j (V_j^0 + V_j^1) + \sum_j \sum_k (V_{jk} + V_{jk}^1) + V_L + \sum_j V_{Lj}$$

where the summations extend over all the molecular units in the unit cell. Discussing the case of water  $V_j^0$  is the potential energy of the  $j^{\text{th}}$  free water molecule as a function of its internal coordinates and  $V_j^1$  is the perturbation in it due to the equilibrium field of the crystal at the site of  $j$ . Thus  $V_j^0$  determines the internal mode vibrations and magnitude and variations of  $V_j^1$  from site to site may lead to static field shifts and site splittings.

$V_{jk}$  represents the contributions due to the cross terms between the internal coordinates of the  $j^{\text{th}}$  and  $k^{\text{th}}$  molecular units. Such an interaction between corresponding vibrations of molecules at equivalent sites in the unit cell lifts the degeneracy and gives rise to splitting of bands. Each split frequency corresponds to a specific phase relation between vibrations of the different molecules. This additional splitting ( $C_F$  site splitting) is called correlation field or dynamic field splitting. The term  $V'_{jk}$  is parallel to  $V_{jk}$ , except that it involves the position and orientation of coordinates and expresses an interaction which leads to correlation field splitting of the external modes (librations and translations). The site splitting of the external modes is due to the unequal contributions from the coordinates of non-equivalent sites to  $V_L$ .

$V_L$  is the lattice potential energy expressed as a function of the position and orientation of the coordinates of the molecular units, treating them to be in the equilibrium configurations.  $V_L$ , thus, determines the lattice modes (both the librations and translations in the case of water).

$V_{Lj}$  represents a perturbation in  $V_L$  due to the  $j^{\text{th}}$  molecular unit. It, thus, represents the dynamic interaction between the external and the internal



modes. For water in hydrates the maximum value of the external (librational) mode has been reported in the region  $1080 \text{ cm}^{-1}$  (26) as given in Table 1.2. The internal mode ( $\nu_2$ ) has the smallest reported value  $1495 \text{ cm}^{-1}$  (27) and hence the coupling corresponding to  $V_{Lj}$  terms is not significant.

### 1.3 ISOTOPIC DILUTION

From the preceeding discussion it is quite obvious that to obtain useful information about the vibrations of a molecule in a condensed phase, it will be useful to determine the transitions corresponding to the uncoupled levels, because the intermolecularly uncoupled transition frequencies which are involved in calculating the intramolecular force constants. Thereafter one can determine the magnitude of coupling where it occurs.

The isotopic dilution technique provides the necessary means of uncoupling the motions of neighbouring molecules, thus eliminating the interactions arising from correlation field splittings. This technique thereby makes it possible to distinguish between static field and correlation field effects (28,29). As its name implies, the isotopic dilution technique involves the study of solid solutions with an isotopic species. The static field for the molecule remains almost unchanged, while the dynamic coupling of the motion of

the molecule with its neighbours is eliminated as long as the transition frequencies of the two species are sufficiently far apart. The intermolecularly uncoupled frequencies can therefore be determined. This technique was applied to hydrates by J. Schiffer (7).

In a hydrate, the uncoupled frequencies for a given isotopic species of water may be obtained from the spectrum of a sample containing a small percentage of the molecule in question surrounded by the molecules of the other two isotopic species in the crystal. For example, in order to find out the uncoupled  $\text{H}_2\text{O}$  frequencies, the hydrated sample is prepared having a low percentage of pure  $\text{H}_2\text{O}$  molecules, the others being HOD and  $\text{D}_2\text{O}$ . Four different sample concentrations as shown in Table 1.3 are sufficient to obtain the desired information (30), in principle at least.

The uncoupled  $\text{H}_2\text{O}$  and  $\text{D}_2\text{O}$  frequencies may be found from the third and second samples respectively. Similarly, the first sample gives the coupled  $\text{H}_2\text{O}$  and the fourth the coupled  $\text{D}_2\text{O}$  frequencies. The uncoupled HOD bands may either be found from sample first or from the fourth. However, the uncoupled OH stretching band of HOD, often referred to as  $\nu_{\text{OH}}$ , is most conveniently found from sample four because the spectrum of this sample does not contain  $\nu'_3$  and  $\nu_1$  bands of  $\text{H}_2\text{O}$  on opposite sides of the HOD absorption. Similarly, the

uncoupled OD stretching band of HOD ( $\nu_{OD}$ ) is usually found from the first sample. In general, for HOD, unlike  $H_2O$  and  $D_2O$ , it is not always possible to obtain completely coupled frequencies because no sample would ever contain more than 50% HOD.

#### 1.4.1 STRUCTURE OF HYDRATES

The structure of hydrates has been treated extensively (32-35) and only those points of the structure of hydrates will be emphasized here which are relevant to the present study.

Since X-ray diffraction does not yield accurate measurements on the positions of H-atoms, neutron diffraction (ND) methods have been used to obtain the geometry of water molecules in hydrates. Table 1.4 summarizes some relevant data (5, 15B, 26, 31, 36-40). Ferraris and Franchini-Angela (31) have given a valuable survey of ND studies of hydrates. They observed that the actual geometry varies in various hydrates, but in general the O-H bond length,  $r(O_W-H)$  and the interbond angle,  $2\alpha$  become larger in the bound state as compared with free water.

Hydrogen positions in hydrates have also been estimated from proton magnetic resonance study. Initial work on these lines has been carried out by Pake in gypsum (41). Later on McGrath and Silvidi studied numerous hydrates by this method (42).

#### 1.4.2 SYMMETRY OF WATER IN CRYSTAL HYDRATES

The free water molecule has  $C_{2v}$  symmetry. The symmetry is often reduced in a hydrate due to environmental effects. Even in the absence of orientational disorder or rotation, a water molecule in the crystal can occupy a site having the symmetry of the point group  $C_{2v}$  or one of its sub-groups  $C_2$ ,  $C_s$  or  $C_1$ . If the two hydrogens of a  $H_2O$  molecule form hydrogen bonds of different strengths, the  $C_2$  axis as well as one mirror plane are lost, and the symmetry is reduced to  $C_s$ . Further, in many crystals the special environments above and below the plane of the water molecule are non-equivalent, consequently the symmetry is reduced further to  $C_1$ .

ND evidence shows that 76 out of the 90 water molecules in a total of 47 hydrates studied (31) lost  $C_{2v}$  symmetry. However, it is not unlikely that comparatively small inequalities in bond lengths existed in other molecules also (which could be of spectroscopic significance), though they remained undetected because of uncertainties in position measurements (26). Falk and Knop (15B) observed that as many as 570 out of 663 different water molecules involved in the hydrates examined by him have only  $C_1$  site symmetry.

There is yet another consequence of the particular shape and symmetry of the water molecule. Water in true hydrates is often found as water of coordination forming a fully hydrated  $M(OH_2)_n^{m+}$  aquo-complex, where M is the

central cation,  $m$  is the charge of cation and ' $n$ ' has most common value six as in the present case. The highest symmetries which these complexes may attain in crystals are lower than those ideally possible for  $MX_n$  configuration involving monatomic ligands. The use of a symmetry sensitive local probe, such as Mössbauer, EPR or NMR active atom at the cation (M) site may reveal the true symmetry or distribution of symmetries around the M-ion.

An  $M(OH_2)_6$  complex, which can have the highest possible symmetry of  $O_h$  with essentially localized hydrogen atoms, can also attain one of the  $T_d$ ,  $T_h$  or  $T$  symmetries.

#### 1.4.3 STRUCTURE OF DIVALENT METAL PERCHLORATE HEXAHYDRATES

- (a) The  $C_{2v}^7$  Structure of  $M(ClO_4)_2 \cdot 6H_2O$   
(M = Mg, Mn, Co, Ni and Zn)

Using X-ray diffraction technique, West (43) determined the detailed RT crystal structure of  $Mg(ClO_4)_2 \cdot 6H_2O$ , a representative member of the isomorphous series  $M(ClO_4)_2 \cdot 6H_2O$ . These crystals are found to be pseudohexagonal with an orthorhombic bimolecular unit cell in the space group  $C_{2v}^7 (P_{mn}^{2_1})$ . A projection of an orthorhombic unit cell on  $ab$  plane is shown in Fig. 1.1. The six nearest neighbours of Mg ion are  $H_2O$  molecules forming an octahedron  $Mg(OH_2)_6$  with  $Mg-O_w$  distance as 2.14 Å. These  $H_2O$  molecules may be considered to be situated on the faces of a cube, elongated along its body diagonal as depicted in Fig. 1.2. This elongated diagonal is parallel to

the crystallographic C-axis. The Mg ion site has a trigonal symmetry with its three-fold axis parallel to the C-axis. One of the three octahedron axes joining two opposite  $\text{H}_2\text{O}$  molecules lies in the bc plane, the two  $\text{H}_2\text{O}$  making angles of about  $+55^\circ$  and  $-55^\circ$  respectively, with the C-axis in the bc plane. The remaining two axes of each octahedron lie in the other two equivalent planes of the hexagonal crystal.

The two  $\text{H}_2\text{O}$  octahedra in the unit cell (Fig. 1.1) make an angle of  $60^\circ$  with each other in the ab plane. The configuration about the second Mg ion site in the unit cell is obtained from the first by a rotation of  $60^\circ$  about the C-axis. There are six  $\text{ClO}_4$  tetrahedra ( $\text{Cl-O} = 1.5 \text{ \AA}$ ) lying outside the octahedron of  $\text{H}_2\text{O}$  molecules surrounding the Mg ion (Fig. 1.1).

The pseudohexagonal structure of the crystals is the result of combination of a body-centred orthorhombic metal lattice (M-lattice) and a base-centred dihexagonal water-perchlorate lattice (P-lattice). Low symmetry M-lattice is triply twinned (43) along a three-fold vertical twinning axis so as to assume a hexagonal form (Figs. 1.3 and 1.4). The twinning does not apply to the high symmetry P-lattice. At the twinning boundaries the P-lattice is continuous, whereas the M-lattice is discontinuous. West (43) has coined the term hermaprodite for this type of twinning. Such a twinning may be called repeated twinning (44, 45) or mimetic twinning (45, 46) forming a triplet similar to that occurring in the structure of aragonite (45, 46). All the Mg ions within a twin boundary have the same first and second coordination spheres of neighbour

(water molecules and perchlorates) as in the untwinned structure. Detailed examination shows that their higher coordination spheres differ from those in the untwinned structure.

If the trigonal symmetry at the Mg ion site is exact and the twinning components match perfectly and also the first and the second coordination spheres are considered, then all the Mg ion sites will be equivalent in the hexagonal crystal. The sites may become inequivalent in two ways. Firstly, the trigonal symmetry is exact but there is a little mismatch of the twinning components as has been reported in the structure of aragonite (44). The positions of the Mg ions of one component in the twin boundary may not exactly correspond to those of the other components. This mismatch will be more for the first and the second coordination spheres (44). So far no experimental observation has been made to determine the amount of mismatch in the series. However, a small amount of mismatch has been reported for  $\text{Co}(\text{ClO}_4)_2 \cdot 6\text{H}_2\text{O}$  (43) through a measurement of interfacial angle of the crystal which were found to differ from the ideal angle of  $60^\circ$  by less than  $2'$ . Secondly, if trigonal symmetry is not exact, two metal cation sites in the unit cell in one twinning component may be inequivalent and rotated by  $120^\circ$  relative to those of the other two components. This results in six inequivalent sites in the crystal.

West (43) observed some diffuse streaks in the Laue and oscillation photographs of  $\text{Zn}(\text{ClO}_4)_2 \cdot 6\text{H}_2\text{O}$  crystals. He concluded that they appeared due to some disorder in the structure, but did not make any detailed study. Later on Ghosh and Ray (47)

by an X-ray analysis verified its twinning and explained the nature of disorder in terms of mistakes in repetition along the b-axis of the orthorhombic cell of each of the three twin components. The dimensions of the unit cell are given in Table 1.5.

(b) The  $C_{3v}^1$  Structure of  $M(ClO_4)_2 \cdot 6H_2O$  ( $M = Cd$  and  $Hg$ )

The preliminary observations by West (43) from X-ray crystallography show that both  $Cd(ClO_4)_2 \cdot 6H_2O$  and  $Hg(ClO_4)_2 \cdot 6H_2O$  have trigonal unimolecular unit cell with space group  $C_{3v}^1$ . West (43) did not determine the atomic positions in these crystals and found that as far as the positions of perchlorate groups and those of water molecules were concerned, the structure totally resembled that of hexagonal  $LiClO_4 \cdot 3H_2O$ . Fig. 1.5 shows the projection along C-axis of four unit cells of  $Cd(ClO_4)_2 \cdot 6H_2O$  (adopted from  $LiClO_4 \cdot 3H_2O$  (48,49)) having the trigonal symmetry. The Cd (or Hg) atom in the unit cell, with coordinates  $00 \frac{1}{2}$  is at the center of water octahedra which form columns along the direction of the C-axis. The two neighbouring water octahedra in a column share two sheets of three water molecules between them, i.e., each pair of Cd(or Hg) atoms is separated by two layers of three water molecules. The positions and arrangements of all other atoms and groups were proposed to remain essentially the same. The  $ClO_4^-$  ions lie between the columns and are hydrogen bonded to them as shown in Fig. 1.6. The dimensions of this unit cell are also given in Table 1.5.



## 1.5 GROUP THEORETICAL ANALYSIS

### (a) Perchlorate Systems with $C_{2v}^7$ Space Group

The hydrated perchlorates of Mg, Mn, Co, Ni and Zn belong to space group  $C_{2v}^7$  with two molecules in the unit cell. Therefore, there are twelve water molecules, four perchlorate groups and two metal cations in the unit cell. In the space group, the possible site symmetries are  $C_s(2)$  and  $C_1(4)$ . Now to select the site symmetry of the metal cation,  $H_2O$  and  $ClO_4^-$  group we must always have the number of equivalent atoms or molecules equal to the accommodational value of the site symmetry. Therefore, the four  $ClO_4^-$  groups and two metal cations in the unit cell must occupy the site symmetry  $C_1(4)$  and  $C_s(2)$  respectively. However, there is no site symmetry which can accommodate the twelve water molecules of the unit cell. As mentioned previously the metal cation and six water molecules forming the aquo-complex  $M(OH_2)_6$ , which is taken as a single group, can be in the  $C_s$  site symmetry in addition to the metal cation. Thus in the space group  $C_{2v}^7$ , the  $[M(OH_2)_6]^{2+}$  and  $ClO_4^-$  groups can only have  $C_s$  and  $C_1$  site symmetries respectively. Therefore, the twelve equivalent water molecules in the unit cell can be assumed to have the same site symmetry  $C_s$ , which is of course a subgroup of the point group  $C_{2v}$  of free water molecule. The other possibility is that the twelve  $H_2O$  molecules in the unit cell can have three  $C_1(4)$  site symmetries. However, this possibility has been ruled out, because a single bending mode has been

observed in these hydrates experimentally. The correlation table for the symmetry species of the point group (of ion or molecule) to the space group is given in Table 1.6.

(b) Perchlorate Systems with  $C_{3v}^1$  Space Group

$Cd(ClO_4)_2 \cdot 6H_2O$  and  $Hg(ClO_4)_2 \cdot 6H_2O$  belong to space group  $C_{3v}^1$  with one molecule in the unit cell. In this space group the possible site symmetries are  $3C_{3v}(1)$ ,  $C_s(3)$  and  $C_1(6)$ . Therefore the six water molecules can occupy the  $C_1(6)$  site. The metal cation would naturally occupy the  $C_{3v}(1)$  site which will remain the site for the single metal aquo-complex  $M(OH_2)_6$ .

In both  $C_1$  and  $C_{3v}$  site symmetries all the six water molecules are equivalent to give a single bending mode spectroscopically. The two perchlorate ions in the unit cell cannot have site symmetry  $C_s(3)$  or  $C_1(6)$  because the accommodational number of  $C_s$  and  $C_1$  are both greater than 2. Thus the only possible site symmetries for the two  $ClO_4^-$  ions are the remaining two distinguishable  $C_{3v}(1)$  sites, which can accommodate one  $ClO_4^-$  group each. The correlation table for the symmetry species of the point group (of ion or molecule) to the space group is given in Table 1.7.

## 1.6 FERMI RESONANCE

Fermi resonance (FR) (50) occurs when two different energy levels of a molecule, having the same symmetry species, lie close together in energy. Their interaction results in the mutual repulsion of the levels and large enhancement in

the intensity of the weaker transition.

(a) Calculation of FR Parameters

From the spectra of the complexes the observed intensity ratio ( $R > 1$ ) and the frequency separation ( $\Delta$ ) of the FR doublet (say  $\nu_1$  and  $2\nu_2$  in the case of water) can be used to determine the separation of the unperturbed levels ( $\Delta_0$ ) and the Fermi coupling coefficient ( $\Omega$ ) using an approximation method (51,52) giving equations 1) and 2) below :

$$\Delta_0 = \Delta \frac{R - 1}{R + 1} \quad \dots\dots 1)$$

$$\Omega = \frac{(\Delta^2 - \Delta_0^2)^{1/2}}{2} \quad \dots\dots 2)$$

(b) Calculation of the Unperturbed Frequencies

The unperturbed frequencies of the doublet members ( $\nu_{10}$ ,  $2\nu_{20}$ ) can then be calculated from equation 3) below :

$$(\nu_{10}, 2\nu_{20})_{\text{H}_2\text{O}} = \frac{\nu_1 + 2\nu_2}{2} \pm \frac{\Delta_0}{2} \quad \dots\dots 3)$$

(c) FR Displacement Parameter

The FR interaction may be characterized by  $\Omega$ . If  $\Delta$  is large enough, effect of  $\Delta_0$  becomes negligible in equation 2) and  $\Omega$  will approximately be equal to  $\frac{\Delta}{2}$ . We suggest, therefore, that FR may be characterized by the displacement of the two perturbed levels,  $\Delta F$  determined as

$$\Delta F = \Delta - \Delta_0 \quad \dots\dots 4)$$

In strong proton acceptors higher  $\Delta F$  can be observed. This statement was confirmed by Wolff (53).

### 1.7 ELECTRICAL AND MECHANICAL ANHARMONICITIES

Electrical anharmonicity of a given normal mode is associated with an asymmetric variation of the dipole moment with mechanical motion for that mode. The mechanical anharmonicity is associated with deviations of the potential well for a given mode from the harmonic (parabolic) form. The induced dipole moment  $\mu$ , the potential function of the well  $V$  and the energy level  $E(v)$  for the  $v^{\text{th}}$  vibrational number are given, in the diatomic approximation, by

$$\mu = \mu_0 + \mu_1 Q + \mu_2 Q^2 + \dots \quad \dots \quad 1)$$

$$V = \frac{1}{2} K_2 Q^2 + K_3 Q^3 + \dots \quad \dots \quad 2)$$

$$\frac{1}{hc} E(v) = W_e (v + \frac{1}{2}) + W_e X_e (v + \frac{1}{2})^2 + \dots \quad \dots \quad 3)$$

From above equations and observed values of  $\nu_2$ ,  $2\nu_2$ , and their intensities ( $I_{\nu_2}$  and  $I_{2\nu_2}$ ), the anharmonicities  $W_e X_e$  (54), the fundamental harmonic frequencies  $W_e$  (54), cubic potential constants  $K_3$  (55) and the dipole coefficient ratios  $(\mu_2/\mu_1)$  (56) can be deduced approximately :

$$W_e X_e = \frac{2(\nu_2) - 2\nu_2}{2} \quad \dots \quad 4)$$

$$W_e = \nu_2 + 2W_e X_e \quad \dots \quad 5)$$

$$K_3 = \left[ \frac{4W_e (W_e X_e)}{15} \right]^{\frac{1}{2}} \quad \dots \quad 6)$$

$$\frac{\mu_2}{\mu_1} = \frac{-(K_3/W_e) \pm [I_2 \nu_2 \cdot \nu_2 / I_{\nu_2} \cdot 2 \nu_2]^{\frac{1}{2}}}{1 \pm 5(K_3/W_e) [I_2 \nu_2 \cdot \nu_2 / I_{\nu_2} \cdot 2 \nu_2]^{\frac{1}{2}}} \dots\dots\dots 7)$$

## 1.8 PREVIOUS VIBRATIONAL STUDIES IN IR AND RAMAN

IR work (57-60) on  $M(\text{ClO}_4)_2 \cdot 6\text{H}_2\text{O}$  ( $M = \text{Mg, Mn, Co, Ni}$  and  $\text{Zn}$ ) so far has been limited to room temperature spectra and the region  $600$  to  $1200 \text{ cm}^{-1}$  and  $3000$  to  $4000 \text{ cm}^{-1}$ . Low temperature spectra have not been covered, and region  $1200$  to  $3000 \text{ cm}^{-1}$  and below  $600 \text{ cm}^{-1}$  remains uninvestigated. Deuteration studies are not available. Raman spectra are available (61-63) only for the salts with  $M = \text{Mg, Ni, Zn}$  and  $\text{Cd}$  and these are for polycrystalline samples only. IR spectra for salts with  $M = \text{Cd}$  and  $\text{Hg}$  are not available and no Raman spectra for salts with  $M = \text{Mn, Co}$  and  $\text{Hg}$  are available. The reported data are reproduced in Table 1.8. Estimates of intensities and half widths are not available in any of the reported cases, and in many cases the assignments need a closer examination.

### 1.9.1 PHASE TRANSITIONS

The cross-disciplinary subject of phase transitions is of growing interest to physicists, chemists, metallurgist, ceramists and others involved in the study of solids from the view point of its theoretical importance or technological relevance. Computer core storage in magnetized ferrite rings and liquid crystal digital displays, polymorphism, crystal

structure and electrical, magnetic, dielectric and thermal properties form some of the important aspects of such studies. Newer systems undergoing transitions and newer kinds of transitions such as incommensurable structural phase transitions, quasi-low dimensional systems, systems containing lattice disorder due to impurities or as mixed crystals and multicritical points are constantly being reported. The subject of phase transformations in solids has been reviewed by Staveley (64), Ubbelohde (65), Smoluchowski (66), Rao et al (67,68), Owens et al (69), Tayal et al (70) and Muller et al (71). A brief critical account of the topics on phase transformations relevant in view of this thesis will be presented here.

### 1.9.2 CLASSIFICATION OF PHASE TRANSITIONS

#### (a) Early Attempts for Classifications

The two classes early established are :

##### (i) The first-order (or discontinuous) transformations

Such transitions involve a sharp and discrete change in internal and free energies at the transformation temperature and therefore the system shows discontinuity in almost all the physical and chemical properties at the transition temperature.

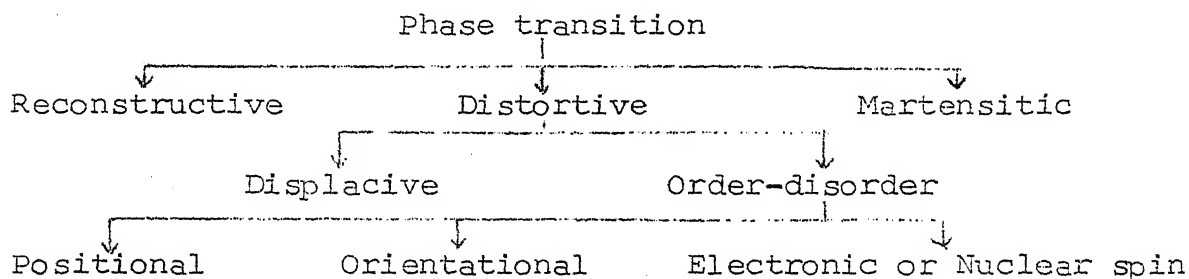
##### (ii) Second (or higher) order (or continuous) transformations

This category of phase-transitions occur over a large temperature range and are generally associated with continuous

increase in disorder, internal energy and specific heat with rise in temperature (67).

(b) The Buerger Classification

According to this classification the change of crystal structure at a phase transition in solids is summarized as follows :



Martensite transformation does not fall under the present study and will not be discussed here. About the reconstructive and distortive processes a brief description follows :

(i) Reconstruction of lattice

In the reconstructive phase transitions, the atoms of a solid reconstruct a new lattice as shown in Fig. 1.7. Thermal transformation of  $\text{CsCl}$  at  $479^\circ\text{C}$  (73),  $\text{NH}_4\text{Cl}$  at  $180^\circ\text{C}$  (74), aragonite-calcite transformation of  $\text{CaCO}_3$  at 723 K (75) with coordination number of Ca changing from 9 to 6; transformation of carbon from graphite to diamond (76); tin (white to gray) (77,78); phosphorous (yellow to black) (79); glass (amorphous to crystalline) (80); and crystal hydrates (normal to pseudohydrate;  $\text{Cd}(\text{ClO}_4)_2 \cdot 6\text{H}_2\text{O}$  and  $\text{Hg}(\text{ClO}_4)_2 \cdot 6\text{H}_2\text{O}$  in present case) all belong to this class.

(ii) Distortion of lattice

In distortive type of phase transition the regular lattice is distorted slightly without disrupting the linkage in any way. This can occur in two ways :

- (A) Displacive transformation, which involves small displacements in the lattice position of a single atom or a molecular unit.
- (B) Order-disorder transformation, which involves the ordering of atoms or molecules among various equivalent positions.

(A) Displacive transformations: These are associated with the very small changes in the energy and are usually fast. The high temperature form is usually more open (higher specific volume) and has high specific heat and symmetry. Examples of displacive transformations include the transition of  $\text{SiO}_2$  (Tridymite-Quartz (81-83));  $\text{ZnS}$  (Sphalerite-Wurtzite, (84));  $\text{FeS}_2$  (Pyrite-Mercasite, (85,86));  $\text{Sb}_2\text{O}_3$  (Senarmonite-Volentinite) (85-86));  $\text{As}_2\text{O}_3$  (Arsenolite-Clandelite, (85-86)) and  $\text{TiO}_2$  (Brookite-Rutile, (85,86)). Phase transformation of  $\text{SrTiO}_3$  appears to be truly displacive, while transitions of  $\text{BaTiO}_3$  and  $\text{PbTiO}_3$ , often considered to be displacive, can also be described in terms of an order-disorder transition (87,88). As we shall see in section 4.2.4 in our present case also  $\text{Mn}(\text{ClO}_4)_2 \cdot 6\text{H}_2\text{O}$  and  $\text{Co}(\text{ClO}_4)_2 \cdot 6\text{H}_2\text{O}$  appear to be truly displacive. Transitions of  $\text{Mg}(\text{ClO}_4)_2 \cdot 6\text{H}_2\text{O}$  and  $\text{Ni}(\text{ClO}_4)_2 \cdot 6\text{H}_2\text{O}$  can also be described in terms of order-disorder mechanism as discussed in section 3.2.6.



(B) Order-disorder transitions: An ideal state of crystalline arrangement corresponds to perfect order and is realized ideally at the absolute zero temperature. At higher temperatures the extent of order is expressed in terms of an order parameter. If an order-disorder transition takes place discontinuously, we call it a first-order transition. In a higher-order cooperative transition the change occurs gradually and behaves like a  $\lambda$ -transition. Some order-disorder transitions have features of both the cooperative and discontinuous transitions (89).

### 1.9.3 MECHANICS OF ORDER-DISORDER TRANSITIONS

In an order-disorder transition, the increase in entropy is made up of electronic, vibrational, rotational and configurational contributions

$$\Delta S = \Delta S_{el} + \Delta S_{vib} + \Delta S_{rot} + \Delta S_c \quad \dots\dots (1)$$

where the subscripts are self-explanatory. The component  $\Delta S_{el}$  can generally be ignored except in metal-insulator or similar transitions. The vibrational entropy term  $\Delta S_{vib}$  is determined by the vibrational spectra of the material in the ordered and disordered phases, and it is considerable when the change in volume at the transition is large or when the disordered state has a different crystal symmetry. The rotational entropy term  $\Delta S_{rot}$  becomes important only if free rotation in one, two or three degrees of freedom occurs in one of the phases (necessarily in the disordered phase). The last term  $\Delta S_c$ , the configu-

rational entropy increase, is the dominant term in most of the order-disorder transitions, so that one can write

$$\Delta S \simeq \Delta S_c \quad \dots\dots (2)$$

If, in the ordered and disordered phases, the total number of configurations (whether it be positional or orientational in origin) are  $W_1$  and  $W_2$  respectively, then

$$\Delta S_c = K \ln \left( \frac{W_2}{W_1} \right) \simeq \Delta S \quad \dots\dots (3)$$

This simple equation often provides tremendous physical insight into the order-disorder transitions. The rate at which the full value of the disorder (or order) is attained is generally different in different directions. Let  $Q$  be a measured property which is dependent on disorder. If the environment is changed so that  $Q_f$  is the value of  $Q$  proper to that environment, and  $Q_i$  is the instantaneous value of  $Q$ , the change proceeds with time with characteristic first-order kinetics (90) defined by :

$$\frac{dQ_i}{dt} = \frac{1}{\tau} (Q_f - Q_i) \quad \dots\dots (4)$$

where  $\tau$  is known as the relaxation time. Upon integration equation (4) becomes

$$Q_i = Q_f - (Q_f - Q_o) \exp(-t/\tau) \quad \dots\dots (5)$$

where  $Q_o$  is the initial value of the quantity which is being measured. Relaxation time for ordering is very sensitive to temperature and its value decreases with the temperature

approaching  $T_c$ . However, as  $T_c$  is approached, the free energy difference between the ordered and disordered states decreases to such a low value that the processes of ordering and disordering get very much retarded. This results in a marked increase in relaxation times. Thus, the relaxation time exhibits a minimum in the region just below  $T_c$ .

Three principal kinds of disordering transitions may be distinguished :

- (a) positional disordering
- (b) orientational disordering and
- (c) spin disordering

(a) Positional Disordering

It arises either when atoms or ions occupy inappropriate sublattice positions or when more positions are available for the atoms than are necessary (90-95). Positional disorder has been observed in various inorganic compounds such as AgI (96),  $\text{RbAg}_4\text{I}_5$  (90,97,98) and  $\text{Fe}_3\text{O}_4$  (99).

(b) Orientalional Disordering

This can take place in situations where more than one distinguishable orientations become possible for a unit in the lattice. Orientalional disordering has been observed in KCN (100-103), NaHS (104), KNCS (105-108),  $\text{NaNO}_2$  (109,110),  $\text{KNO}_2$  (111,112),  $\text{NaNO}_3$  (113,114) and  $\text{NH}_4\text{Cl}$  (115-119).

### (c) Spin Disordering

In solids the orbital motions of electrons are known to be quenched (i.e. not free to reorient), but the spins are free to reorient. An ordering of spins imparts magnetism to the lattice. As the temperature increases, these elementary magnet spins flip over to other orientations, i.e. disorder sets in.

There are quite a number of materials which do not undergo complete ordering even on cooling to absolute zero. The entropies of these will be +ve at absolute zero. This is in apparent contradiction to the third law of thermodynamics. Examples of this are  $H_2O$  (89,120), and hydrates like  $ZnF_2 \cdot 4H_2O$  (121). There are also transitions involving disordering defects like vacancies (122,123).

### 1.9.4 EXPERIMENTAL TECHNIQUES USED FOR PHASE TRANSITION STUDIES

The various techniques used in these investigations are X-ray diffraction (96), neutron diffraction (97), electron diffraction (98), electrical resistivity (99), Hall coefficient (100), thermoelectric power (101), heat capacity (102), diamagnetic susceptibility (103) and elastic constants (104).

#### (a) X-ray Diffraction

It is used for crystal structure determination. Using Laue and Weissenberg photographs of a single crystal, coexistence of phases or formation of hybrid crystals during a

transformation can be known (72). Examination of crystal axes in single crystals during the transformation is sometimes useful.

(b) Neutron Diffraction

This technique is used to monitor changes in the positions of light atoms and magnetic structures (71) in the crystals.

(c) Optical and Electron Microscopy

These techniques are used to study moment of boundaries, growth of nuclei and changes in grain size and to identify the pressure induced transitions.

(d) UV-VIS-IR and Raman Spectroscopy

Spectroscopic techniques involving ultraviolet, infrared and Raman studies take advantage mainly of the thermosensitive transitions in the respective regions. These studies not only give evidence of a phase transition but also help in understanding the mechanisms involved (70,71).

(e) Magnetic Resonance

Magnetic resonance techniques dealing with NMR, EPR, NQR and Mössbauer spectroscopy have yielded information regarding the local static and dynamic changes associated with the transformations (68).

(f) Electrical Measurements

The A.C. or D.C. conductivities and dielectric constants are measured and plotted with temperature. Phase transitions are inferred from a discontinuity or a break on these curves. Such techniques are especially useful in the study of order-disorder transformations of alloys, semiconductors and ferroelectrics.

(g) Magnetic Susceptibility and Anisotropy Measurements

Magnetic transitions or polymorphic changes have been studied by measuring changes in these quantities with temperature (69).

(h) Differential Thermal Analysis

This technique is powerful to study the changes in enthalpy, activation energy and thermal hysteresis during a transformation (109,124).

Besides these modern techniques the measurements of the heat capacity, the Youngs modulus and thermal expansion of solids etc. are some other classical techniques which have sometimes been employed for the study of phase transitions in solids.

1.9.5 PREVIOUS STUDIES ON PHASE TRANSITIONS IN  $M(\text{ClO}_4)_2 \cdot 6\text{H}_2\text{O}$   
(M = Mg, Mn, Co, Ni, Zn, Cd and Hg)

While details of the pertinent results on perchlorates undertaken for the present study are summarized at the beginning of each chapter, a synopsis of various observed phase transitions in  $M(\text{ClO}_4)_2 \cdot 6\text{H}_2\text{O}$  is given in Table 1.9.

REFERENCES

1. G.C. Pimental and A.L. McClellan, 'The Hydrogen Bond', W.H. Freeman and Co., San Francisco, Calif. (1960).
2. W.C. Hamilton and J.A. Ibers, 'Hydrogen Bonding in Solids', W.A. Benjamin, Inc., New York (1968).
3. S.N. Vinogradov and R.H. Linnell, 'Hydrogen Bonding', Van Nostrand Reinhold company New York (1971).
4. P. Schuster and G. Zundel. (eds.), 'The Hydrogen Bond', North Holland, Amsterdam (1976).
5. W.S. Benedict, N. Gailar and E.K. Plyler, J. Chem. Phys. 24, 1139 (1956).
6. K. Kuchitsu and L.S. Bartell, J. Chem. Phys. 36, 2460 (1962).
7. J. Schiffer, Ph.D. thesis, Princeton University (1963) and references therein.
8. J. Schiffer and D.F. Hornig, J. Chem. Phys. 49, 4150 (1968).
9. M. Falk and T.A. Ford, Can. J. Chem. 44, 1699 (1966).
10. D. Eisenberg and W. Kauzmann, 'The Structure and Properties of Water', Oxford University Press, New York (1969).
11. J. Lascombe (ed.), 'Molecular Motions in Liquids', D. Reidel Publishing Company, Dordrecht Holland (1974).
12. R.J.H. Clark and R.E. Hester (eds.), 'Adv. Infrared Raman Spectrosc.', Vol. 2, Chap. 6, Heyden, London (1976).
13. W.A.P. Luck and D. Schioberg, Adv. in Mol. Relaxation and Interaction Processes 14, 277 (1979).
14. J.R. Scherer, in 'Advances in Infrared and Raman Spectroscopy', Vol. 5, Chap. 3, Heyden, (1978) and references therein.

15. F. Franks (ed.), 'Water - A Comprehensive Treatise', Plenum, New York, (A) Vol. 1, Chap. 4 and 5 (1972); (B) Vol. 2, Chap. 2 (1973) and references therein and (C) Vol.3, Chap. 5 and 6 (1973).
16. H.S. Frank, Proc. Roy.Soc. (London), A247, 481 (1958).
17. G. Nemethy and H.A. Scheraga, J. Chem. Phys. 36, 3382 (1962).
18. R. Bansil, J. Wiafe-Akenten and J.L. Taaffe, 'Raman Spectroscopy of Supercooled Water', J. Chem. Phys. 000, Feb. (1982).
19. (a) C.A. Angell, 'Water - A Comprehensive Treatise Vol. 7, F. Franks (ed.), Plenum, New York (1981) and references therein;(b) L. Bosio, J. Teixeira and H.E. Stanley, Phys. Rev. Lett. 46, 597 (1981).
20. (a) M.G. Sceats, M. Stavola and S. Rice, J. Chem. Phys. 70, 3927 (1979); (b) S.A. Rice and M.G. Sceats, J. Phys. Chem. 85, 1108 (1981); (c) F.H. Stillinger, Science 209, 541 (1980) and H.E. Stanley, J. Teixeira, A. Geiger and R.L. Blumberg, Physica 106A, 260 (1981) and references therein.
21. J.E. Bertie and E. Whalley, J. Chem. Phys. 40, 1637 (1944).
22. L. Pauling, J. Am. Chem. Soc. 57, 2680 (1935).
23. W. Vedder and D.F. Hornig , 'Infrared Spectra of Crystals', Chapter in "Advances in Spectroscopy" Vol. II, H.W. Thompson (ed.), Interscience Publ. Co. Inc., New York (1961) Page 189 (and references therein).
24. S. Krim, in 'Infrared Spectroscopy and Molecular Structure', M. Davies, (ed.), Elsevier, Amsterdam (1963).



25. P.M.A. Sherwood, 'Vibration Spectroscopy of Solids', Cambridge University Press (1972).
26. V.P. Tayal, B.K. Srivastava, D.P. Khandelwal and H.D. Bist, Appl. Spectros. Reviews 16, 43 (1980).
27. V.P. Tayal, D.P. Khandelwal and H.D. Bist, Chem. Phys. Lett. 55, 136 (1978).
28. G.L. Hiebert and D.F. Hornig, J. Chem. Phys. 20, 918 (1952).
29. H.J. Hrostowski and G.C. Pimentel, J. Chem. Phys. 19, 661 (1951).
30. R.A. Fifer, Ph.D. thesis, Temple University, Michigan (1970).
31. G. Ferraris and Franchini-Angela, Acta Cryst. B28, 3572 (1972).
32. A.F. Wells, Quart. Rev. (London) 8, 380 (1954).
33. W. Fuller, J. Phys. Chem. 63, 1705 (1959).
34. D. Hadzi (ed.), 'Hydrogen Bonding' Pergamon Press, New York (1959) Page 1 and 7.
35. A.F. Wells, 'Structural Inorganic Chemistry', Oxford, England (1962) Page 565.
36. Z.A. Gabrichidze and I.W. Dzhaparidze, Chem. Abstr. 69, 6925b (1968).
37. B. Klewe and E. Pedersen, Acta Cryst. B30, 2363 (1974).
38. S.H. Simonsen and M.H. Mueller, J. Inorg. Nucl. Chem. 27, 309 (1965).
39. S.K. Sikka and R. Chidambaram, Acta Cryst. B25, 310 (1969).
40. A. Sequeira, S. Srikantha and R. Chidambaram, Acta Cryst. B26, 77 (1970).
1. G.E. Pake, J. Chem. Phys. 16, 327 (1948).
2. J.W. McGrath and A.A. Silvidi, J. Chem. Phys. 34, 322 (1961) and references therein.

43. C.D. West, Z. Kristallogr. 91A, 480 (1935).
44. M.H. Battey, 'Mineralogy for Students', Oliver and Boyd, Edinburgh, Scotland (1972) Page 69.
45. F.D. Bloss, 'Crystallography and Crystal Chemistry', Holt, Rinehart and Winston, Inc., New York (1971) Page 328.
46. D. and C McKie, 'Crystalline Solids', Thomas Nelson and Sons Ltd., Great Britain (1974) Page 90.
47. M. Ghosh and S. Ray, Z. Kristallogr. 145, 146 (1977).
48. C.D. West, Z. Kristallogr. 88, 198 (1934).
49. A. Sequeira, I. Bernal, I.D. Brown and R. Faggiani, Acta Crystallogr. 31, 1735 (1975).
50. E. Fermi, Z. Physik 71, 250 (1931).
51. J.F. Bertran, L. Ballester, L. Dorriholova, M. Sanches and R. Arrieta, Spectrochim. Acta 24A, 1765 (1968).
52. J. Overent, 'Infrared Spectroscopy and Molecular Structure', M. Davies (ed.), Elsevier (1963) Page 350.
53. H. Wolff and D. Horn, Ber. Bunsenges Physik. Chem. 72, 419 (1968).
54. G. Herzberg, 'Molecular Spectra and Molecular Structure', Van Nostrand, Princeton, N.J. (1950) Vol. I, Page 95.
55. A. Foldes and C. Sandorfy, J. Mol. Spectrosc. 20, 262 (1966).
56. R.C. Herman and K.E. Shuter, J. Chem. Phys. 22, 481 (1954).
57. S.D. Ross, Spectrochim. Acta 18, 225 (1962).
58. B.J. Hathaway and A.E. Underhill, J. Chem. Soc. 3091 (1961).
59. T.G. Balicheva and S.N. Andreev, J. Struct. Chem. 5, 23 (1964).
60. F.A. Miller and C.H. Wilkin, Ann. Chem. 24, 1253 (1952).
61. J.P. Mathieu, J. Chem. Phys. 50, 9 and 79 (1953).

62. Annettle Weil and J.P. Mathieu, *Comp. Rend.* 238, 2510 (1954).
63. J.M. Janik, A. M. Mikuli, E. Mikuli, T. Stanck, Krakow Report No. 1113/PS, Krakow (1980).
64. L.A.K. Staveley, *Quart. Rev.* 3, 64 (1949).
65. A.R. Ubbelohde, *Quart. Rev.* 11, 246 (1957).
66. R. Smoluchowski (ed.), 'Phase Transformations in Solids', John Wiley and Sons, Inc., New York (1957).
67. C.N.R. Rao and K.J. Rao, in 'Progress in Solid State Chemistry', H. Reiss (ed.), Vol. 4, Pergaman Press, Oxford (1967).
68. C.N.R. Rao and K.J. Rao, 'Phase Transitions in Solids', McGraw-Hill Inc. (1978).
69. F.J. Owens, C.P. Poole, Jr., and H.A. Farach (eds.), 'Magnetic Resonance of Phase Transitions', Academic Press, New York, San Francisco, London (1979).
70. V.P. Tayal, B.K. Srivastava, D.P. Khandelwal and H.D. Bist, *Appl. Spectros. Rev.* 16, 89 (1980).
71. K.A. Muller and H. Thomas (eds.), 'Structural Phase Transitions', Springer-Verlog Berlin, Heidelberg, New York (1981).
72. A.R. Ubbelohde, 'Reactivity of Solids', J.H. De Boer (ed.), Elsevier Publishing Co., Amsterdam (1961).
73. K.J. Rao, G.V.S. Rao and C.N.R. Rao, 'Trans. Farad. Soc.' 63, 1013 (1967).
74. A. Arell, *Ann. Acad. Sci. Fenn.*, Ser AUI No. 57 (1960).
75. M. Dufy, *Ann. Chim.* 107 (1960).
76. H.P. Eovenkerk, F.P. Bundy, H.T. Hall, H.M. Strong and R.H. Wentorf, Jr. *Nature* 184, 1094 (1959).
77. J.H. De Boer, *Discuss. Farad. Soc.* 23, 171 (1957).

78. W.G. Buergers and L.J. Gruen, 'Discuss. Farad. Soc.' 23  
183 (1957).
79. V.B. Butuzov and S.S. Boksha, Doklady, Soveshchaniya 311 (1956).
80. A.I. Berenhnoi, 'Glass-Ceramics and Photo-Sitalls' Plenum  
Press, New York (1970).
81. A.L. Roberts, 'Kinetics of High Temperature Processes',  
W.D. Kingery (ed.), John Wiley, New York (1959).
82. S.R. Yoganarasimhan and C.N.R. Rao, Trans. Farad. Soc. 58,  
1579 (1962).
83. C.N.R. Rao, Canad. J. Chem. 39, 498 (1961).
84. F.A. Kroger, Z. Krist. A102, 136 (1939).
85. M.J. Buerger, Fortscher. Miner, 39, 9 (1961).
86. M.J. Buerger, 'Phase Transformations in Solids',  
R. Smoluchowski (ed.), John Wiley, New York (1957).
87. J.F. Scott, Rev. Mod. Phys. 46, 33 (1974).
88. G. Shirane, Rev. Mod. Phys. 46, 437 (1974).
89. L.A.K. Staveley, 'Technica', Revista de Engenharia, Separate  
10, No. 414, Page 173, Lisbon (1972).
90. M.A. Krivoglaz and A. Smirnov, 'The Theory of Order-Disorder  
in Alloys', H. Warlimont (ed.), Springer-Verlog, Berlin (1974)  
p. 148.
91. J.M. Cowley, J. Appl. Phys. 21, 24 (1950).
92. H. Lipson, 'Progress in Metal Physics', B. Chalmers (ed.),  
Vol. 2, Pergamon Press, New York (1957).
93. L. Guttman, in 'Solid State Physics', F. Seitz and D. Turnbull  
(eds.), Vol. 3, Academic Press, New York (1956).

94. H. Yamouchi and D. de Fontaine, in 'Order-Disorder Transformation in Alloys', H. Warlimont (ed.) Springer-Verlog, Berlin (1974) p. 148.
95. B.H. Kear, T. Sims, N.S. Stoloff and J.H. Westbrook (eds.), 'Ordered Alloys, Structural Applications and Physical Metallurgy', Claitors Publishing Division, Baton Rouge (1970).
96. W. Van Gool, in 'Fast Ion Transport in Solids', W. Van Gool (ed.), North-Holland, Amsterdam (1973).
97. S. Geller, Science 157, 310 (1967).
98. H. Wiedersich and S. Geller, in 'The Chemistry of Extended Defects in Non-metallic Solids', L. Eyring and M.O. Keefe (eds.), North-Holland, Amsterdam (1970) p. 629.
99. K. Kamigaki, M. Ohashi and T. Kanekto, in 'Ferrites', Y. Hoshino, S. Iida and M. Sugimoto (eds.), University Park Press, Baltimore (1971), p. 598.
100. H. Suga, T. Matsno and S. Seki, Bull. Chem. Soc. Japan 38, 1115 (1965).
101. M. Aloji, J. Chem. Phys. 54, 3514 (1971).
102. E. Fukishima, J. Chem. Phys. 49, 4721 (1968).
103. D.E.O. Reilly, E.M. Peterson, C.E. Scheie and P.K. Kadaba, J. Chem. Phys. 58, 3018 (1973).
104. J.J. Rush, L.A. de Graaf and R.C. Livingston, J. Chem. Phys. 58, 3439 (1973).
105. C. Akers, S.W. Peterson and R.D. Willett, Acta Cryst. B24, 1125 (1968).
106. M. Sakiyama, H. Suga and S. Seki, Bull. Chem. Soc. Japan 36, 1025 (1963).

107. R. Savoie and M. Pezolet, Can. J. Chem. 45, 1677 (1967).
108. Z. Iqbal, L.H. Sarma and K.D. Moller, J. Chem. Phys. 57, 4728 (1972).
109. Y. Yamada, I. Shibuya and S. Hoshino, J. Phys. Soc. Japan 18, 1594 (1963).
110. E.V. Chisler and M.S. Shur, Phys. Stat. Solidi 17, 163 and 173 (1966).
111. J.F. Solbakk and K.O. Stromme, Acta Chem. Scand 23, 300 (1969).
112. K.O. Stromme, Z. Anorg. Allg. Chem. 389, 315 (1972).
113. F.C. Kracek, J. Amer. Chem. Soc. 53, 2609 (1931).
114. R.A. Schroeder, C.E. Weir and E.R. Lippincott, J. Res. Natl. Bur. Standards 66A, 407 (1962).
115. A. Arell, Ann. Acad. Sci. Fenn. Ser. A6, No. 57, 204 (1966).
116. P. Schwartz, Phys. Rev. B4, 902 (1971).
117. H.A. Levy and S.W. Peterson, Phys. Rev. 86, 766 (1952), J. Chem. Phys. 21, 366 (1953).
118. R. Bersohn and H.S. Gutowsky, J. Chem. Phys. 22, 651 (1954).
119. C.H. Wang and R.E. Wright, J. Chem. Phys. 58, 1411 (1973).
120. L. Pauling, 'Nature of the Chemical Bond', Cornell University Press, Ithaca (1960).
121. R.O. Cook, A. Davies and L.A.K. Staveley, Proc. First Int. Con. Calorimetry and Thermodynamics (1969).
122. H. Warlimont (ed.), 'Order-Disorder Transformation in Alloys', Springer-Verlog, Berlin (1974).
123. N.G. Parsonage and L.A.K. Staveley, 'Disorder in Crystals', Oxford University Press (1977).

124. G.M. Bartenev and A.A. Ramizova, Zhur. Fiz. Khim. 31, 2534 (1957).
125. M.J. Buerger, in 'Phase Transformations in Solids', R. Smoluchowski, J.E. Mayer and W.A. Weyl (eds.), John Wiley, New York (1951).
126. M.J. Buerger, Fortshr. Miner. 39, 9 (1961).
127. I. Dezsi and L. Keszthelyi, Solid State Commun. 4, 511 (1966).
128. A.K. Jain and G.C. Upreti, Private Communications.
129. R. Dayal, D.R. Rao and P. Venkateswarlu, Can. J. Phys. 56, 1175 (1978).
130. E. Mikuli, A.M. Mikuli, M. Rachwalska and T. Stanek, Physica 104B, 326 (1981).
131. I. Svare, B.O. Fimland, K. Otnes, J.A. Janik, J.M. Janik, E. Mikuli and A.M. Mikuli, Physica 106B, 195 (1981).
132. I. Svare and B.O. Fimland, J. Chem. Phys. 74, 5977 (1981).
133. J.M. Janik, A.M. Mikuli, E. Mikuli and T. Stanek, Krakow - Report No. 1113/PS, Krakow (1980).
134. M.B. Patel and H.D. Bist, J. de Physique, C6, 917 (1981).
135. B.K. Chaudhuri, J. Phys. C-7, 3962 (1974).
136. B.K. Chaudhuri, Solid State Commun. 16, 767 (1975).
137. A.K. Jain and G.C. Upreti, J. Phys. C13, 5177 (1980).
138. R. Dayal, D.R. Rao and P. Venkateswarlu, J. Magn. Reson. 36, 99 (1979).
139. J.C. Sartorelli, S. Isotani, J.A. Ochi, W. Sano and A. Piccini, Chem. Phys. Lett. 57, 608 (1978).
140. M. Rachwalska and T. Stanek, Phys. Stat. A48, 297 (1978).

- 141. B.K. Chaudhuri, J. Phys. C8, 1884 (1975).
- 142. M.P. Sinha, A. Pal and S.K. Dutta Roy, J. Phys. C9, 2783 (1976).
- 143. B.K. Chaudhuri, J. Phys. C9, 1285 (1976).
- 144. A.K. Jain and G.C. Upreti, Solid State Commun. 23, 571 (1978).
- 145. R. Dayal, Ph.D. thesis, I.I.T. Kanpur, India (1976).
- 146. M.B. Patel and H.D. Bist, S331, NPSSP (1980).
- 147. A.K. Jain and G.C. Upreti, Phys. Stat. Sol. A50, 155 (1980).
- 148. R. Dayal, D.R. Rao and P. Venkateswarlu, J. Chem. Phys. 70, 2487 (1979).



Table 1.1: Frequencies of water in the vapour state

	HOH	HOD	DOD
	3755.79	3707.47	2788.05
(a)	3656.65	2726.73	2671.46
	1594.54	1402.20	1178.33
	3942.53	3889.84	2688.78
(b)	3832.17	2824.32	2763.80
	1648.47	1440.21	1206.39

(a) experimental observed frequencies, (b) harmonic frequencies.

Table 1.2: Librational and bending modes in typical crystal hydrates.

Modes	Typical values	Ref.	Modes	Typical values	Ref.
Libra- tional	115 - 1080 $\text{cm}^{-1}$	26	Transla- tional	200 - 490 $\text{cm}^{-1}$	15B
Bending	1495-1732 $\text{cm}^{-1}$	27,15B	Stretching	2850-2625 $\text{cm}^{-1}$	15B

Table 1.3: Percentage of  $\text{H}_2\text{O}$ ,  $\text{HOD}$  and  $\text{D}_2\text{O}$  in the crystal to obtain uncoupled bands.

Sample No.	% $\text{H}_2\text{O}$	% $\text{HOD}$	% $\text{D}_2\text{O}$	Uncoupled bands
1	95	5	0	$\nu_{\text{OD}}(\text{HOD})$
2	56	39	5	$\nu_1, \nu_3(\text{D}_2\text{O})$
3	5	39	56	$\nu_1, \nu_3(\text{H}_2\text{O})$
4	0	5	95	$\nu_{\text{OH}}(\text{HOD})$

Table 1.4: Geometry of water in crystal hydrates

Quantity	Magnitude in free water(a)	Magnitude in hydrates	References for data in col. 3
$r(\text{O}_\text{W}-\text{H})$	$0.9743 \text{ \AA}^\circ$	$0.850 \text{ \AA}^\circ - 1.070 \text{ \AA}^\circ$	15 B
$2\angle$	$104.52 \text{ \AA}^\circ$	$102.5^\circ - 115.5^\circ$	15 B
$r(\text{O}_\text{W} \dots \text{X})$	...	$2.6 \text{ \AA}^\circ - 3.364 \text{ \AA}^\circ$	36, 37
H-bond angle	...	$180^\circ - 120^\circ$	38
$r(\text{M}-\text{O}_\text{W})$	...	$1.62 \text{ \AA}^\circ - 2.907 \text{ \AA}^\circ$	39, 40

(a) from Benedict, et al (5).

Table 1.5: Dimension of the unit cell

Crystal lattice (cation)	Axes ( $\text{\AA}^\circ$ )		
	a	b	c
Mg	7.76	13.44	5.26
Mn	7.85	13.60	5.30
Co	7.76	13.44	5.20
Ni	7.73	13.39	5.17
Zn	7.76	13.44	5.20
Cd	7.96	13.79	5.30
Hg	-	-	-

Table 1.6: Correlation table for point group  $C_{2v}$  and  $T_d$   
with space group  $C_{2v}^7$ .

Point group	Site Symmetry	Space group	Site Symmetry	Point group
$C_{2v}(\text{H}_2\text{O})$	$C_s$	$C_{2v}^7$	$C_1$	$T_d(\text{ClO}_4^-)$

The diagram illustrates the correlation of irreducible representations (irreps) between the point groups  $C_{2v}$  and  $T_d$  via their site symmetries  $C_s$  and  $C_1$ .

- Left side ( $C_{2v}$ ):**
  - $A_1(\gamma_1, \gamma_2, T_z)$
  - $B_2(\gamma_3, R_x, T_y)$
  - $A_2(R_z)$
  - $B_1(R_y, T_x)$
- Middle ( $C_s$ ):**
  - $A'$  (receives arrows from  $A_1$  and  $B_2$ )
  - $A''$  (receives arrows from  $A_2$  and  $B_1$ )
- Right side ( $C_1$ ):**
  - $A$  (receives arrows from  $A'$  and  $A''$ )
  - $A''$  (receives arrows from  $A_1$  and  $A_2$ )
- Far right ( $T_d$ ):**
  - $A_1(\gamma_1)$
  - $A_2$
  - $E(\gamma_2)$
  - $F_1(R_{x,y,z})$
  - $F_2(\gamma_3, \gamma_4)$
  - $T_{x,y,z}$

Arrows indicate the correlation paths:  $A_1 \rightarrow A' \rightarrow A$ ,  $B_2 \rightarrow A' \rightarrow A$ ,  $A_2 \rightarrow A'' \rightarrow A''$ ,  $B_1 \rightarrow A'' \rightarrow A''$ ,  $A_1 \rightarrow A''$ , and  $A_2 \rightarrow A''$ .

Table 1.7: Correlation table for point group  $C_{2v}$  and  $T_d$   
with space group  $C_{3v}^1$

Point group	Site Symmetry	Space group	Site Symmetry	Point group
$C_{2v}(H_2O)$	$C_1$	$C_{3v}^1$	$C_{3v}$	$T_d(ClO_4^-)$
$A_1(\nu_1, \nu_2, T_z)$				$A_1(\nu_1)$
$A_2(R_z)$				$F_2(\nu_3, \nu_4, T_{x,y,z})$
$B_1(T_x, R_y)$				$E(\nu_2)$
$B_2(\nu_3, T_y, R_x)$				$F_1(R_{x,y,z})$
				$A_2$

or (other possible correlation between the space group  $C_{3v}^1$  and point group  $C_{2v}$ ).

Point group	Site Symmetry	Space group	Site Symmetry	Point group
$C_{2v}(H_2O) \sigma_v(zx)$	$C_{3v}$	$C_{3v}^1$	$C_{3v} \sigma_v(yz)$	$C_{2v}(H_2O)$
$A_1(\nu_1, \nu_2, T_z)$				$A_1(\nu_1, \nu_2, T_z)$
$B_1(T_x, R_y)$				$B_2(\nu_3, T_y, R_x)$
$A_2(R_z)$				$A_2(R_z)$
$B_2(\nu_3, T_y, R_x)$				$B_1(T_x, R_y)$

IRREFRAC

REFR

Cation (M)	$\gamma_3(p)$	Ross (57) $\gamma_1(p)$	$\gamma_2(p)$	Hatheway et al (58)	Balicheva et al (59) single crystal (H <sub>2</sub> O)	Miller et al (60)	Mathieu (61)	Janik et al (63) (ClO <sub>4</sub> <sup>-</sup> )
	1087		627		3515	652	1130	465
Mg	1111	940			3460	945	1625	
	1143		635			962	2100	630
						1060	3540	
Mn					3530			
					3440			
	1037		628		3530			
Co	1114	943						
	1143		637		3460			
								465
Ni	1105	942		1030-1196	3540			630
			628					
			633	930	3450			
	1093		625		3530			
Zn	1111	941	628					3505
	1143		637					

Expt. Tech.	Mg (a)	Ni (a)	Co (a)	Mn (a)	Zn (a)	Cd (a)	Hg
Mossbauer	83-113 (127)	83 (127)	148-163 (127)				
Magnetic susceptibility		225 (135, 136)	245-264 (142) 166 (136, 141)	120 (143)			
EPR	335 (128) 328 (123) 324 (128) 272 (128, 129) 193 (129) 103 (128, 129)	361 (137) 311 (137) 245 (137) 223 (138, 139)	354 (137)  264 (138) 243 (137) 155 (137) 148-161 (138)		346 (144) 284 (144, 145)	353 (147) 272 (147, 148) 259 (147) 116 (147, 148)	
Specific heat	325.03 (130) 272.97 (130) 168 (130) 108 (130)	361.05 (140) 311.4 (140) 225 (140)	263 (142) 240 (142) 215 (142)	134 (142)			
PMR & NQS	325 (131) 273 (131) 133 (131) 110-120 (131)						
Piezoelectric	324-328 (132) 110-120 (132)	250 (132)	160 (132)	160 (132) 89 (132)	160 (132)	274 (132) 110 (132)	
Raman	325 (133)	361 (133)					

contd.

M<sup>2+</sup>

Expt. Tech.	Mg (a)	Ni (a)	Co (a)	Mn (a)	Zn (a)	Cd (a)	Hg (a)
Infrared (b)	450	355	333	341	284 (134, 146)	272	272
	422	311	288	248	256.5 (134, 146)	259	243
	370	223	240	161	233 (134, 146)	162	137
	335	180	166			120	
	225.5 (134)					248	
	193 (134)						
	110 (134)						

- (a) The figures in parentheses denote the references cited at the end of the chapter.
- (b) Present study.

# FIGURE CAPTIONS

- Fig.1.1: A projection on ab plane of an orthorhombic unit cell of  $\text{Mg}(\text{ClO}_4)_2 \cdot 6\text{H}_2\text{O}$ . A six ring of three waters and three perchlorate oxygens is outlined (43). The number indicates the height of the atom, along the c-axis, taking  $c = 1$  (zero or one if no number).
- Fig.1.2: Water octahedron surrounding the metal ion.
- Fig.1.3: Cyclic threeeling of  $\text{Mg}(\text{ClO}_4)_2 \cdot 6\text{H}_2\text{O}$ . Triangles in two different orientations are  $\text{ClO}_4$  tetrahedra at two different heights, all pointing in the same direction normal to the plane of projection. Two kinds of circles are metal atoms in two layers separated by  $c/2$ . Full lines are twinning boundaries (43).
- Fig.1.4: Three-fold vertical twinning of Mg lattice. The closed and open circles are Mg atoms in two different layers,  $c/2$  apart. Triangles in two different orientations are  $\text{ClO}_4$  tetrahedrons at two different heights.
- Fig.1.5: Four unit cells of  $\text{Cd}(\text{ClO}_4)_2 \cdot 6\text{H}_2\text{O}$  structure projected along the c-axis; z-coordinates of the Cl atoms are marked and those of Cd atoms are  $\frac{c}{4}$  (or  $\frac{3c}{4}$ ) (after Ghosh and Ray (47) adopted from  $\text{LiClO}_4 \cdot 3\text{H}_2\text{O}$ ). The triangles denote the set of three water molecules.
- Fig.1.6: Hydrogen bonding in  $\text{Cd}(\text{ClO}_4)_2 \cdot 6\text{H}_2\text{O}$ . The projection of octahedra represents the  $[\text{Cd}(\text{OH}_2)_6]^{2+}$  group and  $\text{ClO}_4$  tetrahedron. The acceptor  $\text{H} \cdots \text{O}$  bonds are shown as broken lines (after Sequeria et al (49) adopted from  $\text{LiClO}_4 \cdot 3\text{H}_2\text{O}$ ).
- Fig.1.7: Transformation from the structure A to any of the other structures requires breaking of first-coordination bonds. Transformations among B, C and D are only distortional (after Buerger (125,126)).



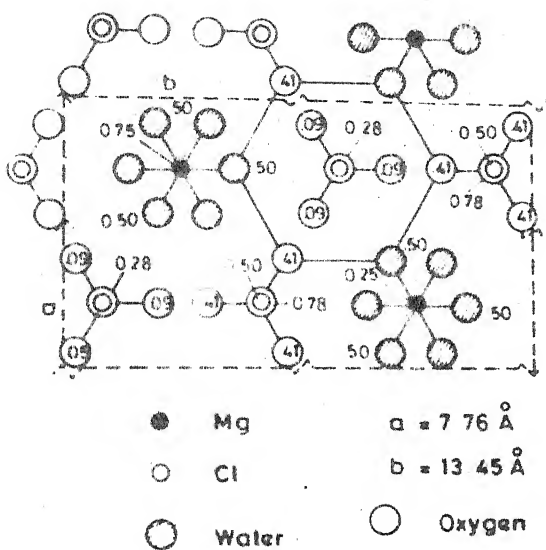


FIG. 1.1

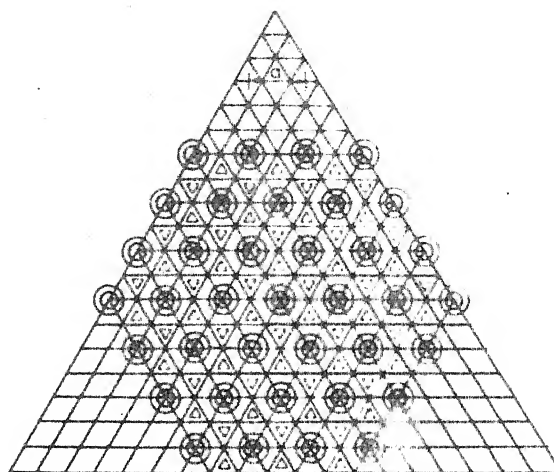


FIG. 1.3

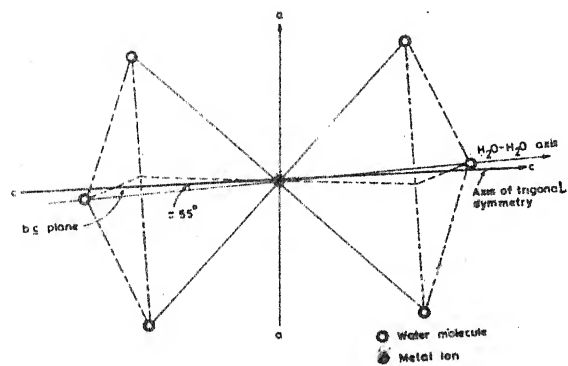


FIG. 1.2

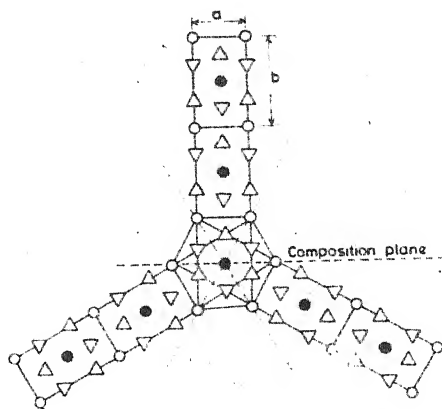


FIG. 1.4

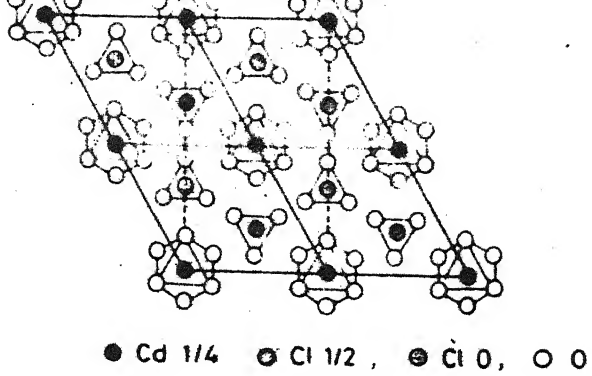


FIG 1.5

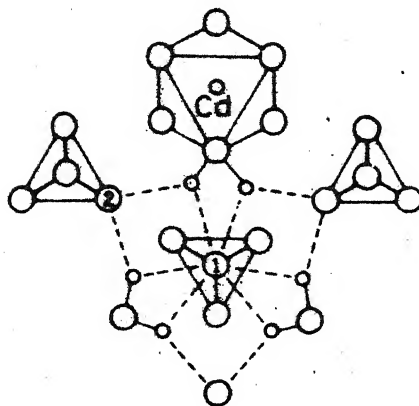


FIG. 1.6

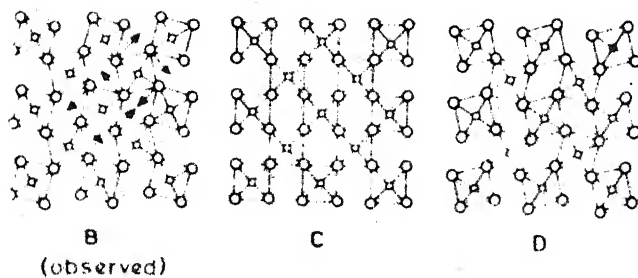
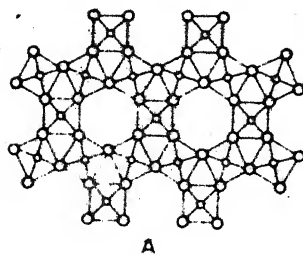


FIG 1.7

## CHAPTER II

### EXPERIMENTAL TECHNIQUES

#### 2.1.1 INFRARED SPECTRA OF SOLIDS

We present here, in a nutshell, the main techniques to record the infrared spectra emphasizing the roles of those techniques adopted by us. The four principal methods, used to obtain infrared spectra of solid substances are the following :

##### (a) Single Crystals

This is seldom done with salt crystals using normal transmission method since thin samples ( $\sim$ micron thickness usually) are needed for infrared transmission studies. Beam condensers could be helpful to get better signal-to-noise ratio but may result in overheating of the sample. However, attenuated total reflectance (ATR) technique is used to record single crystal absorption with moderately large crystals.

##### (b) Thin Films:

The sample is crystallized from solution (including  $H_2O$ ,  $D_2O$  under controlled environment) or is condensed from the vapour (in case of volatile materials) onto the surface of a proper infrared window. (In the later case the film must frequently be annealed to affect a transition from an amorphous to a crystalline state.) By preparing thin films, it is also possible to obtain polarized infrared spectra, if the crystals are uniformly oriented. This method is not

suitable for the present study because of very hygroscopic, highly absorbtive and reactive (with IR windows) nature of the samples.

(c) Mulls

Finely ground particles of a sample are mixed with nujol (or a fluorinated hydrocarbon) to prepare a mull and the resultant mull is then coated onto an infrared window. We used this method, because the surface layer of nujol prevents to some extent (i) the interaction between the sample and infrared windows and (ii) the absorption of moisture by the sample while preparing the mull. Therefore this method is better than thin film technique for these samples.

(d) Pellets (i.e. the potassium bromide technique)

In this technique the sample is finely ground and dispersed in a powdered halide, which is then pressed into a clear disc. This method is most widely used, but has several serious disadvantages (1). Other than the possibility of chemical changes such as reaction, complex formation or mixed crystal formation with the suspended material, there are dangers inherent in the mechanical procedures used. Grinding and pelleting sometimes promote polymorphic transitions. Of one immediate concern is the fact that it might easily result in dehydration of a hydrate or transfer of water molecules to the surrounding medium, so that the degree of hydration of the sample would not be known. Finally, excessive grinding of a solid may result in distortion of the crystal structure, producing a spectrum characteristic of

almost an amorphous state of the sample. In the present study, it was observed that dehydration of a hydrate and complex formation (observed by colour change) was taking place except in the case of  $\text{Mg}(\text{ClO}_4)_2 \cdot 6\text{H}_2\text{O}$  and  $\text{Ni}(\text{ClO}_4)_2 \cdot 6\text{H}_2\text{O}$ . Therefore this method was applied for  $\text{Mg}(\text{ClO}_4)_2 \cdot 6\text{H}_2\text{O}$  and  $\text{Ni}(\text{ClO}_4)_2 \cdot 6\text{H}_2\text{O}$  only and rest of them were studied in mull.

Spectra of crystalline substances prepared by the above methods frequently exhibit deviations from ideal appearance due to various scattering effects (1). The recorded spectra may be affected significantly by the following effects :

#### 2.1.2 FACTORS AFFECTING IR SPECTRA IN SOLIDS

##### (a) Particle Size

Ideally, the particles should be small compared to the wavelength of light being absorbed. When this is the case, decrease in light transmission (i.e. apparent absorption) due to the sample will occur only at characteristic absorption bands and the measured band intensities will correspond to the true intensities. With larger particles, there will be a general decrease in light transmission over the entire recorded spectrum, this light loss being greater at the higher frequencies (where the wavelength is smaller). Furthermore, the measured absorption intensity will be less than expected on the basis of the true extinction coefficient. In the limiting case, for large crystal particles, all light hitting the crystals will be scattered, reflected or totally absorbed and no bands will be seen in the spectrum. Thus the relative band intensities cannot be deter-

mined in the presence of large particles.

(b) Refractive Index

A difference between the refractive indices of the material and the surrounding medium may produce changes in the spectrum, similar to those discussed in the previous paragraph, by promoting loss of light by reflection (especially with increasing particle size). In the pressed pellet and mull methods, a medium with refractive index close to that of the sample is chosen to produce better spectra. Of more importance is the rapid change in refractive index of a substance in the vicinity of an absorption band. This gives rise to the Christiansen effect, characterized by asymmetrical and anomalous band shapes (2). Due to this effect the absorption on the low frequency side of a band is greater than that of its high frequency side; this was observed to varying extents in almost all spectra recorded but the bands maxima were not shifted by the effect (1).

2.2 RAMAN SPECTRA OF SOLIDS

Two principal methods can be used to obtain Raman spectra of solid substances :

(a) Single Crystals

CENTRAL LIBRARY.  
I. I. T., Kanpur.

Acc. No. A 82827

The single crystal polarization spectra give very useful information for classification of phonons and phase transitions. The main problem in this method is to grow a single crystal and determine its axes. The crystals which are stable and not hygroscopic are suitable for Raman study.

(b) Polycrystalline Samples

(i) Capillary method

We have used mostly this technique, because of very hygroscopic nature of the samples. The hygroscopic sample is powdered in an adequately dehumidified chamber and filled in a capillary tube which is then sealed. The sample in the capillary is used for Raman studies.

(ii) Rotating method.

Some compounds are very sensitive to the laser light and the temperature and get decomposed when laser beam falls on them. Some of the coloured samples absorb both the incident and scattered radiations. In such cases, the sample is prepared as a disc, which can be fitted in the rotating sample holder which gives a relative motion between the sample and the laser beam. The speed of rotation can be chosen according to the requirements.

2.3 INFRARED SPECTROPHOTOMETER - P.E.-580

The infrared spectra were recorded on the Perkin Elmer-580 spectrophotometer, having dry air purging system and polarizing assembly. It is a self recording, high performance, double beam, ratio recording machine with 'live' zero and single beam facility covering the range  $4000$  to  $180\text{ cm}^{-1}$ . All scan speeds, slit-widths and noise filtering are fully integrated in one control giving 31 combinations.

Four gratings (whose spectral ranges and grooves per cm are summarized in Table 2.1 are used, all in their first order. The gratings are mounted back-to-back, in pairs on two grating tables as shown in the optical diagram (Fig. 2.1).

Seven interference filters and one Yoshinaga transmission filter are used to cover the complete range of the instrument. The eight filters are mounted on a wheel. Automatically changes occur approximately at 2400, 1525, 1000, 690, 490, 370 and 250  $\text{cm}^{-1}$ . Additional filtering is provided over the range of the last grating by an additional scatter grating, which automatically substitutes for mirrors M(F)14 and M(F)15.

The best resolution conditions are selected for recording the spectra. The accuracy (0.5 to 1.5  $\text{cm}^{-1}$ ) of the frequency scale depends upon the frequency range with repeatability  $\pm 0.5 \text{ cm}^{-1}$  in the range 4000-2000  $\text{cm}^{-1}$  to 0.25  $\text{cm}^{-1}$  in the range 2000-180  $\text{cm}^{-1}$ .

An on-axis ellipsoid mirror M(E)18, and a CsI lens on the thermocouple (the detector) reduce the dimensions of the slit image falling on the target; a 1.4 mm x 0.45 mm strip of blackened gold leaf is welded to two pins. This produces a thermoelectric voltage representative of the intensity of the radiation.

For the calibration of the frequency scale, the spectrum of polystyrene was used.



## 2.4 LASER RAMAN SPECTROPHOTOMETER -SPEX 1403

The Raman data were obtained with a Spex model 1403 Ramalog spectrophotometer equipped with a 5 watt Spectra Physics model 165-09 argon ion laser operated at 514.5 nm on light control mode. Fig. 2.2 shows the optical diagram for the instrument.

The three phase 400 volts line voltage stabilized with the help of a EMS-10 (20 KVA) automatic voltage stabilizer to operate the laser through its 265 exciter run on three phase 203 volts, through a power transformer. The HX-500 chilling plant from Neslab was used to cool the laser and its power supply. The water temperature was maintained at 20°C. The chiller heat was dissipated by tap water. The maximum power obtainable at 514.5 nm near the output end was approximately 2 watt. The beam from the laser was passed onto the UVISIR illuminator through the laser-mate (a grating device to isolate background plasma lines before the radiation enters the Spex 1459 UVISIR illuminator) by a beam deflector attached to the output end of the laser tube. A low focal length fused silica condenser lens focusses the beam (of approximate diameter 1.5 mm) to a spot of 10 $\mu$ m in diameter at the focus of an elliptical collector mirror, which refocusses the scattered radiation onto the entrance slit of the 1403 monochromator. The scattered light falls (after passing through four slits, two gratings (1800 gr/mm) and five mirrors in the monochromator) into a thermoelectrically cooled C31034 photo-multiplier tube which was used as a detector. The signal was analysed by the Spex digital photon counting DPC-2

system fitted with a linear strip chart recorder coupled to the monochromator through a compudrive to record the spectra.

## 2.5 5 WATT ARGON ION LASER

The CW model 165 Ar<sup>+</sup> ion laser consists of a laser head which contains a rugged and trouble free plasma tube closed at each end by Brewster angle windows, a solenoid and an optical resonator. Dust particles on the windows which cause serious reduction in power are intercepted by bellows. The optical resonator is formed by a spherical reflector at the output end and a prism assisted with a flat mirror (to select wavelengths) at the back end. The tube is supported on a kinematically adjustable mount so that it may be positioned exactly on the mirror center line. External thumbwheel controls are provided for wavelength selection and changes of intra-cavity aperture. Table 2.2 summarizes the operating wavelengths ( $\lambda$ ) and available power.

The 265 Exciter contains all the necessary electronic-circuits to create, sustain and monitor the ion discharge in the plasma tube; to monitor and control the output power; and to supply and regulate the solenoid current of the 165 Ar<sup>+</sup> ion laser. The laser head and the 265 Exciter are cooled continuously by flow of chilled distilled water at constant temperature (20°C) supplied from the Neslab HX-500 chiller plant.

To get constant optical power, we operate in 'light control' mode(half an hour after starting the laser).

### 2.6.1 LOW TEMPERATURE CELL

Out of the numerous cells designed for absorption studies at liquid nitrogen (3-5) or liquid helium (6-12) temperatures, we have used the Specac variable temperature unit which works in the temperature range 83 K to 523 K on a Dewar principle utilising vacuum of 0.5 mm of Hg.

### 2.6.2 THE SPECAC LOW TEMPERATURE CELL

A line diagram of the cell is shown in Fig. 2.3. In this cell the top plate fits the top adaptor via O-ring of the vacuum tight jacket. The refrigerant chamber with sample cell holder, electrical connection leads, vacuum pump connection, copper constantan thermocouple are all conveniently arranged inside the jacket. The refrigerant chamber can be rotated for alignment in the optical beam. For convenience of location of the position of the cell in the optical path a pin is fixed in the top adaptor. The whole assembly is mounted in the spectrophotometer by means of a standard 3" x 2" plate.

The sample cell holder is fitted with two heaters (5 ohms each) in parallel, which enable us to maintain the temperature of the sample cell between 83 to 523 K; 83 K is obtained with liquid nitrogen. All temperatures above LNT are incrementally obtained with automatic control heater and mushroom arrangement, which is as given in Table 2.3. The mushroom and bung play a very important role in refrigerant chamber efficiency. To measure the temperature copper constantan thermocouple is used and desired temperature is obtained by its automatic control

unit. To minimize the fogging in outer windows, heaters are used to keep the windows warmer than the ambient temperature.

## 2.7 DE-HUMIDIFIER

The perchlorates are very hygroscopic in nature. To work in a moisture free atmosphere we installed a de-humidifier in our lab. (is shown in Fig. 2.4). This is an automatically regulated, dual tower desiccant type space de-humidifier. There exists an automatic (on-off) control of the machine according to the required level of humidity. The two heaters are on one side of the main body. Valve channels and two silica-jel packet plates are fixed on the top on the other end of the machine. Silica jel outlet plates are on the side-end and are used for the replacement of the gel. On the top of the body two small centrifugal blowers are mounted directly on motor shafts. Blower housing is connected with glass wool filters. The humid air from room is sucked out and dry air at room temperature is blown to the room till the humidity acquires a required level, set up in the control unit.

## 2.8 PREPARATION AND PURIFICATION OF PERCHLORATES

The perchlorates were prepared by the action of aqueous perchloric acid on the oxides of Zn and Hg, and carbonates of Mg, Co, Ni, Cd and Mn. They were repeatedly crystallized by slow evaporation at room temperature inside a desiccator containing concentrated sulphuric acid. To obtain the pure salt, every time, the solutions were prepared in distilled water. The perchlorate hexahydrate crystals grow in the form of long

the sample in D<sub>2</sub>O at room temperature. In the third stage D<sub>2</sub>O from the aqueous solution was transferred to the empty flask by a similar method, leaving the deuterated salt. The above process was repeated several times to get the deuterated sample .

## 2.10 RESOLUTION OF THE OVERLAPPING BANDS

Only few bands of interest appear as distinct isolated bands in the IR absorption spectra. Often the neighbouring bands overlap considerably. It was therefore necessary to resolve such spectra geometrically. This resolution depends on the knowledge of expected shapes of the components. In the condensed phase theoretical considerations justify the Lorentzian shape for the band contours (14). Gaussian curves are found to be good for the description of electronic absorption bands but not of IR bands (15). In fact, neither of these two functions is found to give a complete fit to the experimental curves and hence their Voigt like combinations (16) have been often used. However, in cases where the actual band-width is much larger than the instrumental slit-width, the Lorentzian shape alone gives a reasonably good fit, especially if one is not to go far into the tail of the band. This was the situation in the present case. Hence we used the Lorentzian analysis to analyse the complex structure in the overlapping regions by replotting the transmission spectra in linear absorbance scale and subtracting the contribution from the base line. A Lorentzian function is given as

$$I(\nu) = I(\nu_0) \frac{b^2}{b^2 + (\nu - \nu_0)^2}$$

Here  $\nu_0$  is the frequency at peak intensity  $I(\nu_0)$  and  $2b$  is the full band-width at half the maximum intensity, designated as  $\Delta\nu_{1/2}$ . Similarly the full band-width at  $\frac{1}{10}, \frac{2}{10}, \frac{3}{10}, \frac{4}{10}, \frac{5}{10}, \frac{6}{10}, \frac{7}{10}, \frac{8}{10}, \frac{9}{10}$  of the maximum intensity are  $6b, 4b, 3.06b, 2.44b, 2b, 1.64b, 1.30b, b, 0.66b$  respectively. Fig. 2.6 shows the significance of  $I(\nu_0)$  and  $b$ .

The product of  $I(\nu_0)$  and  $\Delta\nu_{1/2}$  is a measure of the intensity of a band, usually called integrated intensity. It is useful to evaluate the relative integrated intensities (RII) of different bands assigning  $\text{RII} = 100$  to one typical band or group within a spectrum. This procedure is adopted by us.

For the analysis of an overlapping band selection of a proper base line is essential. Two main considerations for this were the following : (a) the base should not touch the tails of a absorption profiles; margin should be left for absorption at the tails (b) selecting a base line with increasing absorption towards lower frequency region is to be avoided because if scattering is a contributor, it increases on the high frequency side and could tilt the base only in opposite sense. Having chosen a base and after accounting for it, the region to be analysed is replotted on a linear absorption scale. Analysis is now made starting with the more obvious components, affixing some  $I_0(\nu)$  and  $\Delta\nu_{1/2}$  parameter to them, obtaining the residues, proceeding to more bands and so on. Three main criteria are used in this analysis :

(a) We tried to search for the minimum number of Lorentzian components warranted by the observed contour. Minor residues

or deviations were not used to introduce bands with doubtful existence, since Lorentzian shape was only an approximation.

(b) In case of alternative analysis giving equally good fit, the one which maintained the peak positions nearer the observed hump was preferred.

(c) A component which was not obvious in the band contour by showing a hump or a clear shoulder was introduced only in those cases where repeated Lorentzian trials otherwise failed by wide margins and there were spectral evidences also for such a component.

The inaccuracies of the derived parameters vary from situation to situation. For frequencies the estimated error level is  $\pm 1 \text{ cm}^{-1}$  for sharp peaks to  $\pm 5 \text{ cm}^{-1}$  for broad but distinct bands and for the shoulders and  $\pm 10 \text{ cm}^{-1}$  for bulges and very weak evidences. For intensities the error level may be 5 to 10% in the case of envelopes with weak overlapping and 10 to 20% in the case of envelopes with strong overlappings.

REFERENCES

1. G. Duyckacrts, *Analyst.* 84, 201 (1959).
2. A.H. Pfund, *Phys. Rev.* 36, 71 (1930).
3. E.L. Wagner and D.F. Hornig, *J. Chem. Phys.* 18, 296 (1950).
4. H.T.J. Chilton, *Spectrochim. Acta* 16, 979 (1960).
5. M. Cadene and C. Deloupy, *J. Phys. Radium* 19, 506 (1958).
6. V. Roberts, *J. Sci. Instr.* 32, 294 (1955).
7. W.H. Durig and I.L. Mador, *Rev. Sci. Instr.*, 23, 421 (1952).
8. L.J. Schoen, L.E. Kuentzel and H.P. Broida, *Rev. Sci. Instr.* 29, 633 (1958).
9. L.F. Keyser and G.W. Robinson, *J. Chem. Phys.* 44, 3225 (1966).
10. F.R. Lipsett, *Rev. Sci. Instr.* 32, 840 (1961).
11. I.S. Pominov, N.N. Vlasov and G.I. Frolov, *Zh. Prikl. Spectrosk.* 4, 287 (1966), *J. Appl. Spectry.* 4, 210 (1966).
12. W. Weltner and D. Mileod, *J. Chem. Phys.* 45, 3096 (1966).
13. R. Dayal, Ph.D. Thesis, I.I.T., Kanpur (1977).
14. H.A. Lorentz, *Koninkl. Ned. Akad. Welenschap. Proc.* 8, 591 (1960).
15. A. Vitek, *Czeckoslov. Chem. Commun.* 39, 366 (1974).
16. W. Voigt, *Munch. Berg.* 1912, 603 (1912).



Table 2.1: The characteristic of gratings in P.E.-580

Grating No.	lines/cm	Range ( $\text{cm}^{-1}$ )	Range with late grating change ( $\text{cm}^{-1}$ )
1	2880	4000 - 1980	4000 - 1950
2	960	1980 - 630	1950 - 600
3	250	630 - 330	600 - 300
4	90	330 - 180	300 - 180

Table 2.2: The available  $\lambda(\text{nm})$  and power (mW) from 5 Watt  $\text{Ar}^+$  ion laser.

$\lambda(\text{nm})$	Power (mW)	$\lambda(\text{nm})$	Power (mW)	$\lambda(\text{nm})$	Power (mW)
1090*	50	496.5	700	465.8	200
528.7*	340	488.0	1500	457.9	350
514.5	2000	476.5	750	454.5*	120
501.7	400	472.7	300	457.7-514.5 (Multiline)	5000

\*require separate mirror.

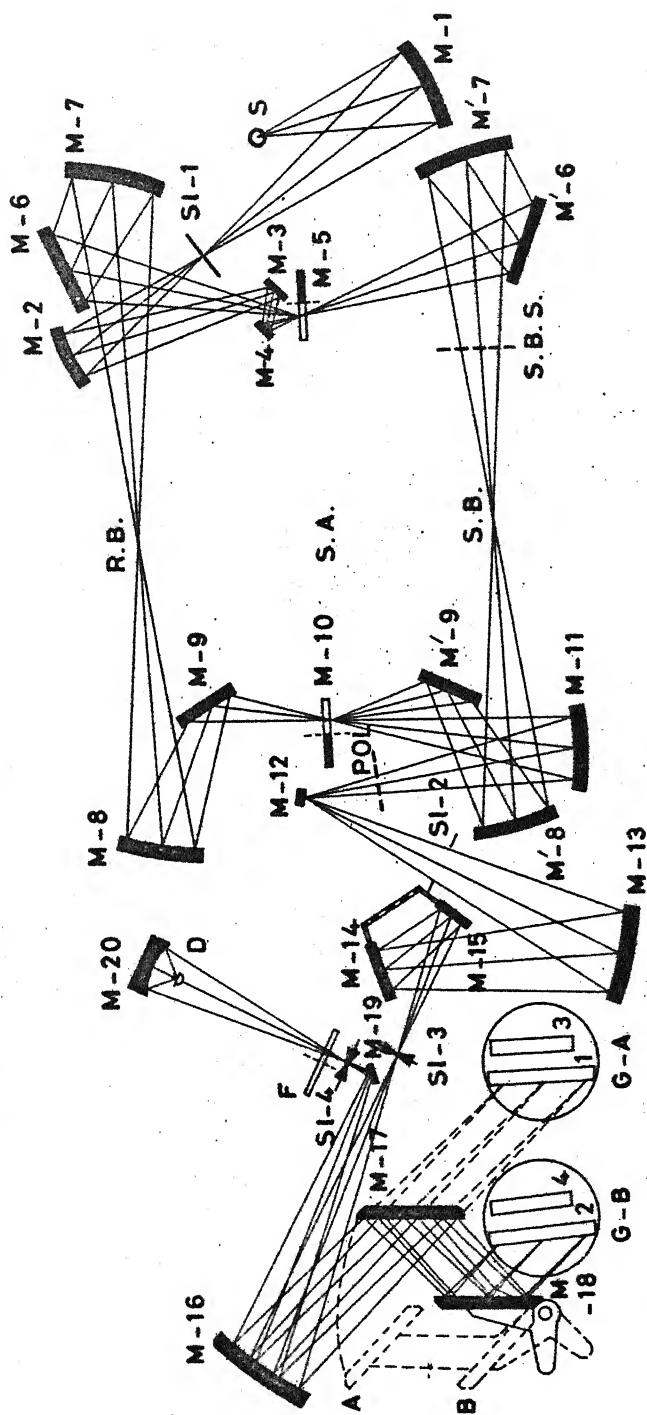
Table 2.3: Mushroom and coolant used for different temperature ranges.

Temperature range	Mushroom	Coolant
Ambient to $+250^{\circ}\text{C}$	None	None
$-100$ to $30^{\circ}\text{C}$	Large	Liquid $\text{N}_2$
$-190$ to $-80^{\circ}\text{C}$	Small	Liquid $\text{N}_2$
$-196$ (lowest) to $-180^{\circ}\text{C}$	None	Liquid $\text{N}_2$

FIGURE CAPTIONS

- Fig. 2.1 Optical diagram of Perkin-Elmer model-580 infrared spectrophotometer.
- Fig. 2.2 Optical diagram of Spectra Physics Laser and Ramalog 1403 spectrophotometer.
- Fig. 2.3 Specac variable temperature cell.
- Fig. 2.4 The De-humidifier machine installed outside the infrared lab.
- Fig. 2.5 Vacuum arrangement used to prepare deuterated analogues of hydrated samples.
- Fig. 2.6 Defining  $I_0$  and  $b$  of a Lorentzian absorption band.

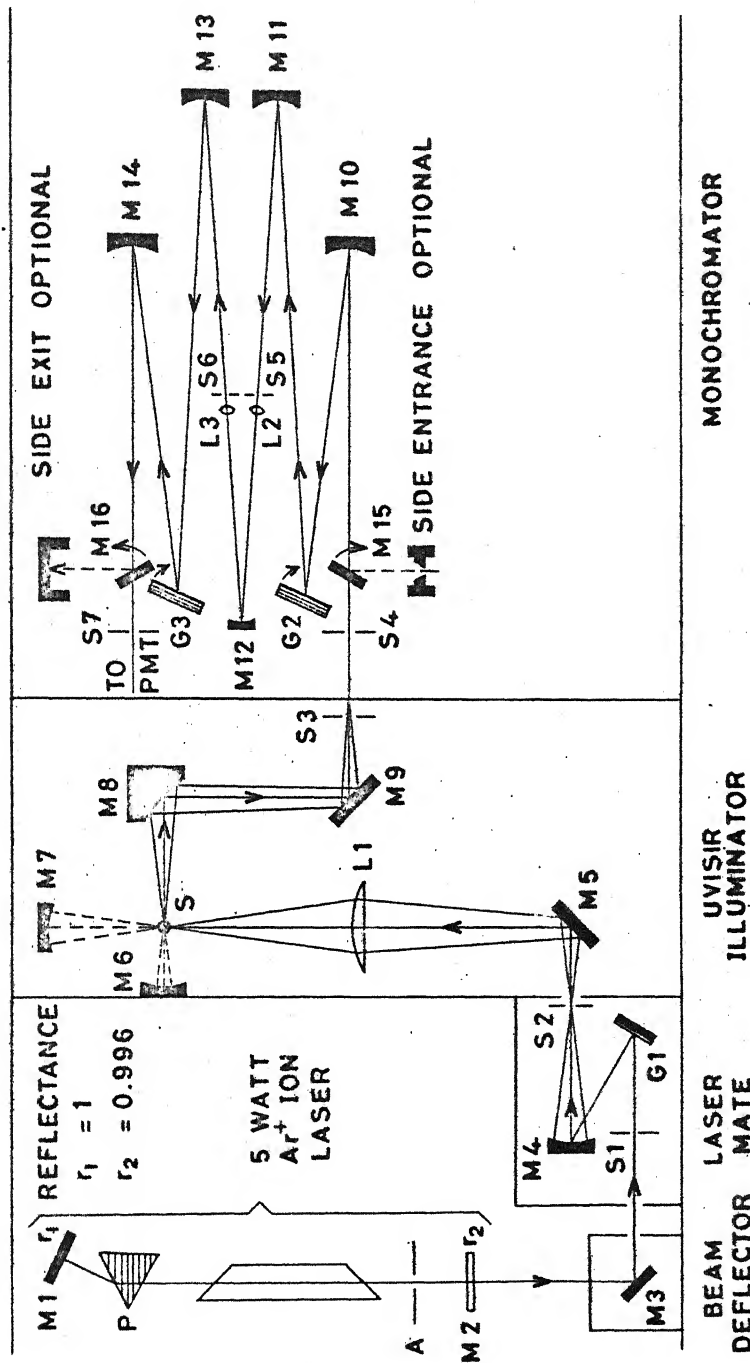
# OPTICAL DIAGRAM OF PERKIN-ELMER MODEL 580 INFRARED SPECTROPHOTOMETER



SOURCE (S); TOROID MIRRORS (M-1, M-2, M-4, M-7, M'-7, M-8, M'-8, M-11, M-12, M-13); CHOPPER MIRRORS (M-5, M-10); REFLECTING AND SCATTER GRATING SURFACE MIRRORS (M-3, M-6, M'-6, M-9, M'-9, M-14, M-15, M-17, M-18, M-19); PARABOLOID MIRROR (M-16); ELLIPSOID MIRROR (M-20); GRATING TABLES (G-A, G-B); BAFFLE AND SECONDARY SOURCE (SI-1); PUPIL BAFFLE (SI-2); ENTRANCE SLIT (SI-3); EXIT SLIT (SI-4); POLARIZER ALLEGORY (POL); OPTICAL FILTERS (F); DETECTOR (D); SAMPLE BEAM SHUTTER (S.B.S.); SAMPLE BEAM (S.B.) SAMPLE AREA (S.A.); REFERENCE BEAM (R.B.).

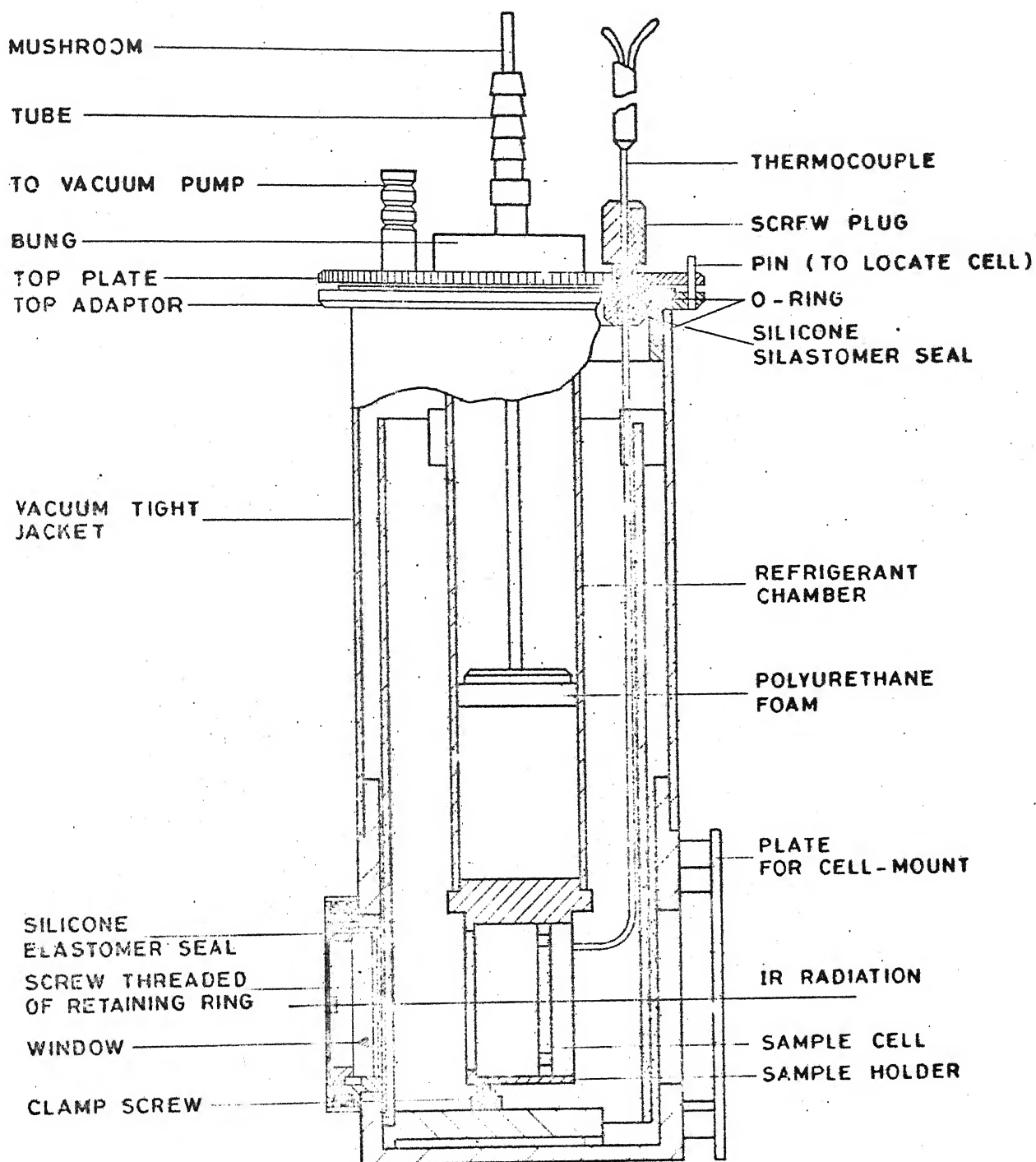
FIG. 2.1

# OPTICAL DIAGRAM OF SPECTRA PHYSICS LASER AND RAMALOG 1403 SPECTROMETER



PRISM (P); APERTURE (A); PLANE MIRRORS (M1, M2, M3, M5, M9, M15, M16); CONCAVE MIRRORS (M4, M6, M7, M10, M11, M12, M13, M14); ELLIPTICAL COLLECTOR MIRROR (M8); SLITS (S1, S2, S3, S4, S5, S6, S7); PLANE GRATINGS (G1, G2, G3); FUSED SILICA CONDENSER LENS (L1); SAMPLE (S), OPTICAL FILTERS (L2, L3); PHOTO MULTIPLIER TUBE (PMT).

FIG. 2.2.



SPECAC VARIABLE TEMPERATURE CELL

FIG. 2.3

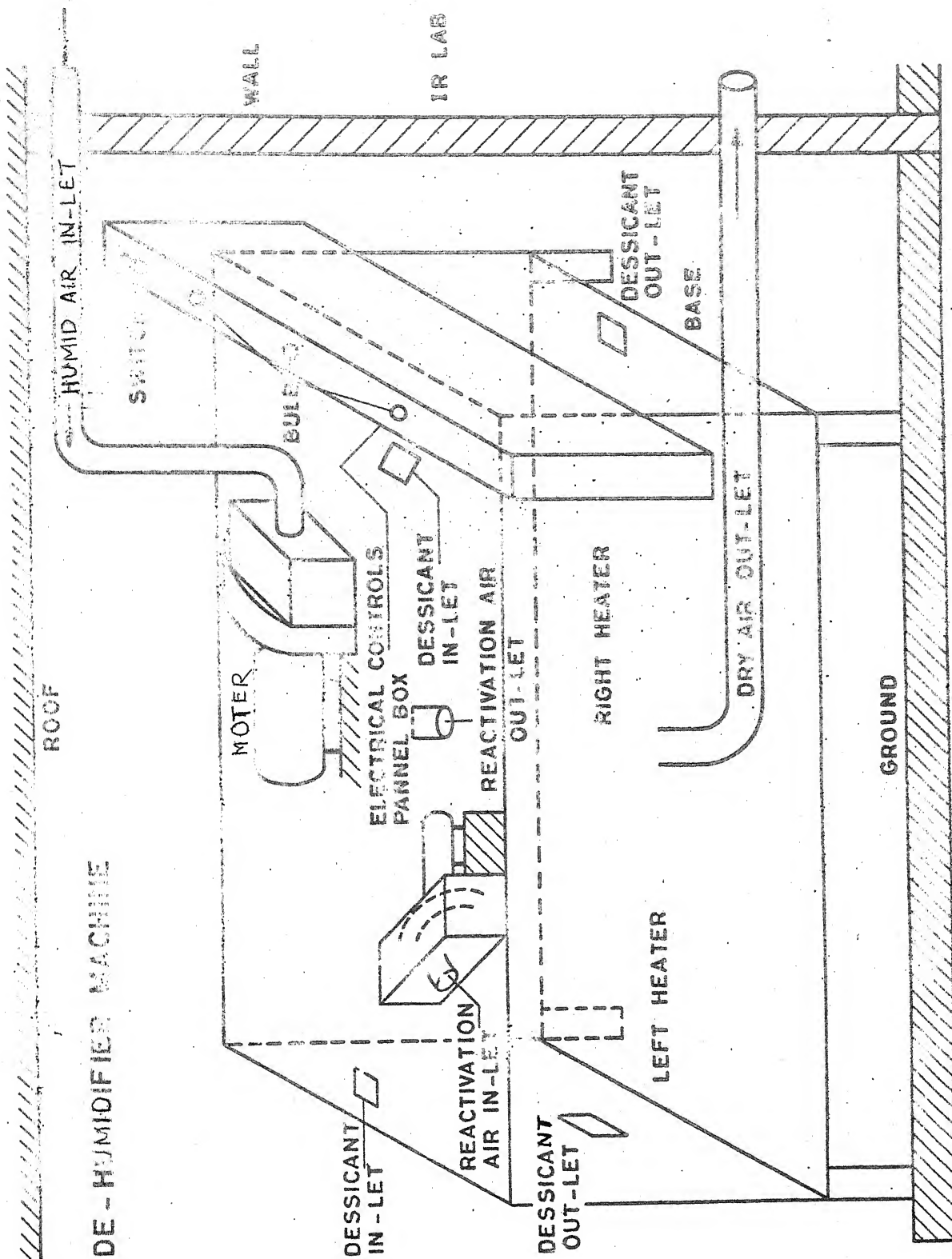


FIG. 2.4

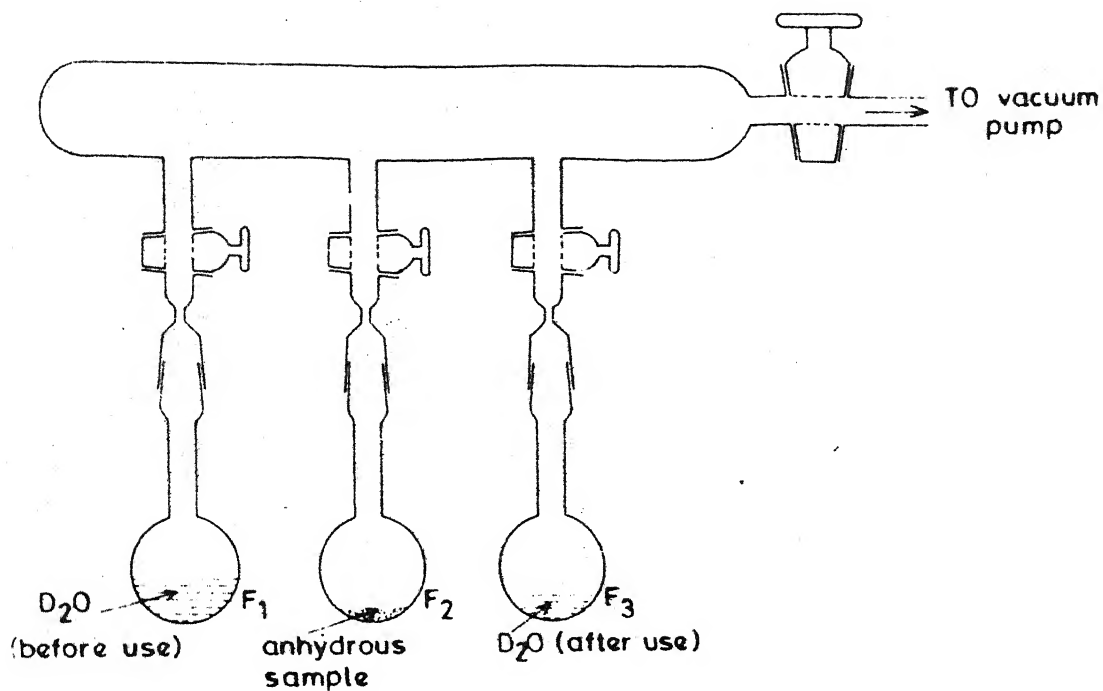


FIG. 2.5

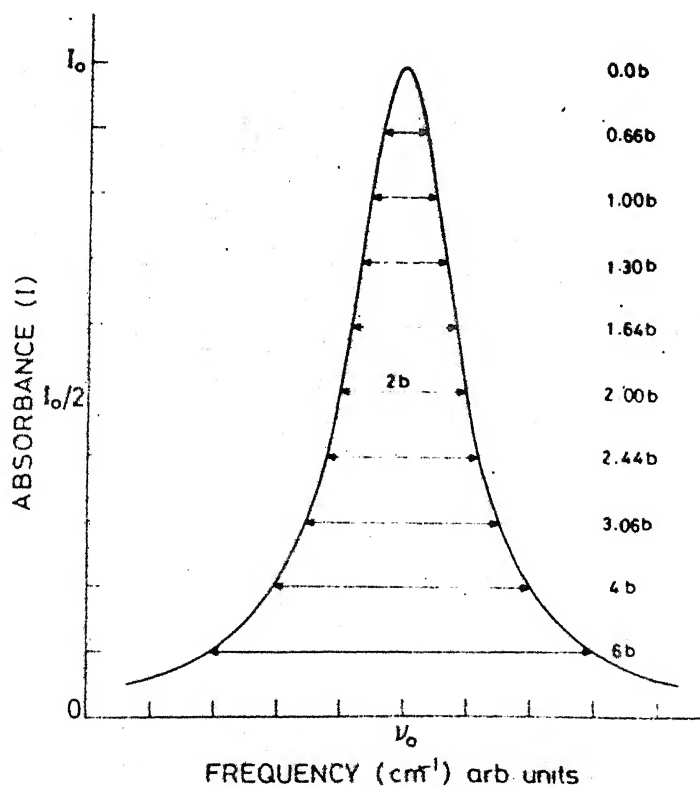


FIG. 2.6

### CHAPTER III

## VIBRATIONAL STUDIES AND PHASE TRANSITIONS IN MAGNESIUM AND NICKEL PERCHLORATE HEXAHYDRATES\*

### ABSTRACT

The observed intensity ratio of  $\nu_3$  and  $\nu_1$  modes and typical  $\nu_3 - \nu_1$  separation are attributed to lowering of symmetry, anharmonic effects and M-O<sub>w</sub> coordination. The planar rocking mode of water couples with its in-plane bending mode  $\nu_2$  to give a combination band and a weak resonance interaction exists between  $2\nu_2$  and  $\nu_1$ . The frequency of the rocking mode of water increases with hydrogen bonding while that of wagging mode increases with M-O<sub>w</sub> coordination.

The temperature evaluation of IR spectra confirms phase transitions at 110, 193 and 335 K in magnesium perchlorate hexahydrate (MPH) and at 223, 311 and 355 K in nickel perchlorate hexahydrate (NPH) and suggests new phase transitions at 225, 370 and 450 K in MPH and at 180 K in NPH. The transitions at 225 and 193 K in MPH & at 223 and 180 K in NPH are triggered by the tumbling motion of metal aquo-complex, while the transitions at 335, 370 and 450 K in MPH & at 311 and 355 in NPH arise due to reorientational motion of water molecule. The transition at 110 K in MPH is associated with positional ordering of hydrogen atoms. The space group below 225 K in MPH and 223 K in NPH is suggested to be C<sub>s</sub><sup>2</sup>.

---

\*Papers based on this study have appeared in

- (I) M.B. Patel and H.D. Bist, J. de. Physique C6, 917 (1981).
- (II) M.B. Patel and H.D. Bist, Appl. Spectros. 36, 185 (1982).



### 3.1 INTRODUCTION

Infrared (IR) survey of magnesium perchlorate hexahydrate (MPH) in  $600\text{--}4000\text{ cm}^{-1}$  region was reported by Miller et al (1) who suggested that the near free state value of OH stretching frequency is due to weak hydrogen bonding in this salt. Likewise Ross (2) and Hathaway et al (3) have reported the fundamental vibrations of perchlorate group. Ross (2) has further suggested that observed splitting in the  $\nu_3(p)$  and  $\nu_4(p)$  bands of perchlorate are due to distortion of  $\text{ClO}_4^-$  tetrahedron in MPH and nickel perchlorate hexahydrate (NPH) in the crystal lattice. Sartorelli et al (4) have observed phase transition in NPH by EPR supported by IR studies, where the doublet band corresponding to  $\nu_4(p)$  at room temperature (RT) becomes triplet at low temperature (LT). This difference in the IR spectra was qualitatively explained due to a change in symmetry at the  $\text{ClO}_4^-$  site and/or due to normal larger band-width at higher temperature (HT). Weil et al (5) have suggested that MPH crystal is hexagonal and the splitting in  $\nu_3(p)$  of  $\text{ClO}_4^-$  ion increases with the size of cation. Recently Janik et al (6) studied half-widths of 465 and  $630\text{ cm}^{-1}$  bands with temperature and confirmed the high temperature (HT) phase transitions previously discovered at 325 and 361 K for MPH and NPH, respectively. Other reported phase transitions in MPH and NPH by different techniques are presented in Table 3.1. The remarks made by different authors, however, differ from one another for the same phase transition. To correlate the structures and the nature of phase transition, we have undertaken a systematic IR study of the aforesaid hydrates along with a

detailed analysis of vibrational bands. The magnitude of distortion, effect of mechanical and electrical anharmonicities (6a), origin of splittings and coupling effects have also been discussed. The study also includes Fermi resonance between  $\nu_1$  and  $2\nu_2$  of water, the correlations between rocking mode frequency ( $\nu_R$ ) and mean OH stretch frequency ( $\nu_{OH}$ ), and wagging mode ( $\nu_W$ ) and metal oxygen (M-O<sub>W</sub>) vibration of  $M(OH_2)_6$  aquo-complex (i.e.  $\nu_6(c)$ ) and calculation of the force constants for displacement of H and O atoms during rocking (R), wagging (W) and twisting (T) motions.

### 3.2 RESULTS AND DISCUSSIONS

#### 3.2.1 INTERNAL VIBRATIONS OF WATER

##### (a) The Hydrate and the Deuterate

The IR spectra of MPH and NPH in the OH stretching region ( $4000-2800\text{ cm}^{-1}$ ) at LT, RT and HT are shown in Fig. 3.1. At RT the  $\nu_1$  and  $\nu_3$  bands of water are superimposed on one another to give a single broad band centered around  $3420$  and  $3405\text{ cm}^{-1}$  for MPH and NPH, respectively. The curves B and D are retraced on absorption scale by subtracting the contribution due to baseline shift, along with the bending mode of water as shown in Figs. 3.2 and 3.3, respectively for MPH and NPH. The  $\nu_1$ ,  $\nu_3$  and several other weaker band contours are analysed fitting the Lorentzian shapes (7) to these components. The resolved bands are shown by dotted curves. The analysed band contours in the region  $2950-2300\text{ cm}^{-1}$  are shown in Figs. 3.4 (A) and 3.5 (A) and in the region  $1700-900\text{ cm}^{-1}$  for MPH and  $1750-850\text{ cm}^{-1}$  for

NPH are shown in Figs. 3.4 (B) and 3.5 (B) respectively for deuterated samples. The Raman spectra of MPH (I) and NPH (II) have been recorded at RT (cf. Fig. 3.6). The absorption frequencies and their assignments along with half-widths and relative intensities are presented in Tables 3.2 and 3.3.

The available structural information (given in section 1.4.3 (a)) on MPH and NPH implies that the two hexahydrates are similar. The structures of the two hydrates are identical is further corroborated by striking similarities between their spectra. The discrete structure and low half-widths of bands indicate that both the hydrates have ordered structures, since disordered crystal spectra are expected to consist of broad bands (8).

(b) Stretching Region

(i) Assignments of bands and determination of magnitude of distortion

The assignments of observed bands in hydrates for  $\nu_1$  and  $\nu_3$  are consistent with the empirical relation (9,10)

$$(3657 - \nu_1) = 0.8333 (3756 - \nu_3) \quad \dots\dots 1)$$

for the shifts found between these bands in symmetrically bound  $H_2O$  molecules; where 3657 and 3756 are  $\nu_1$  and  $\nu_3$  frequencies in the gaseous state of water. The isotopic shifts support the criterion for the assignments as  $\nu_H/\nu_D$  is 1.34. The translatory lattice mode  $\nu_6(c)$  of aquo-complex in the crystal is observed in Far-IR at  $137\text{ cm}^{-1}$  (section 3.2.4) for MPH and is expected

around  $134 \text{ cm}^{-1}$  for NPH in analogy with MPH (11).

The uncoupled doublet of OH (eg.  $3436$  and  $3407 \text{ cm}^{-1}$  for MPH) and OD ( $2550$  and  $2535 \text{ cm}^{-1}$  for MPH) stretching bands indicate that the water molecules in the crystals are distorted from  $C_{2v}$  to  $C_s$  symmetry due to non-equivalent hydrogen bonding (12,13). The magnitude of distortion 'd' is computed from the relation (12)

$$d = \frac{\Delta\nu_{3,1}(C_s) + \Delta\nu_{ui,uj}}{2\Delta\nu_{3,1}(C_s)}$$

where  $\Delta\nu_{3,1}(C_s) = \nu_3 - \nu_1$ , the observed frequency difference and  $\Delta\nu_{ui,uj} = \nu_{ui} - \nu_{uj}$ ,  $ui$  and  $uj$  have been used to denote uncoupled mode of two non-equivalent  $i$  and  $j$  OH oscillators. The values for  $d$  parameter for MPH and NPH are presented in Table 3.4(a) for both  $H_2O$  and  $D_2O$  substitutions. ' $d = 0.701$ ' indicates that 70.1 percent of  $\nu_1(C_s)$  and  $\nu_3(C_s)$  vibrations are localized in individual OH bond vibrations. In the limit of infinite distortion,  $\nu_1(C_s)$  and  $\nu_3(C_s)$  frequencies are those of the individual bond oscillators of the molecule.

(ii) Mechanical and electrical anharmonicities of  $\nu_3$  and  $\nu_1$  modes.

The observed intensity ratio of  $\nu_3$  and  $\nu_1$  bands is  $I(\nu_3)/I(\nu_1) = 1.53$  in MPH and magnesium perchlorate partially deuterated (MPD) and 1.50 for NPH and nickel perchlorate partially deuterated (NPD) as given in Table 3.4(b). Secroun et al (14) have given relations for intensities of fundamental bands of a triatomic molecule having  $C_{2v}$  symmetry. If a simple point charge model for  $H_2O$  is taken and only the mechanical

motions of atoms are considered, these relations lead to

$$I(\nu_3)/I(\nu_1) = \tan^2 \theta \quad \dots\dots 3)$$

where  $\theta$  is the semiband angle of  $H_2O$  in the hydrate. The reported (15) value of  $\theta$  in  $LiClO_4 \cdot 3H_2O$  is  $51.25^\circ$ . Using the same value of  $\theta$  for MPH and NPH (16) the ratio comes out to be 1.57 (cf. Table 3.4(b)). The small difference in the observed value of the intensity ratio may be attributed to the loss of  $C_{2v}$  symmetry of  $H_2O$  due to distortion. If this is the only factor affecting the intensity ratio, we would have  $I(\nu_3)/I(\nu_1)$  for NPH greater than that of MPH, since the distortion in MPH is larger than in NPH.

This discrepancy can be explained by considering mechanical and electrical anharmonicities, which also govern the intensity ratio. The halfwidths of  $\nu_3$  in both the hydrates are quite large ( $\sim 107 \text{ cm}^{-1}$ ) as compared to  $\nu_1$  ( $67 \text{ cm}^{-1}$  cf. Table 3.2) indicating that  $\nu_3$  is mechanically more anharmonic than  $\nu_1$ . Thus one would expect to have intensity ratio greater than 1.57. This ratio is expected to be more for MPH than NPH since the ratio of half-widths between  $\nu_3$  and  $\nu_1$  is larger in MPH than in NPH. Secondly the electrical anharmonicity is also associated with an asymmetric variation of the effective charges with the mechanical motion of :

- (I) the proton along the hydrogen bond and
- (II) water oxygen ( $O_w$ ) along the metal-oxygen bond.

The first factor cancels out the oscillating dipole for the asymmetric  $\nu_3$  mode but adds up for  $\nu_1$  mode. The  $\nu_1$  mode oscillating dipole is directed along  $M-O_w$  bond which is also the

symmetry axis. Hence, the displacements of  $O_w$  in this mode affects asymmetrically the overlapping of electron clouds. Consequently, the effective oscillating dipole will be large. However, in  $\nu_3$  mode the displacements are perpendicular to  $M-O_w$  bond and hence the variations in the effective charge are symmetric and small. Thus the electrical anharmonicity for the  $\nu_3$  mode is small as compared to  $\nu_1$  (6a). Therefore, the observed lower value of intensity ratio compared to theoretical value could be due to the resultant effect of distortion and mechanical and electrical anharmonicities.

(iii) The mean  $\nu_{OH}$  stretching and  $\Delta\nu_{3,1}$  splitting

The observed splitting  $\Delta\nu_{3,1} = (\nu_3 - \nu_1)$  for  $H_2O$  molecules in MPH and NPH are 72 and 77  $cm^{-1}$  respectively. These values are small compared with 99.14  $cm^{-1}$  in the vapour phase (17). Saumagne et al (18) have pointed out that  $\Delta\nu_{3,1}$  decreases with decreasing OH frequency for dilute solutions of  $H_2O$  in a series of inert solvents. The observed splittings by various scientists (12,17-21,29) as listed in Table 3.5 have been plotted against  $\nu_{OH}$  in Fig. 3.7. Several observed values by us (for MPH and NPH) and others do not lie on the straight line of Fig. 3.7. Some reasons suggested for this discrepancy are :

(I) A change in the geometry of water from its  $C_{2v}$  symmetry increases  $\Delta\nu_{3,1}$ .

(II) If a cation forms a bond with the oxygen of water molecule, one of the observed effects would be a decrease in the  $\Delta\nu_{3,1}$  splitting. This has also been shown theoretically by Sartori et

The increase in  $\Delta\nu_{3,1}$  due to distortion of the molecule is obtained from the following relation (12)

$$\Delta\nu_{3,1} = [(\Delta\nu_{u3,u1})^2 + (\Delta\nu_{3,1}(C_{2v}))^2]^{\frac{1}{2}} \dots\dots 4)$$

where  $\Delta\nu_{3,1} (= \nu_3 - \nu_1)$  is the observed frequency difference.  $\Delta\nu_{u3,u1} (= \nu_{u3} - \nu_{u1}$ ; u representing the uncoupled vibration) is the uncoupled splitting separation. This has been obtained by partial deuteration technique.  $\Delta\nu_{3,1}(C_{2v})$  is the hypothetical value for undistorted water (assuming  $C_{2v}$  symmetry) which should fall on the straight line between  $\Delta\nu_{3,1}$  and the mean  $\nu_{OH}$ .

Taking  $\Delta\nu_{u3,u1}$  same for both hydrate and deuterate (cf. Table 3.7) in Eq. 4) we obtained  $\Delta\nu_{3,1}(C_{2v})$  as 26.4 and 32.1  $\text{cm}^{-1}$  for MPH and NPH, respectively, which fall below the straight line by 25.6 and 16.5  $\text{cm}^{-1}$ . If distortion alone were responsible for the observed  $\Delta\nu_{3,1}$ , the calculated value according to Eq. 4) should have fallen on the straight line. This indicates that other factors are also responsible along with the distortion. This view is further supported by the fact that observed  $\Delta\nu_{3,1}$  in MPH is less than NPH though the distortion is more in MPH than NPH. The  $M-O_w$  interaction seems to be responsible for this discrepancy. The effect of  $M-O_w$  has been discussed and analysed by Sartori et al (22,23) who showed that  $\Delta\nu_{3,1}$  splitting of  $H_2O$  decreases in presence of a cation. The cationic effect is expected to be stronger in MPH than that in NPH on account of the stronger  $M-O_w$  bond in the former compound (section 2.2.3(b)). When these factors are taken into account, the  $\Delta\nu_{3,1}$  is expected to fall on the straight line. However, such calculations have not been made. On the other hand, from

the general expression for this splitting (12)

$$\Delta\nu_{3,1} = 0.172 \bar{\nu}_{\text{OH}} - 539.7 \quad \dots \quad 5)$$

the calculated values fall on the straight line.

(c) Bending Region

(i) Hydrogen bonding and M-O<sub>w</sub> coordination

The bending mode observed as a singlet in both the hydrates and their deuterated and partially deuterated analogues indicate that all the twelve water molecules in the unit cell are equivalent, which is in agreement with the X-ray data (24). The frequency of bending mode in MPH is higher than in NPH, though the hydrogen bonding in NPH is stronger than in MPH as inferred from OH-stretching region. The hydrogen bonds involving water hydrogen increase the bending frequency (15,22) with enhanced hydrogen bonding. The higher bending frequency in MPH can be explained by taking into account the stronger cation water interaction in the sample which also increases the bending frequency (15,22). This view point is further supported by our observed M-O<sub>w</sub> vibration (i.e.  $\nu_6(c)$ ) of the aquo-complex value which is on higher frequency side for MPH than NPH (section 3.2.3(b)).

(ii) Mechanical and electrical anharmonicities of  $\nu_2$

The overtone  $2\nu_2$  of bending mode appears as a sharp band in H<sub>2</sub>O, HOD and D<sub>2</sub>O in crystal hydrates. The values of the mechanical anharmonicities ( $W_e X_e$ ) and the fundamental frequencies ( $W_e$ ) of bending mode can be computed from the observed



values of  $\nu_2$ ,  $2\nu_2$  under simple diatomic approximation using the relation :

$$G(v) = (v + \frac{1}{2})W_e - (v + \frac{1}{2})^2 W_e X_e$$

In the above relation the coupling of modes has justifiably been neglected. The calculated values of  $W_e X_e$  and  $W_e$  are shown in Table 3.6(b). From the data in Table 3.2, 3.3, 3.6(a) and 3.6(b) the cubic potential constant ( $K_3$ ) and the dipole coefficient ratio ( $\mu_2/\mu_1$ ) can be deduced (26,27) by using the relations given in section 1.7. The calculated values are also presented in Table 3.6(b).

A comparison of the mechanical anharmonicities  $W_e X_e$  of these hydrates and analogous deuterates for the bending mode can be made with the corresponding vapour phase values of  $H_2O$ ,  $HOD$  and  $D_2O$  which are 17, 11 and  $9\text{ cm}^{-1}$ , respectively (28). These values show that binding in the lattice has made these vibrational modes mechanically more harmonic (except probably for  $D_2O$ ) (6a). This might be due to Fermi resonance (18) between  $\nu_1$  and  $2\nu_2$  bands in the crystal hydrates. Similarly, the larger values of  $I(2\nu_2/I\nu_2)$  and  $\mu_2/\mu_1$  as shown in Table 3.6(a) and 3.6(b), respectively] for  $D_2O$  compared with that for  $HOD$  supports the assumption of Fermi resonance between  $\nu_1$  and  $2\nu_2$  modes. The Fermi resonance between  $\nu_1$  and  $2\nu_2$  in NPH is stronger than in MPH.

#### (d) Fermi Resonance

The resonance interaction between  $\nu_1$  and  $2\nu_2$  modes separated by about  $145\text{ cm}^{-1}$  seems to be weak as is apparent from the

following arguments :

- (I) The intensity of  $2\nu_2$  is expected to increase at the expense of  $\nu_1$  as resonance interaction between them increases. The intensities of  $2\nu_2$  is very *low* relative to that of  $\nu_1$  band.
- (II) Appearance of  $2\nu_2$  band of HOD indicates that the total intensity of  $2\nu_2$  bands of  $\text{H}_2\text{O}$  and  $\text{D}_2\text{O}$  are not only due to Fermi resonance, but also due to electrical anharmonicity which is large as indicated by large value of  $\mu_2/\mu_1$  [Table 3.6(b)].
- (III) The fact that  $2\nu_2$  bands are not observed in Raman (cf. Fig. 3.6) also argues in favour of weak resonance interaction since strong interaction would lead to enhanced Raman intensity for the  $2\nu_2$  peaks.

The observed anharmonicities, however, suggest that a finite Fermi interaction is present. The Fermi interaction parameter  $\Omega$  has been calculated from the relation (30) :

$$\begin{aligned}\Omega &= \langle v_1, v_2, v_3 | H'/hc | v_1-1, v_2+2, v_3 \rangle \\ &= \frac{K_3}{2} \left[ -\frac{v_1}{2} (v_2+1)(v_2+2) \right]\end{aligned}$$

where  $v_1$ ,  $v_2$  and  $v_3$  are the vibrational quantum numbers of the fundamental,  $H'/hc$  is the anharmonic term in the Hamiltonian and  $K_3$  is the cubic force constant in dimensionless normal coordinate space. The resonance between  $\nu_1$  and  $2\nu_2$  requires that  $v_1 = 1$ ,  $v_2 = v_3 = 0$ , where the above equation reduces to

$$\Omega = K_3/2$$

Thus, the interaction constant can be obtained from  $K_3$  and then the unperturbed separation  $\Delta_0$  of the Fermi doublet from the relation

$$\Delta_0 = (\Delta^2 - 4\Omega^2)^{1/2}$$

where  $\Delta$  is observed separation of perturbed level of the Fermi doublet. The method of successive approximation has been applied to obtain consistent values for  $\Omega$ ,  $\Delta_0$ ,  $W_e$ ,  $W_e^X$ ,  $K_3$  and  $\nu_1/\nu_2$ . These values are also presented in Table 3.6(b).

As hydrogen bonding increases in hydrates (and/or with an increased cation effect)  $\nu_1$  is expected to fall (22,23,27) while  $2\nu_2$  is expected to increase in frequency resulting in a decrease in the difference  $\nu_1 - 2\nu_2$ . This prediction holds good in the present case.

### 3.2.2 UNCOUPLED VIBRATIONS OF HOD AND D<sub>2</sub>O

Fig. 3.8 shows the IR spectra of partially deuterated (D) MPH samples containing different percentages of H<sub>2</sub>O, HOD and D<sub>2</sub>O at 300 K and 93 K in the region 2900-2340 cm<sup>-1</sup> and 1710-1100 cm<sup>-1</sup>. At 300 K the peak positions in the OD stretching region are not clearly distinguishable, however, at 93 K they are well resolved. The influence of temperature on band intensities is seen by comparing the spectra at 300 K and 93 K. The D-spectra of NPH are not shown, which are similar to those of D-spectra of MPH. The spectra in the OH stretching region of D-samples remain almost similar to those in the normal hydrate (Fig. 3.1) at 300 K and 93 K for both the compounds. The bending mode remains single both at 300 K and 93 K in the samples with different percentages of D. Its band position changes slightly with the percentage of D.

In 5% D-sample there is a single band in OD stretching region at 300 K, which splits into four at 93 K as shown in Fig. 3.8(E,F). There is also a change in the band positions with D-percentage as seen from the comparison of the band position

of HOD and D<sub>2</sub>O (cf. Tables 3.2, 3.3 and 3.7). The splitting in 5% D-sample cannot arise due to double minimum potential for hydrogen motion, because the bands do not show the temperature effect on their intensities (31). In 5% D-sample, the percentages of H<sub>2</sub>O, HOD and D<sub>2</sub>O are 90, 9 and 1, respectively obtained by considering intensity of bending and stretching modes of H<sub>2</sub>O, HOD and D<sub>2</sub>O. There are twelve water molecules in each unit cell (24). The presence of one HOD surrounded by eleven H<sub>2</sub>O is a good representation for an uncoupled environment. Therefore, out of the four bands two of them, which are strong, are assigned to the uncoupled OD stretching modes of HOD (9%) and the rest two are assigned to the uncoupled  $\nu_3$  and  $\nu_1$  bands of D<sub>2</sub>O (1%). The two uncoupled OD doublets of HOD arise due to different environments for each OD in the hydrates. The corresponding uncoupled bending modes of HOD and D<sub>2</sub>O are also presented in Table 3.7. There is no evident change in position of uncoupled bands of D<sub>2</sub>O and HOD with an increase in the percentage of D. This indicates that the intermolecular coupling is weak. The uncoupled bands of H<sub>2</sub>O cannot be obtained because of experimental difficulties in preparing 95% D-samples.

### 3.2.3 INTERNAL MODES OF PERCHLORATE AND LIBRATIONAL AND TRANSLATIONAL MODES OF WATER

The IR spectra of MPH and NPH have been recorded at LT, RT and HT in the regions 250-1350 cm<sup>-1</sup> and are reproduced in Figs. 3.9(I) and 3.9(II), respectively. The observed bands are presented in Table 3.8 along with the bands observed in Raman at RT (cf. Fig. 3.6). The peak intensities of some of the

observed bands in the IR spectra are extraordinarily thermosensitive. Thus, the bands can be classified into two major groups:

- (a) the internal modes of perchlorate and
- (b) the librational and translational modes of water.

The IR spectra of MPH is plotted again on the absorbance scale (cf. Fig. 3.10). The curves A, B correspond to the curves A, B of Fig. 3.9(I) and A', B' are the corresponding curves for the D-samples. The spectra of NPH have not been replotted on absorbance scale. The temperature variation study of D-sample was performed and the data are given in Table 3.9.

#### (a) Perchlorate Vibrational Modes

The assignments of  $\text{ClO}_4^-$  vibrational modes are given in Table 3.8. The criteria for assignments are :

(I) The free  $\text{ClO}_4^-$  ion belong to point group  $T_d$  for which one expects four fundamental vibrations, all of which are Raman active and only two of them are IR active. The four bands falling around 1100, 940, 630 and 460  $\text{cm}^{-1}$  are  $\nu_3(p)$ ,  $\nu_1(p)$ ,  $\nu_4(p)$  and  $\nu_2(p)$  respectively and are well known from solution Raman spectra (25,32). Therefore, the observed four bands in Raman in the same region are assigned accordingly. Similarly in IR two strong bands are assigned to  $\nu_3(p)$  and  $\nu_4(p)$  and the other two weaker bands to  $\nu_1(p)$  and  $\nu_2(p)$  (Table 3.8) allowed due to factor group selection rules (section 1.5(a)).

(II) The fundamental vibrations of  $\text{ClO}_4^-$  ion in Raman are expected to be much stronger than the librational modes of water.

(III) These bands do not show any shift and remain unaffected on deuteration and on changing the temperature. At RT the triplet

splitting of  $\nu_3(p)$  in IR both for MPH and NPH shows the operation of the factor group selection rules. It could qualitatively be argued that the  $\text{ClO}_4^-$  ion is distorted to  $C_{2v}$  symmetry in the lattice. This is in agreement with the earlier observation (2,24).

(b) The Librational and Translational Modes of Water

The rest of the observed bands, which show D shift and whose peak intensities are strongly affected with the temperature, are assigned as the bands arising due to water molecules in the crystal. The assignments of these bands are presented in Table 3.9 both for MPH and NPH respectively at RT and LT along with the bands in D-sample. The assignments are based on the following criteria :

- (I) the intensity;  $I_W > I_R > I_T$  (33),
- (II) general observed frequency sequence;  $\nu_R > \nu_W > \nu_T$  (33),
- (III) frequency shift on deuteration;  $(\nu_{\text{H}_2\text{O}}/\nu_{\text{HOD}})_R = 1.21$ ,  
 $(\nu_{\text{H}_2\text{O}}/\nu_{\text{HOD}})_W = 1.09$ ,  $(\nu_{\text{H}_2\text{O}}/\nu_{\text{HCD}})_T = 1.22$ ,  
 $(\nu_{\text{H}_2\text{O}}/\nu_{\text{D}_2\text{O}})_R = 1.39$ ,  $(\nu_{\text{H}_2\text{O}}/\nu_{\text{D}_2\text{O}})_W = 1.34$  and  
 $(\nu_{\text{H}_2\text{O}}/\nu_{\text{D}_2\text{O}})_T = 1.41$  (33),
- (IV) observation of a combination band of the bending and rocking mode (33),
- (V) nature of band shape and its behaviour with temperature.

The observed R, W and T positions of water in hydrates and D-samples differed slightly (1 to 7  $\text{cm}^{-1}$ ) at LT. Such shifts are expected due to dynamic splitting of these modes. However, due to small magnitude of the shifts, much significance cannot be attached to these observations.

Comparison of the frequencies of librational modes of MPH and NPH with stretching modes shows that  $\nu_R$  increases with strength of hydrogen bond (whereas  $\nu_{OH}$  decreases (34)). The  $\nu_W$  mode is almost independent of hydrogen bonding. The latter, however, increases linearly with M-O<sub>w</sub> vibration  $\nu_6(c)$  (35). The M-O<sub>w</sub> vibrations (i.e. translational modes of H<sub>2</sub>O) are assigned on the basis of their shift in D-sample and expected positions of these modes studied earlier (11,36) in the transition metal aquo-complexes taking M(OH<sub>2</sub>)<sub>6</sub> complex as a single unit with point group O<sub>h</sub>.

Jain (37) used the relations given by Blue (38) for calculating the force constants assuming a harmonic vibrator. Introducing several simplifications, Jain deduced the following relations :

$$K_H = 0.118 \times 10^{-5} (\nu_T)^2$$

$$K_H = 0.133 \times 10^{-5} (\nu_W)^2 - 0.0078 K_O$$

$$K'_H = 0.123 \times 10^{-5} (\nu_R)^2 - 0.0025 K'_O$$

where  $K_H$  and  $K_O$  are potential constants (m dyne/A<sup>0</sup>) coming into force against the displacement of H and O atoms respectively, when the molecule librates about a-axis.  $K'_H$  and  $K'_O$  are similar constants involved in the libration about c-axis. It was concluded that the force constant  $K_O$  associated with the displacement of O<sub>w</sub> (not along M-O<sub>w</sub> bond) should have a negligible role, as compared with  $K_H$  in controlling the frequencies of the librational modes. Using the above relations, we have computed the force constants both for MPH and NPH (cf. Table 3.10). Comparing the results obtained for MPH and NPH, it is

found that the calculated values (37) of  $K_O$  (13 for MPH and 15 for NPH) are greater in case of NPH and so one infers that  $M-O_w$  frequency is higher in this case which is in contradiction with the observed frequencies for the two cases (cf. Table 3.9).

Similar is the observation for  $K_H$ . This questions the validity of the formula, which has been critically examined recently in a review (33).

### 3.2.4 FAR-IR

Fig. 3.11 shows the Far-IR spectrum of MPH at RT taken at the RSIC, IIT Madras in the typical region  $10\text{ cm}^{-1}$  to  $250\text{ cm}^{-1}$  to study the low frequency vibrations. The observed band frequencies are presented in Table 3.11. The assignment of these bands are made on the basis of previously reported and predicted values of  $M(OH_2)_6$  complex (11,36) and  $ClO_4^-$  ion (39). The four  $ClO_4^-$  groups in the unit cell will give twelve translational modes, out of which three will be acoustic and the rest will be optical modes. The optical translational modes  $Lt_7$ ,  $Lt_5$ ,  $Lt_3$  fall around the same frequency ( $215\text{ cm}^{-1}$ ). Same is the case for  $Lt_9$ ,  $Lt_4$  and  $Lt_2$  ( $152\text{ cm}^{-1}$ ) and  $Lt_8$ ,  $Lt_6$  and  $Lt_1$  ( $72\text{ cm}^{-1}$ ) as suggested earlier (39).

### 3.2.5 COMBINATION BANDS IN THE REGION $1700-2350\text{ cm}^{-1}$

The spectrum in  $1700-2350\text{ cm}^{-1}$  in IR has especially been investigated with higher sample concentration in order to obtain additional evidence for distinguishing R, W and T modes by observing the expected planer combination of  $\nu_2$  and R mode of water.



Fig. 3.12 shows the IR spectra of MPH and its D-analogue (curves B and A respectively) at RT in the range 2350 to 1700  $\text{cm}^{-1}$ . Spectra for NPH and its D-analogue are shown by curves D and C respectively. The observed band positions are presented in Table 3.12 along with their assignments. The assignments are based on the shift of the bands on deuteration, and effect of temperature on them. The assignment of 2230  $\text{cm}^{-1}$  band as a combination of  $\nu_2 + \nu_R$  of water seems to be justifiable because the inplane libration  $\nu_R$  may mix with in-plane bending mode  $\nu_2$  to give the combination mode. In the D-sample this band shifts to 1943  $\text{cm}^{-1}$  which may be a combination of  $\nu_2$  (1440  $\text{cm}^{-1}$ ) +  $\nu_R$  (505  $\text{cm}^{-1}$ ) of HOD. This band is broader than the perchlorate combination in this region. Similar argument hold good for NPH and the assignments are given in the Table 3.12.

### 3.2.6 PHASE TRANSITIONS

#### (a) Phase Transitions Below RT

##### (i) Perchlorate modes

The earlier IR study (4) on NPH suggested that the splitting of  $\nu_4(p)$  from doublet at RT to triplet at LT was due to change of crystal field symmetry at  $\text{ClO}_4^-$  ion site and/or normal decrease in half-width at LT. The perchlorate vibrations both in MPH and NPH do not exhibit any discontinuous changes with temperature. The  $\nu_3(p)$  and  $\nu_4(p)$  bands are expected to show three components each under the  $C_{2v}^7$  space group. The splitting in  $\nu_3(p)$  is evident even at RT, but in  $\nu_4(p)$  the three components are resolved clearly only at LT in the case of NPH.

(ii) Water modes

The IR spectra of MPH and NPH in stretching and librational region are reproduced in Figs. 3.1, 3.9(I) and 3.9(II). The spectra do not show any appreciable change at RT and LP, except in the librational region. In the librational region appearance of the IR inactive T mode with appreciable intensity indicates that the water molecules are distorted. However the temperature dependence of librational modes could not give a definite evidence of phase transition in the normal hydrate because of the overlapping of several bands. Therefore, we have studied the temperature dependence of OD stretching mode of HOD in both MPH and NPH by isotopic dilution technique (40-42).

The IR spectra of OD stretching fundamentals of isotopically diluted HOD(5%) have been recorded at different temperatures and are shown in Figs. 3.13(A) and 3.14(A). The splitting of the OD doublet with temperature is shown in Fig. 3.15 which has discontinuities at  $\sim 225$  and  $193$  K in MPH and  $223$  and  $180$  K in NPH.

The phase transitions at  $225$  and  $223$  K in MPH and NPH respectively indicate that the water molecules are distorted due to nonequivalent hydrogen bonding (12), which is in agreement with EPR (4,43) studies. Tentative conclusion on the basis of IR spectra can be drawn regarding the nature of distortion. On attributing the splitted components to the two asymmetric bond lengths, it is evident that the mirror plane and the two fold screw symmetries are lost as far as H-positions are concerned. However, the glide plane symmetry may still exist. Therefore, the space group  $C_{2v}^7$  is reduced to the two possible

space groups  $C_s^2$  and  $C_s^4$ . If one takes the primitive cell with two formula units, the space group at LT phase is reduced to  $C_s^2$  only. The observation of piezoelectric effect (44) also supports the  $C_s^2$  space group in contradiction to the earlier suggestion of  $C_{2h}^5$  space group (45,46), which should not exhibit the piezoelectric effect.

The flipping motion (47) of water molecules is not responsible for the phase transition, because this motion does not cause any distortion in the water molecules as shown in Fig. 3.16. The asymmetric distortion of O-H bonds in water could be caused by a tumbling or a reorientation motion of the  $H_2O$  groups. The possibility of distortion due to reorientational motion of water seems unlikely as such motion would not give a splitting of OH stretch. Further, no discontinuous changes could be observed in the librational region of water which should have accompanied the phase transition if reorientation was the main reason. Hence, the tumbling motion appears to be the only cause for asymmetric H-bonding producing the distortion.

At 193 K in MPH and 180 K in NPH,  $H_2O$  molecules are further distorted due to the reason discussed above. In this transition no further change in space group takes place. On lowering the temperature further minor discontinuity was observed in MPH around 110 K. The peak intensity enhancement observed at 110 K suggests that the phase transition at this temperature is associated with a positional ordering of hydrogen atoms in crystal as observed earlier in other salts (8,12,48). In this transition the nature of band shape does not change indicating

no further structural change (12). In NPH no phase transition has been observed in this temperature range.

(b) Phase Transitions Above RT

Figs. 3.13(B) and 3.14(B,C) show the spectra of bending modes at different temperatures. The intensities and half-widths of these bands at different temperatures are shown in Figs. 3.17(I) and 3.17(II). The minor discontinuities are observed at 335, 370, 422 and 445 K in MPH and at 311 K in NPH and a sharp discontinuity at 355 K is also observed in NPH. The variation in halfwidth indicates that there is a change in reorientational motion of  $H_2O$ , because this motion increases the half-width. The contribution to half-width due to reorientational motion is obtained by applying Rakov's method (49). If  $\Delta\nu_{1/2} = \Delta\nu_0 + (\Delta\nu_{1/2})_R$  the rotational and vibrational correlation times are calculated using the formula :

$$T_R = \frac{1}{\pi(\Delta\nu_{1/2} - \Delta\nu_0)} \quad \text{and} \quad T_v = \frac{1}{\pi(\Delta\nu_0)}$$

where  $\Delta\nu_{1/2}$  is the observed width at a particular temperature and  $\Delta\nu_0$  is the width due to vibrational relaxation alone, which is independent of temperature and is obtained by extrapolating the halfwidth vs temperature graph upto absolute zero temperature. However, the extraneous effects like those due to slit-width, sample preparation etc. should be avoided and minimized. The calculated vibrational relaxation times for bending modes of  $H_2O$  in MPH and NPH are 0.92 and 0.77 picosecond respectively and for HOD in NPH is 0.84 picosecond. The calculated rotational relaxation times are presented in Table 3.13. Thus any discontinuity

in  $\Delta\nu_{1/2}$  with temperature will also reflect the discontinuity in rotational correlation time because of the reorientational broadening  $\Delta\nu_{1/2} - \Delta\nu'_0$ . The flips of water molecules by  $180^\circ$  alone do not change the dipolar interaction and consequently contribute nothing to the relaxation rate. The  $180^\circ$  flips of  $H_2O$  would not cause broadening of the bands (47).

The exponential increase of half-width and discontinuity in it with temperature are associated with reorientational motion of  $H_2O$  and phase transitions. In phase transformations one can expect changes in potential barrier (57,58) also. To determine the reorientational potential barrier  $V$  in different phases we used Frankel's relation:

$$(\Delta\nu_{1/2} - \Delta\nu'_0) = Ae^{-V/RT}$$

where  $R$  is gas constant and  $A$  is constant. A graph between  $\log_e (\Delta\nu_{1/2} - \Delta\nu'_0)$  vs  $1000/T$  is plotted both for MPH (I) and NPH (II) as shown in Fig . 3.18 from which the value of potential barrier  $V$  and the constant  $A$  in different phases have been computed and summarised in Table 3.14.

# REFERENCES

1. F.A. Miller and C.H. Wilkin, *Ann. Chem.* 24, 1253 (1952).
2. S.D. Ross, *Spectrochim. Acta* 18, 225 (1962).
3. B.J. Hathaway and A.E. Underhill, *J. Chem. Soc.* 3091 (1961).
4. J.C. Sartorelli, S. Isotani, J.A. Ochi, W. Sano and A. Piccini, *Chem. Phys. Lett.* 57, 608 (1978).
5. A. Weil and J.P. Mathieu, *Comp. rend.* 238, 2510 (1954).
6. J.M. Janik, A.M. Mikuli, E. Mikuli and T. Stanek, *Krakow-Report No. 1113/PS Krakow* (1980).
- 6a. M.B. Patel and H.D. Bist, *Appl. Spectros.* 36, 185 (1982).
7. F.J. Bartoli and T.A. Litoritz, *J. Chem. Phys.* 56, 405 (1972).
8. D.F. Hornig, *J. Chem. Phys.* 17, 1346 (1949).
9. D.N. Glew in 'Hydrogen Bonded Solvent Systems' A.K. Covington and P. Jones (eds.) Taylor and Francis, London (1968) page 133.
10. L.J. Bellamy, M.J. Blandamer, M.C.R. Symons and D. Wadlington, *Trans. Faraday Soc.* 67, 3435 (1971).
11. V. Ananthanarayanan, *Z. Phys. Chem.* 222, 102 (1963).
12. J. Shiffer, Ph.D. Thesis, Princeton Univ., Princeton, N.J. 1963.
13. G. Brink and M. Falk, *Can. J. Chem.* 49, 347 (1971).
14. C. Secroun and P. Jouve, *J. Phys. (Paris)* 32, 871 (1971).
15. M. Falk and O. Knop in 'Water - A Comprehensive Treatise' Vol. II F.R. Franks (ed.) Plenum Press, New York-London (1973), page 55 (and references therein).
16. A.F. Wells, 'Structural Inorg. Chem.' Oxford, England (1962) p page 585.
17. W.S. Benedict, N. Gailar and E.K. Plyler, *J. Chem. Phys.* 24, 1139 (1956).
18. P. Saumagne and M.L. Josien, *Bull. Soc. Chim. France* 813 (1958).
19. Y.I. Ryskin, G.P. Stavitskaya and N.A. Toropov, *Russ. J. Inorg. Chem. (English Trans.)* 5, 1315 (1960).
20. J. Lecomte, *J. Chem. Phys.* 50, C54 (1953).
21. M. Van-Thiel, E.D. Becker and G.C. Pimentel, *J. Chem. Phys.* 27, 486 (1957).
22. G. Sartori, C. Furlani and A. Damiani, *J. Inorg. Nucl. Chem.* 8, 119 (1958).
23. G. Sartori and C. Furlani, *Z. Physik, Chem. (Frankfurt)* 15, 336 (1958).
24. C.D. West, *Z. Kristallogr.* 91A, 480 (1935).
25. R.E. Hester and R.A. Plane, *Inorg. Chem.* 3, 768 (1964).
26. A. Foldes and C. Sandorfy, *J. Mol. Spectrosc.* 20, 262 (1966).
27. R.C. Horman and K.E. Shuter, *J. Chem. Phys.* 22, 481 (1954).
28. R. Fifer, Ph.D. Thesis, Temple Univ. (1970).

29. S. Smith and J.W. Linnett, *Trans. Faraday Soc.* 52, 891 (1956).
30. D.F. Smith and J. Overend, *Spectrochim. Acta* A28, 471 (1972).
31. R.L. Somorjai and D.F. Hornig, *J. Chem. Phys.* 36, 1980 (1962).
32. G. Herzberg, 'Molecular Spectra and Molecular Structure' Vol. II  
D. Van. Nostrand Co. Inc., Princeton, N.J. (1945).
33. V.P. Tayal, B.K. Shrivastava, D.P. Khandelwal and H.D. Bist,  
*Appl. Spectrosc. Review* 16, 43, 1980 (and references therein).
34. H.R. Oswald, *Helv. Chim. Acta* 48, 590 (1965).
35. V.P. Tayal, D.P. Khandelwal and H.D. Bist, *Chem. Phys. Lett.* 55,  
136 (1978).
36. I. Nakagawa and T. Shimanouchi, *Spectrochim. Acta* 20, 429 (1964).
37. Y.S. Jain, *Solid State Commun.* 17, 605 (1975).
38. R.W. Blue, *J. Chem. Phys.* 22, 280 (1954).
39. H.D. Lutz and R.A. Becker, *Spectrochim. Acta* 35A, 797 (1979).
40. M. Falk and T. A. Ford, *Can. J. Chem.* 44, 1699 (1966).
41. T.T. Wall and D.F. Hornig, *J. Chem. Phys.* 43, 2079 (1965).
42. R.D. Woldron, *J. Chem. Phys.* 26, 809 (1957).
43. A.K. Jain and G.C. Upreti, *J. Phys.* C13, 5177 (1980).
44. I. Svare and B.O. Fimland, *J. Chem. Phys.* 74, 5977 (1981).
45. B.K. Chaudhuri, *J. Phys.* C7, 3962 (1974).
46. B.K. Chaudhuri, *Solid State Commun.* 16, 767 (1975).
47. I. Svare, B.O. Fimland, K. Otnes, J.A. Janik, J.M. Janik,  
E. Mikuli and A.M. Mikuli, *Physica* 106B, 195 (1981).
48. T.A. Fold and M. Falk, *J. Mol. Struct.* 3, 445 (1969).
49. A.W. Rakov, *Trudg Fiz. Instituta im. Lebedieva* 27, 111 (1964).
50. I. Dezsi and L. Keszthetyi, *Solid State Commun.* 4, 511 (1966).
51. E. Mikuli, A.M. Mikuli, M. Rachwalska and T. Stanek, *Physica*  
104B, 326 (1981).
52. M. Rachwalska and T. Stanek, *Phys. Stat. Sol.* A48, 297 (1978).
53. R. Dayal, D.R. Rao and P. Venkateswarlu, *Can. J. Phys.* 56,  
1175 (1978).
54. R. Dayal, D.R. Rao and P. Venkateswarlu, *J. Magn. Reson.* 36, 99 (1979).
55. A.K. Jain and G.C. Upreti, Private communications.
56. M.B. Patel and H.D. Bist, *J. de Physique* C6, 917 (1981).
57. A.R. Bates, K.W.H. Stevens, *J. Phys.* C2, 1573 (1969).
58. J.M. Janik, J.A. Janik and B. Janik, Report No. 892/PS, 1975  
Krakow, Poland.

Table 3.1: Phase transition temperatures (K) in MPH and NPH

Experimental technique used	Temperatures	
	MPH (a)	NPH (a)
Mössbauer	83-113 (50)	83 (50)
Magnetic suscepti- bility		225 (45, 46)
Specific heat	325.03 (51)	361.05 (52)
	272.97 (51)	311.4 (52)
	168 (51)	225 (52)
	108 (51)	
PMR and QNS	325 (47)	
	273 (47)	
	133 (47)	
	110-120 (47)	
Piezoelectricity	324-328 (44)	250 (44)
	110-120 (44)	
Raman	325 (6)	361 (6)
EPR	335 (55)	361 (43)
	328 (55)	311 (43)
	324 (55)	245 (43)
	272 (55, 53)	223 (4, 54)
	193 (53)	
	103 (55, 53)	
Infrared (b)	450	355
	422	311
	370	223
	335	180
	225.5 (56)	
	193 (56)	
	110 (56)	

(a) Figures in parantheses denote the references cited at the end of the chapter.

(b) Present study.



Table 3.2: Observed bands in IR spectra of MPH in the region of internal vibrations of  $H_2O$  and its deuterated analogue at 93 K and Raman spectra at 300 K.

MPH			MPD			Ratio of fre- quency shift	Assignment	
Infrared		Raman	Infrared					
$\nu$ ( $cm^{-1}$ )	$\Delta\nu_{1/2}$ ( $cm^{-1}$ )	I	$\nu$ ( $cm^{-1}$ )	$\Delta\nu_{1/2}$ ( $cm^{-1}$ )	I			
583	100	17	2675*	40	14	1.34	$\nu_3 + \nu_4(c)$ ( $X_2O$ )	
520	84	18	2618*	38	19	1.34	$\nu_1 + \nu_4(c)$ ( $X_2O$ )	
468	107	100	2581	25	100	1.34	$\nu_3$ ( $X_2O$ )	
436	20	5	2550	15	81	1.35	Uncoupled stretching bands of $X_2O$ and HOD.	
407*	17	3	2535	17	112	1.34		
396	67	65	3530	2510	15	65	1.35	$\nu_1$ ( $X_2O$ )
350*	69	9	2490*	32	10	1.35	$\nu_3 - \nu_4(c)$ ( $X_2O$ )	
274	70	9	2398*	33	9	1.36	$\nu_1 - \nu_4(c)$ ( $X_2O$ )	
			2364.5	17	13	1.13	$2\nu_2'$ (HOD)	
235	15	9	2393	10	5	1.35	$2\nu_2$ ( $X_2O$ )	
			1441	10	44	1.13	$\nu_2$ (HOD)	
530	13	18	1630	1205.5	8	15	1.35	$\nu_2$ ( $X_2O$ )

uch significance can not be attached to the very weak bands marked with asterisk.

= H under column MPH and D under MPD.

$\nu_4(c)$  = Translatory lattice mode of water in  $M(OH_2)_6$  aquo-complex.

Table 3.3: Observed bands in IR spectra of NPH in the region of internal vibrations of  $\text{H}_2\text{O}$  and its deuterated analogue at 93 K and Raman spectra at 300 K.

NPH			NPD			Ratio of frequency shift	Assignment
Infrared		Raman	Infrared				
$\nu$ ( $\text{cm}^{-1}$ )	$\Delta\nu_{1/2}$ ( $\text{cm}^{-1}$ )	I	$\nu$ ( $\text{cm}^{-1}$ )	$\Delta\nu_{1/2}$ ( $\text{cm}^{-1}$ )	I		
3580	110	20	2678*	55	26	1.34	$\nu_3 + \nu_4(\text{c}) (\text{X}_2\text{O})$
3500	85	20	2608*	50	26	1.34	$\nu_1 + \nu_4(\text{c}) (\text{X}_2\text{O})$
3449	110	100	2568	30	100	1.34	$\nu_3 (\text{X}_2\text{O})$
3420*	34	8	2532	15	71	1.35	Uncoupled stretching bands of $\text{X}_2\text{O}$ and HO
3393*	30	5	2520	15	82	1.35	
3372	70	67	3510 2495	19	67	1.35	$\nu_1 (\text{X}_2\text{O})$
3320*	100	18	2455*	42	24	1.35	$\nu_3 - \nu_4(\text{c}) (\text{X}_2\text{O})$
3240*	80	18	2380*	45	18	1.36	$\nu_1 - \nu_4(\text{c}) (\text{X}_2\text{O})$
			2860	23	14	1.13	$2\nu_2 (\text{HOD})$
3230	28	13	2390	18	7	1.35	$2\nu_2 (\text{X}_2\text{O})$
			1438.5	14	45	1.13	$\nu_2 (\text{HOD})$
1628	16	21	1624 1204	12	14	1.35	$\nu_2 (\text{X}_2\text{O})$

Much significance can not be attached to the very weak bands marked with asterisk.

X = H under column NPH and D under NPD.

$\nu_4(\text{c})$  = Translatory lattice mode of water in  $\text{M}(\text{OH}_2)$  aquo-complex.

Table 3.4 (a): Magnitude of distortion parameter 'd' for  $\text{H}_2\text{O}$  and  $\text{D}_2\text{O}$  in MPH and NPH at 93 K

Compound	d-parameter	
	$\text{H}_2\text{O}$	$\text{D}_2\text{O}$
MPH	0.701	0.605
NPH	0.675	0.580

Table 3.4 (b): Intensity ratio  $(I_{\nu_3}/I_{\nu_1})$  for  $\text{H}_2\text{O}$  and  $\text{D}_2\text{O}$  in MPH and  $^3\text{NPH}$  at 93 K.

Compound	$(I_{\nu_3}/I_{\nu_1})$		Theoretical
	$\text{H}_2\text{O}$	$\text{D}_2\text{O}$	
MPH	1.54	1.53	1.57
NPH	1.50	1.49	1.57

Table 3.5: The  $\nu_3$  and  $\nu_1$  bands of water under different environs (The data are taken from references given under col.2 in parantheses)

Symbol	$\text{H}_2\text{O}$ in	(Ref.)	$\nu_3$ ( $\text{cm}^{-1}$ )	$\nu_1$ ( $\text{cm}^{-1}$ )	$\nu_3 - \nu_1$ ( $\text{cm}^{-1}$ )	$\bar{\nu}_{\text{OH}} = \frac{\nu_1 + \nu_3}{2}$ ( $\text{cm}^{-1}$ )
⊙	Vapour	(17)	3755.8	3656.7	99.14	3706.2
○	$\text{N}_2$ Matrix	(29)	3725	3627	98	3676
▽	$\text{CCl}_4$	(18)	3708	3613	95	3660.5
□	$\text{CCl}_4$	(20)	3705	3614	91	3660
▼	$\text{Cs}_2$	(18)	3691	3601	90	3646
○	Beryl	(19)	3690	3598	92	3644
▽	$\text{CHCl}_3$	(18)	3676	3598	78	3637
▽	Toluene	(18)	3670	3592	78	3631
▽	Nitromethane	(18)	3667	3580	87	3623.5
▽	Acetonitrile	(18)	3626	3540	86	3583
▽	Acetone	(18)	3616	3535	80	3575
▽	Dioxene	(18)	3583	3512	71	3547.5
⊖	$\text{NaBr} \cdot 2\text{H}_2\text{O}$	(12)	3462	3410	52.7	3436
⊖	$\text{NaCl} \cdot 2\text{H}_2\text{O}$	(12)	3455	3405	50	3430
○	$\text{Mg}(\text{ClO}_4) \cdot 2 \cdot 6\text{H}_2\text{O}$	*	3468	3396	72	3432
○	$\text{Ni}(\text{ClO}_4) \cdot 2 \cdot 6\text{H}_2\text{O}$	*	3449	3372	77	3410.5

\*Present study.

Table 3.6 (a): Intensity ratio ( $I_2\nu_2/I\nu_2$ ) for  $\text{H}_2\text{O}$ , HOD and  $\text{D}_2\text{O}$  in MPH and NPH at 93 K.

Compound	$(I_2\nu_2/I\nu_2)$		
	$\text{H}_2\text{O}$	HOD	$\text{D}_2\text{O}$
MPH	0.49	0.28	0.34
NPH	0.60	0.32	0.48

Table 3.6 (b): The calculated constants for the bending modes of  $\text{H}_2\text{O}$ , HOD and  $\text{D}_2\text{O}$  in MPH and NPH (i) without considering Fermi resonance and (ii) considering Fermi resonance.

Compound	(i)							(ii)						
	$W_2^X e$ ( $\text{cm}^{-1}$ )	$W_e$ ( $\text{cm}^{-1}$ )	$K_3$ ( $\text{cm}^{-1}$ )	$\mu_2/\mu_1$	$W_2^X e$ ( $\text{cm}^{-1}$ )	$W_e$ ( $\text{cm}^{-1}$ )	$K_3$ ( $\text{cm}^{-1}$ )	$\mu_2/\mu_1$	$\Delta$ ( $\text{cm}^{-1}$ )	$\Delta_0$ ( $\text{cm}^{-1}$ )	$\Delta$ ( $\text{cm}^{-1}$ )	$\Delta_0$ ( $\text{cm}^{-1}$ )	$\Delta$ ( $\text{cm}^{-1}$ )	$\Delta_0$ ( $\text{cm}^{-1}$ )
$\text{H}_2\text{O}$	12.5	1655.0	-74.5	+0.62 -0.41	9.3	1648.6	-63.9	+0.60 -0.42	161	147.8	161	147.8	32.0	32.0
MPH HOD	8.8	1458.5	-58.4	+0.45 -0.31	8.8	1458.5	-58.4	+0.45 -0.31	-	-	-	-	-	-
$\text{D}_2\text{O}$	9.0	1223.5	-54.2	+0.51 -0.34	6.7	1218.8	-46.5	+0.49 -0.35	117	107.4	117	107.4	23.3	23.3
$\text{H}_2\text{O}$	13.0	1654.0	-75.7	+0.68 -0.45	9.3	1646.5	-63.8	+0.66 -0.46	142	126.9	142	126.9	31.9	31.9
NPH HOD	8.5	1455.5	-57.4	+0.48 -0.33	8.5	1455.5	-57.4	+0.48 -0.33	-	-	-	-	-	-
$\text{D}_2\text{O}$	9.0	1222.0	-54.2	+0.58 -0.39	6.5	1216.9	-45.8	+0.56 -0.40	105	94.5	105	94.5	22.9	22.9

Table 3.7: Uncoupled bands of D<sub>2</sub>O and HOD in MPH and NPH stretching and bending regions.

Uncoupled Bands (cm <sup>-1</sup> )					
D <sub>2</sub> O			HOD		
MPH	NPH	Assignment	MPH	NPH	Assignment
1206	1204.5	$\nu_2$	1443	1440	$\nu_2$
2511	2495	$\nu_1$	2535	2521	$\nu_{OD}$
2578	2565	$\nu_3$	2548	2531	$\nu_{OD}$
			3407	3393	$\nu_{OH}$
			3436	3420	$\nu_{OH}$

Table 3.8: Observed Raman and IR bands (cm<sup>-1</sup>) in microcrystalline MPH and NPH powder below 1300 cm<sup>-1</sup>

MPH				NPH				Assignment
Raman		Infrared		Raman		Infrared		
RT	LT	RT	HT	RT	LT	RT	HT	
	1260	1260	1260		1260	1260	1264	$2\nu_4(p)$
	1182	1179	1177		1184	1180	1178	$\nu_3(p) + \nu_L(p)$
1133	1150	1148	1148		1151	1148	1148	$\nu_3(p)$
1116	1112	1110	1110	1118	1114	1112	1110	$\nu_3(p)$
1090	1090	1088	1090	1087	1088	1087	1088	$\nu_3(p)$
	1070				1071			$\nu_3(p) - \nu_L(p)$
935	943	942	940	934	944	942	943	$\nu_1(p)$
	927	926	926		927	926	926	$\nu_1(p) - \nu_L(p)$
	602	605	840		653	658	750	$\nu_R$
	740							$\nu_T + \nu_6(c)$
	640	640	639		640	639	639	$\nu_4(p)$
633				631	632			$\nu_4(p)$
	630	630	630		628	629	629	$\nu_4(p)$
	485	470	480		480	460	625	$\nu_W$
468	460		461	465	460		468	$\nu_2(p)$
402	423				402	395		$\nu_T$
	380				375			$\nu_6(c)$
	360	356			356	352		$\nu_6(c)$
354				395				$\nu_1(c)$
290				315				$\nu_3(c)$
210								$\nu_2(c)$

R, W, T, c, p and L stand for rocking, wagging, twisting modes of water; M(OH<sub>2</sub>)<sub>6</sub> aquo-complex, perchlorate and lattice modes of ClO<sub>4</sub><sup>-</sup> respectively.

Table 3.9: The Librational modes and  $M-O_W$  stretches ( $\text{cm}^{-1}$ ) in hydrated and partially deuterated MPH and NPH at LT and RT.

Compound	Hydrate		Partially deuterate					Frequency shift ratio				Assignment	
	$\nu(\text{cm}^{-1})$		$\nu(\text{cm}^{-1})$		$\nu(\text{cm}^{-1})$			$\nu_{\text{H}_2\text{O}}/\nu_{\text{HOD}}$		$\nu_{\text{H}_2\text{O}}/\nu_{\text{D}_2\text{O}}$			
	LT	RT	H <sub>2</sub> O	HOD	D <sub>2</sub> O	H <sub>2</sub> O	HOD	D <sub>2</sub> O	LT	RT	LT		RT
MPH	360	356	360	354	351	355			1.02		1.03		$\nu_6(\text{c})$
	380		380	375	370				1.02		1.03		$\nu_6(\text{c})$
	423		424	345	290				1.23		1.46		$\nu_{\text{T}}$
	485	470	479	450	335	468	445	330	1.08	1.06	1.45	1.42	$\nu_{\text{W}}$
	602	605	604	523	420	607	505	423	1.15	1.20	1.43	1.43	$\nu_{\text{R}}$
NPH	356	352	356	350	345	352			1.02		1.03		$\nu_6(\text{c})$
	375		375	370	365				1.02		1.03		$\nu_6(\text{c})$
	402	395	398	330	290	392			1.22		1.39		$\nu_{\text{T}}$
	480	460	473	443	350	458	435	345	1.08	1.06	1.36	1.33	$\nu_{\text{W}}$
	653	658	655	540	483	660	545		1.21	1.21	1.35		$\nu_{\text{R}}$

Table 3.10: Frequencies ( $\text{cm}^{-1}$ ) and force constants  $K_H$ ,  $K_O$  ( $\approx K'_O$ ) and  $K'_H$  (m dyne/ $\text{\AA}^0$ ) for librational modes of  $\text{H}_2\text{O}$  molecules in MPH and NPH.

Compound	LT		RT		HT	
	Frequency	Force constant	frequency	Force constant	Frequency	Force constant
MPH	$\nu_T=423$	$K_H=0.211$	$\nu_T^*$	$K_H=0.294$	$\nu_T^*$	$K_H=0.306$
	$\nu_W=485$	$K_O=13.04$	$\nu_W=470$	$K_O = --$	$\nu_W=480$	$K_O = --$
	$\nu_R=602$	$K'_H=0.413$	$\nu_R=605$	$K_H=0.450$	$\nu_R=840$	$K'_H=0.868$
NPH	$\nu_T=402$	$K_H=0.191$	$\nu_T=395$	$K_H=0.189$	$\nu_T^*$	$K_H=0.520$
	$\nu_W=480$	$K_O=14.84$	$\nu_W=460$	$K_O=11.88$	$\nu_W=625$	$K_O = --$
	$\nu_R=653$	$K'_H=0.487$	$\nu_R=658$	$K'_H=0.503$	$\nu_R=750$	$K'_H=0.692$

\*Twist mode is not observed.

Table 3.11: Observed frequencies ( $\text{cm}^{-1}$ ) in the Far-IR spectrum of MPH

$\nu$	Assignment*	$\nu$	Assignment*
215	$\nu_{\text{Lt}_{7,5,3}}$	78	$\nu_{\text{Lr}_c}$
152	$\nu_{\text{Lt}_{9,4,2}}$	72	$\nu_{\text{Lt}_{8,1,6}}$
137	$\nu_4(\text{c})$	41.5	$\nu_{\text{Lt}_a}$
108	$\nu_{\text{Lr}_a}$	27	$\nu_{\text{Lt}_b}$
88	$\nu_{\text{Lr}_b}$	13	$\nu_{\text{Lt}_c}$

\*Explanation of notations is: (c) =  $\text{M}(\text{OH}_2)_6$  aquo-complex.

Lr and Lt = rotational and translational modes of perchlorate group.

Table 3.12: The combination bands ( $\text{cm}^{-1}$ ) in IR spectra of MPH and NPH (and their deuterated analogues) in the range 2350 to  $1700 \text{ cm}^{-1}$ .

MPH	MPD	NPH	NPD	Assignment
2230	2235	2270	2274	$\nu_2 + \nu_R (\text{H}_2\text{O})$
2060	2060	2060	2060	$\nu_3(\text{p}) + \nu_1(\text{p})$
2020	2020	2060	2020	$\nu_3(\text{p}) + \nu_1(\text{p})$
	1943 *		1980 *	$\nu_2 + \nu_R (\text{HOD})$
1843	1845	1838	1840	$2\nu_4(\text{p}) + \nu_R (\text{H}_2\text{O})$
	1740 *		1735 *	$2\nu_4(\text{p}) + \nu_R (\text{HOD})$

\*Extrabands appear on deuterated samples only.

p and R stand for perchlorate and rocking mode.

Table 3.13: Temperature dependence of rotational correlation time  $\tau_R$  (picosecond) in MPH and NPH for bending mode of water.

MPH				NPH ( $\text{H}_2\text{O}$ )			
emp. (K)	$\tau_R$	Temp. (K)	$\tau_R$	Temp. (K)	$\tau_R$	Temp. (K)	$\tau_R$
93	10.6	379	1.9	93	7.3	373	0.3
105	10.6	389	1.6	173	7.3	HOD	
115	7.7	401	1.4	203	4.8	93	13.3
150	7.1	410	1.3	223	3.9	183	13.3
190	7.1	418	1.0	228	3.6	203	5.9
196	6.1	424	0.8	238	3.3	223	4.6
214	4.3	445	0.8	253	3.1	283	4.6
222	3.5	451	0.6	273	2.9	303	4.2
250	3.3	455	0.5	288	2.7	318	3.0
273	3.3	456	0.5	308	2.7	328	3.0
301	3.2	459	0.4	318	2.0	348	2.5
332	3.1	467	0.4	338	1.7	353	2.4
338	2.2	470	0.4	353	1.7	358	0.2
369	2.2	481	0.4	358	0.3	378	0.2



Table 3.14: Potential barrier 'V' and constant 'A' in different phases.

Compound	Phase	Temperature range in K	Potential barrier 'V' in K cal/mole	Constant 'A' in $\text{cm}^{-1}$
MPH	I	below 110	$\approx 0$	1.00
	II	110 - 193	$\approx 0$	1.49
	III	193 - 225	1.83	182.67
	IV	225 - 335	0.28	5.32
	V	335 - 370	$\approx 0$	4.71
	VI	370 - 422	6.26	20434.91
	VII	422 - 445	$\approx 0$	12.807
	VIII	above 445	13.91	78871720
NPH	I	below 180	$\approx 0$	1.45
	II	180 - 223	1.64	130.97
	III	223 - 311	0.37	7.25
	IV	311 - 355	1.74	83.86
	V	above 355	$\approx 0$	37.53

### FIGURE CAPTIONS

Fig.3.1: Infrared spectra in  $4000-2800\text{ cm}^{-1}$  region are reproduced on transmittance scale for  $\text{Mg}(\text{ClO}_4)_2 \cdot 6\text{H}_2\text{O}$  at 480, 93 and 300 K by curves A, B and C respectively and for  $\text{Ni}(\text{ClO}_4)_2 \cdot 6\text{H}_2\text{O}$  at 368, 93 and 300 K by curves F, D and E respectively. The abscissa origins in this figure (as well as in some other figures) for different curves have been suitably shifted for clarity.

Fig.3.2: The curve B of Fig. 3.1 is retraced on absorbance scale (solid lines) along with bending region of water. The dotted lines show the Lorentzian components.

Fig.3.3: The curve D of Fig.3.1 is retraced on absorbance scale (solid lines) along with bending region of water. The dotted lines show the Lorentzian components.

Fig.3.4: Solid lines show parts of observed spectra (retraced on absorbance scale) at 93 K for various percentages of  $\text{H}_2\text{O}$ ,  $\text{HOD}$  and  $\text{D}_2\text{O}$  in  $\text{Mg}(\text{ClO}_4)_2 \cdot 6\text{H}_2\text{O}$ . The dotted lines show Lorentzian components.

<u>curve</u>	<u>region</u>	<u>percentage of</u>		
		$\text{H}_2\text{O}$	$\text{HOD}$	$\text{D}_2\text{O}$
A	OD stretching	38	41	21
B	bending	38	41	21

Fig.3.5: Solid lines show parts of observed spectra (retraced on absorbance scale) at 93 K for various percentages of  $\text{H}_2\text{O}$ ,  $\text{HOD}$  and  $\text{D}_2\text{O}$  in  $\text{Ni}(\text{ClO}_4)_2 \cdot 6\text{H}_2\text{O}$ . The dotted lines show Lorentzian components.

<u>curve</u>	<u>region</u>	<u>percentage of</u>		
		$\text{H}_2\text{O}$	$\text{HOD}$	$\text{D}_2\text{O}$
A	OD stretching	41	41	18
B	bending	41	41	18

Fig.3.6: Room temperature Raman spectra of  $\text{Mg}(\text{ClO}_4)_2 \cdot 6\text{H}_2\text{O}$  (curve I) and  $\text{Ni}(\text{ClO}_4)_2 \cdot 6\text{H}_2\text{O}$  (curve II).

Fig.3.7: The  $\nu_3 - \nu_1 (\Delta\nu_{3,1})$  separation versus mean OH stretching frequency ( $\nu_{OH}$ ) (after reference 12).

Fig.3.8: Infrared spectra in the range 2900-2340 and 1710-1100  $\text{cm}^{-1}$  of partially deuterated  $\text{Mg}(\text{ClO}_4)_2 \cdot 6\text{H}_2\text{O}$  at 300 K (dotted lines) and 93 K (solid lines) with the percentages given below of  $\text{H}_2\text{O}$ , HOD and  $\text{D}_2\text{O}$  in the sample.

curves at		percentage of		
300 K	93 K	$\text{H}_2\text{O}$	HOD	$\text{D}_2\text{O}$
A	B	38	41	21
C	D	76	22	2
E	F	90	9	1

Fig.3.9: Infrared spectra in 1350-250  $\text{cm}^{-1}$  region at various temperatures (K) in transmittance scale for :

(I)  $\text{Mg}(\text{ClO}_4)_2 \cdot 6\text{H}_2\text{O}$  : (A) 93, (B) 300 and (C) 480 K and  
 (II)  $\text{Ni}(\text{ClO}_4)_2 \cdot 6\text{H}_2\text{O}$  : (A) 93, (B) 300 and (C) 368 K.

Fig.3.10: Infrared spectra of  $\text{Mg}(\text{ClO}_4)_2 \cdot 6\text{H}_2\text{O}$  plotted on absorbance scale. The curves A and B correspond to the curves A and B of Fig.3.9(I) and A' and B' are the corresponding curves for its partial deuterate. The dotted lines show Lorentzian analysis.

Fig.3.11: Far-infrared spectrum of  $\text{Mg}(\text{ClO}_4)_2 \cdot 6\text{H}_2\text{O}$  at room temperature in the range 10-250  $\text{cm}^{-1}$ .

Fig.3.12: Infrared spectra in the region 2350-1700  $\text{cm}^{-1}$  at 300 K of  $\text{Mg}(\text{ClO}_4)_2 \cdot 6\text{H}_2\text{O}$  (curve B),  $\text{Ni}(\text{ClO}_4)_2 \cdot 6\text{H}_2\text{O}$  (curve D) and their deuterated analogues (curves A and C respectively).

Fig.3.13: Temperature dependence of OD stretching and  $\text{H}_2\text{O}$  bending modes in  $\text{Mg}(\text{ClO}_4)_2 \cdot 6\text{H}_2\text{O}$  : Curve A - OD stretching (5%D); curve B -  $\text{H}_2\text{O}$  bending (0%D).

Fig.3.14: Temperature dependence of OD stretching,  $\text{H}_2\text{O}$  bending and HOD bending modes in  $\text{Ni}(\text{ClO}_4)_2 \cdot 6\text{H}_2\text{O}$  : Curve A - OD stretching (5% D); Curve B -  $\text{H}_2\text{O}$  bending (39% D); Curve C - HOD bending (39% D).

Fig.3.15: Separation of OD doublet ( $\text{cm}^{-1}$ ) in  $\text{Mg}(\text{ClO}_4)_2 \cdot 6\text{H}_2\text{O}$  (curve I) and  $\text{Ni}(\text{ClO}_4)_2 \cdot 6\text{H}_2\text{O}$  (curve II) of HOD (5% D) versus temperature.

Fig.3.16:  $[M(OH_2)_6]^{2+}$  complex with possible modes of motion indicated;  $180^\circ$  flip of each  $H_2O$  and/or reorientation of each water by an angle  $\theta$  ( $0^\circ < \theta < 180^\circ$  - solid arrows) and tumbling motion of the whole complex (dashed arrows) are shown.

Fig.3.17: Half-width (solid lines) and relative intensities (dotted lines) of bending modes of  $H_2O$  in  $Mg(ClO_4)_2 \cdot 6H_2O$  (curve I) and partially deuterated sample of  $Ni(ClO_4)_2 \cdot 6H_2O$  (curve IIA) and bending mode of  $HOD$  in partially deuterated sample of  $Ni(ClO_4)_2 \cdot 6H_2O$  (curve IIB) are plotted against temperature.

Fig.3.18:  $\log_e (\Delta\nu_{1/2} - \Delta\nu_0)$  versus  $1000/T$  for bending mode of  $H_2O$  in  $Mg(ClO_4)_2 \cdot 6H_2O$  (curve I) and in partially deuterated sample of  $Ni(ClO_4)_2 \cdot 6H_2O$  (curve IIA) and bending mode of  $HOD$  in partially deuterated sample of  $Ni(ClO_4)_2 \cdot 6H_2O$  (curve IIB) are plotted.

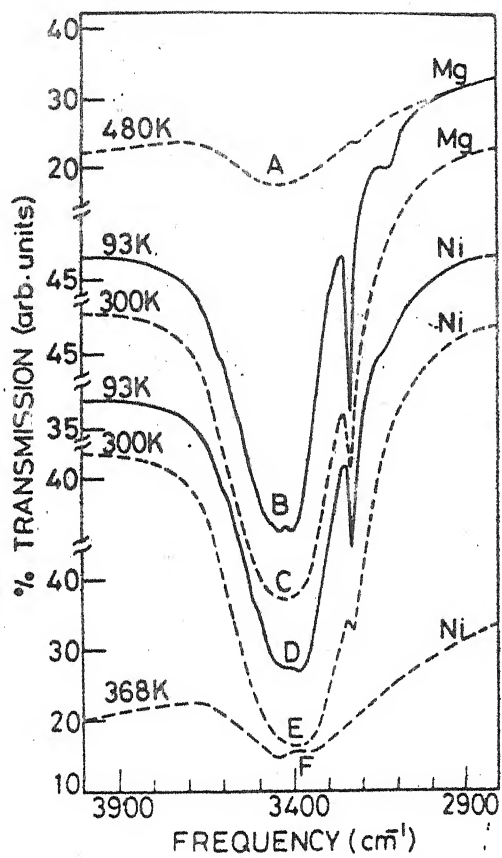


FIG. 3.1

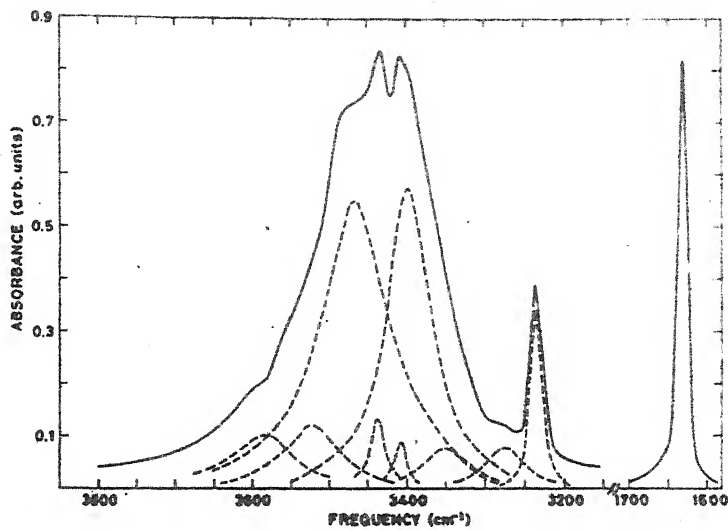


FIG. 3.2

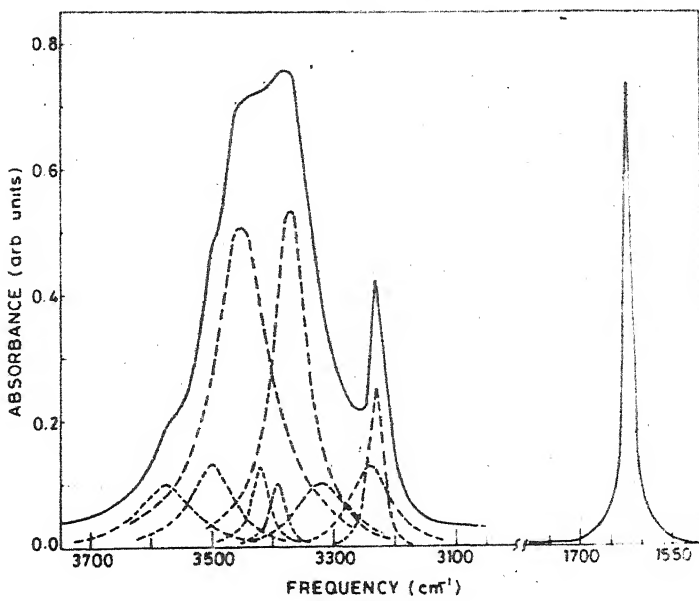


FIG. 3.3

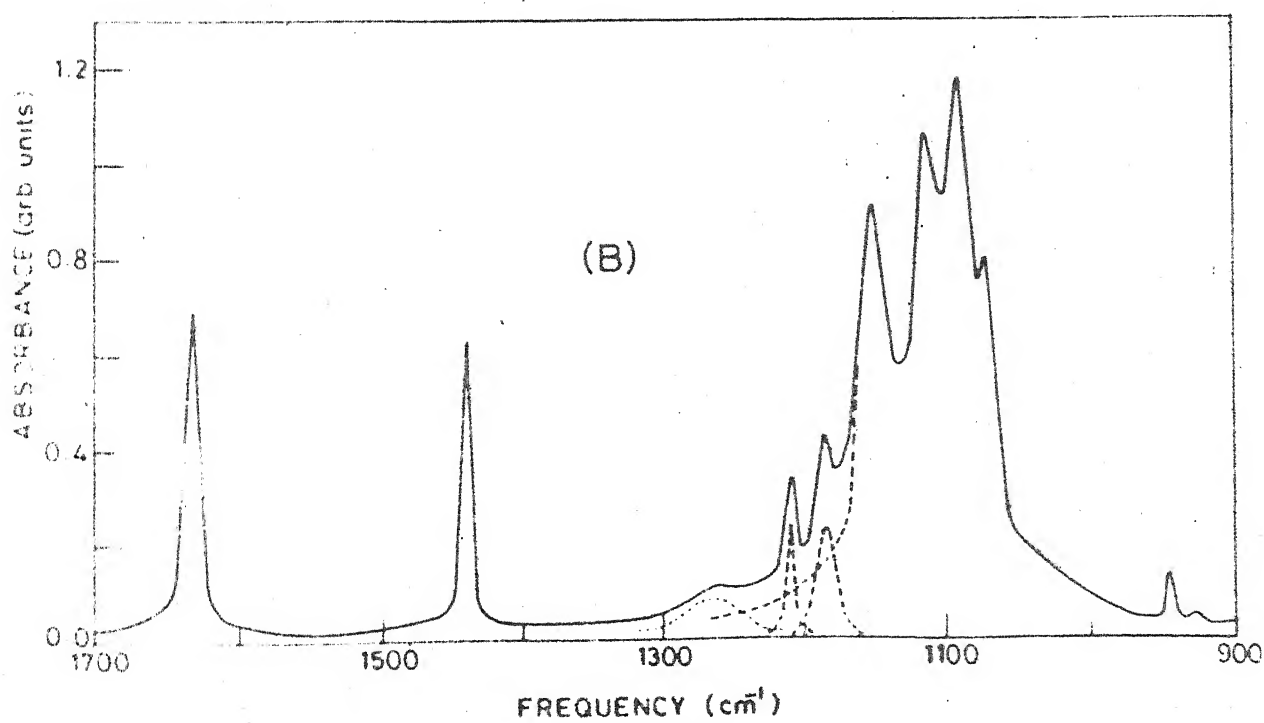
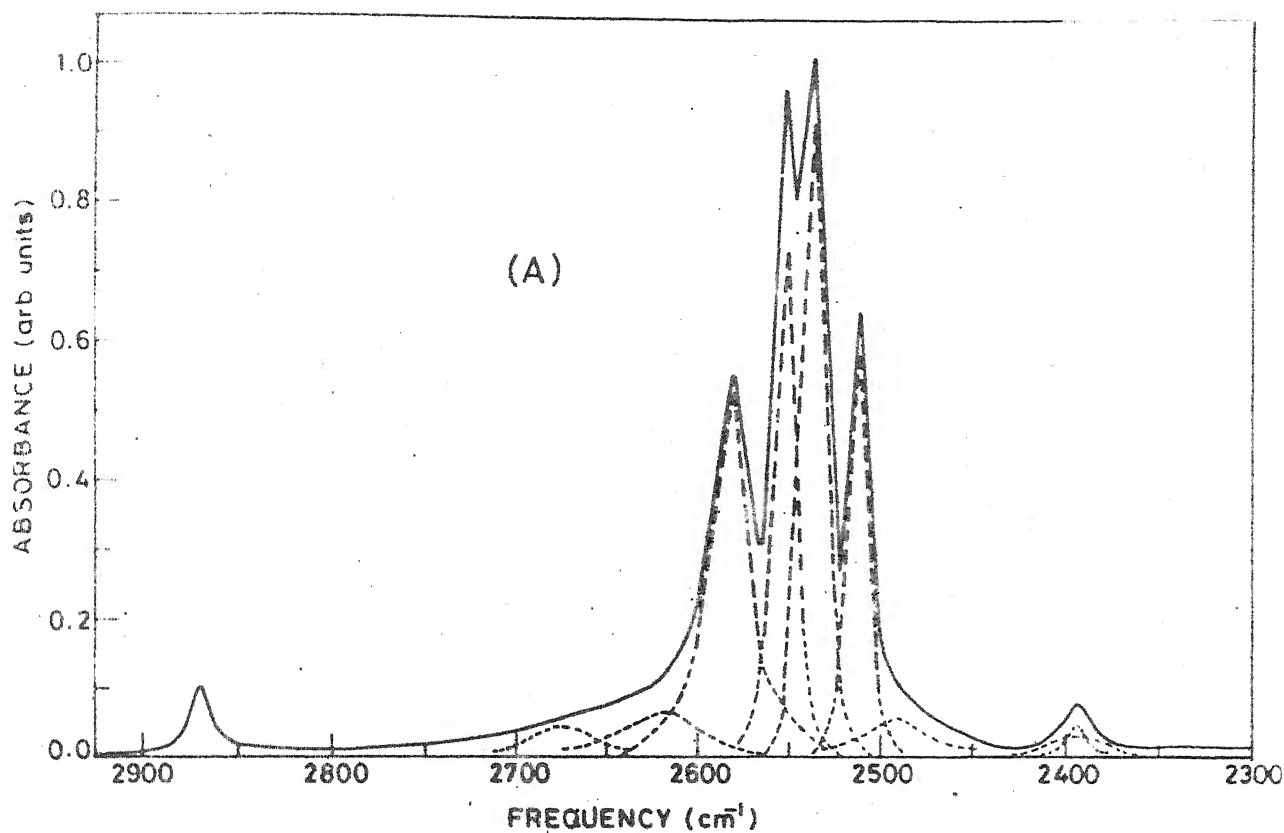


FIG. 3.4

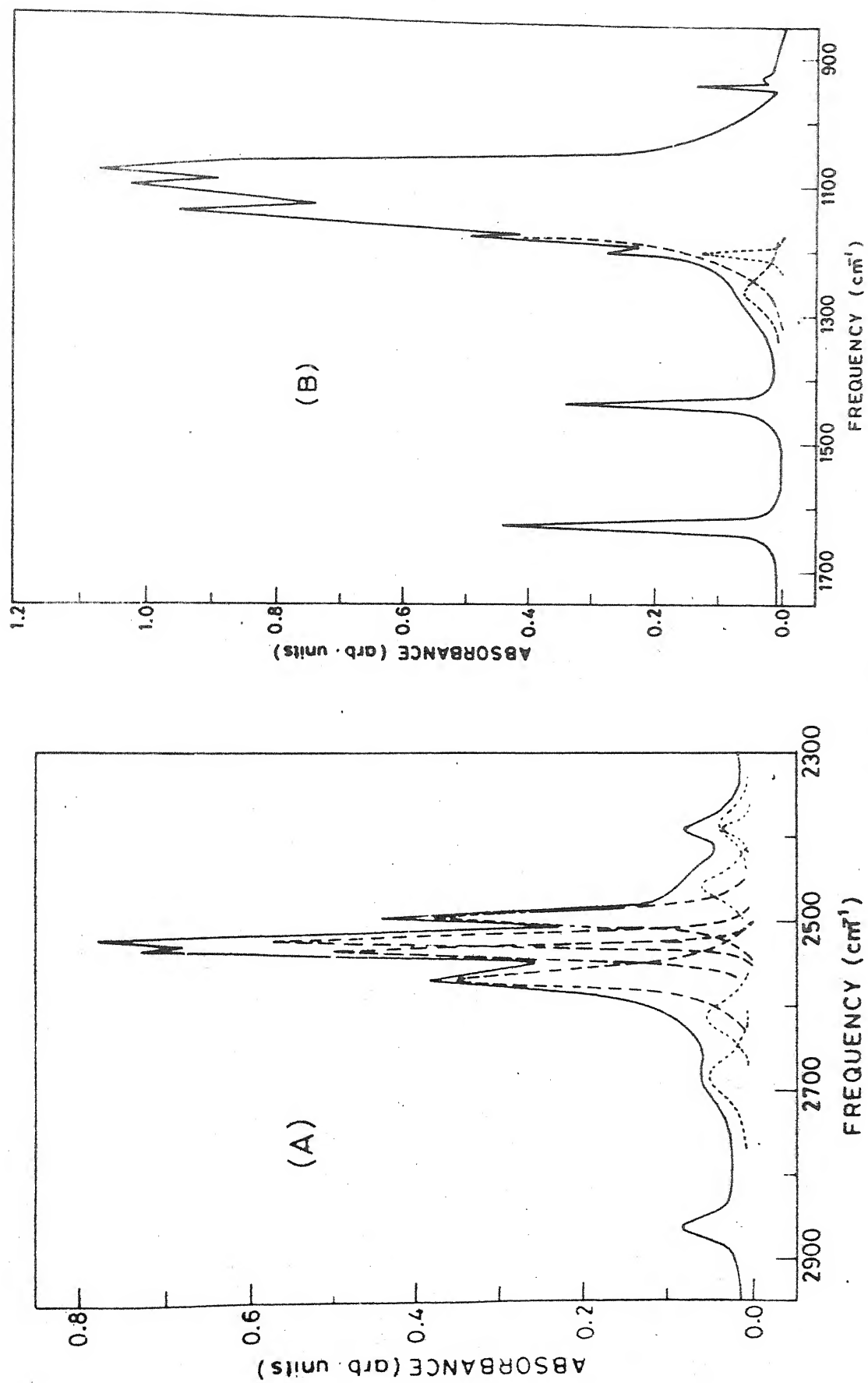


FIG. 3.5

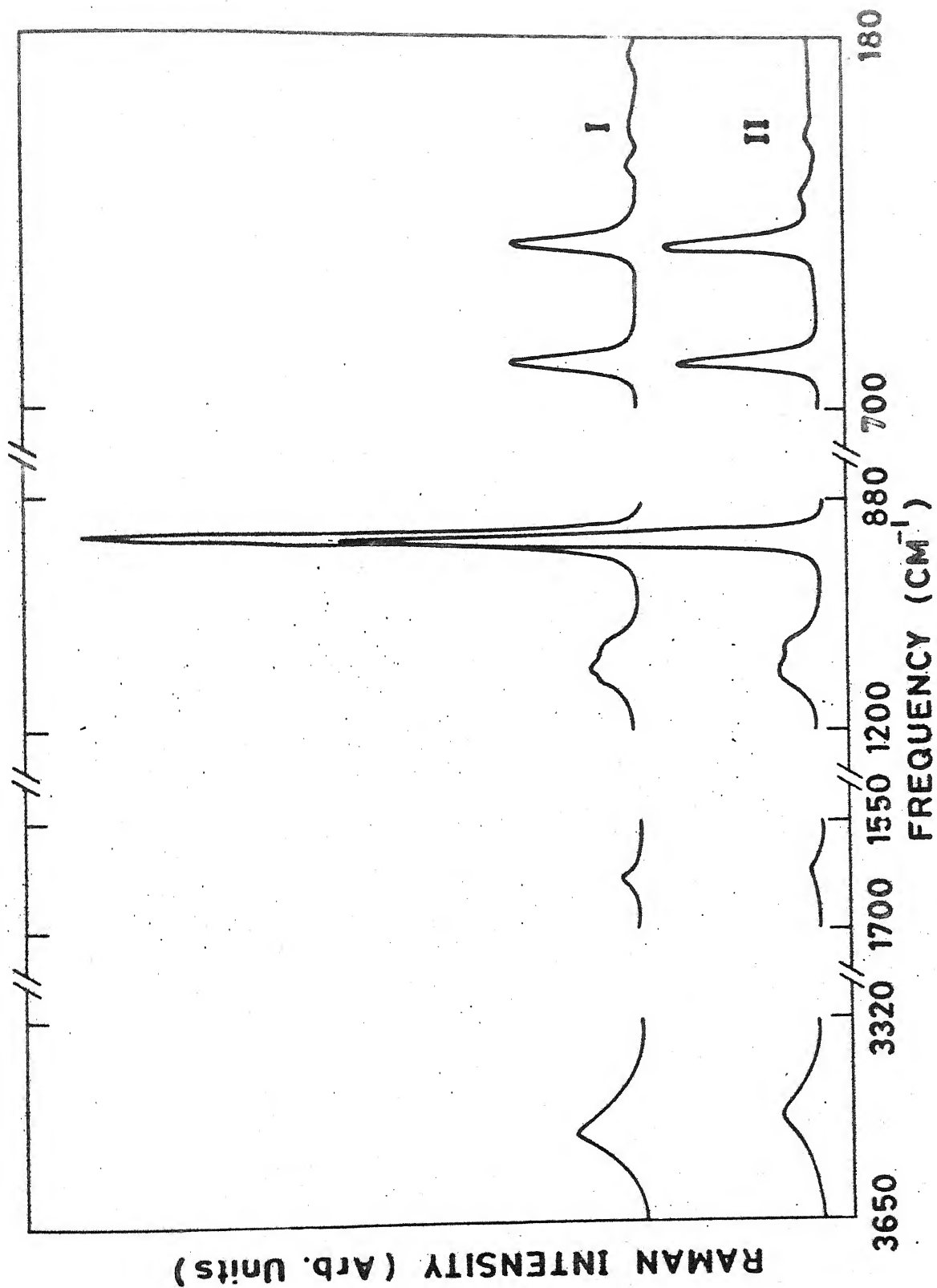


FIG. 3.6



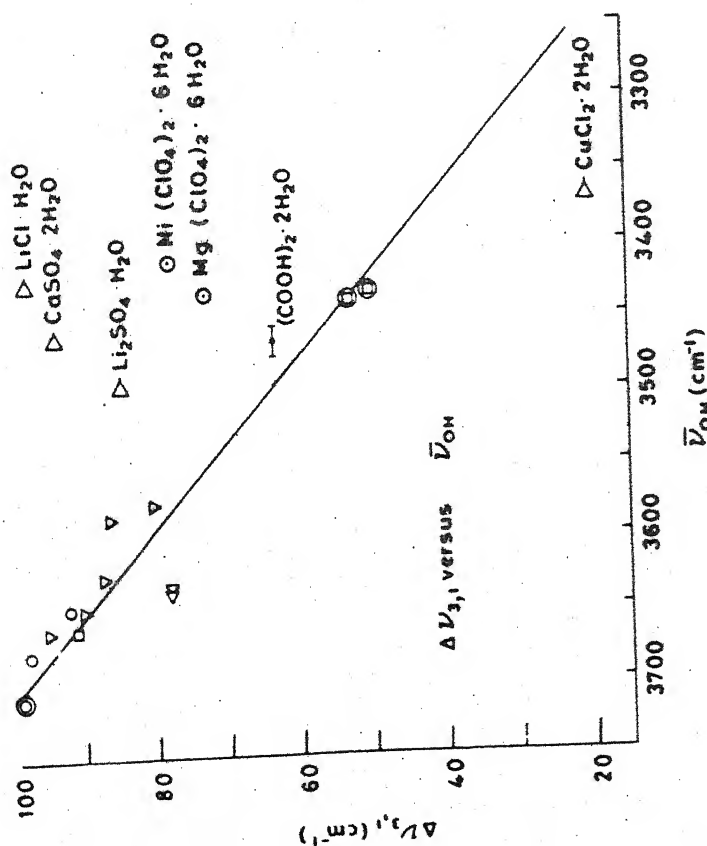
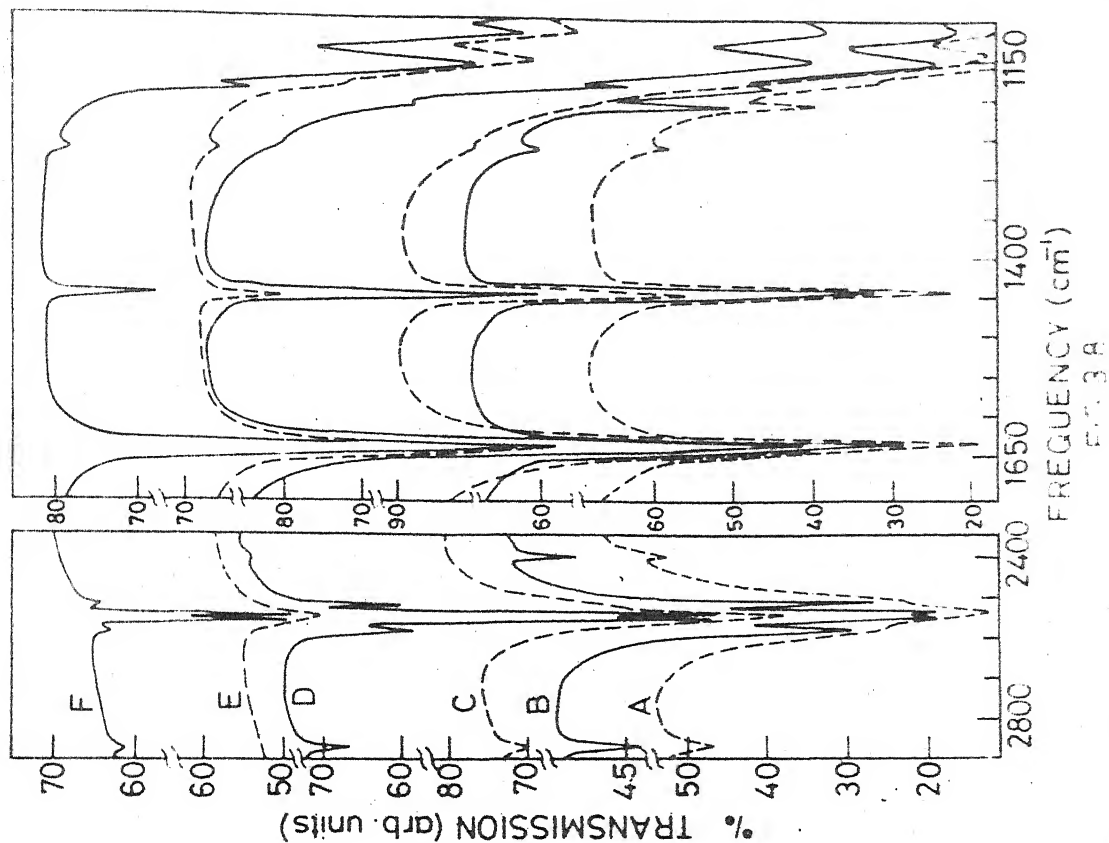


FIG. 3.7

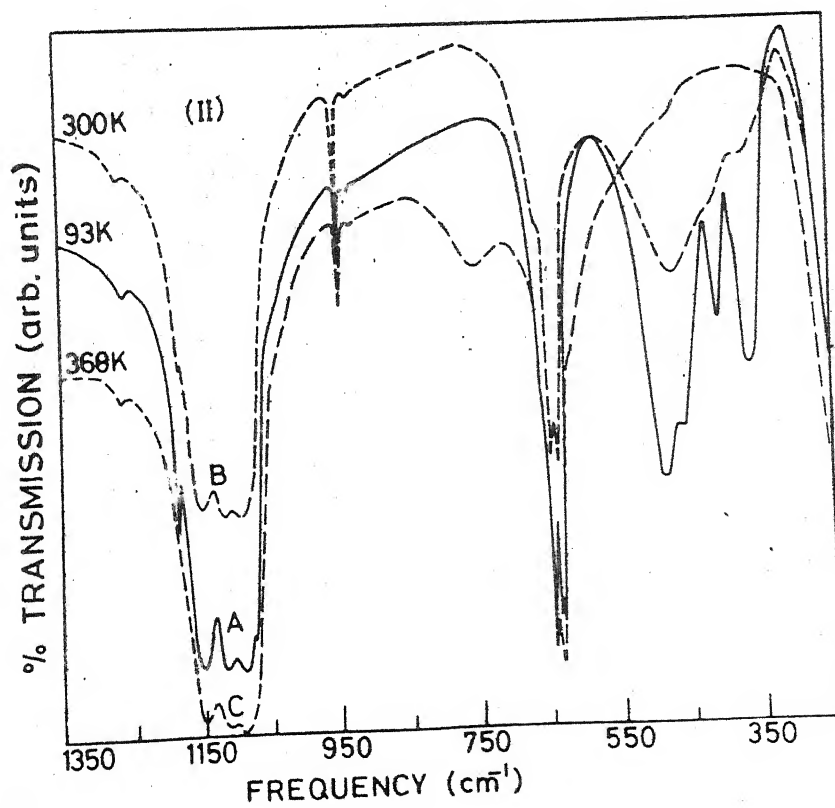
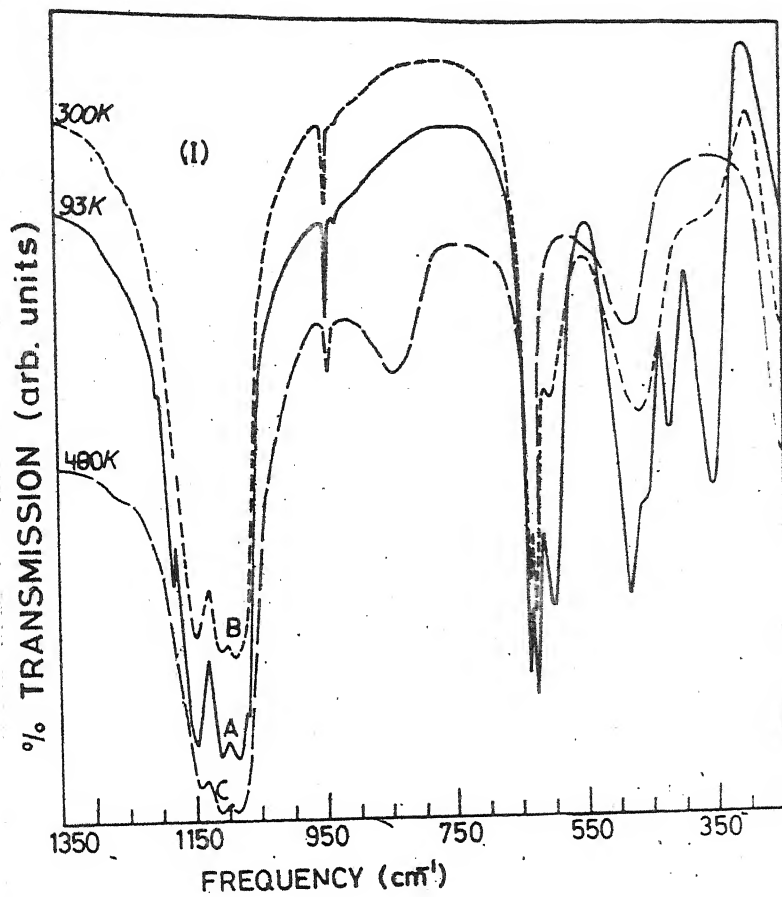


FIG. 3.9

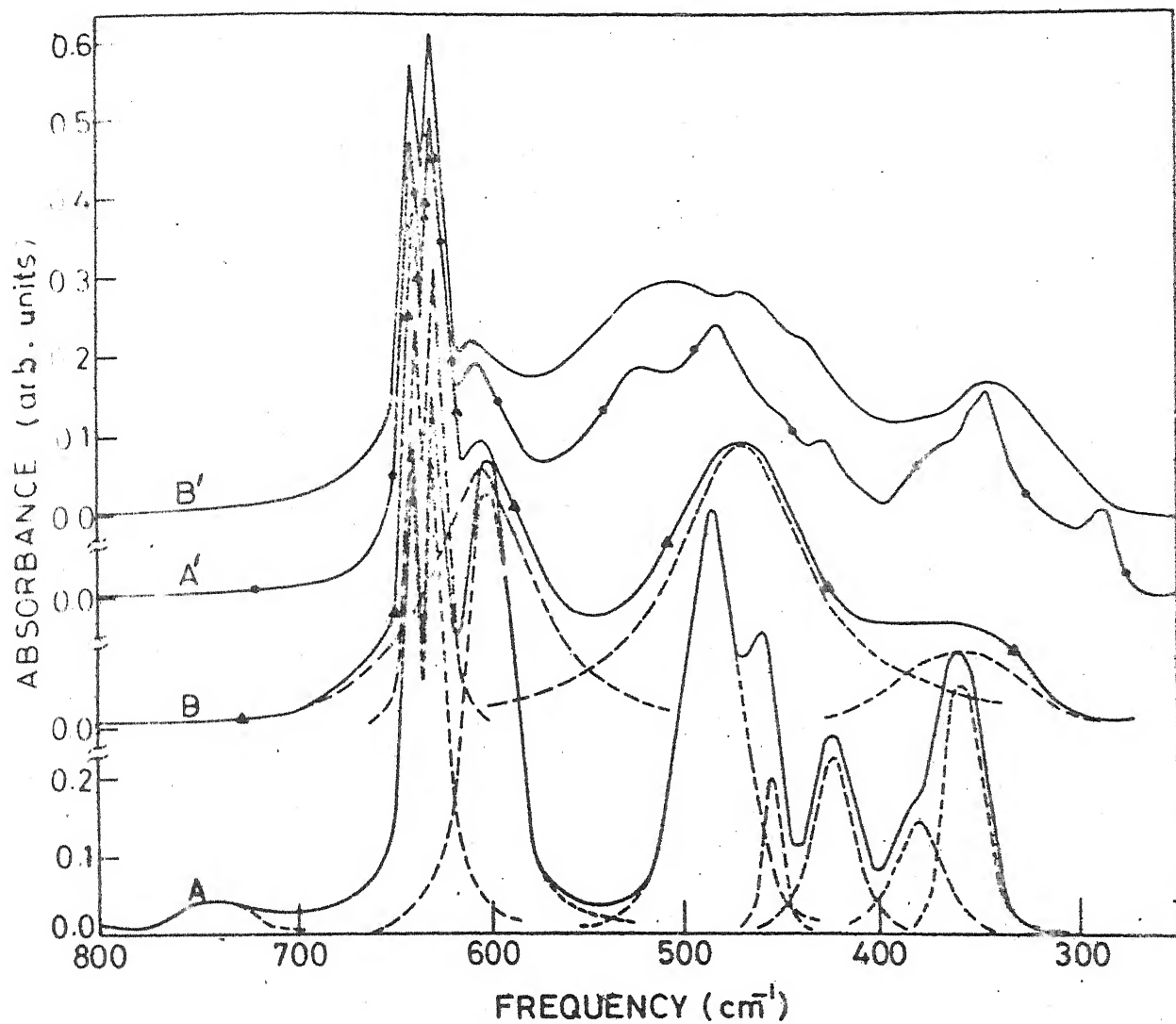


FIG. 3.10

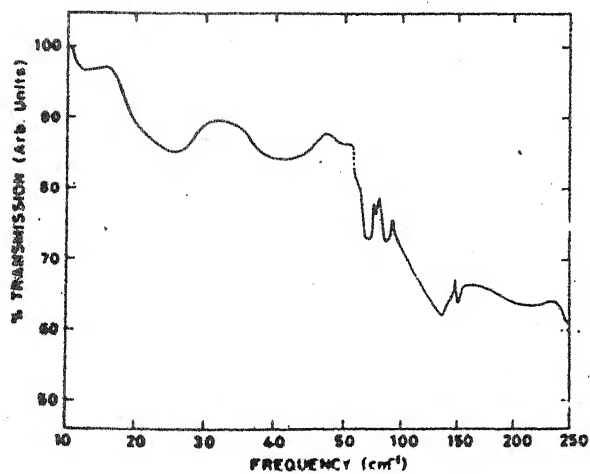


FIG. 3.11

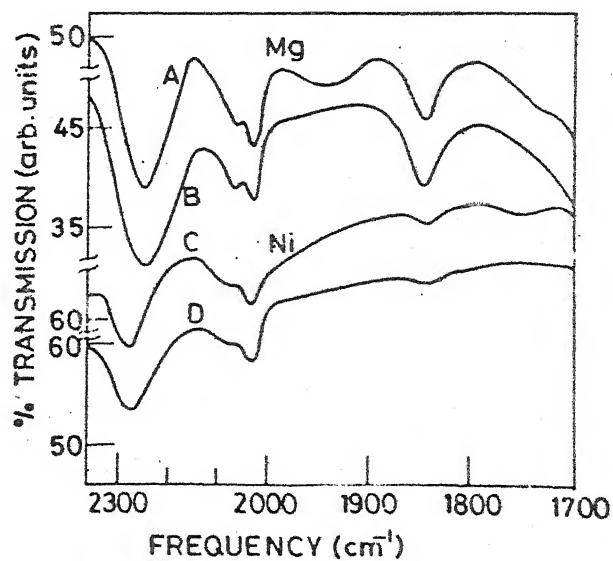


FIG. 3.12

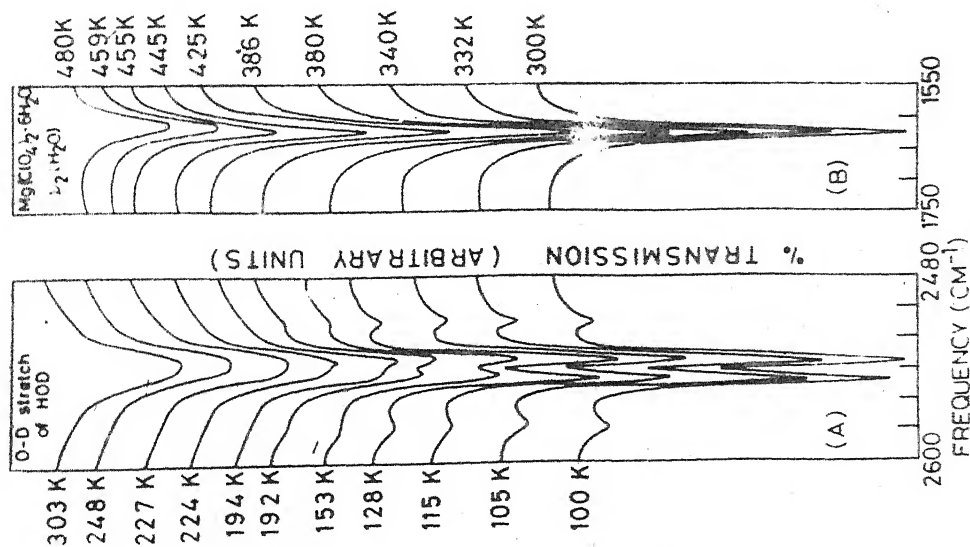


FIG. 313

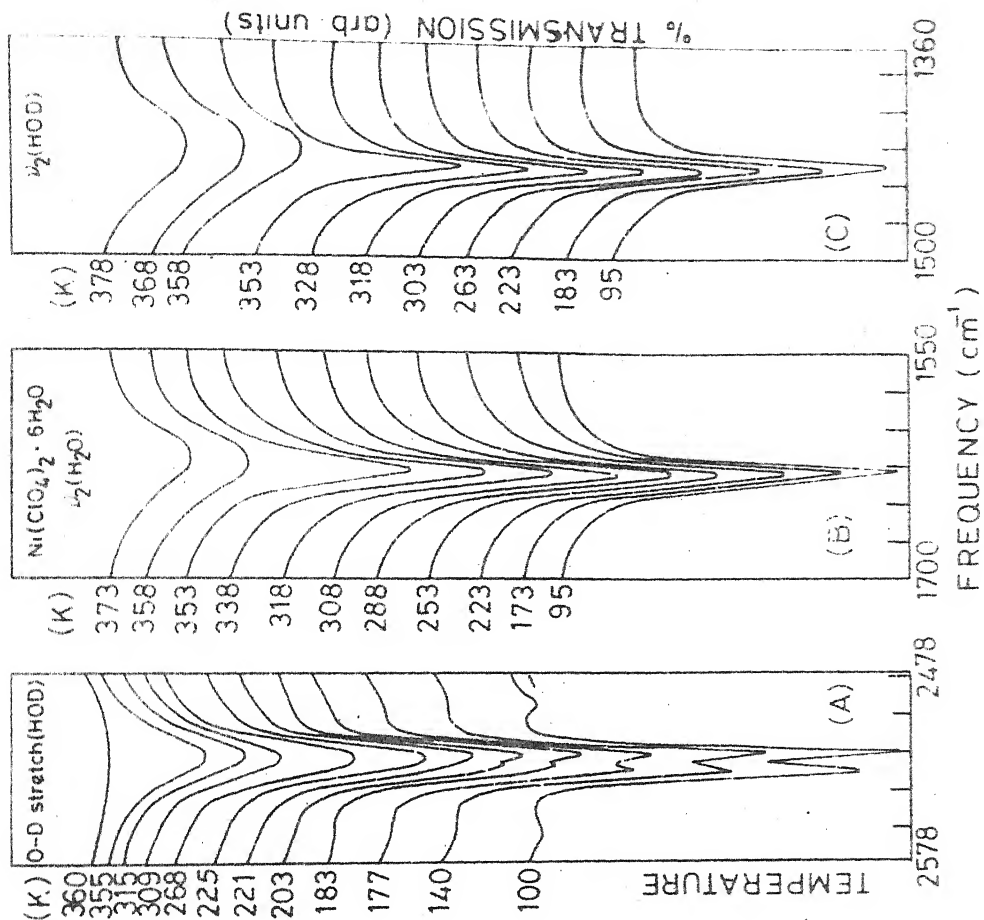


FIG. 314

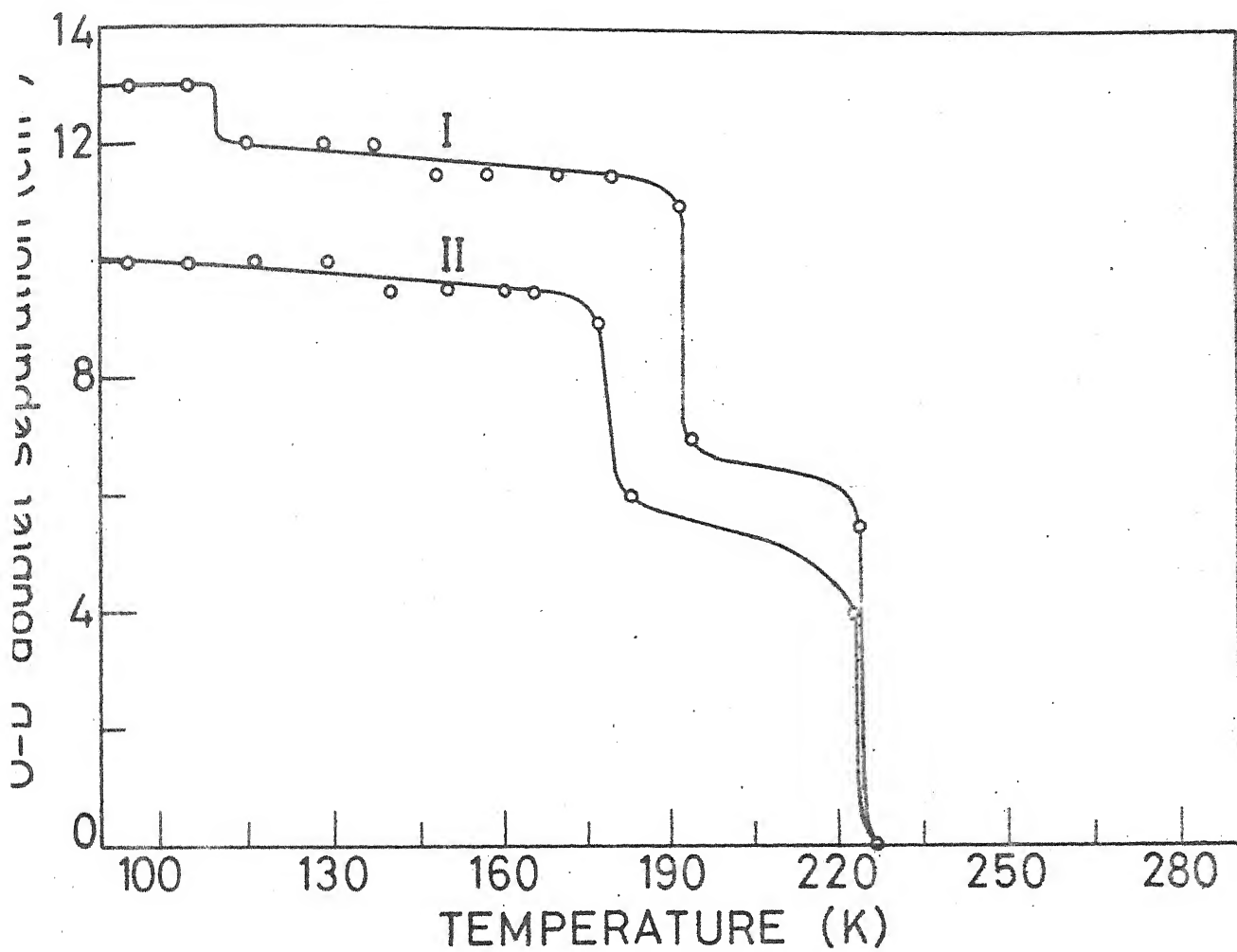


FIG. 3.15

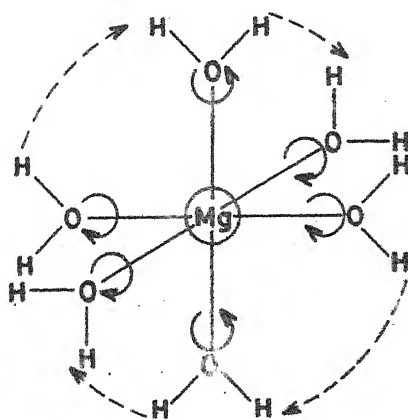


FIG. 3.16

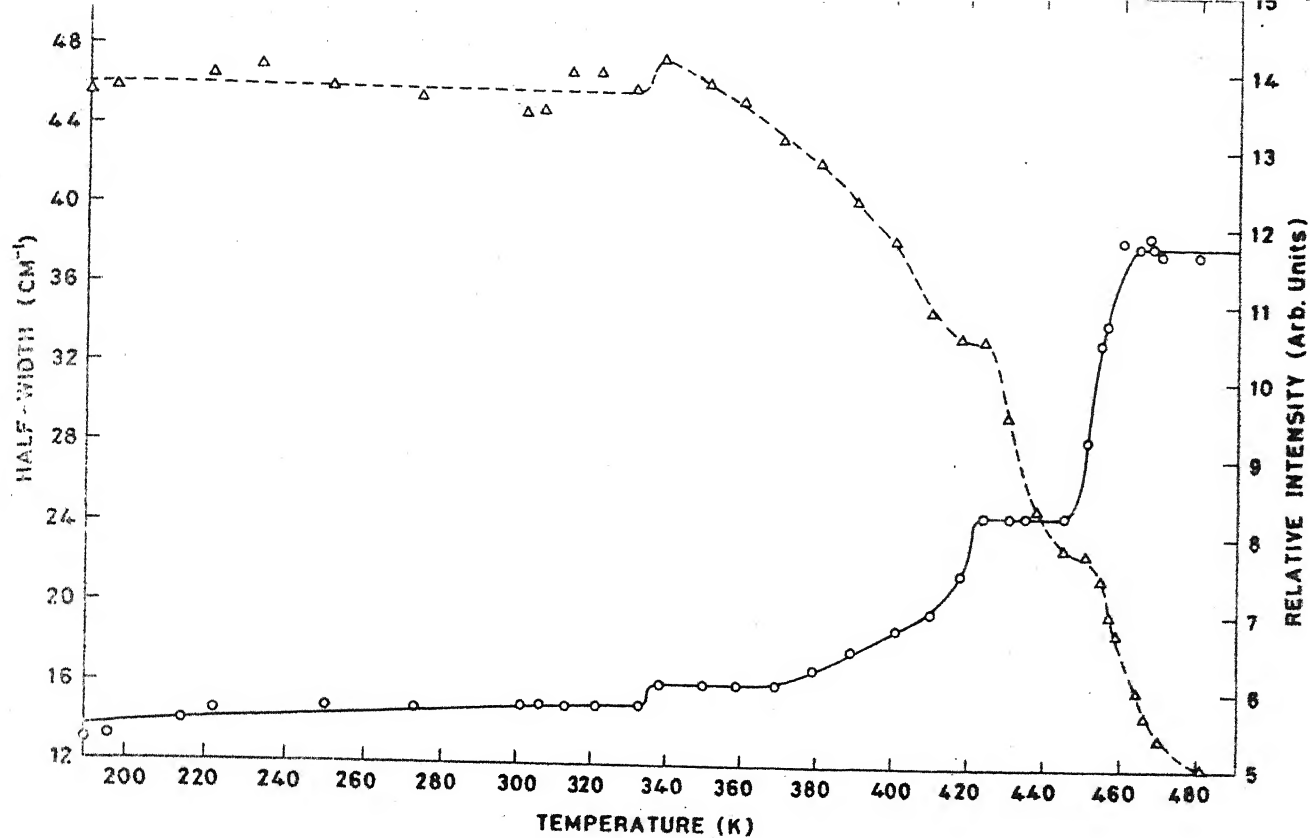


FIG. 3.17 (I)

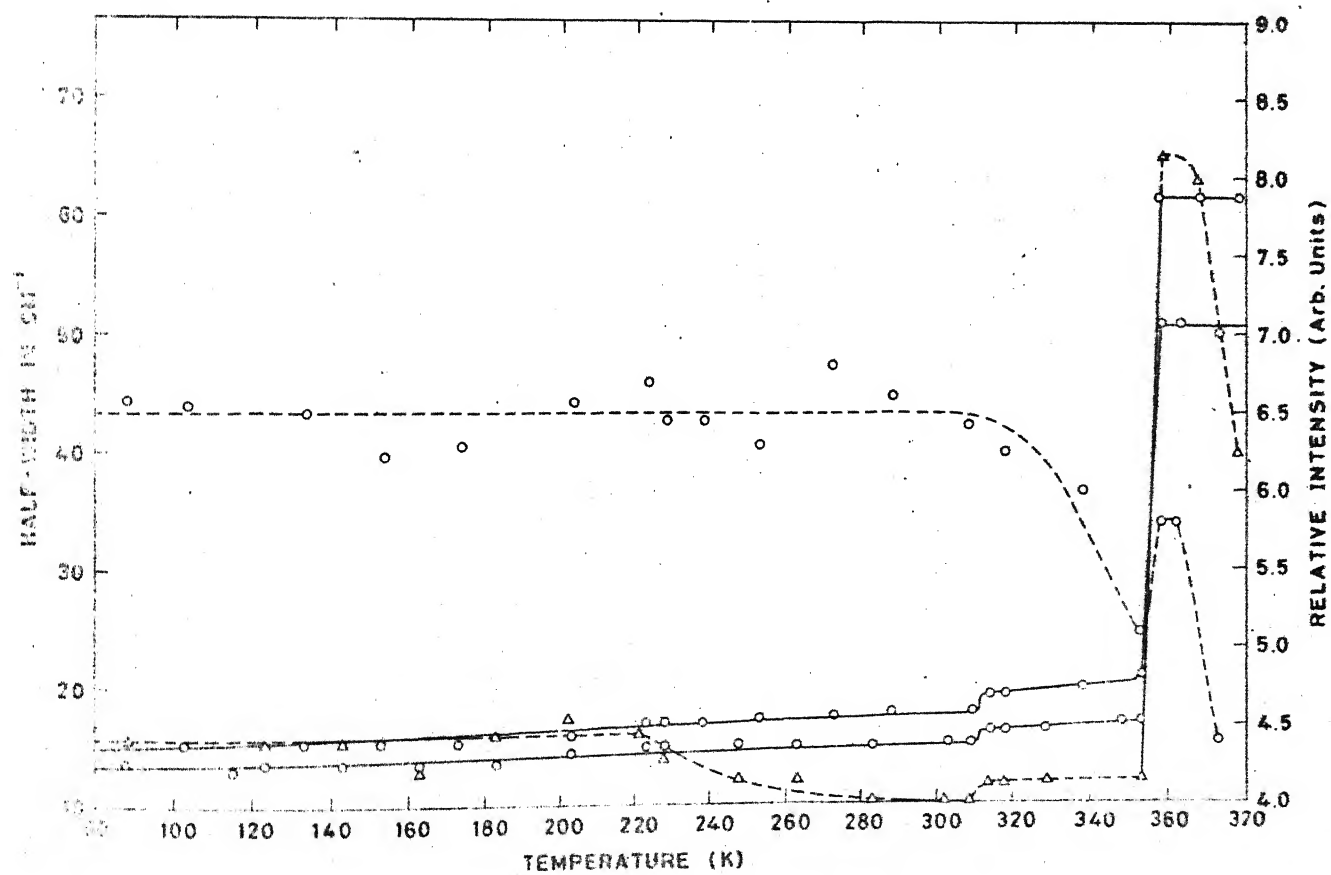


FIG. 3.17 (II)

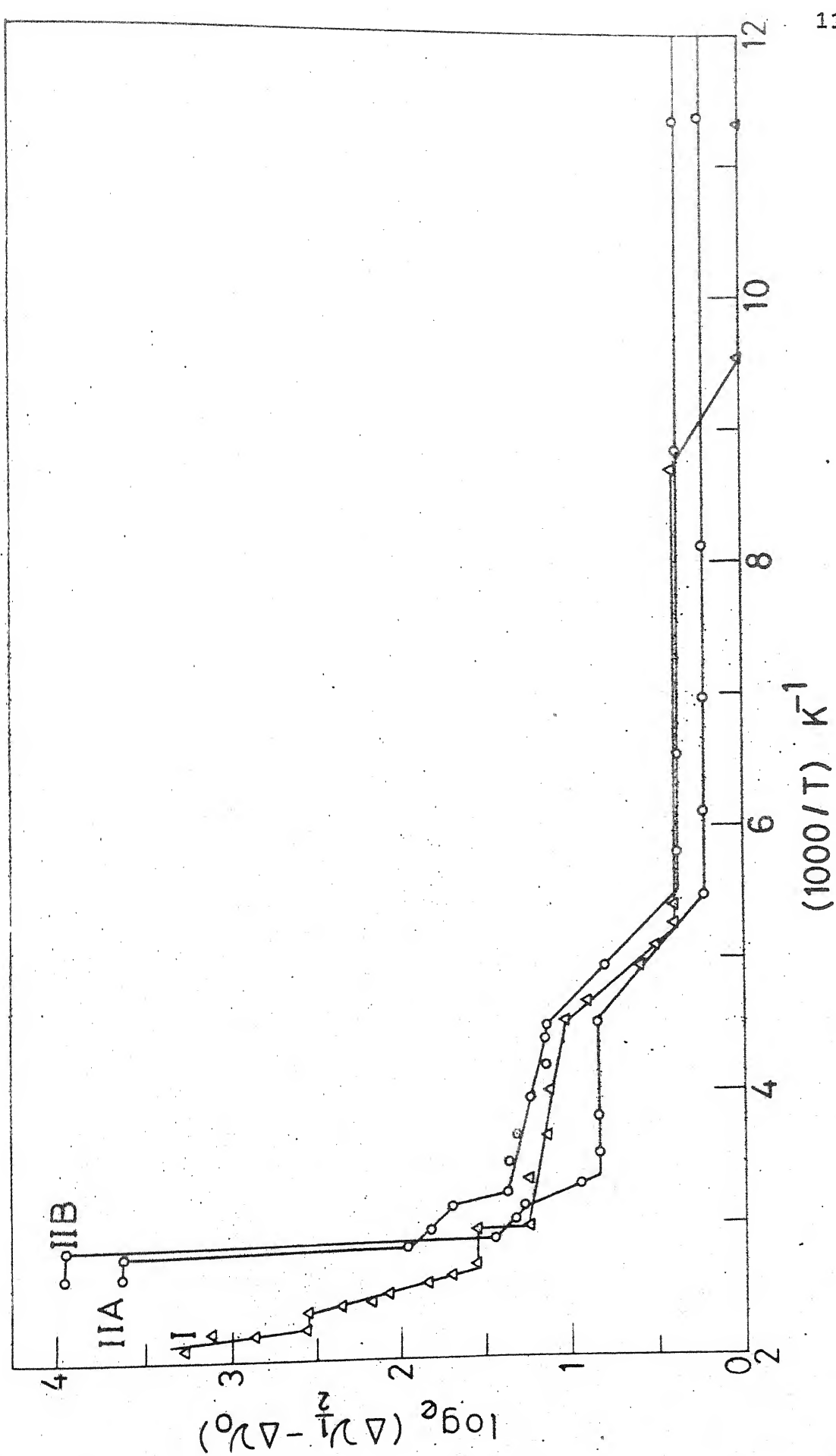


FIG. 3.18

## CHAPTER IV

### VIBRATIONAL STUDIES AND PHASE TRANSITIONS IN COBALT AND MANGANESE PERCHLORATE HEXAHYDRATES

#### ABSTRACT

Detailed vibrational assignments of cobalt and manganese perchlorate hexahydrates (CoPH + MnPH), based on their RT and LT infrared and RT Raman spectra and on comparison with the spectra of MPH and NPH, are proposed. The thermal evaluation of infrared spectra confirms phase transitions at 166, 240-288 and 333 K in CoPH and 161 K in MnPH and further suggests new phase transitions at 248 and 341 K in MnPH. The transition at 240 and 333 K in CoPH and 248 and 341 K in MnPH are assigned to the displacement of water octahedra to two distinguishable site symmetries. At LT the space group changes from  $C_{2v}^7$  to  $C_s^1$  and two types of lattices are identified. Both the lattices are disordered ones in MnPH while one of the lattice is ordered in CoPH. The phase transitions at 166 and 160 K in CoPH and MnPH respectively are attributed to the distortion of water molecules in the crystals.



#### 4.1 INTRODUCTION

The infrared (IR) spectra of cobalt perchlorate hexahydrate (CoPH) have been reported by Ross (1) for the fundamental vibrations of the perchlorate group. He has suggested that the observed splittings in  $\nu_3(p)$  and  $\nu_4(p)$  bands are due to distortion of  $\text{ClO}_4$  tetrahedron in CoPH in the crystal lattice. Later Balicheva et al (2) reported single crystal IR spectra of both CoPH and manganese perchlorate hexahydrate (MnPH) in the OH stretching region. They reported only two bands for each compound and assigned the high frequency band around  $3530\text{ cm}^{-1}$  as OH vibration in  $\text{M-O-H}\dots\text{OClO}_3$  and the lower frequency band around  $3440\text{ cm}^{-1}$  as OH vibration in  $\text{M-O-H}\dots\text{OH}_2$  rather than as  $\nu_3$  and  $\nu_1$  stretching bands of water. However,  $\text{M-O-H}\dots\text{OH}_2$  does not exist in the crystal structure (3) and thus the assignments of Balicheva et al cannot be correct. No other reports are available in literature on IR or Raman studies of these salts.

Various techniques have been used to investigate the phase transitions in CoPH and MnPH. The observed transition temperatures are summarised in Table 4.1. It can be seen that the transition temperatures reported from different techniques differ very much from each other. Therefore, with a view to clarify the structures and the nature of phase transitions we have undertaken the IR studies of the aforesaid compounds along with an analysis of the vibrational bands in analogy with magnesium and nickel perchlorate hexahydrates as discussed in chapter III.

## 4.2 RESULTS AND DISCUSSIONS

### 4.2.1 INTERNAL VIBRATIONS OF WATER

Fig. 4.1 shows the IR spectra of CoPH and MnPH in the region 3800-2700, 1800-1500 and 1300-900  $\text{cm}^{-1}$  at 300 and 100K. Fig. 4.2 shows the Raman spectra of CoPH and MnPH at room temperature (RT). The observed band frequencies both in IR and Raman along with their assignments are presented in Tables 4.2 and 4.3 for CoPH and MnPH respectively.

The available structural information on CoPH and MnPH implies that the two hexahydrates are similar except for a small mismatch in interfacial angle (3) for CoPH. However, no experimental observation has been made to determine the amount of mismatch in MnPH. The structures of the two hydrates are alike is further corroborated by the striking similarities between their spectra at RT (Fig. 4.1). At RT the broadness of bands indicates that both the hydrates have disordered structures, since ordered crystal spectra are expected to consist of narrow bands (4). This conclusion is further supported by similarities between the spectra of CoPH and MnPH with Zinc perchlorate hexahydrate (will be discussed in chapter V) at RT, whose crystal structure is known to have a disordered structure (5). At LT the nature of the spectra changes, both in CoPH and MnPH, indicating that structural changes are taking place (6) in both these hydrates in going from RT to LT.

(a) Bending Region

At RT a single bending mode is observed for each hydrate (Fig. 4.1), which indicates that all the twelve water molecules in the unit cell have the same site symmetry. This is in agreement with the crystal structure (3). However, the single bending mode becomes a doublet at LT in both the hydrates. Thus, at LT the water molecules in the unit cell occupy sites of two different symmetries, so that the crystal structure no more has  $C_{2v}^7$  space group. Though the bending mode becomes doublet in both the hydrates at LT, yet the nature of band shapes is different in the two salts. In the case of CoPH the central component is intense and sharp and it is superimposed on a broad band. The shape of the intense and sharp band is identical with that of MPH and NPH as discussed in chapter III. In MnPH there is clear splitting into two broad bands, but the band-width of each is less as compared to that of the broad bending mode of CoPH. Since the positions and shapes of the bands belonging to the bending mode are very sensitive to the intermolecular forces in the crystal, which are both distance and orientation dependent, the above observation can be attributed to the change of intermolecular forces which behave differently at different sites in the crystal lattice. To differentiate between two types of water, we have taken the sharp bending mode as type one (I) in CoPH and the higher frequency side bending mode as type one (I) in MnPH. The other component in each case is taken as due to second type water (II). The assignments given in Tables 4.2 and 4.3 have been made accordingly.

(b) Stretching Region

In the OH stretching region (Fig. 4.1), the peak positions of  $\nu_1$  and  $\nu_3$  bands of water are not distinguishable at RT and they overlap to give a single band with a weak shoulder around  $3195\text{ cm}^{-1}$ . The asymmetric broad band can be resolved into three peaks, where the central one has the maximum intensity and that at  $3195\text{ cm}^{-1}$  is the weakest. These three components are assigned as  $\nu_1$ ,  $\nu_3$  and  $2\nu_2$  on the basis of their intensities. The antisymmetric stretch band  $\nu_3$  is stronger in intensity than the symmetric band  $\nu_1$  in IR and vice versa in Raman, while  $2\nu_2$  is the weakest in IR and was not observed in Raman. Although there will be strong mixing between the stretching modes  $\nu_1$  and  $\nu_3$ , yet we have retained the nomenclature  $\nu_1$ ,  $\nu_2$  and  $\nu_3$  for  $\text{H}_2\text{O}$  bands. The band position of  $\nu_1$  is greater than that of  $\nu_3$  agrees with model given by Sartori (7). The observed higher frequency of band  $\nu_1$  in comparison to  $\nu_3$  may be due to change in stretch-stretch interaction constant as also reported earlier (7a).

In going from RT to LT the spectrum of CoPH shows a marked change. But the spectrum of MnPH does not show any remarkable change in the nature of band shape, intensity or band positions, except that the shoulder  $2\nu_2$  is more pronounced. Therefore  $\nu_1$  and  $\nu_3$  bands for the two types of water cannot still be separated out. It seems that they fall at the same frequencies for both types of water and both the frequencies ( $\nu_1$  and  $\nu_3$ ) remain the same as at RT. In the case of CoPH, the

spectrum at LT is a broad band (like that at RT) superposed with some sharp bands. The nature and shape of the sharp bands are similar to those of the bands in MPH (discussed in chapter III), therefore these bands are assigned in analogy with MPH. The peak positions of the broad band are not identified, but one can expect that they will remain the same as in RT, as is the case in MnPh. Thus, the bands due to two types of water become different at LT in the case of CoPH and their frequencies and assignment are given in Tables 4.2 and 4.3.

#### 4.2.2 INTERNAL MODES OF PERCHLORATE, LIBRATIONAL MODES OF WATER AND METAL-OXYGEN LATTICE VIBRATIONS

Figs. 4.1 and 4.3 show the IR spectra in the ranges 1300-900 and 900-200  $\text{cm}^{-1}$  respectively for CoPH and MnPH at 300 and 100K. The observed band positions are also presented in Tables 4.2 and 4.3 along with their assignments. The bands around 1100, 940, 630 and 460  $\text{cm}^{-1}$  in both IR and Raman (Fig. 4.2) are assigned to the well-known fundamental vibrations  $\nu_3(\text{p})$ ,  $\nu_1(\text{p})$ ,  $\nu_4(\text{p})$  and  $\nu_2(\text{p})$  respectively of  $\text{ClO}_4^-$  ion in both the hydrates on the same basis as discussed in section 3.2.3(a).

The librational modes show up very weakly in both the hydrates. At RT only one very weak band is observed in each hydrate, and it is assigned as wagging mode, because wagging mode is the most intense in IR among the librational modes (8). The other librational modes are apparently too weak to be observed. But the position of rocking mode can be obtained indirectly from the observation of a weak combination band at 2240  $\text{cm}^{-1}$  in CoPH

and at  $2200\text{ cm}^{-1}$  in MnPH. This is assigned as the combination  $\nu_2(\text{water}) + \nu_R(\text{Rock})$  because both these modes involve in-plane motion already discussed in detail in section 3.2.5. The assignment leads to the conclusion that the rocking mode frequency is around  $620\text{ cm}^{-1}$  in CoPH and  $577\text{ cm}^{-1}$  in MnPH. This falls in the band profile of  $\nu_4(p)$  of  $\text{ClO}_4^-$  ion and so its presence cannot be ascertained there.

At LT a few additional bands appear weakly in the IR spectra of CoPH and MnPH. These bands are assigned as the librational modes of water and metal oxygen vibrations of the two types of water in the lattice on the following basis :

- (i) nature of band shapes
- (ii) appearance of combination mode  $\nu_2 + \nu_R$  (8),
- (iii) intensity  $I_W > I_R > I_T$  in IR (8),
- (iv) frequency sequence  $\nu_R > \nu_W > \nu_T$  (8),
- (v) effect of  $\text{M-O}_W$  coordination and hydrogen bonding on the bending mode (7,9) and
- (vi) the expected frequencies of metal-oxygen vibration (10,11).

In the case of CoPH, for water molecules (I), which show band shapes similar to those in MPH and NPH, the relations between  $\nu_{\text{OH}}$  (average) and  $\nu_R$ , and  $\nu_W$  and  $\nu_{\text{M-O}_W}$  [i.e.  $\nu_6(c)$ ] are shown in Table 4.4. When hydrogen bonding enhances, the  $\nu_{\text{OH}}$  decreases and  $\nu_R$  increases as also suggested by Oswald (12) and when  $\text{M-O}_W$  coordination occurs,  $\nu_{\text{M-O}_W}$  and  $\nu_W$  increase as also suggested by Tayal et al (13).

In the Raman spectra, the bands at  $410\text{ cm}^{-1}$  in CoPH and  $420\text{ cm}^{-1}$  in MnPH are assigned tentatively to the twist mode of

water, since it has the highest intensity in Raman. The bands at 360, 288 and  $214\text{ cm}^{-1}$  are assigned as  $\nu_1(A_{1g})$ ,  $\nu_3(F_{2g})$  and  $\nu_2(E_g)$  of metal-oxygen vibration in the octahedral aquo-complex as expected in analogy with the aquo-complex in other compounds (10). However, these bands are not observed in the case of CoPH because of poor scattered radiation due to red colour of the substance.

#### 4.2.3 COMBINATION BANDS

The bands around 2060, 2020, 1260, 1177 and  $1070\text{ cm}^{-1}$  are assigned as the combinations  $\nu_3(p) + \nu_1(p)$  ( $2060\text{ cm}^{-1}$ ),  $\nu_3(p) + \nu_1(p)$  ( $2020\text{ cm}^{-1}$ ),  $2\nu_4(p)$  ( $1260\text{ cm}^{-1}$ ),  $\nu_3(p) + \nu_L(p)$  ( $1177\text{ cm}^{-1}$ ) and  $\nu_3(p) - \nu_L(p)$  ( $1070\text{ cm}^{-1}$ ) respectively of  $\text{ClO}_4^-$  ion as in the cases of MPH and NPH (cf. Table 4.2). The combination bands involving rocking mode of water are weak, because the rocking modes themselves are very weak and broad. But in the case of CoPH at LT the combination mode appears identically as observed in MPH and NPH. Thus, it indicates that the mixing of bending and rocking modes is stronger for sharp bands but becomes weaker as the widths of the bands increase.

#### 4.2.4 PHASE TRANSITIONS

Figs. 4.1 and 4.3 show the observed bands in the IR spectra of CoPH and MnPH at RT and LT. The nature of band shapes at RT and LT indicates that some structural change is taking place in these hydrates on lowering of temperature. Therefore, we have carried out the temperature dependence study of the most thermosensitive band of water, viz.  $\nu_2$ , to detect

the transition temperatures. This temperature dependence for both the hydrates CoPH and MnPH is shown in Fig. 4.4. For CoPH the intensity of bending mode is plotted against temperature in Fig. 4.5 (dotted line). The intensity of this sharp band increases with lowering of temperature without any appreciable change in the band position and it shows discontinuities at 166, 240-288 and 333 K.

For MnPH the half-width of the bending mode is also plotted against temperature in Fig. 4.5 (solid line). The half-width enhances in MnPH with decrease of temperature without any appreciable change in peak intensity. This plot shows discontinuities at 161, 248 and 341 K.

The discontinuities near 240 in CoPH and 248 K in MnPH are associated with the appearance of a doubling in the bending mode, which indicates that in the new phase not all the water molecules in the unit cell are equivalent, but they occupy two distinguishable sites in the new lattice. There are two possible ways that the water molecules can occupy two different sites. They are :

- (i) There are two aquo-octahedral complexes in the unit cell at RT, which are distributed randomly at RT but are ordered by displacements or reorientation to occupy two distinguishable sites at LT, or
- (ii) the water molecules form two different sets (each of three) in one aquo-octahedral complex and get reoriented at LT in such a way that the sets become distinguishable. The former possibility



seems to be more probable than the latter, which cannot explain the observed two different  $M-O_w$  vibrations from  $M(OH_2)_6$  complex (10). Two different  $M-O_w$  vibrations (having similar natures of band shape in CoPH and MnPH in the same region) are also not observed in the case of MPH and NPH as described in section 3.2.3(b). Hence the formation of two different  $M(OH_2)_6$  complexes in the unit cell is more probable. Two distinguishable  $Mn^{2+}$  complexes in CoPH have been observed by EPR (14,15), which gives direct evidence of formation of distinguishable complexes. As given in Table 4.1 the reported transition temperatures are around 264 K, 243 K (or both). Our plot of the peak intensity of the bending mode with temperature (Fig. 4.5 dotted line) shows that in the cooling process the transition actually starts at 288 K and is completed at 240 K.

Some tentative conclusions on the basis of observed spectra can be drawn regarding the site symmetries of  $H_2O$  molecules in the crystal. In CoPH one of the site symmetries of aquo-complex has identical situation with that in MPH (chapter III) and the other one with that in Zinc perchlorate hexahydrate (ZPH). Thus, the two basal planes in the crystal (3,6) are no more identical at LT as they are at RT because of displacement and/or reorientation of aquo-complex, resulting in two different site symmetries. Similar arguments are also applicable for MnPH. Now on attributing the doublet in bending mode to the two aquo-complexes of different site symmetries, it is evident that the two fold screw and glide plane symmetries are lost in the crystal. However, the mirror plane symmetry may still exist.

Therefore, the space group  $C_{2v}^7$  is reduced to one of the following two possible space groups,  $C_s^1$  and  $C_s^3$ . If one takes the primitive cell having two distinguishable site symmetries (with two formula units), the space group below the transition temperature is reduced to  $C_s^1$  only. Jain et al (15) observed two different spectra of  $Mn^{2+}$  complex in CoPH, but suggested that the space group did not change from  $C_{2v}^7$ . This appears untenable because in  $C_{2v}^7$  space group no two distinguishable sites are possible.

The minor discontinuities at 166 K in CoPH and at 161 K in MnPH have been observed in other studies also (14,15,18-20). They do not give conclusive evidence about the mechanism of phase transition, but from CoPH spectra it appears that distortion of water molecules might be responsible for it. A detailed study of this distortion is not possible in the present case because of the broadness of the bands unlike those in MPH. However, if the molecules get distorted in this transition, then the mirror plane symmetry will be lost further. Therefore, no symmetry will exist and the space group  $C_s^1$  is reduced to  $C_1^1$  only. The piezoelectric effect in CoPH and MnPH reported by Svare et al (19) might be due to this reduction in the space group symmetry.

From Fig. 4.4 one can see that as the temperature rises above RT asymmetry appears in the bending mode around 333 K in CoPH and 341 K in MnPH. However, these modes are not well resolved as in the LT phase because of thermal broadening. The appearance of asymmetry in this mode indicates that all the twelve water molecules in the unit cell are not equivalent and occupy two different sites as at LT. Thus we can say that the mechanisms

of transitions in CoPH and MnPH at high (333 and 341 K) and low temperatures (288 and 248 K) respectively, are the same. This observation is in agreement with EPR (15) study. Therefore, the space group above the transition temperature is  $C_s^1$ , with two molecules per unit cell.

#### REFERENCES

1. S.D. Ross, Spectrochim. Acta 18, 225 (1962).
2. T.G. Balicheva and S.N. Andreev, J. Struct. Chem. 5, 23 (1964).
3. C.D. West, Z. Kristallogr. 91A, 480 (1935).
4. D.F. Hornig, J. Chem. Phys. 17, 1346 (1949).
5. M. Ghosh and S. Ray, Z. Kristallogr. 145, 146 (1977).
6. J. Shiffer, Ph.D. Thesis, Princeton Univ., Princeton, N.J. (1963).
7. G. Sartori, C. Furlani and A. Damiani, J. Inorg. Nucl. Chem. 8, 119 (1959).
- 7a. D.F. Hornig, H.F. White and F.P. Reding, Spectrochim. Acta 12, 338 (1958).
8. V.P. Tayal, B.K. Srivastava, D.P. Khandelwal and H.D. Bist, Appl. Spectros. Rev. 16, 43 (1980) (and references therein).
9. M. Falk and O. Knop, in "Water - A Comprehensive Treatise" Vol. II, F. Franks (ed.), Plenum Press, New York-London (1973) page 55 (and references therein).
10. V. Ananthanarayanan, Z. Phys. Chem. 222, 102 (1963).
11. I. Nakamoto and T. Shimanouchi, Spectrochim. Acta 20, 429 (1964).
12. H.R. Oswald, Helv. Chim. Acta 48, 590 (1965).
13. V.P. Tayal, D.P. Khandelwal and H.D. Bist, Chem. Phys. Lett. 55, 136 (1978).
14. R. Dayal, D.R. Rao and P. Venkateswarlu, J. Magn. Reson. 36, 99 (1979).
15. A.K. Jain and G.C. Upreti, J. Phys. C13, 5177 (1980).
16. M.P. Sinha, M. Pal and S.K. Dutta Roy, J. Phys. C9, 2783 (1976).
17. B.K. Chaudhuri, Solid State Commun. 16, 767 (1975).
18. B.K. Chaudhuri, J. Phys. C8, 1884 (1975).
19. I. Svare and B.O. Fimland, J. Chem. Phys. 74, 5977 (1981).
20. I. Dezsi and L. Keszthelyi, Solid State Commun. 4, 511 (1966).
21. B.K. Chaudhuri, J. Phys. C9, 1285 (1976).

Table 4.1: Phase transition temperatures observed in CoPH and MnPH by different techniques.

Experimental techniques used	Temperatures (K)			
	CoPH <sup>(a)</sup>		MnPH <sup>(a)</sup>	
Magnetic susceptibility and anisotropy	245-264	(16)	120	(17, 21)
	166	(17, 18)		
Specific heat	263	(16)	134	(16)
	240	(16)		
	215	(16)		
Piezoelectricity	160	(19)	160	(19)
			89	(19)
Mössbauer	148-163	(20)		
EPR	264	(14)		
	148-161	(14)		
	354	(15)		
	243	(15)		
	155	(15)		
Infrared <sup>(b)</sup>	333		341	
	240-288		248	
	166		161	

(a) The figures in paranthesis denote the references cited at the end of the chapter.

(b) Present study.

Table 4.2: Frequencies (in  $\text{cm}^{-1}$ ) of IR and Raman bands of micro-crystalline CoPH powder.

Infrared		Raman		Assign- ment	Infrared		Raman		Assign- ment
LT	RT	RT			LT	RT	RT		
3525	3525	3515	$\nu_1(\text{II}, \text{w})$		1083	1085	1084	$\nu_3(\text{p})$	
3460			$\nu_3(\text{I})$		1070			$\nu_3(\text{p}) - \nu_{\text{L}}(\text{p})$	
3440	3440		$\nu_3(\text{II}, \text{w})$		943	943	930	$\nu_1(\text{p})$	
3413	}		Uncoupled stretching bands (I)		926	924		$\nu_1(\text{p}) - \nu_{\text{L}}(\text{p})$	
3385					638	637		$\nu_4(\text{p})$	
3370			$\nu_1(\text{I})$		631		630	$\nu_4(\text{p})$	
3222			$2\nu_2(\text{I})$		627	628		$\nu_4(\text{p})$	
3190	3195		$2\nu_2(\text{II}, \text{w})$		636			$\nu_{\text{R}}(\text{I})$	
2250	2240		$\nu_2 + \nu_{\text{R}}(\text{I}, \text{II}, \text{w})$			515		$\nu_{\text{W}}(\text{w})$	
2060	2060		$\nu_3(\text{p}) + \nu_1(\text{p})$		493			$\nu_{\text{W}}(\text{II})$	
2020	2020		$\nu_3(\text{p}) + \nu_1(\text{p})$		455	455	459	$\nu_2(\text{p})$	
1622			$\nu_2(\text{I})$		462			$\nu_{\text{W}}(\text{I})$	
1618	1620	1610	$\nu_2(\text{II}, \text{w})$		440			$\nu_{\text{T}}(\text{I})$	
1260	1260		$2\nu_4(\text{p})$				410	$\nu_{\text{T}}(\text{w})$	
1182	1177		$\nu_3(\text{p}) - \nu_{\text{L}}(\text{p})$		382			$\nu_6(\text{cI})$	
1146	1142		$\nu_3(\text{p})$		352			$\nu_6(\text{cI})$	
1107	1109	1116	$\nu_3(\text{p})$		345			$\nu_6(\text{cII})$	

R, W, T and L stand for rocking, wagging, twisting modes of water and lattice modes of perchlorate, respectively.

p, I, II, w and c stand for perchlorate, water molecules of type one, water molecules of type two, water molecules when both type one and type two are equivalent or same type and aquo-complex  $\text{M}(\text{OH}_2)_6$ , respectively.

Table 4.3: Frequencies (in  $\text{cm}^{-1}$ ) of IR and Raman bands of micro-crystalline MnPH powder.

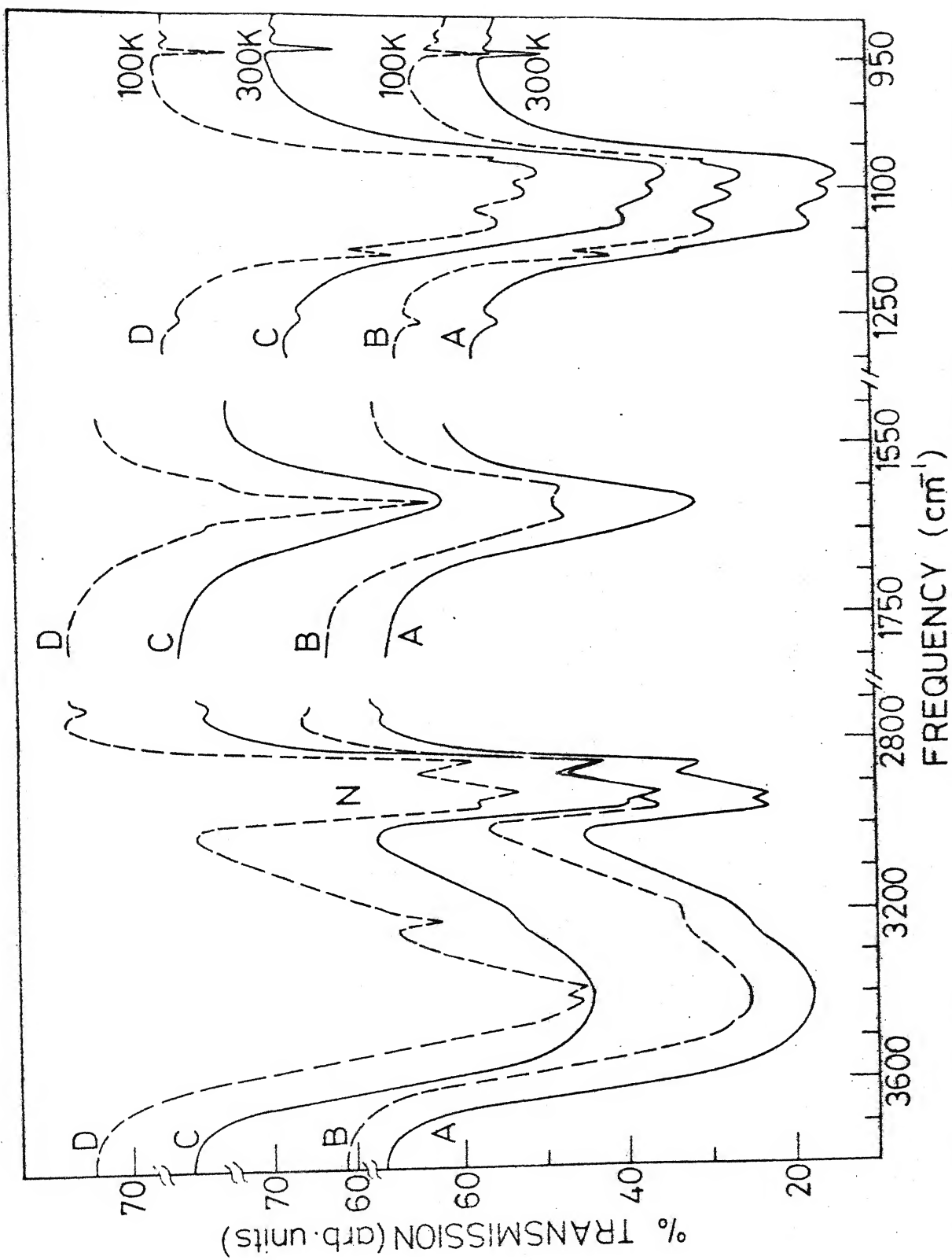
<u>Infrared</u>		<u>Raman</u>		<u>Assignment</u>	<u>Infrared</u>		<u>Raman</u>		<u>Assignment</u>
LT	RT	RT			LT	RT	RT		
3520	3520	3524		$\nu_1(\text{I, II, w})$	1086	1088	1086		$\nu_3(\text{p})$
3420	3420			$\nu_3(\text{I, II, w})$	1070				$\nu_3(\text{p}) - \nu_L'(\text{p})$
3240				$2\nu_2(\text{I})$	943	943	934		$\nu_1(\text{p})$
	3200			$2\nu_2(\text{w})$	927	926			$\nu_1(\text{p}) - \nu_L'(\text{p})$
3170				$2\nu_2(\text{II})$	636	637			$\nu_4(\text{p})$
2270				$\nu_2(\text{I}) + \nu_R'(\text{I})$	631	631	634		$\nu_4(\text{p})$
	2200			$\nu_2(\text{w}) + \nu_R'(\text{w})$	625	627			$\nu_4(\text{p})$
2180				$\nu_2(\text{II}) + \nu_R'(\text{II})$	575				$\nu_W(\text{I})$
2060	2060			$\nu_3(\text{p}) + \nu_1(\text{p})$		525			$\nu_W(\text{w})$
2020	2020			$\nu_3(\text{p}) + \nu_1(\text{p})$	493				$\nu_W(\text{II})$
1640				$\nu_2(\text{I})$	458	458	466		$\nu_2(\text{p})$
	1623	1623		$\nu_2(\text{w})$			420		$\nu_T(\text{w})$
1605				$\nu_2(\text{II})$			360		$\nu_1(\text{cw})$
1261	1260			$2\nu_4(\text{p})$	355				$\nu_6(\text{cI})$
1182	1178			$\nu_3(\text{p}) + \nu_L'(\text{p})$	344				$\nu_6(\text{cII})$
1148	1143			$\nu_3(\text{p})$			288		$\nu_3(\text{cw})$
1110	1108	1115		$\nu_3(\text{p})$			214		$\nu_2(\text{cw})$

R, W, T and L stand for rocking, wagging, twisting modes of water and lattice modes of perchlorate, respectively.

p, I, II, w and c stand for perchlorate, water molecules of type one, water molecules of type two, water molecules when both type one and two are equivalent or same type and aquo-complex,  $\text{M}(\text{OH}_2)_6$ , respectively.

FIGURE CAPTIONS

- Fig.4.1: Infrared spectra in the ranges 3800-2700, 1800-1500 and 1300-900  $\text{cm}^{-1}$  of:  $\text{Mn}(\text{ClO}_4)_2 \cdot 6\text{H}_2\text{O}$  at 300 K (curve A) and 100 K (curve B);  $\text{Co}(\text{ClO}_4)_2 \cdot 6\text{H}_2\text{O}$  at 300 K (curve C) and 100 K (curve D).
- Fig.4.2: Room temperature Raman spectra of  $\text{Mn}(\text{ClO}_4)_2 \cdot 6\text{H}_2\text{O}$  (curve A) and  $\text{Co}(\text{ClO}_4)_2 \cdot 6\text{H}_2\text{O}$  (curve B).
- Fig.4.3: Infrared spectra in ranges 2490-1900 and 900-200  $\text{cm}^{-1}$  of:  $\text{Mn}(\text{ClO}_4)_2 \cdot 6\text{H}_2\text{O}$  at 300 K (curve A) and 100 K (curve B);  $\text{Co}(\text{ClO}_4)_2 \cdot 6\text{H}_2\text{O}$  at 300 K (curve C) and 100 K (curve D).
- Fig.4.4: Temperature dependence of bending mode of water in  $\text{Mn}(\text{ClO}_4)_2 \cdot 6\text{H}_2\text{O}$  and  $\text{Co}(\text{ClO}_4)_2 \cdot 6\text{H}_2\text{O}$ .
- Fig.4.5: Solid line: Half-width versus temperature of bending mode of water in  $\text{Mn}(\text{ClO}_4)_2 \cdot 6\text{H}_2\text{O}$ .  
Dotted line: Peak intensity versus temperature of bending mode of water in  $\text{Co}(\text{ClO}_4)_2 \cdot 6\text{H}_2\text{O}$ .





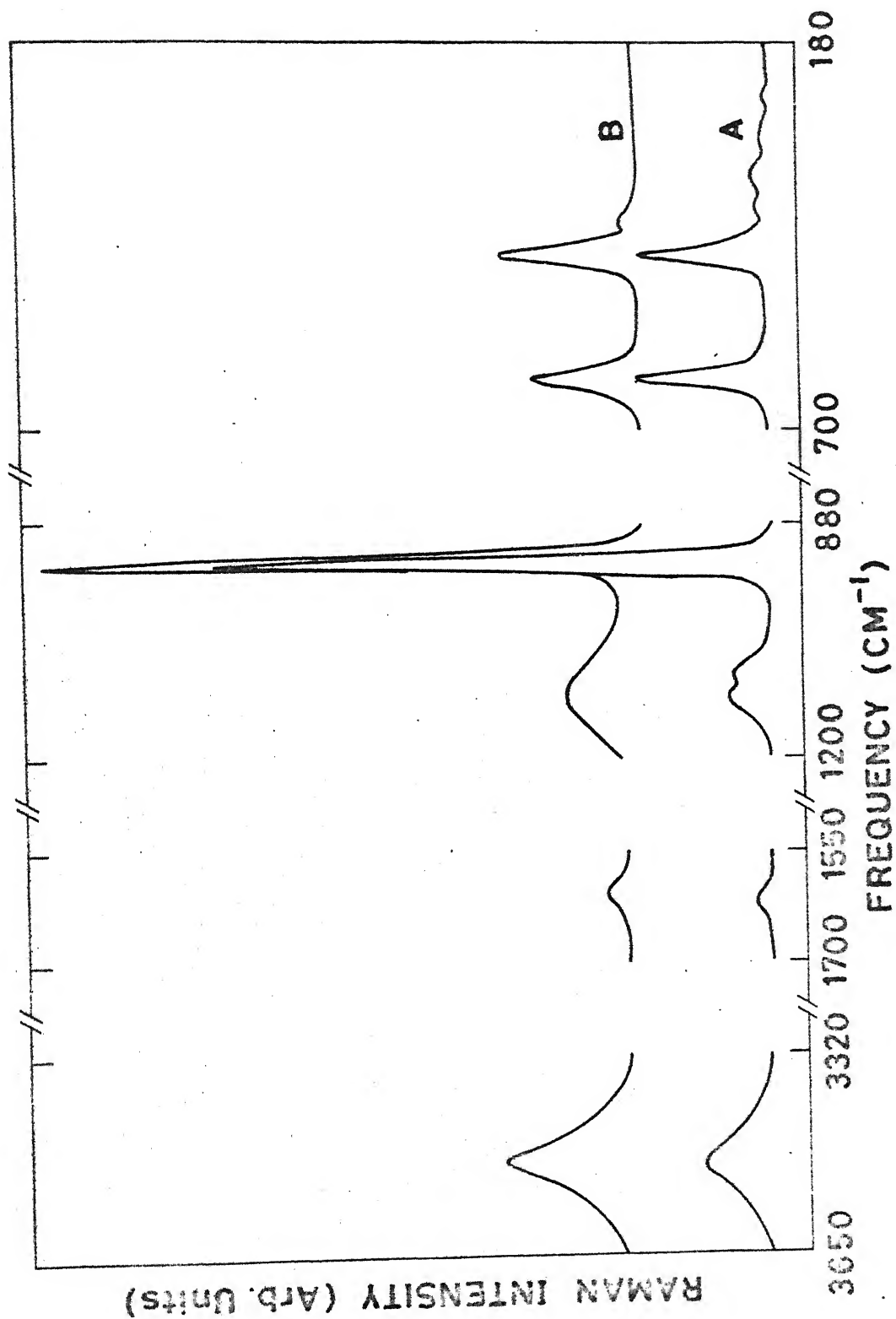
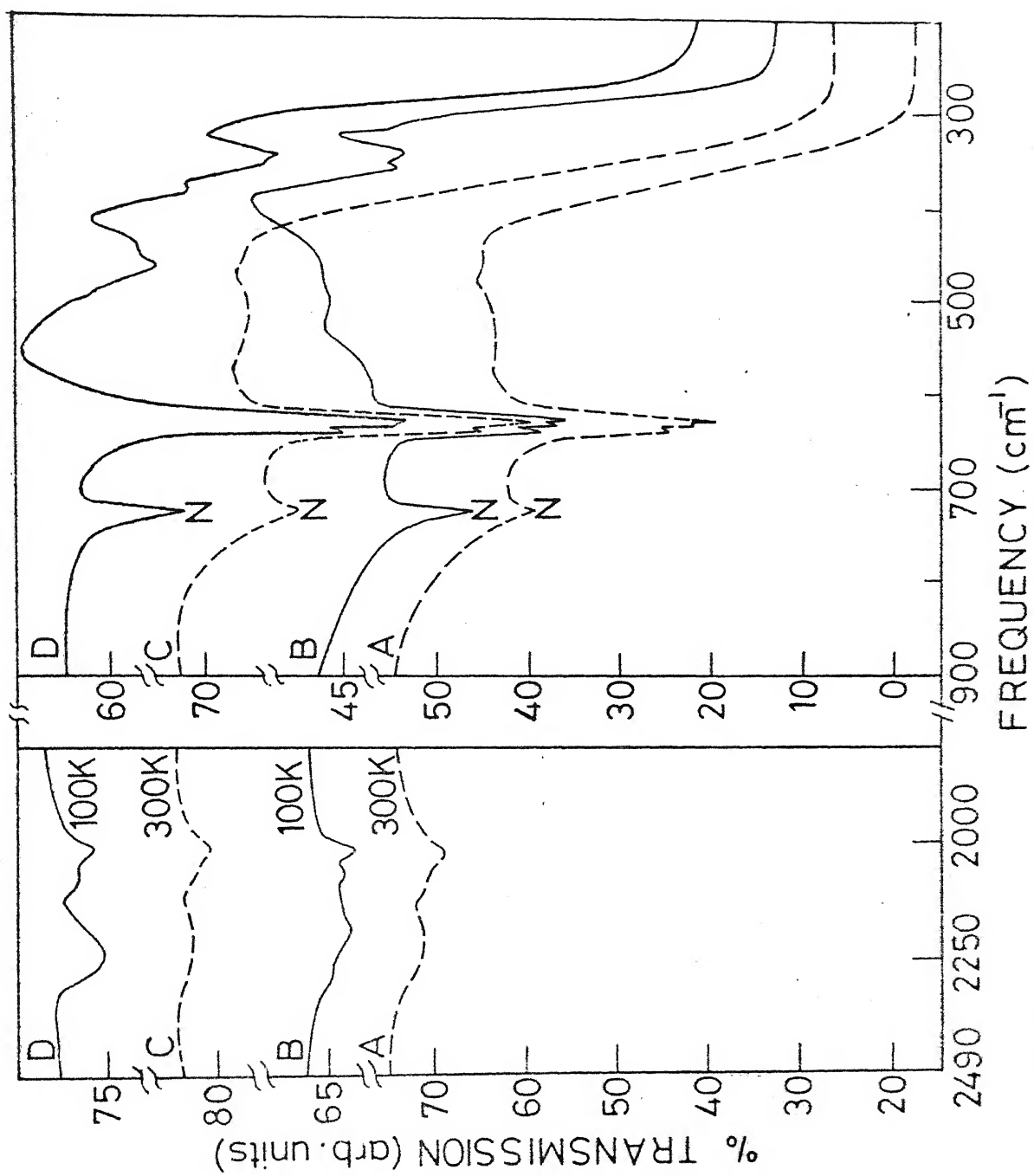


FIG. 4.2



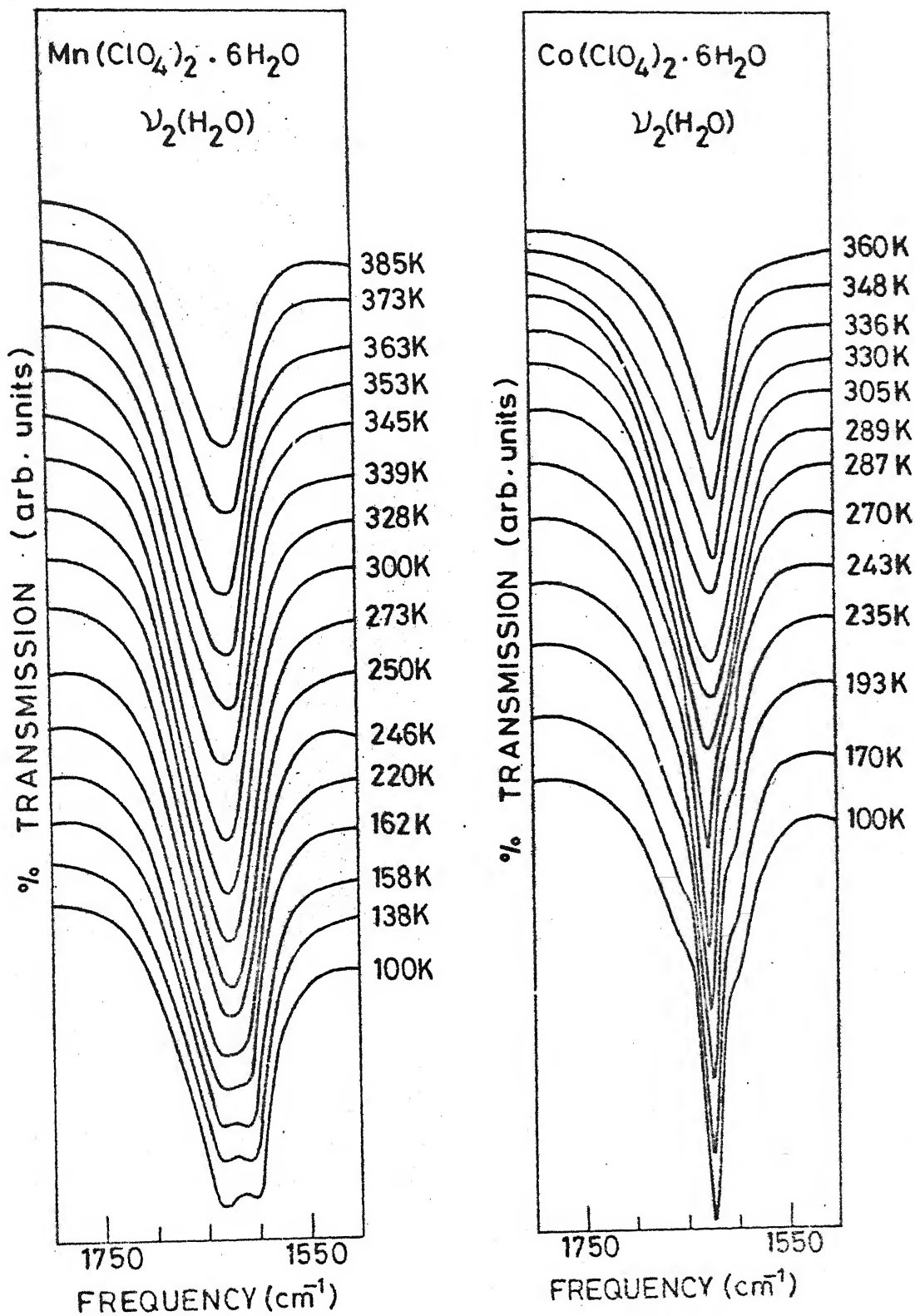


FIG. 4.4

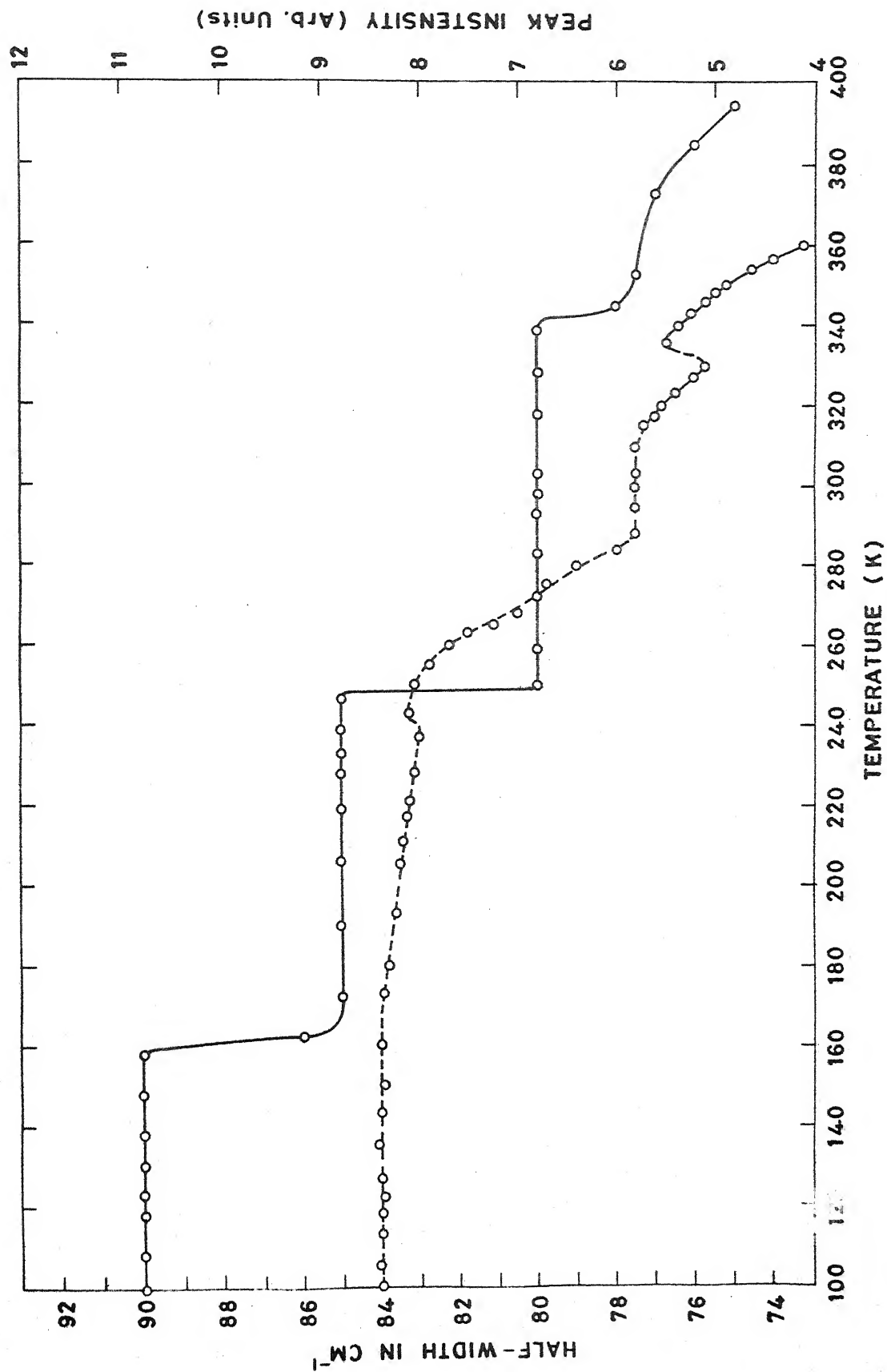


FIG. 4.5

## CHAPTER V

### VIBRATIONAL STUDIES AND PHASE TRANSITIONS IN ZINC PERCHLORATE HEXAHYDRATE\*

#### ABSTRACT

The assignments of the vibrations associated with  $\text{ClO}_4^-$ ,  $\text{H}_2\text{O}$  and  $\text{M}(\text{OH}_2)_6$  complex in zinc perchlorate hexahydrate (ZPH) have been discussed. The sharp discontinuities observed at 284, 256.5 and 233 K in the curves exhibiting variations of integrated intensities, full-widths at half the maximum intensities and positions of the bands associated with stretching, bending and librational modes of water and internal modes of  $\text{ClO}_4^-$  ion have been used to identify new phase transitions and their mechanisms in ZPH.

---

\* Papers based on this study have appeared in :

- (I) M.B. Patel, V.N. Sarin and H.D. Bist, Proc. VIIth Int. Conf. Raman Spectroc. p. 126, (1980) Ed. W.F. Murphy, North-Holland, Ottawa, New York.
- (II) M.B. Patel and H.D. Bist, S331, NPSSP (1980).
- (III) M.B. Patel and H.D. Bist, J. de Physique C6, 917 (1981).
- (IV) M.B. Patel and H.D. Bist, J. Chem. Phys. 000, May (1982).

## 5.1 INTRODUCTION

Ross (1) reported the infrared (IR) spectra of zinc perchlorate hexahydrate (ZPH) for the fundamental vibrations of perchlorate group and suggested that the observed splitting in  $\nu_3(p)$  and  $\nu_4(p)$  bands was due to distortion of  $\text{ClO}_4^-$  tetrahedron in ZPH. Balicheva et al (2) reported two bands in the OH stretching region from IR study on single crystal of ZPH and assigned the bands around  $3530\text{ cm}^{-1}$  and  $3440\text{ cm}^{-1}$  as OH vibrations of water bonded to metal and bonded to perchlorate and water respectively. However, according to X-ray data (3,4), a water-water direct bonding does not exist in the crystal structure. Weil et al (5) reported the Raman spectra of three perchlorates including ZPH and observed that the splitting of  $\nu_3(p)$  band of  $\text{ClO}_4^-$  ion increases with the size of cation. They also suggested that the crystal is hexagonal.

Phase transitions have been detected in ZPH by EPR at 346 K (6) and 284K(6,7) and by piezoelectric study at 160 K (8). Preliminary EPR results suggest that the transition at 284 K is due to lowering of site symmetry from trigonal to monoclinic with  $\text{Zn}^{2+}$  at the  $C_h$  site at lower temperature phase. To verify these results and especially to check the transition below 284 K we have undertaken the vibrational study of ZPH including the temperature dependence of IR spectra.

## 5.2 RESULTS AND DISCUSSIONS

### 5.2.1 INTERNAL MODES OF WATER

Figure 5.1 shows the IR spectra of ZPH (A) at 300 K and (B) at 123 K in the region  $4000 - 2100$  and  $1800 - 1500 \text{ cm}^{-1}$ . Figure 5.2 shows observed bands in Raman spectra at RT in the region  $3650 - 3320$ ,  $1700 - 1550$ ,  $1200 - 880$  and  $700 - 180 \text{ cm}^{-1}$ . The observed band positions (in  $\text{cm}^{-1}$ ) both in IR and Raman are presented in Table 5.1 along with their assignments. The details are given in the text below.

At RT large half-widths of the bands indicate that ZPH has disordered crystal structure, since ordered crystal spectra are expected to consist of narrow bands (9). This conclusion is also supported by the observed disordered crystal structure of ZPH by X-ray (4) study. The spectrum at 300 K is completely different from that at 123 K. This clearly indicates that structural change is taking place in the crystal on lowering the temperature, which has been observed earlier by EPR (6,7) and piezoelectric (8) studies.

#### (a) OH Stretching Region

At RT the IR band shape is similar to that of CoPH and MnPH. The assignment of the bands is made on the same basis as discussed in section 4.2.1(b). The broad band centered around  $3450 \text{ cm}^{-1}$  at RT shows hypochromic effect and bathochromic shifts at LT with the appearance of three distinct peaks at 3365, 3220 and  $3125 \text{ cm}^{-1}$ . The bathochromic shift in the stretching region is

a quite common observation (10,11) and is explained qualitatively as being due to strengthening of hydrogen bonding. It is well known that the increased hydrogen bonding on lowering the temperature results in the enhancement of the integrated intensity (11-15) by a factor of upto ten or more and the half-width from 30 to 100  $\text{cm}^{-1}$  or even more.

Fig. 5.3 shows the absorption versus frequency ( $\text{cm}^{-1}$ ) graph which was replotted from Fig. 5.1 to get the relative intensities. While replotting the contribution due to the base line was separated out and the overlap of nujol bands was also subtracted. Then areas under the curves were measured with a planimeter to give the total integrated intensities of the bands in the whole OH-stretching region. (The resulted components of the low temperature spectrum are discussed later in this chapter.) This method gives the ratio of the total integrated intensities in this region at temperatures 300 K and 123 K as 5:4. This is not in confirmity with already stated fact that normally the intensity for strong hydrogen bonding at low temperature enhances by an order of magnitude. Thus, the hypochromic effect and bathochromic shift indicate that there is a definite structural change in the sample on lowering the temperature. Details about it will be discussed in section 5.2.3. At lower temperature the observed band at 3365, 3220 and 3125  $\text{cm}^{-1}$  are assigned as  $\nu_3$ ,  $\nu_1$  and  $2\nu_2$ , respectively, on the basis of intensity  $I_{\nu_3} > I_{\nu_1} > I_{2\nu_2}$  and increase in the intensity of  $2\nu_2$  as the temperature is lowered as shown in Fig. 5.4a. The intensity of  $2\nu_2$  increases because of the Fermi-resonance (FR).



The FR-interaction increases as the temperature decreases, because the separation between  $\nu_1$  and  $2\nu_2$  decreases due to increase of hydrogen bonding. The intensity of  $2\nu_2$  band indicates a strong FR between  $\nu_1$  and  $2\nu_2$ . The FR parameters, were computed by using the relations given in section 1.6, are

$$\text{Fermi coupling constant } \Omega = 47.1$$

$$\text{Unperturbed level separation } \Delta_0 = 12.3 \text{ cm}^{-1}$$

$$\text{Perturbed level separation } \Delta = 95 \text{ cm}^{-1}.$$

Although there is strong mixing between the stretching modes  $\nu_1$  and  $\nu_3$  and also between the Fermi doublets ( $3220$  and  $3125 \text{ cm}^{-1}$  bands), yet we have retained the nomenclature  $\nu_1$ ,  $\nu_2$  and  $\nu_3$  for water bands. The  $\nu_1$  band has been observed (15a) at higher frequency than  $\nu_3$  band at RT due to change in stretch-stretch interaction constant.

#### (b) Bending Region

The single broad bending mode at RT indicates that all the water molecules in the unit cell are equivalent and disordered in agreement with crystal structure (4). The medium intense  $\nu_2$  mode at 300 K disappears almost completely at 123 K. This is an unexpected result and has not been observed in any crystal hydrate so far. When hydrogen bonding increases on lowering the temperature the bending mode of water should not show any substantial intensity change or band broadening (12). Therefore, the hypochromic effect in the bending mode and increase in its half-width are also in contradiction with the above stated fact. Thus, these changes support the view of

structural change in crystal hydrates (cf section 5.2.3). Details about it will be discussed later.

### 5.2.2 PERCHLORATE VIBRATIONS, LIBRATIONAL MODES AND METAL OXYGEN VIBRATIONS

Fig. 5.5 shows the IR spectra (A) at 300 K and (B) at 123 K in the region  $1550$  to  $200\text{ cm}^{-1}$ . Raman spectrum has already been depicted in Fig. 5.2. The observed band positions both in IR and Raman have also been presented in Table 5.1 along with their assignments. The bands around  $1100$ ,  $940$ ,  $630$  and  $460\text{ cm}^{-1}$  both in IR and Raman are assigned as  $\nu_3(p)$ ,  $\nu_1(p)$ ,  $\nu_4(p)$  and  $\nu_2(p)$  fundamental vibrations of perchlorate on the same basis as discussed in section 3.2.3(a). The observed frequencies agree well with the reported values by Ross (1). The  $\nu_3(p)$  band is observed as triplet both in IR and Raman and is in agreement with the space group  $C_{2v}^7$ .

The position of band maximum, its full width at half the maximum intensity (FWHMI) and the relative integrated intensity (RII) in the Raman spectrum of ZPH have been examined. The Raman spectrum exhibits about a dozen bands. The totally symmetric mode of perchlorate ion  $\nu_1(p)$  at  $932\text{ cm}^{-1}$  carries almost two-fifth of the total RII of the whole Raman spectrum. The doubly degenerate bending mode of  $\text{ClO}_4^-$ ,  $\nu_2(p)$  at  $468\text{ cm}^{-1}$  has approximately three-tenth of the RII of  $\nu_1(p)$  mode. But the FWHMI of both  $\nu_1(p)$  and  $\nu_2(p)$  are similar in magnitude,  $18\text{ cm}^{-1}$  and  $20\text{ cm}^{-1}$  respectively. In the asymmetric stretching region  $\nu_3(p)$  of perchlorate ion, the triply degenerate mode

splits into three bands at 1140, 1116 and 1080  $\text{cm}^{-1}$ . The FWHMI of each component is twice that of  $\nu_2'(p)$ . The combined RII of  $\nu_3(p)$  is equal to RII of  $\nu_4(p)$  at 630  $\text{cm}^{-1}$ , which has a FWHMI (20  $\text{cm}^{-1}$ ) similar to that of  $\nu_2(p)$  and  $\nu_1(p)$ .

The infrared (ZPH at RT) perchlorate modes  $\nu_3(p)$  (at 1135, 1107 and 1085  $\text{cm}^{-1}$ ) and  $\nu_4(p)$  (at 633, 630 and 627  $\text{cm}^{-1}$ ) exhibit three components each. The  $\nu_4(p)$  components have lower FWHMI than the  $\nu_3(p)$ . The sharpest and the weakest intensity band in the whole spectrum is  $\nu_1(p)$  at 940  $\text{cm}^{-1}$  with FWHMI of 3  $\text{cm}^{-1}$ . The splitting at 465  $\text{cm}^{-1}$  could not be seen at RT spectrum even under best conditions. Few overtones and combination bands of the modes of  $\text{ClO}_4^-$  ion, are also observed. Their frequencies and assignments are also given in Table 5.1. These bands do not show any appreciable change in intensity or position on lowering the temperature.

The librational modes are very weak in IR at 300 K as in the case of CoPH and MnPH. At 300 K they are assigned on the basis outlined already in section 4.2.2. At 123 K a strong, broad, asymmetric band centered around 850  $\text{cm}^{-1}$  appears and no other band is present having librational character. Taking intensity and combination band criteria into consideration it seems that both rock and wag fall in the same region. They overlap each other to give a strong asymmetric broad band. Few other weak bands appearing in IR and Raman spectra are assigned on the basis of previously known values of metal-oxygen vibrations of  $\text{M}(\text{OH}_2)_6$  complex (16) and lattice vibration of perchlorate ion (17) in other compounds.

### 5.2.3 PHASE TRANSITIONS

Fig. 5.1 and 5.5 show the IR spectra of ZPH (A) at 300 K and (B) at 123 K. The bands due to perchlorate ion do not show any appreciable change in positions and intensities but the bands due to water show very drastic changes. The temperature dependence of the thermosensitive bands of water in ZPH are shown in Fig. 5.4 (a,b,c) in the stretching ( $4000-3000\text{ cm}^{-1}$ ), bending ( $1850-1500\text{ cm}^{-1}$ ) and librational ( $1000-700\text{ cm}^{-1}$ ) regions respectively. The variation of RII with temperature for the stretching region is shown in Fig. 5.6. Likewise, the variation of FWHMI and middle intense peak position with temperature for the stretching modes are given in Fig. 5.7. The variation of RII and FWHMI with temperature for the bending mode is given in Fig. 5.8. In these curves discontinuities are observed at 284, 256.5 and 233 K.

In the stretching region, as the temperature decreases from RT, there also occurs a decrease in RII as shown in Fig. 5.6. The variation of RII against temperature exhibits discontinuities around 284, 256.5 and 233 K. Below  $\sim 233\text{ K}$  the RII exhibits a monotonous increase in its value.

The FWHMI is insensitive to temperature changes below 233 K as shown in Fig. 5.7. The most prominent discontinuity in FWHMI in this region is near 233 K, although the minor change is observed at 256.5 K also. The change at 284 K is not noticeable. The variation of frequency of the middle intense peak in stretching region also exhibits only minor changes between RT

and 258 K but a sudden shift of  $147\text{ cm}^{-1}$  towards lower frequency occurs at 256.5 K. Further a gradual shift of  $30\text{ cm}^{-1}$  is exhibited between 243-223 K. But lowering temperature below 223 K shift in band position is very small. The shape of the stretching band remains unchanged from RT to 258 K and shows a sudden change at 256.5 K as shown in Fig. 5.4(a). On further decreasing the temperature, the FWHMI decreases and the band is gradually resolved into three distinct peaks.

Fig. 5.8 shows the variation of RII against temperature in the bending region which also exhibits discontinuities around 284, 256.5 and 233 K. The FWHMI shows minor variations between RT and 258 K. However, discontinuous changes are exhibited at 256.5 K and in the range 243-223 K. On further lowering the temperature the whole region remains insensitive to temperature changes due to large FWHMI, the frequency of bending mode shows minor variations towards higher side without a sharp discontinuity. The shape of bending mode remains unchanged upto 258 K and changes occur at 256.5 K as shown in Fig. 5.4(b). The FWHMI shows a gradual enhancement on further decreasing the temperature. The RII against temperature shows a hysteresis of  $3^\circ$  for the transition at 256 K as shown in Fig. 5.9.

In the region  $1000-700\text{ cm}^{-1}$  (Fig. 5.4a) there is no indication of librational band upto 258 K and a band appears abruptly near 256.5 K. Further the RII shows a discontinuity in between 243-223 K. However, the  $\nu_1(p)$  of  $\text{ClO}_4^-$  ion increases in intensity as the temperature is lowered. The variation with temperature is shown in Fig. 5.10, which indicates only two

minor discontinuities near 284 and 256 K. It shows that the  $\text{ClO}_4^-$  ion gets more and more distorted on lowering the temperature.

#### 5.2.4 MECHANISM OF PHASE TRANSITIONS

The above studies show that only minor changes occur at 284 K which are indicative of a 2nd or higher order phase transition. The shapes of bands associated with stretching, bending and librational regions and also with  $\text{ClO}_4^-$  vibrations do not show significant variations and thus indicate that in this phase transition no structural change is taking place (18). These findings may be attributed to the axial compression of water molecules caused by distortion of  $\text{ClO}_4^-$  ion in the crystal hydrates. This mechanism has been suggested earlier by Reiff et al (19) from their Mössbauer study in  $\text{Fe}(\text{ClO}_4)_2 \cdot 6\text{H}_2\text{O}$  in analogy with  $\text{Ti}(\text{urea})\text{ClO}_4$  (20-22) and  $\text{Al}(\text{urea})(\text{ClO}_4)_3$  (23).

The sharp changes at 256.5 K in bands associated with water indicate that 1st order phase transition is taking place. Changes of band shapes also indicate that structural change is taking place at this temperature (18). We have already pointed out that the hypochromic effect in bending mode and large bathochromic shift in stretching band are not due to increased hydrogen bonding. Therefore, almost complete disappearance of the bending mode (Figs. 5.1 and 5.3) could be attributed to the formation of a pseudohydrate (14,15) by ZPH at lower temperature. However, this possibility has been ruled out because of the absence of a sharp OH stretching band around  $3600\text{ cm}^{-1}$  and broad

bands near  $3000\text{ cm}^{-1}$  for the oxonium ion.

The EPR studies (6,7) of  $\text{Mn}^{2+}$  doped ZPH suggest that the space group  $C_{2v}^7$  at RT changes its structure to space group  $C_{2h}^5$  at low temperature. It has already been shown by Ananthanarayanan (24) in the double sulfate hexahydrate tutton salts belonging to space group  $C_{2h}^5$  that the water molecules surrounded the cation octahedrally in the crystals and in such cases the bending mode of water is very weak (24). Group theoretical considerations (section 1.5(a)) show that under  $C_{2v}^7$  space group the  $\text{M}(\text{OH}_2)_6$  group can only have  $C_s$  site symmetry. Taking twelve equivalent water molecules the  $A_1$  mode will go to  $6A_1 + 6B_2$  species of the space group  $C_{2v}^7$ , where each of the species  $A_1$  and  $B_2$  are IR and Raman active. However, this correlation is not possible for  $C_{2h}^5$  space group since  $\text{M}(\text{OH}_2)_6$  complex is known to be at  $C_i$  site and  $\text{H}_2\text{O}$  can also be assumed to be at  $C_i$  site. The  $C_i$  site, however, does not form a subgroup of point group  $C_{2v}$ . Thus from the above considerations it can be concluded that the phase transition at 256.5 K is due to structural change from  $C_{2v}^7$  to  $C_{2h}^5$  with  $z = 2$  (25-27). EPR studies (6,7) suggest that the phase transition at 284 K is due to the change of  $\text{Zn}^{2+}$  site from trigonal to monoclinic ( $C_h$ ) and phase transition at 346 K is related to distortion of  $\text{ClO}_4^-$  ion. In our present case we did not observe the phase transition at 346 K, hence spectra above RT have not been given. But from the mechanism of phase transitions it seems that the two phase transitions at 346 and 284 K are similar to the phase transitions at 284 and 256.5 K respectively. The large difference in transition

temperatures may arise due to a small quantity of  $Mn^{2+}$  doped in their samples. We may say that the difference in ionic radii of dopant may produce an internal strain which may cause the change.

The discontinuity in between 243-223 K shows that this phase transition is superimposed on the 1st order. This 3rd transition itself could be of second or higher order. The change in FWHMI in the stretching region indicates that the phase transition near 233 K is order-disorder type (9).

The gradual decrease in frequency and increase of RII (Fig. 5.6) in stretching region below 223 K is attributed to increased hydrogen bonding which is a very well known fact (11-13). If the hydrogen bonding of both the hydrogens are not equal, then the space group  $C_{2h}^5$  will further be reduced to lower symmetry giving rise to the known piezoelectric effect at low temperature (8).



# REFERENCES

1. S.D. Ross, Spectrochim. Acta 18, 225 (1962).
2. T.G. Balicheva and S.N. Andreev, J. Struct.Chem. 5, 23 (1964).
3. C.D. West, Z. Kristallogr. 91A, 480 (1935).
4. M. Ghosh and S. Ray, Z. Kristallogr. 145, 146 (1977).
5. A. Weil and J.P. Mathieu, Comp. Rend. 238, 2510 (1954).
6. A.K. Jain and G.C. Upreti, Solid State Commun. 28, 571 (1978).
7. R. Dayal, Ph.D. Thesis, I.I.T. Kanpur, India (1976).
8. I. Svare and B.O. Fimland, J. Chem. Phys. 74, 5977 (1981).
9. D.F. Hornig, J. Chem. Phys. 17, 1346 (1949).
10. V.P. Tayal, B.K. Srivastava, D.P. Khandelwal and H.D. Bist, Appl. Spectros. Rev. 16, 43 (1980).
11. R. Fifer, Ph.D. Thesis, Temple University (1970).
12. C.M. Hugging and G.C. Pimentel, J. Phys. Chem. 60, 1615 (1956).
13. S.N. Vinogradov and R.H. Linnell, 'Hydrogen Bonding', Van Nostrand, Reinhold Company, New York (1971), Chapter III.
14. M. Falk and O. Knop, in 'Water - A Comprehensive Treatise', Vol. II, F.Franks (ed.) Plenum Press, New York (1973) Chapter II.
15. W.C. Hamilton and J.A. Ibers, in 'Hydrogen Bonding in Solid', W.A. Benjamin, Inc., New York (1968).
- 15a. D.F. Hornig, M.F. White and F.P. Reding, Spectrochim.Acta 12, 338 (1958).
16. V. Ananthanarayanan, Z. Phys. Chem. 222, 102 (1963).
17. H.D. Lutz and R.A. Becker, Spectrochi.Acta 35A, 797 (1979).
18. J. Sheffer, Ph.D. Thesis, Princeton Univ., Princeton, New York (1963).
19. W.M. Reiff, R.E. Frankel and C.R. Abelod, Chem. Phys. Lett. 22, 124 (1973).
20. B.M. Figgis and L.G.B. Wadley, J. Graham, Acta Cryst. B24, 187 (1972).
21. B.M. Figgis and L.G.B. Wadley, Australian J. Chem. 25, 2233 (1972).
22. B.M. Figgis, L.G.D. Wadley and M. Gerloch, J. Chem. Soc. Dalton 238, (1973).
23. J.H.N. Mooy, H.J. de. Long, M. Glasbeck and J.D.W. Van Voorst, Chem. Phys. Lett. 18, 51 (1973).
24. V. Ananthanarayanan, Z. Phys. 163, 144 (1961).
25. M.B. Patel and H.D. Bist, S331, NPSSP (1980).
26. M.B. Patel and H.D. Bist, J. de. Physique C6, 17 (1981).
27. M.B. Patel and H.D. Bist, J. Chem. Phys. 000, May (1982).

Table 5.1: Observed frequencies in IR and Raman spectra of microcrystalline ZPH powder.

IR (RT)			IR (LT)			Raman (RT)			Assignment
$\nu$ ( $\text{cm}^{-1}$ )	$\Delta\nu_2$ ( $\text{cm}^{-1}$ )	$I_R$	$\nu$ ( $\text{cm}^{-1}$ )	$\Delta\nu_2$ ( $\text{cm}^{-1}$ )	$I_R$	$\nu$ ( $\text{cm}^{-1}$ )	$\Delta\nu_2$ ( $\text{cm}^{-1}$ )	$I_R$	
520	340	101	3220	120	89				$\nu_1$
450	340	215	3365	185	114				$\nu_3$
240	210	39.0	3125	100	69				$2\nu_2$
195	150	10.0	2345	360	54				$\nu_2 + \nu_R$
020	55	9.0	2020	50	10				$\nu_3(p) + \nu_1(p)$
635	80	42.0	1625	200	11	1622	28	4	$\nu_2$
255	60	5.1	1255	60	5.1				$2\nu_4(p)$
135	110	78.1	1135	110	78.1	1140	45	6.3	$\nu_3(p)$
107	90	45.2	1110	90	45.2	1116	35	9.8	$\nu_3(p)$
085	115	100	1082	115	100	1080	40	10.1	$\nu_3(p)$
070	100	22.0	1070	100	22				$\nu_3(p) - \nu_L(p)$
940	3	0.8	939	3	0.9	932	18	100	$\nu_1(p)$
			850	200	134				$\nu_R$ and $\nu_W$
633	20	16.7	633	20	16.7				$\nu_4(p)$
630	20	16.7	630	20	16.7	630	20	29.2	$\nu_4(p)$
627	20	16.7	627	20	16.7				$\nu_4(p)$
510	135	27.9							$\nu_W(w)$
			500		vw				$\nu_2(c) + \nu_5(c)$
465		vw	465		vw	468	20	30	$\nu_2(p)$
430		vw	430		vw				$\nu_5(c) + \nu_4(c)$
402		vw	402		vw				$\nu_5(c) + \nu_4(c)$
						388	38	5.9	$\nu_1(c)$
375		vw	375		vw				$\nu_6(c)$
						356	28	3.1	$\nu_T$
325		vw	325		vw				$\nu_5(c)$
						306	32	2.3	$\nu_3(c)$
305		vw	305		vw				$\nu_5(c)$
						208	24	1.4	$\nu_2(c)$

R, W, T, L, p, c and vw stands for rock, wag, twist modes of water, lattice modes of perchlorate,  $\text{ClO}_4^-$ ,  $\text{M}(\text{OH}_2)_6$  and very weak, respectively.

FIGURE CAPTIONS

- Fig.5.1: IR spectra of  $\text{Zn}(\text{ClO}_4)_2 \cdot 6\text{H}_2\text{O}$  in the range 4000-2100 and 1300-1500  $\text{cm}^{-1}$  at 300 K (curve A) and 123 K (curve B). N in this figure as well as in other figures represents nujol band.
- Fig.5.2: Raman spectrum of  $\text{Zn}(\text{ClO}_4)_2 \cdot 6\text{H}_2\text{O}$  at room temperature.
- Fig.5.3: Replot of curves A and B of Fig.5.1 in absorbance scale (in the range 4000-2800 and 1900-1500  $\text{cm}^{-1}$ ) and their Lorentzian analysis (dotted curves).
- Fig.5.4: Temperature dependence (in the range 305-123 K) of :  
(a) stretching (4000-3000  $\text{cm}^{-1}$ ), (b) bending (1850-1550  $\text{cm}^{-1}$ ) and (c) librational modes (1000-700  $\text{cm}^{-1}$ ) of water.
- Fig.5.5: IR spectra of  $\text{Zn}(\text{ClO}_4)_2 \cdot 6\text{H}_2\text{O}$  in the range 1550-200  $\text{cm}^{-1}$  at 300 K (curve A) and 123 K (curve B).
- Fig.5.6: Total integrated intensity versus temperature for the stretching mode of water.
- Fig.5.7: Plot of band position (solid line) and full-width at half the maximum intensity (FWHMI - dotted line) versus temperature for the stretching mode of water.
- Fig.5.8: Plot of total integrated intensity (solid line) and FWHMI (dotted line) versus temperature for the bending mode of water.
- Fig.5.9: Thermal hysteresis curve for the bending mode of water for 256 K transition.
- Fig.5.10: Plot of peak absorbance versus temperature of  $\nu_1$  mode in  $\text{ClO}_4^-$  ion.

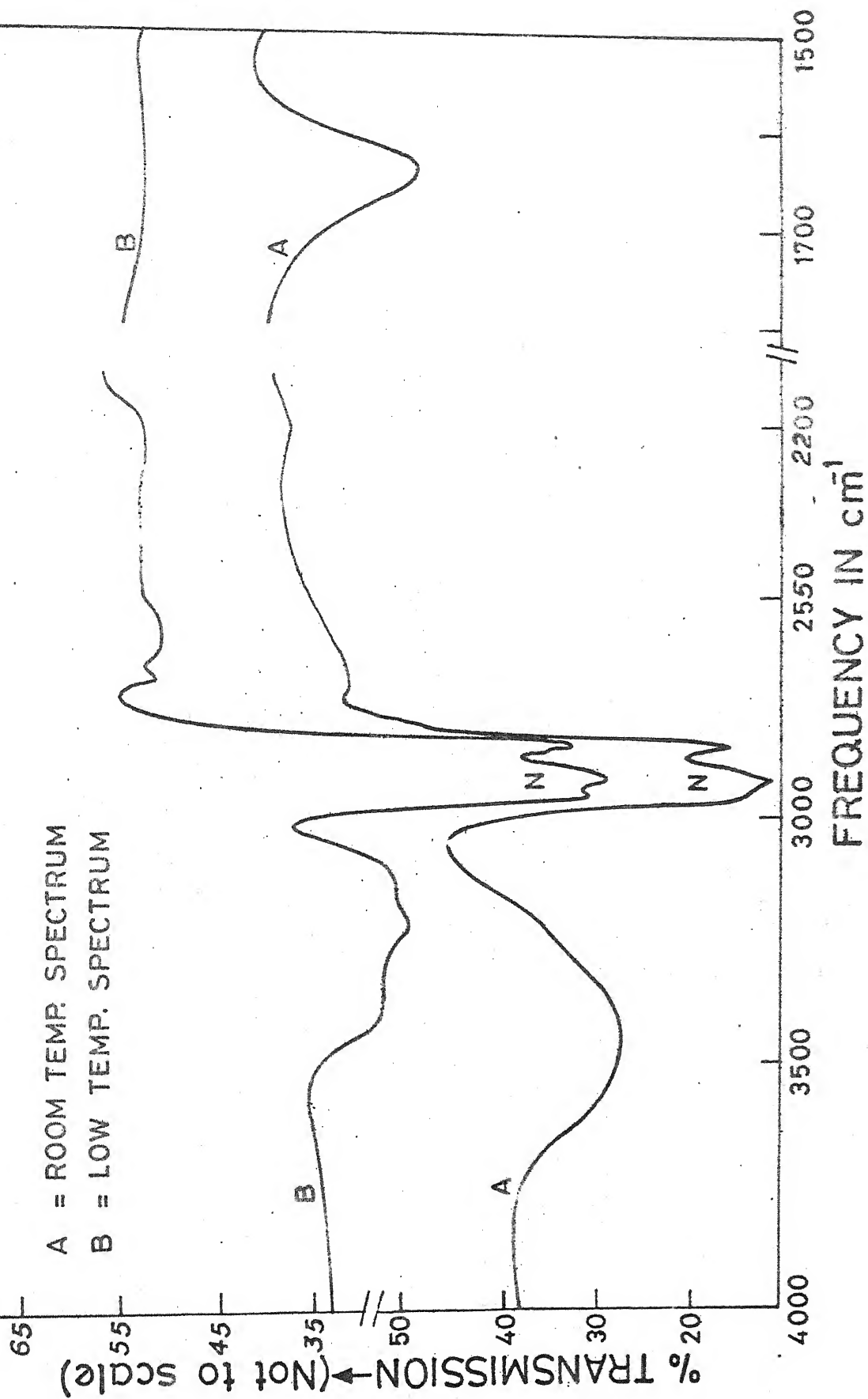


FIG. 5.1

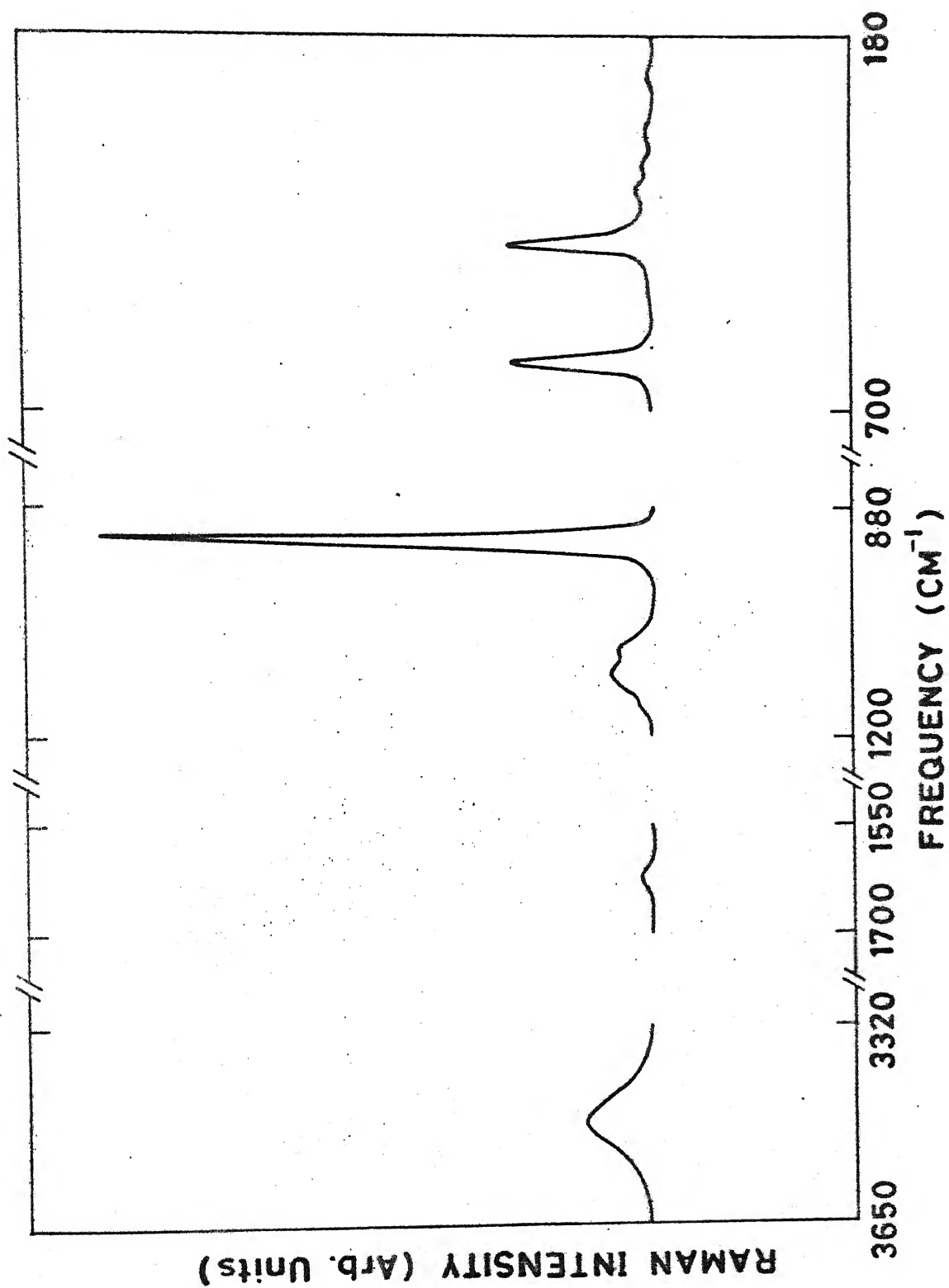


FIG. 5.2

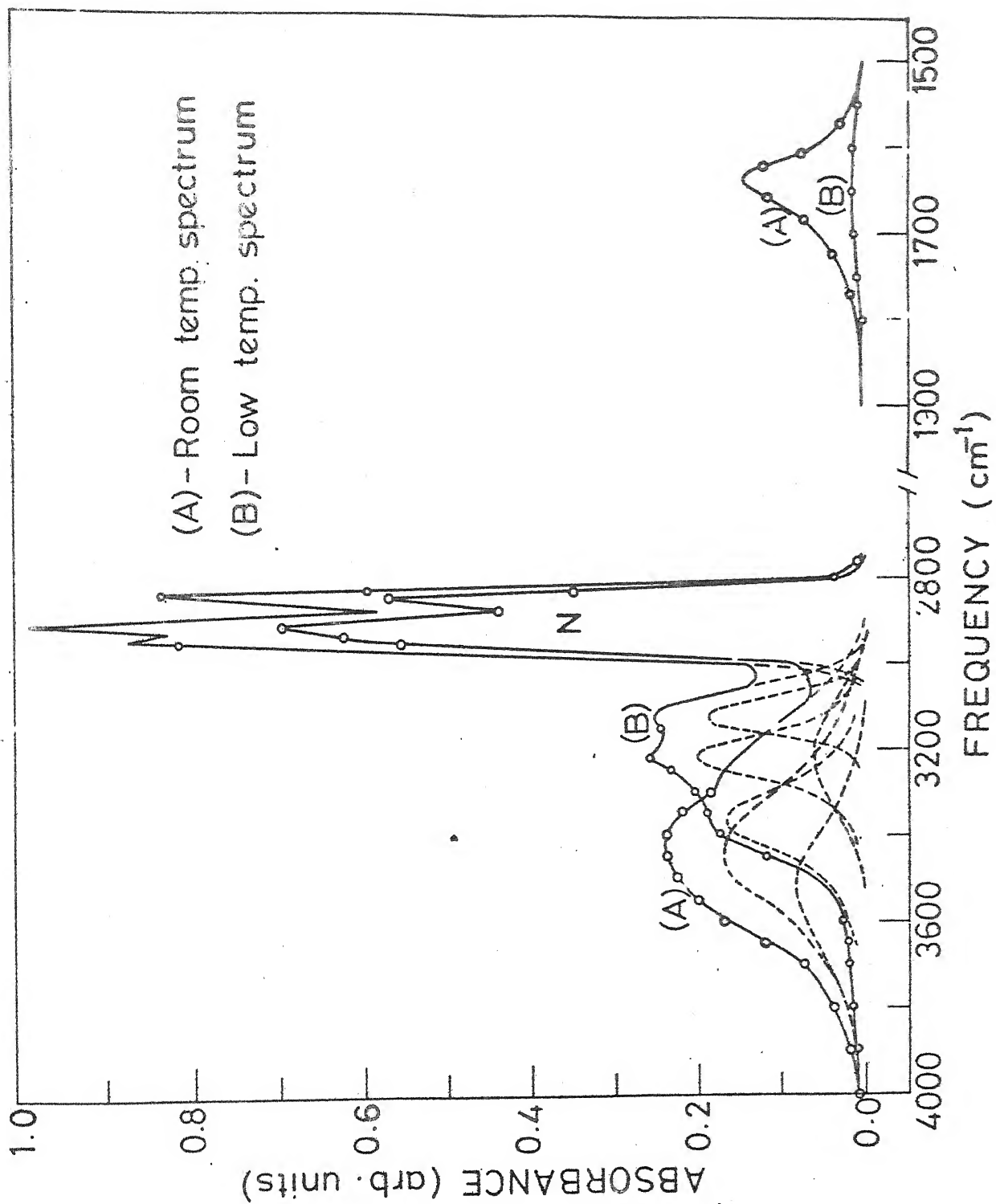


FIG. 5.3

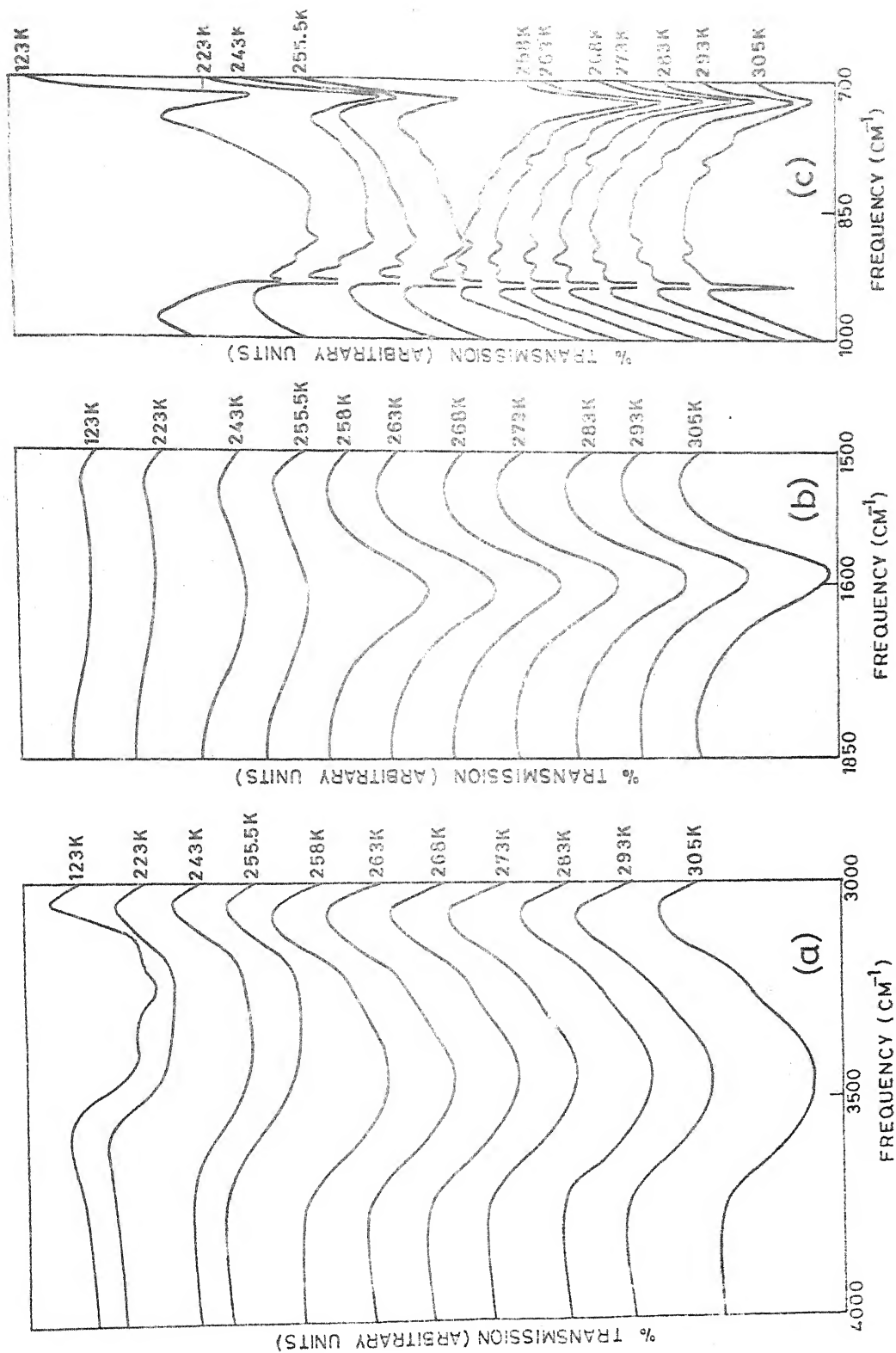


FIG. 5.4

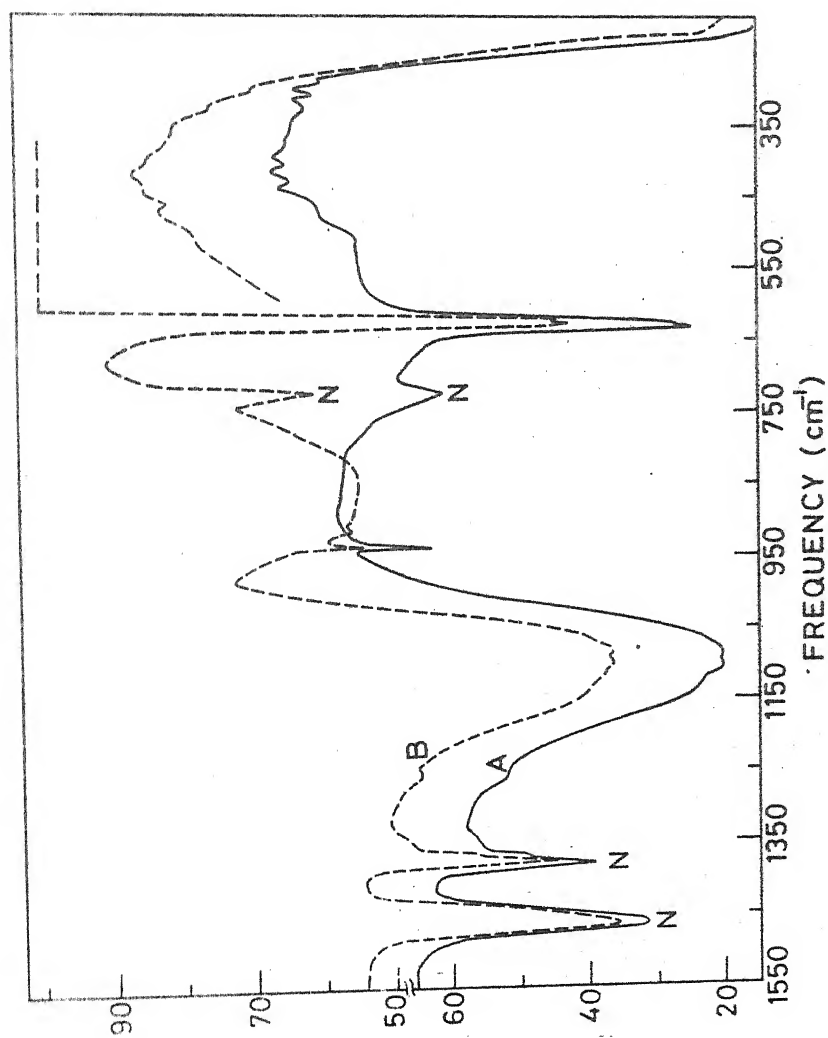


FIG. 5.5

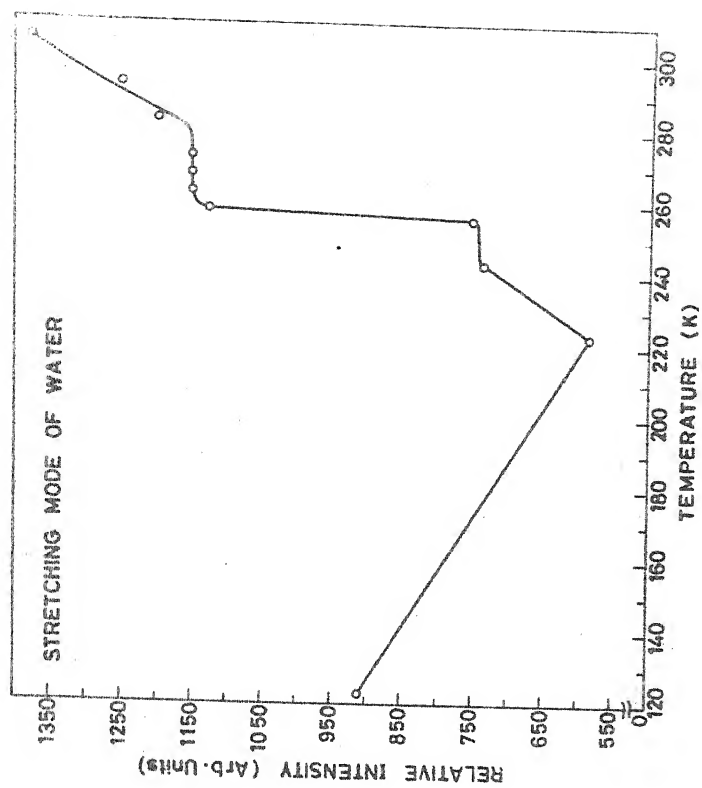


FIG. 5.6



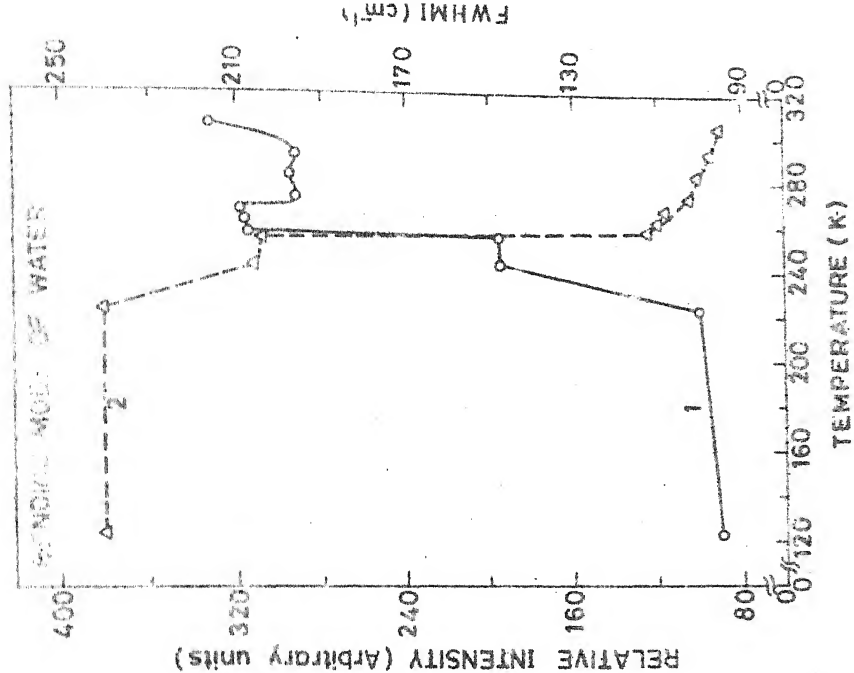


FIG. 5.8

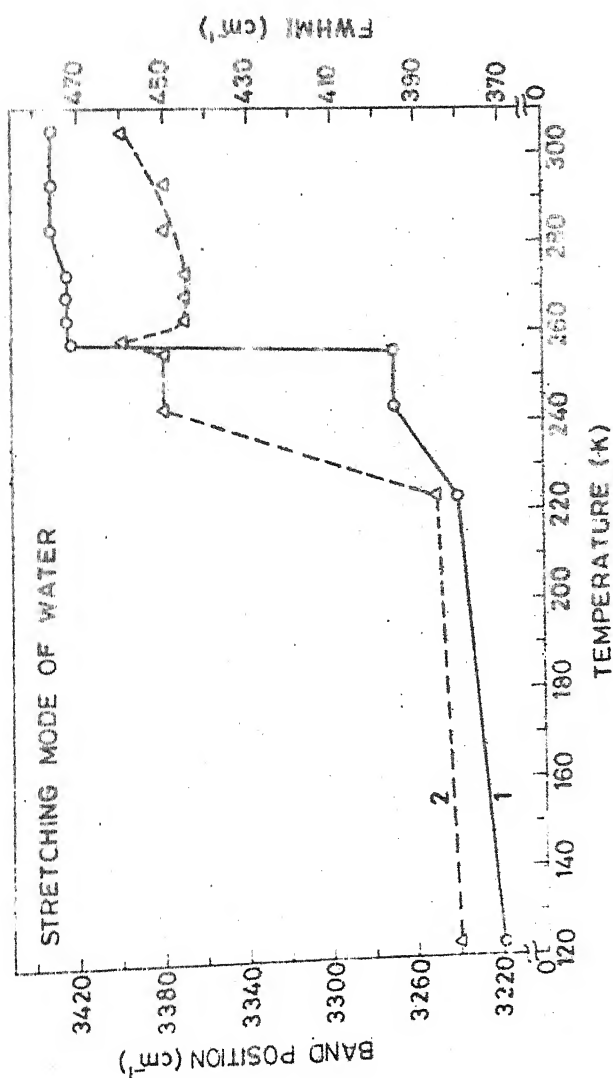


FIG. 5.7

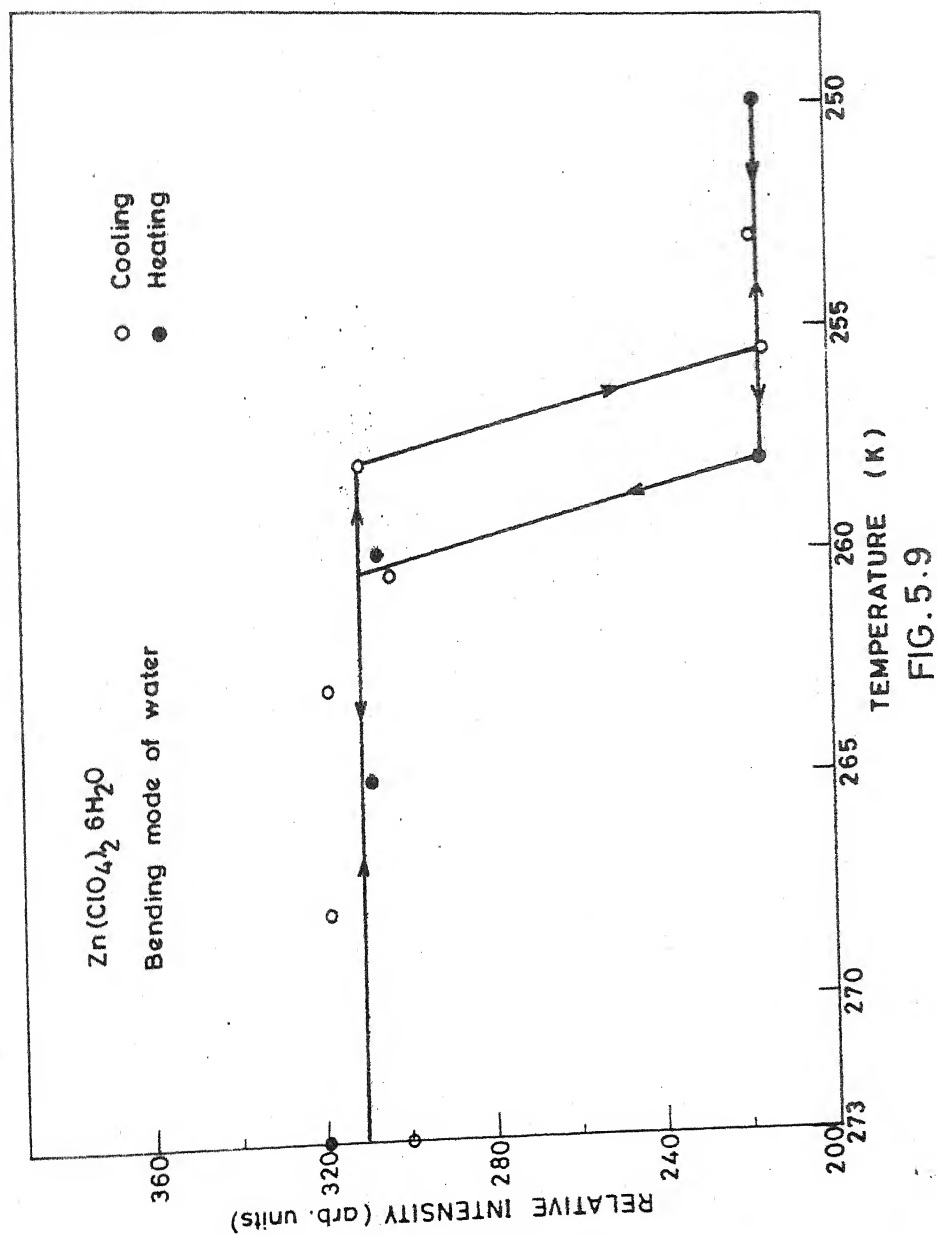


FIG. 5.9

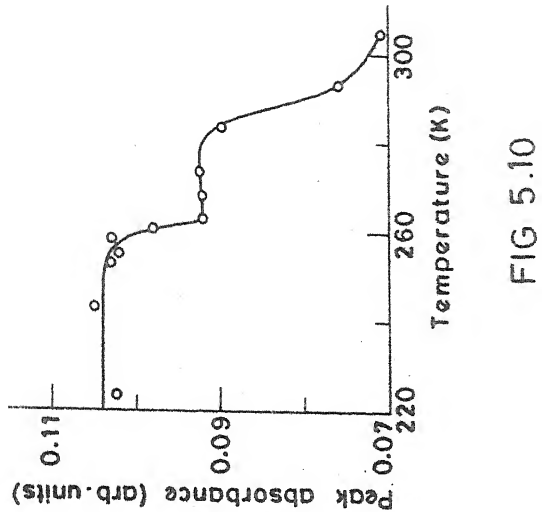


FIG 5.10

## CHAPTER VI

### VIBRATIONAL STUDIES AND PHASE TRANSITIONS IN CADMIUM AND MERCURY PERCHLORATE HEXAHYDRATES

#### ABSTRACT

On the basis of detailed infrared and Raman studies of cadmium and mercuric perchlorate hexahydrates (CPH and HPH) complete vibrational assignments are proposed for room and low temperature phases. The characteristic changes in the stretching, bending and librational mode regions of  $H_2O$  show that the normal hydrate at RT turns out to be a pseudohydrate at LT in both compounds. In pseudohydrate the presence of  $H_3O^+$  ion is demonstrated. The five phase transitions (two for the first time) in CPH and three in HPH (all for the first time) between 300 K and 100 K are being reported and discussed.

## 6.1 INTRODUCTION

Raman study on cadmium perchlorate hexahydrate (CPH) in polycrystalline form was conducted by Weil et al (1). They published Raman spectra of three perchlorates and suggested that CPH is trigonal and the splitting of  $\nu_3(p)$  of  $\text{ClO}_4^-$  ion increases with the size of the cation. Hester et al (2) reported the Raman spectra of saturated aqueous solutions of fifteen perchlorates. Mercury perchlorate hexahydrate (HPH) is one of them. They reported only four fundamental vibrations. No IR study has been carried out in these compounds.

In CPH phase transition studies have been carried out by EPR (3,4) and piezoelectric (5) measurements. The reported phase transitions are at  $T_1 = 363 \text{ K}$  (4),  $T_2 = 272 \text{ K}$  (3-5),  $T_3 = 259 \text{ K}$  (4) and  $T_4 = 115 \text{ K}$  (3-5). No phase transitions have ever been reported for HPH.

## 6.2 RESULTS AND DISCUSSIONS

### 6.2.1 INTERNAL MODES OF WATER

Figs. 6.1 and 6.2 show the IR spectra of CPH and HPH at 100 K (A,C) and 300 K (B,D) for hydrated (C,D) and partially deuterated (A,B) samples, respectively, in the range  $3800\text{--}2000 \text{ cm}^{-1}$  and  $1800\text{--}1500 \text{ cm}^{-1}$ . Raman spectra of CPH and HPH are shown in Figs. 6.3 and 6.4, respectively at RT. The observed frequencies both in IR and Raman are presented in Table 6.1 for both the hydrated compounds along with their assignments. The curves C in Figs. 6.1 and 6.2 are retraced on absorbance scale (solid lines) in the range  $2800\text{--}3800 \text{ cm}^{-1}$  as shown in Figs. 6.5 and 6.6.

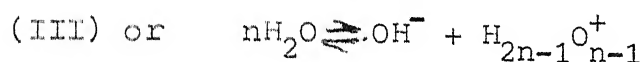
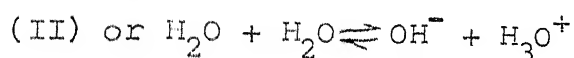
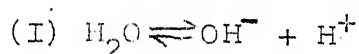
respectively. The dotted lines show the Lorentzian components.

The observed striking similarities in the spectra of the two hydrates reflect that they may have trigonal structures which are alike. At RT the broadness of the bands indicates that both the hydrates have disordered structures (6). At LT the nature of the spectra changes completely, both in CPH and HPH, indicating that structural changes are taking place (7) in these hydrates.

(a) Stretching Region

At RT the  $\nu_3$  and  $\nu_1$  bands of water overlap (cf. Figs. 6.1 and 6.2) but their peak positions can be obtained from the shoulders in the spectra. The  $\nu_3$  and  $\nu_1$  are assigned on the basis that  $\nu_3$  has higher frequency and intensity than  $\nu_1$  in IR, whereas in Raman the intensity of  $\nu_3$  is less than that of  $\nu_1$ .  $2\nu_2$  is very weak in IR and is not observed in Raman for normal water geometry in hydrates. The broad asymmetric peak at RT around  $3500\text{ cm}^{-1}$  could be resolved into three peaks (i.e.  $\nu_3$ ,  $\nu_1$  and  $2\nu_2$ ) at  $3550$ ,  $3460$  and  $3195\text{ cm}^{-1}$  for CPH and  $3550$ ,  $3470$  and  $3190\text{ cm}^{-1}$  for HPH. On lowering the temperature, the bands show bathochromic shifts and are observed at  $3360$ ,  $3220$  and  $3130\text{ cm}^{-1}$  for CPH and  $3365$ ,  $3220$  and  $3125\text{ cm}^{-1}$  for HPH. As discussed earlier (section 5.2.1(a)) the stronger hydrogen bonding as a cause of occurrence of these changes may be ruled out. Further, the appearance of sharp bands at  $3642\text{ cm}^{-1}$  for CPH and  $3595\text{ cm}^{-1}$  for HPH indicates the presence of relatively free  $\text{OH}^-$  ions which are weakly bonded to the cation and/or anions. Hence the ordinary water of crystallization no more

exists in the crystal hydrates at LT (8). Water present in this form in the crystal is referred to as water of constitution and the hydrates containing it as pseudohydrates rather than normal hydrates. In pseudohydrates the  $H_2O$  exists in one or more of the following forms :



Many hydrated compounds (8,9) which have been formulated as true hydrates have turned out to be pseudohydrates at RT. However, no evidence is available in literature where a true hydrate at RT turns out to be pseudohydrate at LT.

(b) Bending Region

At RT, the appearance of a broad single bending band at  $1620\text{ cm}^{-1}$  in CPH and at  $1625\text{ cm}^{-1}$  in HPH (Figs. 6.1 and 6.2) spectra indicates that all the water molecules in the unit cell are equivalent, i.e. they have same site symmetry in agreement with crystal structure (10). At LT both the hydrates show hypochromic effect and the band becomes very broad and simultaneously a sharp band also appears at  $1579\text{ cm}^{-1}$  for CPH ( $1605\text{ cm}^{-1}$  for HPH). As discussed earlier (section 5.2.1(b)), the decreased intensity of the bending mode at LT does not support the increased hydrogen bonding but it indicates the formation of pseudohydrates (11). In partially deuterated samples the bending mode of water remains almost at the same position as in hydrated sample, at RT which indicates

weak intermolecular coupling.

(c) Identification of Oxonium ion in Pseudohydrate

(i) The hydrate spectra

Out of the several possibilities for the forms of pseudohydrate mentioned above in the LT phase, the spectra presented in Fig. 6.1 and 6.2 converge only in one pseudohydrate  $\text{H}_3\text{O}^+$ . The possibility of  $\text{H}_2\text{O} \rightleftharpoons \text{OH}^- + \text{H}^+$  can be ruled out because  $\text{H}^+$  can only make bond with the oxygen of  $\text{ClO}_4^-$  ion; thus only one relatively free OH vibration is possible, hence the observed bands at 3360, 3220, 3130  $\text{cm}^{-1}$ , etc. should not arise from the above chemical composition.

The next possibility is  $\text{H}_2\text{O} + \text{H}_2\text{O} \rightleftharpoons \text{OH}^- + \text{H}_3\text{O}^+$ . As  $\text{H}_3\text{O}^+$  is isoelectronic with  $\text{NH}_3$  with a very little mass difference, it might be expected that their spectra would be similar. Crystalline  $\text{NH}_3$  has absorption (12) bands  $\nu_1$  at 3223,  $\nu_2$  at 1060,  $\nu_3$  at 3378 and  $\nu_4$  at 1646  $\text{cm}^{-1}$ . Therefore, assuming that  $\text{H}_3\text{O}^+$  has also pyramidal structure in these crystals at LT phase, we can assign our observed bands around 3360  $\text{cm}^{-1}$  as  $\nu_3$  and 3220  $\text{cm}^{-1}$  as  $\nu_1$  both for Cd and Hg compounds and 1620  $\text{cm}^{-1}$  for CPH (1625 for HPH) as  $\nu_4$  because of similarity in frequencies. This assignment appears to be reasonable from the consideration of intensities and band positions because the asymmetric stretch in general has higher frequency and intensity than symmetric one as is the case in most of the crystal hydrates. The symmetric bending mode  $\nu_2$  of  $\text{H}_3\text{O}^+$ , which in general occurs in between 1050-1200  $\text{cm}^{-1}$  as reported (13,14) for several

other systems, is not identified in both the samples, because it is masked by the strong asymmetric stretching band  $\nu_3(p)$  of the  $\text{ClO}_4^-$  ion. To resolve these difficulties a deuterated sample is helpful. (Indeed we observed  $\nu_2$  band in partially deuterated  $\text{HD}_2\text{O}^+$  samples around 880 and 885  $\text{cm}^{-1}$  for CPH and HPH respectively. (cf. Table 6.4, to be discussed later); the corresponding  $\nu_2$  frequency will be around 1150  $\text{cm}^{-1}$  in hydrated compounds.) The near coincidence of the observed bands show that the  $\text{H}_3\text{O}^+$  ion has analogous pyramidal structure with  $\text{NH}_3$  in the crystal at LT. Therefore, the observed four fundamental bands agree with the presence of  $\text{H}_3\text{O}^+$  ion with pyramidal structure (as observed in other cases also, cf. Table 6.2). Further evidence of the presence of  $\text{H}_3\text{O}^+$  ion is obtained from other bands in the spectra. This is discussed below :

In the OH stretching region at low temperature the band centred around 3130  $\text{cm}^{-1}$  is assigned to the first overtone of the fundamental bending mode  $\nu_4$  of  $\text{H}_3\text{O}^+$  ion in both the compounds (cf. Table 6.1). The intensity of  $\nu_4$  band is weak in both the compounds, though it is IR active. Therefore, one can expect that the overtone will not be observed. However, the appreciable intensity of the overtone indicates that a strong Fermi resonance (FR) is taking place between the bands  $\nu_1$  and  $2\nu_4$  of  $\text{H}_3\text{O}^+$  ion, thus resulting in a large mechanical anharmonicity. The same argument has been applied in the case of ice (15) in order to assign 3140  $\text{cm}^{-1}$  as the first overtone of bending mode at 1620  $\text{cm}^{-1}$ . The FR parameters are computed from the relations given in section 1.6.1 and presented in Table 6.3 for  $\nu_1$  and



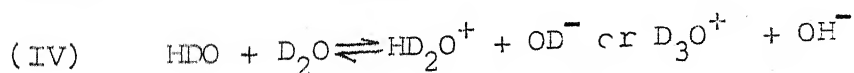
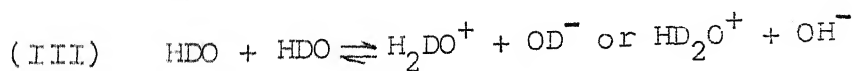
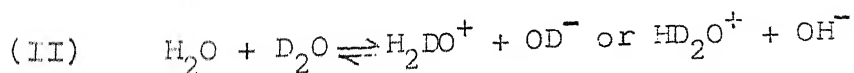
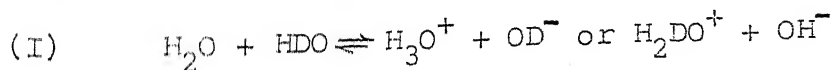
2 $\nu_4$  vibrations of  $\text{H}_3\text{O}^+$  group.

(ii) The partially deuterated spectra

(A) The  $\text{H}_2\text{DO}^+$  and  $\text{HD}_2\text{O}^+$  stretches

Our assignment is further supported by the partially deuterated spectra (Fig 6.1 and 6.2). The observed bands in IR for the partially deuterated samples of both the compounds are presented in Table 6.4 along with their assignments. Though partially deuterated spectra seem to be more complex yet they help in making unambiguous assignments.

In the partially deuterated spectra, the formation of  $\text{H}_2\text{DO}^+$  and  $\text{HD}_2\text{O}^+$  is more probable than the formation of  $\text{H}_3\text{O}^+$  and  $\text{D}_3\text{O}^+$ . As we have mentioned  $\text{H}_2\text{O} + \text{H}_2\text{O}$  gives  $\text{OH}^-$  and  $\text{H}_3\text{O}^+$ , therefore, in the crystal  $\text{H}_3\text{O}^+$  is formed because of the chemical interaction between the two neighbouring water molecules. In the partially deuterated sample, from the statistical point of view, the nearest neighbour of  $\text{H}_2\text{O}$  is either  $\text{D}_2\text{O}$  or  $\text{HDO}$  and the nearest neighbour of  $\text{HDO}$  is either  $\text{D}_2\text{O}$  or  $\text{H}_2\text{O}$  or  $\text{HDO}$ , because the percentage of  $\text{HDO}$  is equal to the sum of the percentages of  $\text{H}_2\text{O}$  and  $\text{D}_2\text{O}$ . Therefore, by the neighbourhood interaction process, in the partially deuterated samples, the formation of isotopic oxonium ions are as follows from the statistical considerations.



The formation of  $\text{H}_2\text{DO}^+$  and  $\text{HD}_2\text{O}^+$  are more probable compared to  $\text{H}_3\text{O}^+$  and  $\text{D}_3\text{O}^+$  in steps (I) and (IV) respectively, because it is observed experimentally that in divalent metal perchlorate hexahydrates the formation of hybrid species like  $\text{H}_2\text{DO}^+$ ,  $\text{HD}_2\text{O}^+$  and  $\text{HOD}$  are maximum. This observed fact might be due to their hygroscopic nature. Therefore, in partially deuterated spectra the bands are primarily due to  $\text{H}_2\text{DO}^+$  and  $\text{HD}_2\text{O}^+$ .

In  $\text{H}_2\text{DO}^+$  and  $\text{HD}_2\text{O}^+$  the  $C_{3v}$  point group symmetry of  $\text{H}_3\text{O}^+$  becomes  $C_s$  due to which the two fold degeneracy of  $\nu_3$  and  $\nu_4$  vibrations of  $\text{H}_3\text{O}^+$  (or  $\text{D}_3\text{O}^+$ ) is lifted. Therefore, from the above considerations we expect three stretching bands, two from  $\text{H}_2\text{DO}^+$  belonging to  $A'$  and  $A''$  species and the third from the  $\text{HD}_2\text{O}^+$  (the uncoupled OH band). Similar is the case in the OD stretching region. Indeed we observe three bands in both OH and OD stretching regions in agreement with our predictions. Further, in the partially deuterated spectrum we do not observe the band around  $3130\text{ cm}^{-1}$  which is quite strong in the hydrated sample. This indicates that there is no more Fermi resonance taking place in the system. The loss of Fermi resonance interaction could be explained as follows :

(I) the bending mode and its overtone shift towards lower frequency side; therefore, the resonance interaction becomes weak and the overtone band is not observed,

(II) in  $C_s$  point group the double degenerate bending mode  $\nu_4$  of point group  $C_{3v}$  goes to  $A'$  and  $A''$  species and they might give combination mode of  $A''$  species rather than overtone, which belongs to  $A'$  species; thus no interaction is possible and the

summation band will not be observed. Therefore, the assignment of the three intense bands in the OH stretching region of  $\text{H}_3\text{O}^+$  is strongly supported by the spectra of partially deuterated sample. The summary of vibrations of  $\text{H}_2\text{DO}^+$  and  $\text{HD}_2\text{O}^+$  under  $\text{C}_s$  point group is also given in Table 6.2.

(B) The  $\text{OH}^-$  bands

The  $\text{OH}^-$  bands appearing in the LT spectra of CPH and HPH are summarized in Table 6.5. The free  $\text{OH}^-$  ion gives a band at  $3706\text{ cm}^{-1}$ . The lower frequencies of  $\text{OH}^-$  ion in HPH denotes that the H-bonding in HPH is stronger than in CPH. The two frequencies in the partially deuterated samples (e.g. 3635 and  $3592\text{ cm}^{-1}$  in CPH) are due to the two possible deuterated species  $\text{H}_2\text{DO}^+$  and  $\text{HD}_2\text{O}^+$  attached to the free  $\text{OH}^-$  groups.

(C) The  $\text{H}_2\text{DO}^+$  and  $\text{HD}_2\text{O}^+$  bending modes

The observed weak band around  $2250\text{ cm}^{-1}$  in both the compounds (Figs. 6.1 and 6.2) at LT is assigned as the first overtone of  $\nu_2$  of  $\text{H}_3\text{O}^+$  ion. The fundamental band corresponding to  $\nu_2(\text{H}_3\text{O}^+)$  is masked by the strong asymmetric stretching band of the  $\text{ClO}_4^-$  ion. This assignment seems to be correct because in the deuterated spectra the  $\nu_2$  band appears around  $880\text{ cm}^{-1}$  for  $\text{HD}_2\text{O}^+$  and  $1120\text{ cm}^{-1}$  for  $\text{H}_2\text{DO}^+$ . The latter, however, is masked by the  $\nu_3(\text{p})$  of  $\text{ClO}_4^-$  ion. From these observations and the overtone band, one can conclude that the  $\nu_2$  band of  $\text{H}_3\text{O}^+$  ion would be somewhere in the range  $1125\text{--}1200\text{ cm}^{-1}$  and most probably around  $1150\text{ cm}^{-1}$ .

In the partially deuterated sample at RT the bending modes of  $\text{H}_2\text{O}$ ,  $\text{HOD}$  and  $\text{D}_2\text{O}$  appear at around 1620, 1420 and 1190  $\text{cm}^{-1}$  respectively for both the compounds. At LT two sharp bands appear at 1581 and 1391  $\text{cm}^{-1}$  for CPH and 1603 and 1410 for HPH and the very broad bands for both the compounds appear around 1605  $\text{cm}^{-1}$  and 1200  $\text{cm}^{-1}$ , whose positions are not exactly identified because the overtone of librational mode also fall around the same region. The sharp band is assigned to bending mode of  $\text{H-O-H}$ , which agree well with the observed two sharp bending modes, one for each  $\text{H-O-H}$  and  $\text{M-O-D}$  in the deuterated sample as shown in Figs. 6.1, 6.2, 6.7 and 6.8.

#### (D) Other possibilities

The possibility of  $\text{H}_2\text{O} + \text{H}_2\text{O} + \text{H}_2\text{O} \rightleftharpoons \text{OH}^- + \text{H}_5\text{O}_2^+$  can be ruled out because of the absence of the characteristic fundamental bands of  $\text{H}_5\text{O}_2^+$  ion as expected from group theoretical considerations and observed (17) in the case of  $(\text{H}_5\text{O}_2)^+(\text{ClO}_4)^-$ . Similarly the possibility of higher oxonium ions  $(\text{H}_{2n-1}\text{O}_{n-1})^+$  can also be ruled out, whose existence is not yet detected experimentally.

#### 6.2.2 WATER LIBRATIONS AND TRANSLATIONS

Figs. 6.7 and 6.8 show the IR spectra of CPH and HPH at 100 K (curves A,C) and 300 K (curves B,D) for hydrated (C,D) and partially deuterated (A,B) samples respectively in the range 1350-250  $\text{cm}^{-1}$ . The observed frequencies both in IR and Raman (as already pointed out in section 6.2.1) are presented in Table

6.1 for both the hydrated compounds along with their assignments. The observed bands in IR for partially deuterated samples for both compounds are presented in Table 6.4 along with their assignments.

(a) Librational Modes

At RT the librational modes are not observed in IR and Raman for the two hydrates. At LT a moderately strong and broad band centred around  $860\text{ cm}^{-1}$  for CPH ( $850\text{ cm}^{-1}$  for HPH) and another weaker band at  $360\text{ cm}^{-1}$  for CPH ( $443\text{ cm}^{-1}$  for HPH) are attributed to librational lattice modes of the  $\text{H}_3\text{O}^+$  ion. Out of three librational modes of the  $\text{H}_3\text{O}^+$  ions, the one about the threefold axis i.e.  $R_z$  should be weak in IR since it has little change in the dipole moment. Therefore, the weak bands at  $360\text{ cm}^{-1}$  and  $443\text{ cm}^{-1}$  in CPH and HPH, respectively, are assigned to  $A_1(R_z)$ . The bands at  $860\text{ cm}^{-1}$  in CPH and  $850\text{ cm}^{-1}$  in HPH belong to doubly degenerate  $E(R_{x,y})$  species. These assignments of librational modes agree with the general behaviour and appearance of the bands. The  $E(R_{x,y})$  modes ( $\sim 855\text{ cm}^{-1}$ ) of the two samples are unusually high in frequency compared to the corresponding librational mode of  $\text{NH}_3$  ( $\sim 520\text{ cm}^{-1}$ ). However, in the IR spectra of the hydronium halides (13), this assignment has been made for bands in the range  $750\text{--}800\text{ cm}^{-1}$ . Moreover, in ice a value of  $850\text{ cm}^{-1}$  (18) and in crystal hydrates a maximum value of  $1080\text{ cm}^{-1}$  have been reported for librational lattice modes of water under ordinary circumstances (19). From the above reported values and the fact that the hydronium ion is more likely

to be strongly hydrogen bonded in perchlorates than in halides, it appears that a value around  $850\text{ cm}^{-1}$  is quite reasonable.

In partially deuterated sample we observed two strong librational bands around  $810\text{ cm}^{-1}$  and  $640\text{ cm}^{-1}$ , while in the hydrated sample it appears around  $860\text{ cm}^{-1}$ . Thus the deuteration shift ratios of 1.06 ( $860/810$ ) and 1.34 ( $860/640$ ), respectively, as expected in analogy with  $\text{H}_2\text{O}$  (19), not only support the assignment of librational band but also formation of  $\text{H}_2\text{DO}^+$  and  $\text{HD}_2\text{O}^+$  in the partially deuterated sample at LT. Similarly the band at  $360\text{ cm}^{-1}$  in CPH and  $443\text{ cm}^{-1}$  in HFH show librational character and support the formation of  $\text{H}_2\text{DO}^+$  and  $\text{HD}_2\text{O}^+$  in partially deuterated samples at LT as shown in Table 6.4. On partial deuteration this librational band splits into two. This can be understood from the following consideration; the oxonium ion does not have exact  $\text{C}_{3v}$  symmetry. If it is  $\text{C}_{3v}$  symmetry, then the  $\text{H}_2\text{DO}^+$  and  $\text{HD}_2\text{O}^+$  species are space degenerate with respect to rotation about the molecular  $\text{C}_3$  axis (the space degeneracy is with respect to its potential environment but not necessarily to its geometric environment), so the librational frequency is unchanged by such a rotation and will appear as a single band. If  $\text{H}_3\text{O}^+$  ion does not have exactly  $\text{C}_{3v}$  symmetry (i.e. one O-H bond length is larger or smaller than the rest two which are equal or all three are different) then the  $\text{H}_2\text{DO}^+$  and  $\text{HD}_2\text{O}^+$  do not have a  $\text{C}_3$  symmetric axis with respect to the potential environment. Consequently, the space degeneracy is removed and gives either doublet or triplet. In this situation if it splits into three, then all of them have equal intensities.

and if it splits into two, then the intensity ratio will be 2:1. In our case we observed a doublet, the ratio of their intensities is 2:1, which is in agreement with the above view. Thus the doublet in twist librational mode arises due to space degeneracy with respect to its potential environment.

(b) Translational modes

The other bands around  $345\text{ cm}^{-1}$  in CPH and  $360$  and  $306\text{ cm}^{-1}$  in HPH could be attributed to translational lattice modes. There are three translational modes of the  $\text{H}_3\text{O}^+$  ion. The weaker one is  $T_z$  involving the displacement along the dipole axis, hence is low in intensity.  $T_z$  causes only a slight bending of the hydrogen bonds hence has a low frequency (14). The maximum value of it reported so far is  $265\text{ cm}^{-1}$  (14). Therefore, the aforesaid bands are not due to  $T_z$  of oxonium ion. For the same reason, one can expect that the doubly degenerate translational mode (represented by  $T_{xy}$ ) would have higher intensity and frequency than that denoted by  $T_z$ . Thus from the nature and shape of the band (which do not shift much in position on deuteration) the bands at  $345\text{ cm}^{-1}$  and  $306\text{ cm}^{-1}$  are assigned to the translational doubly degenerate lattice mode of CPH and HPH respectively. The other weak band at  $360\text{ cm}^{-1}$  in HPH is assigned as metal-oxygen vibration of the metal Hg and oxygen of  $\text{OH}^-$  ion. However, this band could not be identified in CPH, because the librational ( $R_z$ ) band also falls in the same region, whose intensity is large as compared to M-O vibration and hence the latter is completely merged in the former. However, M-O band

appears at  $365\text{ cm}^{-1}$  on deuteration.

The possibility of higher oxonium ions  $(\text{H}_{2n-1}\text{O}_{n-1})^+$  (i.e.  $\text{H}_5\text{O}_2^+$  next to  $\text{H}_3\text{O}^+$ ) is ruled out due to lack of observed bands in the case of  $(\text{H}_5\text{O}_2)^+(\text{ClO}_4)^-$  (17) in the region  $1000\text{--}250\text{ cm}^{-1}$ .

The observed bands in the Raman spectra of CPH and HPH at RT are assigned in analogy with previously reported values (20,21) of vibrational frequencies of  $\text{M}(\text{OH}_2)_6$  complex in other compounds.

### 6.2.3 PERCHLORATE VIBRATIONS

The bands in IR and Raman spectra of CPH and HPH as shown in Figs. 6.3, 6.4, 6.7 and 6.8 around  $1100\text{ }(\nu_3(\text{p}))$ ,  $935\text{ }(\nu_1(\text{p}))$ ,  $630\text{ }(\nu_4(\text{p}))$  and  $460\text{ cm}^{-1}\text{ }(\nu_2(\text{p}))$  are well known fundamental vibrations of perchlorate ion which remain unaffected on deuteration. These bands do not show any appreciable change in intensity with temperature. The  $\nu_3(\text{p})$  and  $\nu_4(\text{p})$  bands split further into several components at LT. The band positions at RT and LT are presented in Tables 6.1 and 6.4.

The  $\nu_3(\text{p})$  band shows a doublet and a triplet for CPH and HPH respectively in Raman spectra at RT. But in IR it shows triplet with two shoulders for both the compounds. Group theoretical analysis (cf. section 1.5(b)) reveals that  $\nu_3(\text{p})$  band of  $\text{ClO}_4^-$  ion belonging to  $\text{f}_2$  species should split into two (i.e.  $\text{a}_1 + \text{e}$ ) species which is exactly the case as observed for CPH in Raman. More than two bands as observed in the other spectra may arise due to the following reasons :



(I) The two perchlorate groups in the unit cell occupying two distinguishable sites may cause site group splitting.

(II) The bands might be combinations of  $\nu_2(p)$  and  $\nu_4(p)$ ,  $\nu_1(p)$  and lattice modes, and  $\nu_3(p)$  and lattice modes of  $\text{ClO}_4^-$  ion.

Though a specific assignment for these bands can be done only after performing the single crystal studies, but with the above considerations the crystal structure proposed by West (10) is in agreement with our observed results. However, detailed crystal structure studies are needed to ascertain the crystal structure of CPH and HPH. Further splitting in  $\nu_3(p)$  and  $\nu_4(p)$  at LT in IR spectra indicate a change in symmetry at the  $\text{ClO}_4^-$  ion site, resulting from the structural phase transformation which is corroborated from the observed changes in the bands of water in these crystal hydrates, as discussed earlier. Thus the low temperature crystal structure does not belong to  $C_{3v}^1$  space group.

#### 6.2.4 CONCLUSION

From the above studies we concluded that the normal hydrates at RT change to pseudohydrates at LT. In pseudohydrates the presence of  $\text{H}_3\text{O}^+$  ion which has pyramidal structure, is confirmed from the observed spectra of the normal hydrates as well as their deuterated analogues. The structure of both the hydrates at RT is  $[\text{M}(\text{OH}_2)_6]^{2+}(\text{ClO}_4^-)_2$  which becomes  $[\text{M}(\text{OH}^-)_3(\text{H}_3\text{O}^+)_3]^{2+}(\text{ClO}_4^-)_2$  at LT.

#### 6.2.5 PHASE TRANSITIONS

As has already been discussed, the nature of the spectra at RT and LT are quite different from each other, which indicates that structural phase transition is taking place. To find out the transition temperatures we have studied the temperature dependence of the stretching and bending modes of water in CPH and HPH, which are shown in Figs. 6.9 and 6.10 respectively. In the OH stretching region, temperature dependence of the band position of middle peak shows discontinuities at 120, 162 and 248 K in CPH (dotted line) and at 137 and 243 K in HPH (solid line) as shown in Fig. 6.11. Similarly, the temperature dependence of relative intensity (solid line) and half-width (dotted line) of bending mode of  $\text{H}_2\text{O}$  (after transition,  $\text{H}_3\text{O}^+$ ) in CPH and HPH are shown in Figs. 6.12 and 6.13 respectively. These curves show minor discontinuities at 272 and 259 K in CPH and at 272 K in HPH, but a sharp discontinuity at 248 K in CPH and at 243 K in HPH. Fig. 6.14 shows the hysteresis effect for the transition at around 248 K in CPH (solid line) and 243 K in HPH (dotted line).

The minor discontinuity observed at 272 K has been earlier reported for CPH in EPR (3,4) and piezoelectric (5) studies. They suggested that this transition is associated with thermal contraction of lattice. Our present studies show that in both the hydrates, the formation of pseudohydrate starts at this temperature as is indicated by the decrease of intensity (Figs. 6.12, 6.13) and appearance of weak and sharp band in the bending region (Fig. 6.9). This seems to arise due to lattice contraction because as the lattice contracts, the two layers of water

become closer in the crystal. As no cation is present in between the layers (cf. section 1.4.3(b)) the bonds break due to the jump of proton in order to form pseudohydrate, as happens in the case of  $\text{HClO}_4 \cdot \text{H}_2\text{O}$  (22-24). With the contraction of lattice the formation of pseudohydrate increases. The transition in CPH at 259 K, as observed in EPR (4), has also the same mechanism for the phase transition. The transition at 248 K in CPH and 243 K in HPH also involves the same mechanism, but the rate of formation of pseudohydrate, i.e. the reconstruction of new lattice is very fast and below this temperature the compound almost completely changes to pseudohydrate. This transition shows hysteresis of three degrees in the case of CPH and no hysteresis has been observed in the case of HPH (Fig. 6.14). The presence of  $\text{H}_3\text{O}^+$  ion with pyramidal structure in the pseudohydrate at low temperature phase has been confirmed and discussed in the vibrational study (cf. section 6.2.1(c)).

The discontinuities at 162 K and 120 K in CPH and 137 K in HPH indicate that there is an increase in hydrogen bonding of  $\text{H}_3\text{O}^+$  ion which appears to be due to reorientation of  $\text{H}_3\text{O}^+$  ion in the pseudohydrate. The transition at 120 K in CPH has been reported in EPR (3,4) and piezoelectric(s) studies. EPR study (3) has suggested that in this transition the principal axes are oriented in different directions and the site of metal ion also changes. Our present study cannot reveal the change of site of metal ion but it reflects the change in orientation of  $\text{H}_3\text{O}^+$  ion. NMR study (22) in  $\text{HClO}_4 \cdot \text{H}_2\text{O}$  ( $\text{H}_3\text{O}^+\text{ClO}_4^-$ ) also suggests that the phase transition at 143 K in  $\text{H}_3\text{O}^+\text{ClO}_4^-$  is associated with

the reorientational motion of  $\text{H}_3\text{O}^+$  ion. Thus out of the five transitions observed in CPH between RT and LT the 248 K transition is the most prominent one and is manifested both by OH-stretching and bending modes. Same is the case with 243 K transition in HPH.

#### REFERENCES

1. A.Weil and J.P.Mathieu, Comp. Rend. 238, 2510 (1954).
2. R.E. Hester and R.A. Plane, Inorg. Chem. 3, 769 (1964).
3. R.Dayal, D.R.Rao and P.Venkateswarlu, J.Chem.Phys.70, 2487(1979).
4. A.K.Jain and G.C.Upreti, Phys. Stat. Sol. (a) 58, 155 (1980).
5. I.Svare and B.O.Fimland, J.Chem.Phys. 74, 5977 (1981).
6. D.F.Hornig, J.Chem.Phys.17, 1346 (1949).
7. J.Shiffer, Ph.D. Thesis, Princeton Univ. Princeton, N.J.(1963).
8. M.Falk and O. Knop, in 'Water - A Comprehensive Treatise' Vol.II, F.Franks (ed.), Plenum Press, New York-London (1973), page 55 (and references therein).
9. W.C.Hamilton and J.A.Ibers, in 'Hydrogen Bonding in Solid', W.A.Benjamin, Inc., New York (1968), page 115 (and references therein).
10. C.D.West, Z.Kristallogr. 91A, 480 (1935).
11. S.N. Vinogradov and R.H. Linnell, ('Hydrogen Bonding', Van Nostrand Reinhold Company, New York (1971) Chapter III.
12. D.E.Bethell and N. Shappard, J.Chem.Phys. 21, 1421 (1953).
13. C.C. Ferriso and D.F. Hornig, J.Chem. Phys. 23, 1464 (1955).
14. R. Savoie and P.A. Giguere, J. Chem. Phys. 41, 2698 (1964).
15. D.F. Hornig, H.E.White and F.P.Reading, Spectrochim. Acta 12, 338 (1953).
16. C.C. Ferrico and D.F. Hornig, J. Am. Soc. 75, 4113 (1953).
17. A.C. Pavia and P.A. Giguere, J. Chem. Phys. 52, 3551 (1970).
18. P.A. Giguere and K.B. Harvey, Can. J. Chem. 34, 798 (1956).
19. V.P. Tayal, B.K.Srivastava, D.P.Khandelwal and H.D.Bist, Appl. Spectrosc.Rev. 16, 43 (1980)(and references therein).
20. V.Ananthanarayanan, Z. Phys. Chem. 222, 102 (1963).
21. R.E. Hester and R.A. Plane, Inorg. Chem. 3, 768 (1964).
22. R.C.Taylor and G.L.Vidale, J. Am. Chem. Soc. 78, 5999 (1956).
23. K. Czarniecki, J.A. Janik, J.M. Janik, G. Pytasz, M.Rachwaska and T. Waluga, Physica 85B, 291 (1977).

6.1: Observed frequencies (in  $\text{cm}^{-1}$ ) in Raman and IR spectra of microcrystalline CPH and HPH powder.

CPH			HPH			Assignment
Infrared		Raman	Infrared		Raman	
at 100K	at 300K	at 300K	at 100K	at 300K	at 300K	
3642			3595			$\nu(\text{OH})^-$
	3550			3550	3524	$\nu_3(\text{w})$
	3460	3508		3470	3476	$\nu_1(\text{w})$
3360			3365			$\nu_3(\text{H}_3\text{O})^+$
3220			3220			$\nu_1(\text{H}_3\text{O})^+$
	3195			3190		$2\nu_2(\text{w})$
3130			3125			$2\nu_4(\text{H}_3\text{O})^+$
2250			2250			$2\nu_4(\text{H}_3\text{O})^+$
2060	2060		2060	2060		$\nu_3(\text{p}) + \nu_1(\text{p})$
2020	2020		2020	2020		$\nu_3(\text{p}) + \nu_1(\text{p})$
1620			1625			$\nu_4(\text{H}_3\text{O})^+$
	1621	1618		1619		$\nu_2(\text{w})$
1579			1605			$\beta(\text{M-O-H})$
1260	1260		1260	1260		$2\nu_4(\text{p})$
1185	1180 sh		1180	1178 sh		$\nu_3(\text{p})$
1148	1145	1132	1142	1140	1164	
1112	1112	1068	1110	1109	1106	
1090	1090		1089	1088		
1083			1080			
1071	1070 sh		1070	1070 sh	1026	
944	943	935	943	942	924	$\nu_1(\text{p})$
860			850			$\nu_{\text{R}_{x,y}}(\text{H}_3\text{O})^+$
638	640		638	637		$\nu_4(\text{p})$
630	630	630	630	628	626	
625			625			
460	460	461	460	460	456	$\nu_2(\text{p})$
360			443			$\nu_{\text{R}_z}(\text{H}_3\text{O})^+$
		348			384	$\nu_1(\text{c})$
365			360			$\nu_{\text{T}}(\text{OH})$
					310	$\nu_3(\text{c})$
			306			$\nu_{\text{T}_{x,y}}(\text{H}_3\text{O})^+$
					222	$\nu_2(\text{c})$
					150	$\nu(\text{c})$

Table 6.2: Normal modes of  $\text{H}_3\text{O}^+$  ion under  $C_{3v}$  symmetry and of  $\text{H}_2\text{DO}^+$  and  $\text{HD}_2\text{O}^+$  ions under  $C_s$  symmetry (attained due to a loss of symmetry from  $C_{3v}$ ).

Modes $\nu(\text{cm}^{-1})$ in $\text{NH}_3$	Approximate frequency ( $\text{cm}^{-1}$ ) in $\text{H}_3\text{O}^+$ ion	Symmetry species in		Approximate frequency ( $\text{cm}^{-1}$ ) in		Modes Modes
		$\text{C}_{3v}$	$\text{C}_s$	$\text{H}_2\text{DO}^+$	$\text{HD}_2\text{O}^+$	
$\nu_1$ 3223	3220	$A_1$	$A'$	2440	3280	$\nu_1$
$\nu_2$ 1060	1150*	$A_1$	$A'$	1120*	880	$\nu_2$
$\nu_3$ 3378	3360	E	$A'$	3230	2330	$\nu_3$
			$A''$	3380	2510	$\nu_3'$
$\nu_4$ 1646	1620	E	$A'$	1600 <sup>a</sup>	1200 <sup>a</sup>	$\nu_4'$
			$A''$			$\nu_4''$
						4

\*Inferred from  $\nu_2$  position in  $\text{HD}_2\text{O}^+$

a - Bands  $\nu_4^i$  and  $\nu_4''$  are not resolved.

Table 6.3: Fermi Resonance parameters in CPH (HPH) between bands 3220 (3220) and 3130 (3125)  $\text{cm}^{-1}$  assigned as  $\nu_1$  and  $2\nu_4$  of  $\text{H}_3\text{O}^+$  ion.

Fermi Resonance Parameters		CPH	HPH
Unperturbed level separation	$\Delta_0$	20.5 $\text{cm}^{-1}$	17.3 $\text{cm}^{-1}$
Fermi coupling coefficient	$\Omega$	43.8	46.7
Fermi resonance displacement	$\Delta - \Delta_0$	69.5 $\text{cm}^{-1}$	77.7 $\text{cm}^{-1}$

Table 6.4: Observed frequencies (in  $\text{cm}^{-1}$ ) in IR spectra of partially deuterated CPH and HPH at 100 and 300 K.

CPH		HPH		Assignment
$\nu$ in $\text{cm}^{-1}$		$\nu$ in $\text{cm}^{-1}$		
at 100 K	at 300 K	at 100 K	at 300 K	
	3850		3840	$\nu_{\text{OD}}(\text{HOD}) + \nu_2(\text{HOD})$
3635		3590		$\nu(\text{OH})^{\text{---}}(\text{H}_2\text{DO})^+$
3592		3560		$\nu(\text{OH})^{\text{---}}(\text{HD}_2\text{O})^+$
	3520		3510	$\nu_{\text{OH}}(\text{HOD})$
3380		3390		$\nu_3(\text{H}_2\text{DO})^+$
3280		3280		$\nu_{\text{OH}}(\text{HD}_2\text{O})^+$
3230		3250		$\nu_1(\text{H}_1\text{DO})^+$
2702		2668		$\nu(\text{OD})^{\text{---}}(\text{H}_2\text{DO})^+$
2642		2620		$\nu_3(\text{OD})^{\text{---}}(\text{HD}_2\text{O})$
	2620		2640	$\nu_3(\text{D}_2\text{O})$
	2530		2530	$\nu_{\text{OD}}(\text{HOD})$
2510		2510		$\nu_3(\text{HD}_2\text{O})^+$
2435		2430		$\nu_{\text{OD}}(\text{H}_2\text{DO})^+$
	2390		2390	$2\nu_2(\text{D}_2\text{O})$
2335		2320		$\nu_1(\text{HD}_2\text{O})^+$
2060	2060	2060	2060	$\nu_3(\text{p}) + \nu_1(\text{p})$
2020	2020	2020	2020	$\nu_3(\text{p}) + \nu_1(\text{p})$
	1620		1620	$\nu_2(\text{H}_2\text{O})$
1600		1610		$\nu_4(\text{H}_2\text{DO})^+$
1581		1603		$\beta(\text{M-O-H})$
	1422		1420	$\nu_2(\text{HOD})$
1391		1410		$\beta(\text{M-O-D})$
1260	1260	1260	1260	$2\nu_4(\text{p})$
1200		1200		$\nu_4(\text{HD}_2\text{O})^+$
	1190		1190	$\nu_2(\text{D}_2\text{O})$
1120		1120		$\nu_2(\text{H}_2\text{DO})^+$
1185	1180	1180	1178	$\nu_3(\text{p})$
1148	1145	1142	1140	
1112	1112	1110	1109	
1090	1090	1089	1088	
1083		1080		
1071	1070	1070	1070	

contd.. Table 6.4

CPH		HPH		Assignment
$\nu$ in $\text{cm}^{-1}$		$\nu$ in $\text{cm}^{-1}$		
at 100 K	at 300 K	at 100 K	at 300 K	
944	943	943	942	$\nu_1(\text{p})$
880		885		$\nu_2(\text{HD}_2\text{O})^+$
810		816		$\nu_{R_{x,y}}(\text{H}_2\text{DO})^+$
640		640		$\nu_{R_{x,y}}(\text{HD}_2\text{O})^+$
638	640	638	637	$\nu_4(\text{p})$
630	630	630	628	
625		625		
475		480		$\nu_2(\text{p})$
460	460	460	460	
345		438		$\nu_{R_z}(\text{H}_2\text{DO})^+$
335		424		$\nu_{R_z}(\text{H}_2\text{DO})^+$
365		360		$\nu_T(\text{OH})^-$
350		345		$\nu_T(\text{OD})^-$
265		332		$\nu_{R_z}(\text{HD}_2\text{O})^+$
255		322		$\nu_{R_z}(\text{HD}_2\text{O})^+$
340		302		$\nu_{T_{x,y}}(\text{H}_2\text{DO})^+$

$\text{p}$ ,  $\beta$ ,  $\text{R}$  and  $\text{T}$  stand for  $\text{ClO}_4^-$ , bending, libration and translation, respectively.

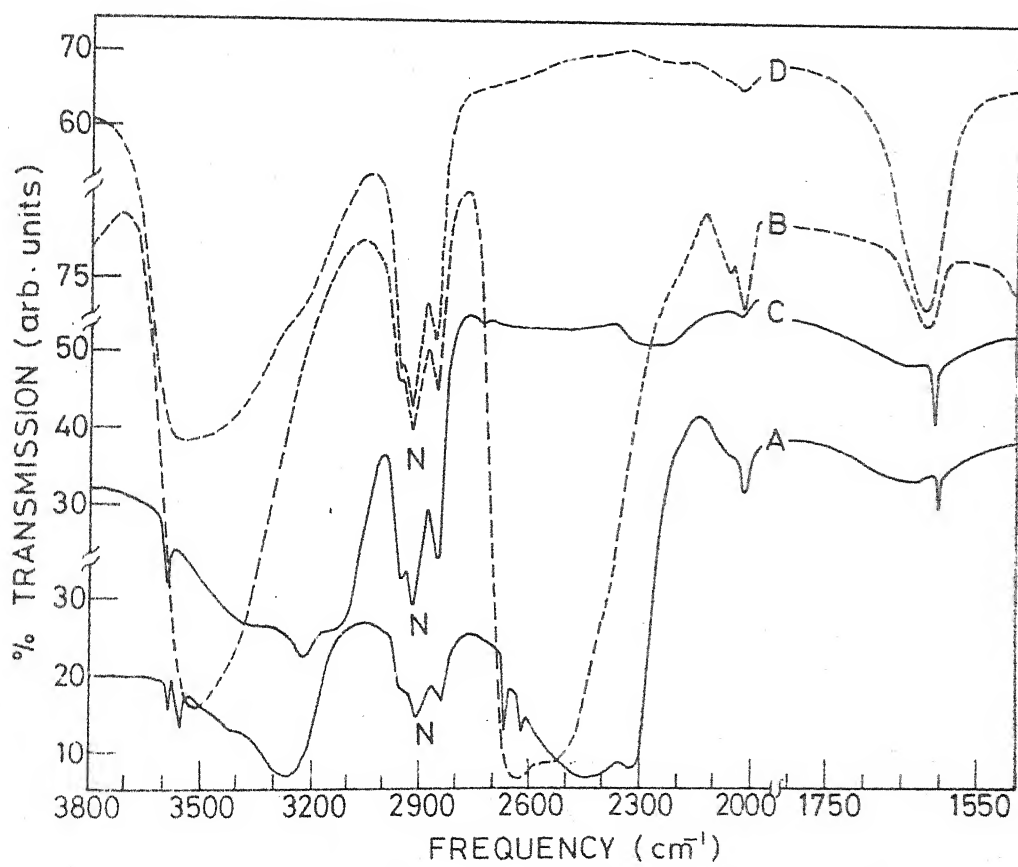
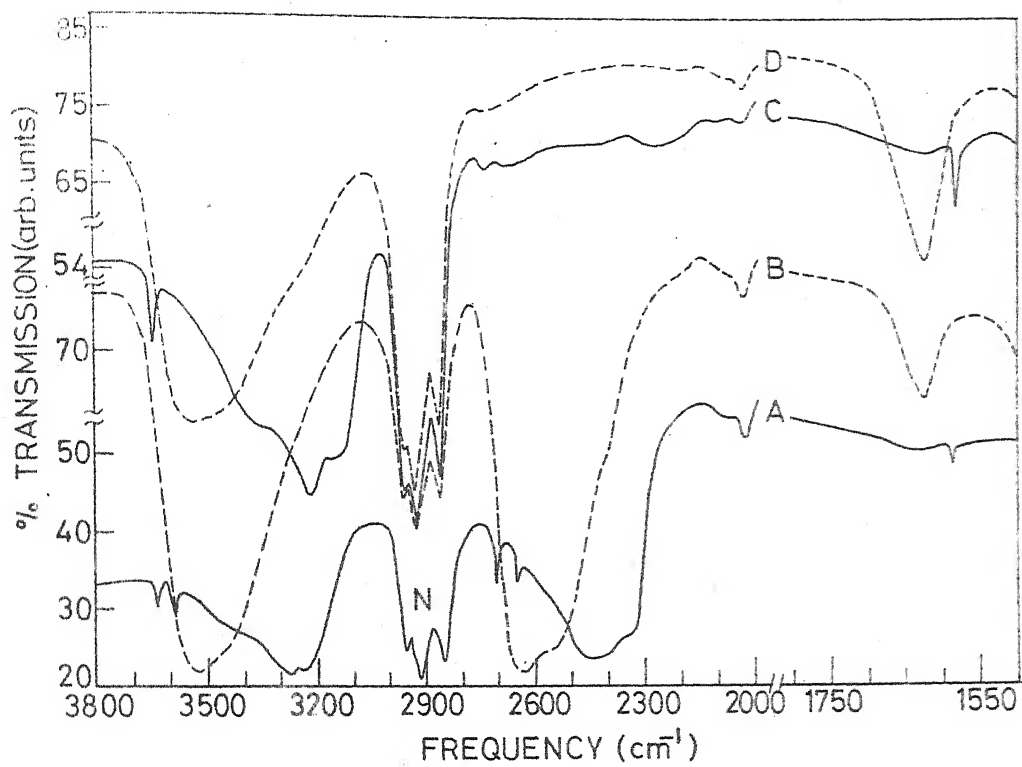
Table 6.5: The  $\text{OH}^-$  bands in hydrated and partially deuterated CPH and HPH at LT.

species compounds	$\nu(\text{OH})^-$ in $\text{cm}^{-1}$		
	$\text{H}_3\text{O}^+$	$\text{H}_2\text{DO}^+$	$\text{HD}_2\text{O}^+$
CPH	3640	3635	3592
HPH	3595	3590	3560



# FIGURE CAPTIONS

- Fig.6.1: Infrared spectra of  $\text{Cd}(\text{ClO}_4)_2 \cdot 6\text{H}_2\text{O}$  at 100 K (curve C) and at 300 K (curve D) and its partially deuterated sample at 100 K (curve A) and at 300 K (curve B) in 3800-2000 and 1800-1500  $\text{cm}^{-1}$  regions. N in this figure as well as in other figures represents nujol band.
- Fig.6.2: Infrared spectra of  $\text{Hg}(\text{ClO}_4)_2 \cdot 6\text{H}_2\text{O}$  at 100 K (curve C) and at 300 K (curve D) and its partially deuterated sample at 100 K (curve A) and at 300 K (curve B) in 3800-2080 and 1800-1500  $\text{cm}^{-1}$  regions.
- Fig.6.3: Raman spectrum of  $\text{Cd}(\text{ClO}_4)_2 \cdot 6\text{H}_2\text{O}$  at room temperature.
- Fig.6.4: Raman spectrum of  $\text{Hg}(\text{ClO}_4)_2 \cdot 6\text{H}_2\text{O}$  at room temperature.
- Fig.6.5: The curve C of Fig.6.1 is plotted in absorbance scale (solid line). The Lorentzian analysis is shown by dotted lines.
- Fig.6.6: The curve C of Fig.6.2 is plotted in absorbance scale solid line. The Lorentzian analysis is shown by dotted lines.
- Fig.6.7: Infrared spectra of  $\text{Cd}(\text{ClO}_4)_2 \cdot 6\text{H}_2\text{O}$  at 100 K (curve C) and 300 K (curve D) and its partially deuterated sample at 100 K (curve A) and 300 K (curve B) in 1350-250  $\text{cm}^{-1}$  region.
- Fig.6.8: Infrared spectra of  $\text{Hg}(\text{ClO}_4)_2 \cdot 6\text{H}_2\text{O}$  at 100 K (curve C) and at 300 K (curve D) and its partially deuterated sample at 100 K (curve A) and at 300 K (curve B) in 1350-250  $\text{cm}^{-1}$  region.
- Fig.6.9: Temperature dependence of OH stretching modes in  $\text{Cd}(\text{ClO}_4)_2 \cdot 6\text{H}_2\text{O}$  and  $\text{Hg}(\text{ClO}_4)_2 \cdot 6\text{H}_2\text{O}$ .
- Fig.6.10: Temperature dependence of bending mode of water in  $\text{Cd}(\text{ClO}_4)_2 \cdot 6\text{H}_2\text{O}$  and  $\text{Hg}(\text{ClO}_4)_2 \cdot 6\text{H}_2\text{O}$ .
- Fig.6.11: Temperature dependence of the frequency of the peak at 3220  $\text{cm}^{-1}$  at 100 K for  $\text{Cd}(\text{ClO}_4)_2 \cdot 6\text{H}_2\text{O}$  (dotted line) and  $\text{Hg}(\text{ClO}_4)_2 \cdot 6\text{H}_2\text{O}$  (solid line).
- Fig.6.12: Half-width (dotted line) and relative intensities (solid line) of bending modes of water in  $\text{Cd}(\text{ClO}_4)_2 \cdot 6\text{H}_2\text{O}$  versus temperature.
- Fig.6.13: Half-width (dotted line) and relative intensities (solid line) of bending modes of water in  $\text{Hg}(\text{ClO}_4)_2 \cdot 6\text{H}_2\text{O}$  versus temperature.
- Fig.6.14: Thermal hysteresis curves for  $\text{Cd}(\text{ClO}_4)_2 \cdot 6\text{H}_2\text{O}$  (solid lines) and  $\text{Hg}(\text{ClO}_4)_2 \cdot 6\text{H}_2\text{O}$  (dotted line) for transition at 248 and 243 K respectively.



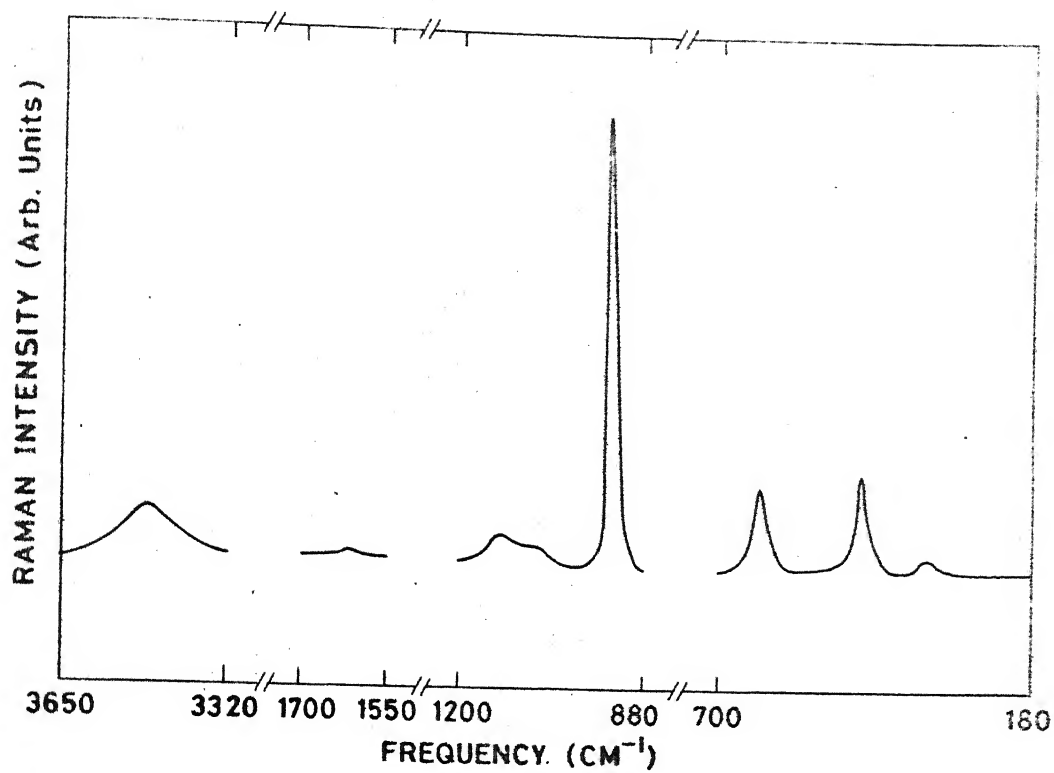


FIG. 6.3

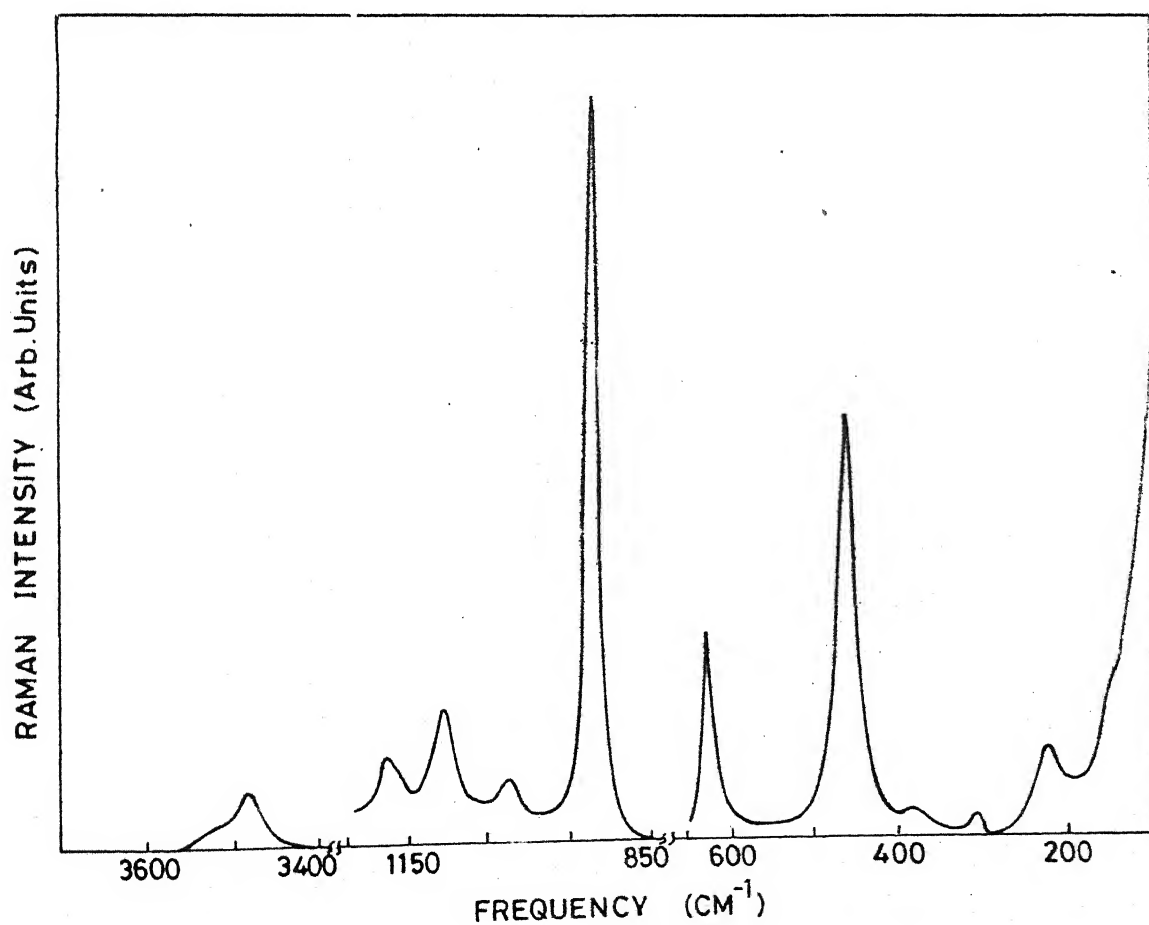
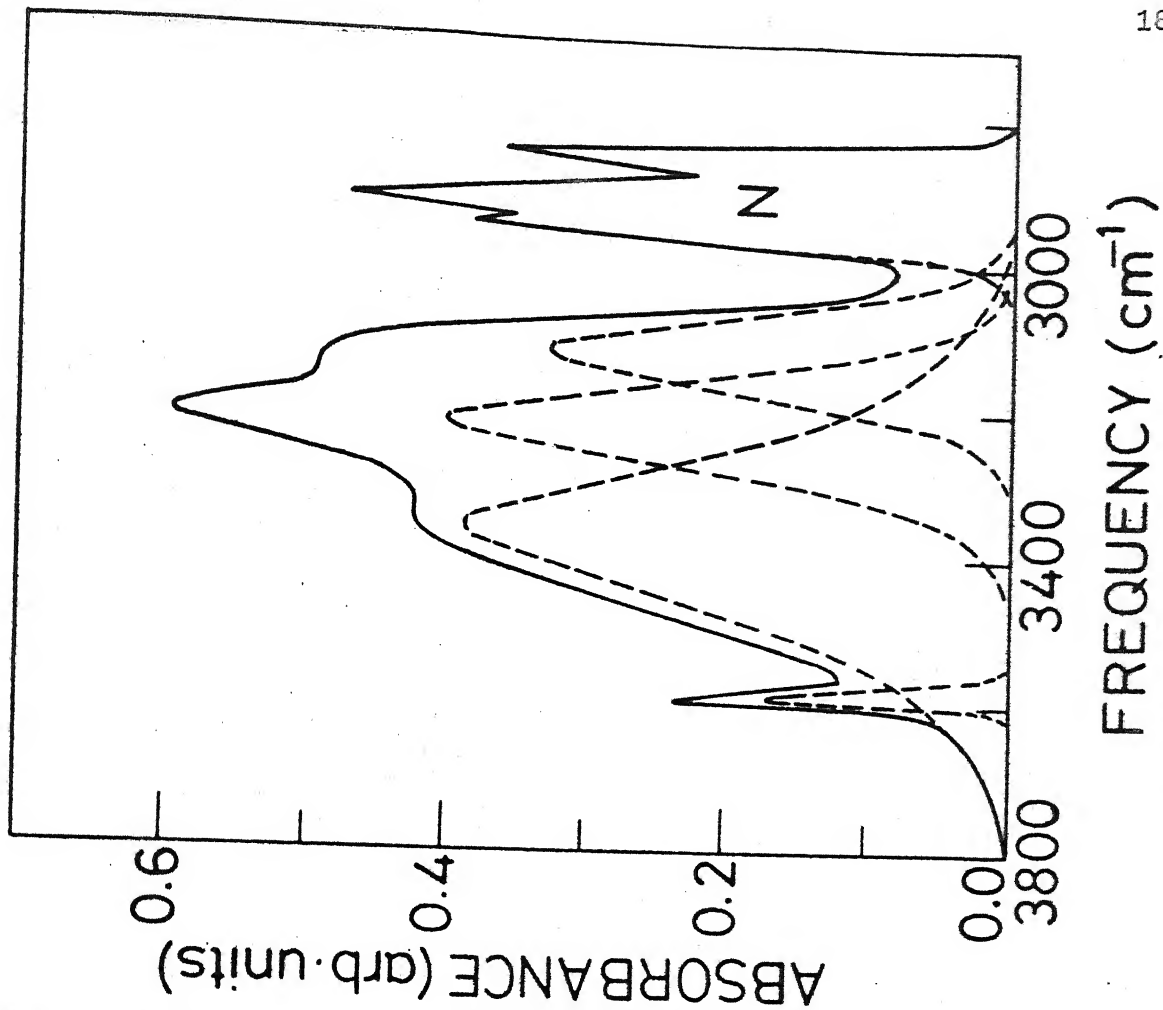
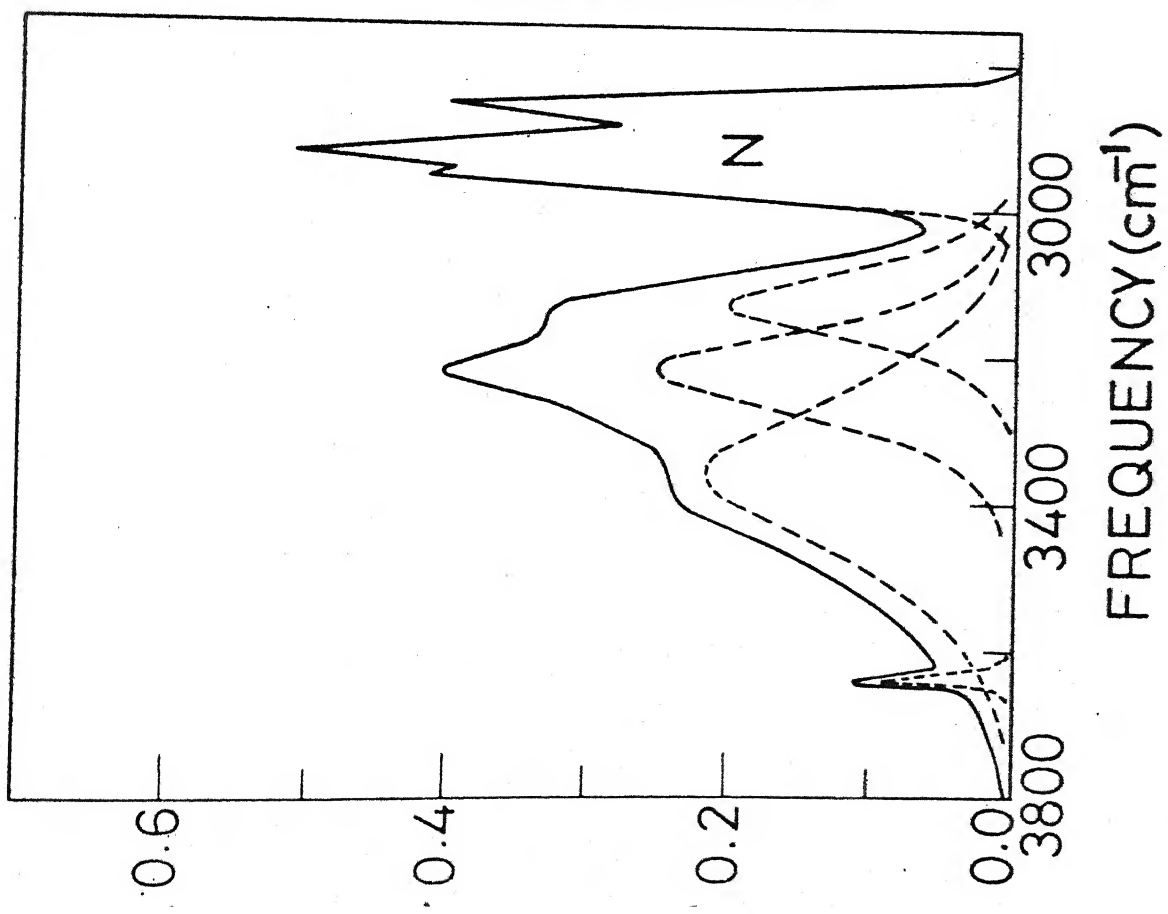


FIG. 6.4



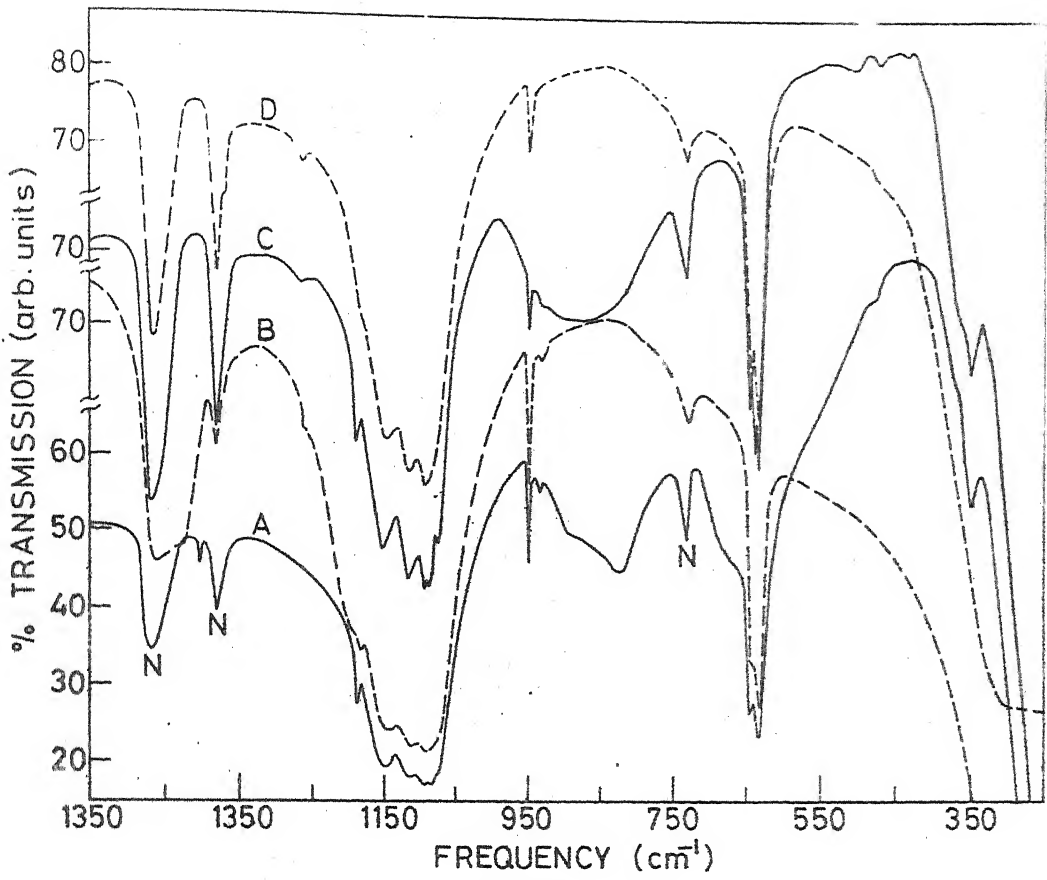
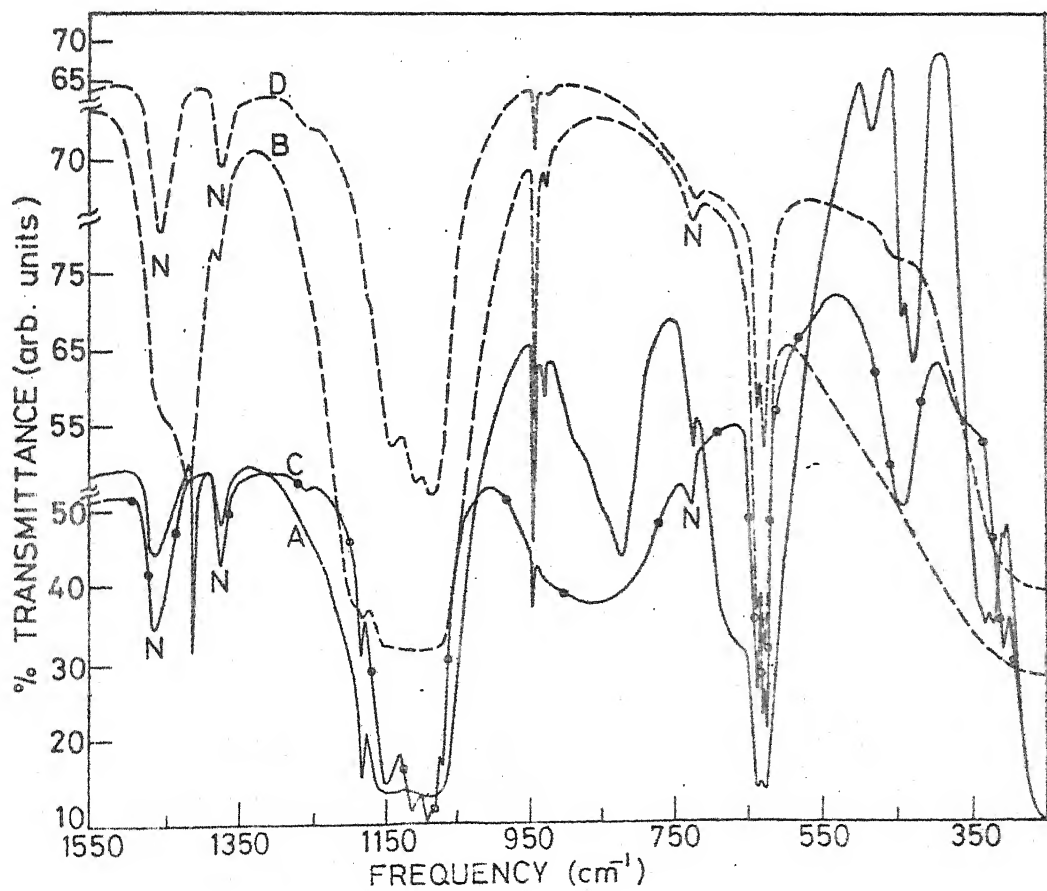


FIG. 6.7



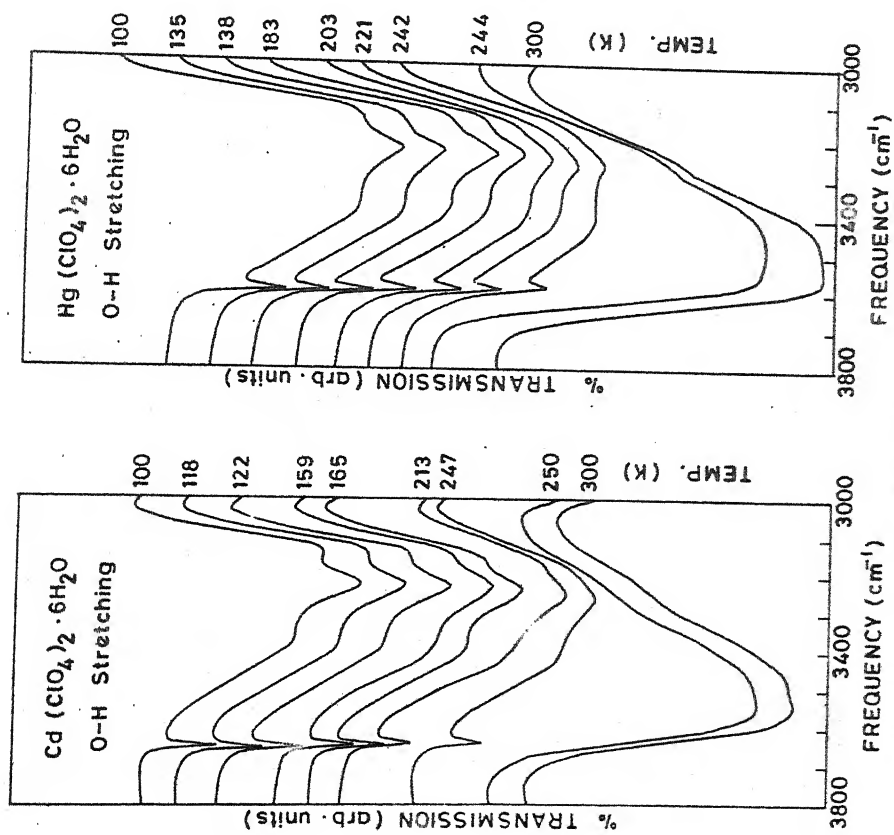


FIG. 6.9

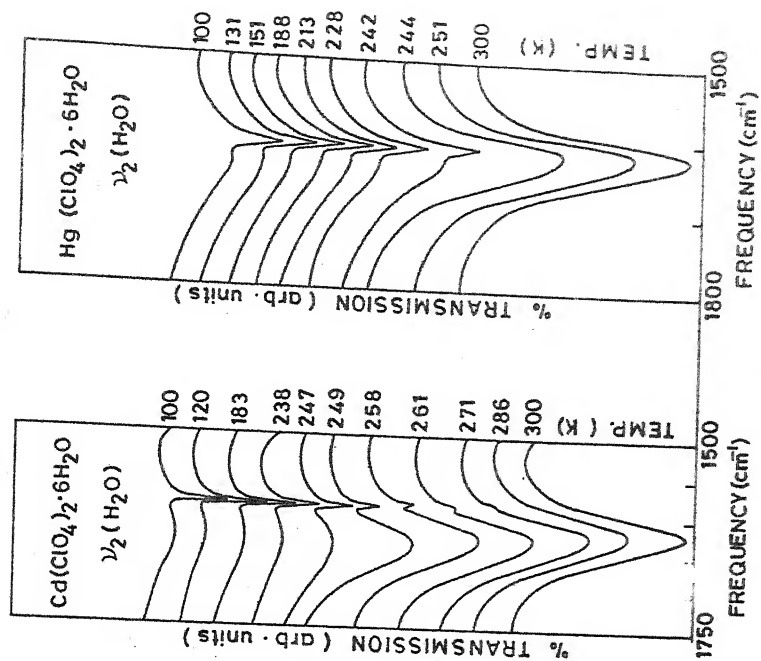


FIG. 6.10

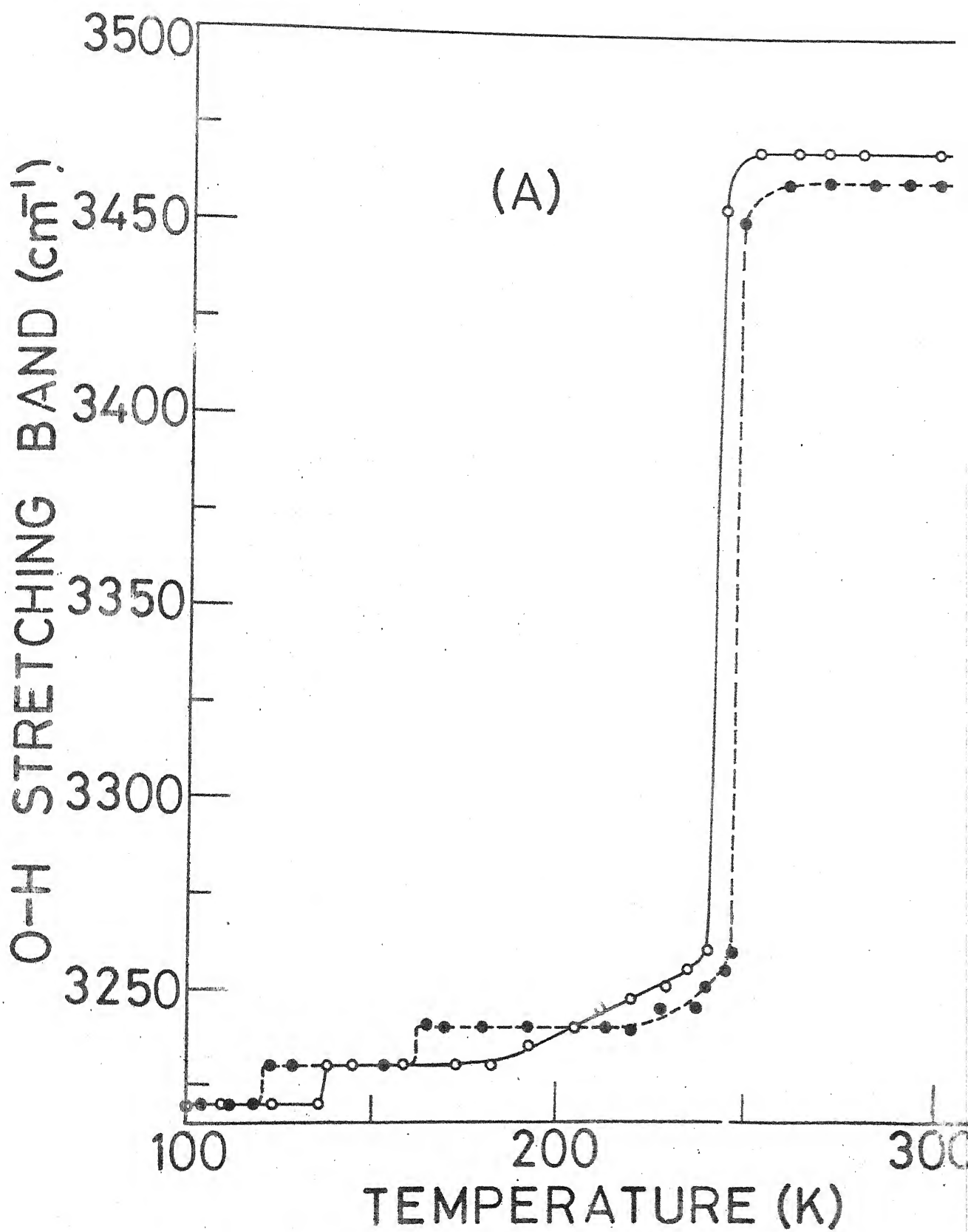


FIG. 6.11

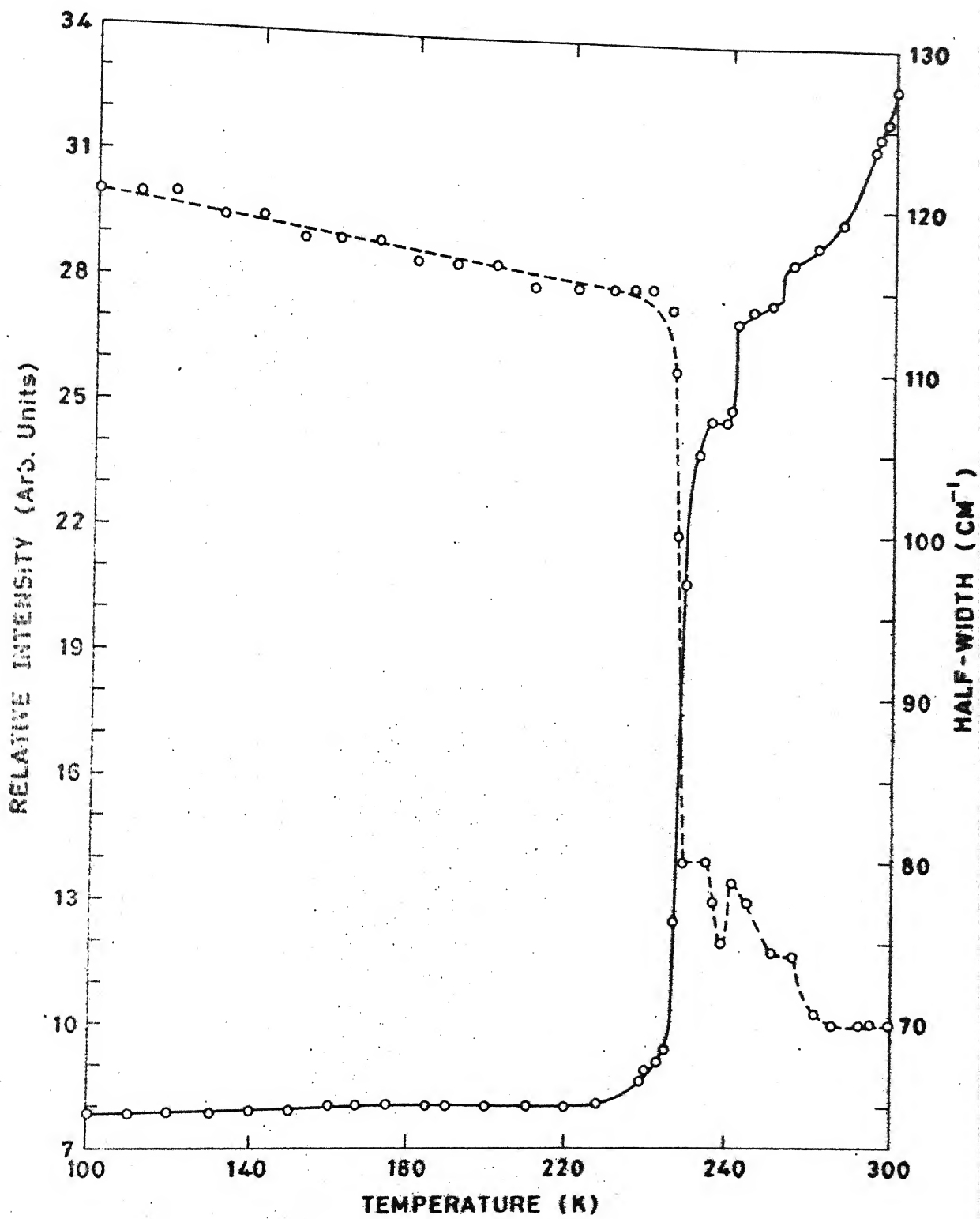


FIG. 6.12



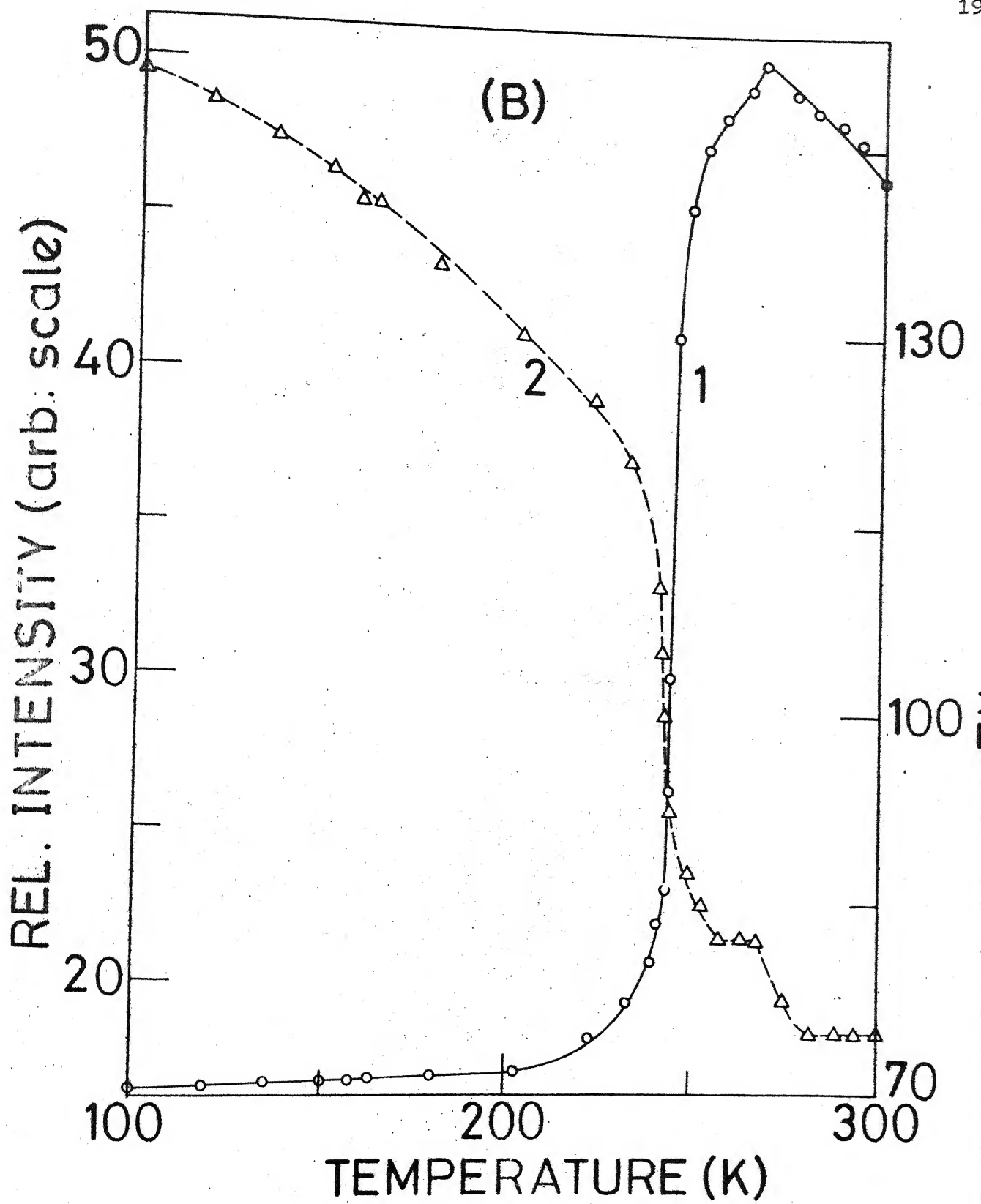
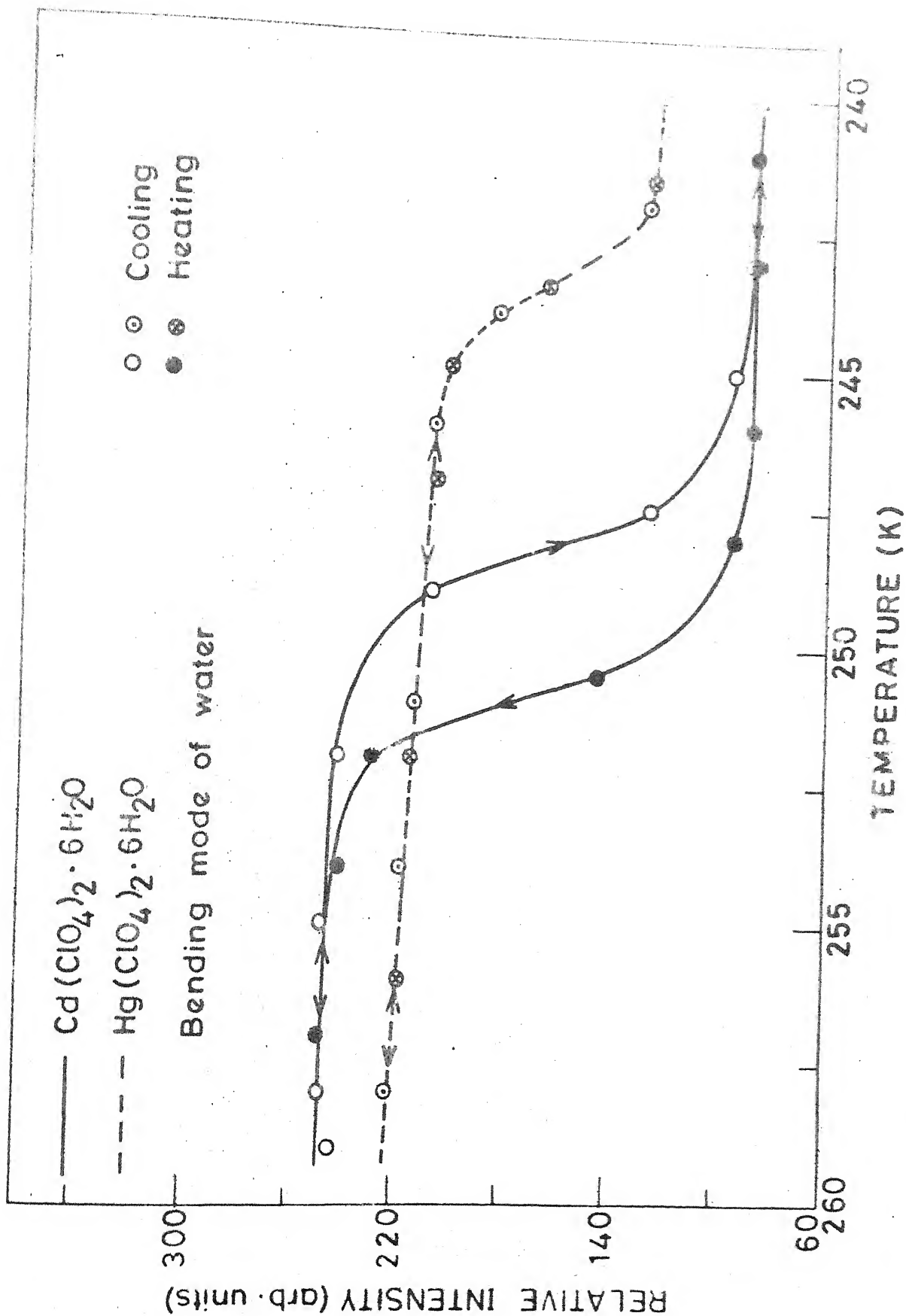


FIG. 6.13



## CHAPTER VII

### BACKGROUND AND THE OBJECTIVE

#### 7.1 BACKGROUND OF THE WORK

The hexahydrates of divalent metal perchlorates  $M(ClO_4)_2 \cdot 6H_2O$  where  $M = Mg, Ni, Co, Mn, Zn, Cd$  and  $Hg$  are chosen for comprehensive IR absorption and Raman scattering studies to examine (I) the vibrational assignments, (II) phase transition temperatures and (III) phase transition mechanisms. The aforesaid salts belong to two different systems, i.e. orthorhombic ( $Mg, Ni, Co, Mn$  and  $Zn$ ) and trigonal ( $Cd$  and  $Hg$ ). The detailed crystal structures and all the bond lengths in these compounds are not known, but the arrangements of  $H_2O$  and  $ClO_4^-$  ion are reported to be similar. Thus the changes observed in the spectra going from one salt to other must be attributed to changes in the metal coordination effects.

Earlier IR studies of these samples at RT were in the OH stretching and fundamental vibrational regions of  $ClO_4^-$  ion only. The same was the case with Raman studies except for  $Mg$  and  $Ni$  (perchlorate hexahydrates) whose temperature dependence studies for  $ClO_4^-$  ion vibrational modes were available. Studies on deuterated samples were not available. No attempts had been made earlier to deduce and study half-widths and relative integrated intensities of the bands at varying temperatures. So these studies were undertaken in the present work.

## 7.2 CONTRIBUTION OF THE PRESENT WORK

Following are the new observations made to complete some of the informations not available in the literature :

- (I) IR spectra of Cd and Hg, and Raman spectra of Co, Mn, and Hg perchlorate hexahydrates are presented for the first time.
- (II) IR spectra of Mg, Ni, Co, Mn and Zn perchlorate hexahydrate are extended to  $600-200\text{ cm}^{-1}$  region.
- (III) Raman spectra of Mg, Ni, Zn and Cd perchlorate hexahydrates are extended to  $20-450\text{ cm}^{-1}$  and  $1300-4000\text{ cm}^{-1}$  regions.
- (IV) IR spectra of all the compounds have been studied at LT ( $\sim 93\text{ K}$ ) for the first time in the region  $4000-200\text{ cm}^{-1}$ .
- (V) An analysis of the IR spectra and Raman spectra (except for the fundamental vibration of  $\text{ClO}_4^-$  ion) have been made for the first time.
- (VI) The temperature dependence of thermosensitive bands are presented for the first time in all the aforesaid salts using IR technique.
- (VII) The study of phonons and phase transitions in Mg, Ni, Co, Mn, Zn, Cu and Hg perchlorate hexahydrates are reported in chapters III, IV, V and VI. In each case the IR spectra ( $4000-200\text{ cm}^{-1}$ ) have been recorded at different temperatures while Raman spectra ( $20-4000\text{ cm}^{-1}$ ) are recorded at RT only. From the analysis of these data, we have arrived at several new conclusions and correlations which have already been summarized in the synopsis and details are given in respective chapters of this work.

### 7.3 SUGGESTIONS FOR FUTURE WORK

Further, we can make the following observations, for extending the present work in future on the following lines which we could not do due to certain limitations.

- (I) Single crystal and temperature dependence study in Raman.
- (II) Careful IR study and its temperature dependence for all the observed modes near transition temperatures which were reported by other techniques and are not observed in the present investigation.
- (III) Study of the vibrational spectra of hydrates containing strong hydrogen bonds, paying particular attention to resonance interaction between  $\nu_1$  and  $2\nu_2$  and the origin of hydrogen bonds.
- (IV) To distinguish the various influences on the stretching modes of water molecule in condensed systems using the correlation between  $\Delta\nu_{3,1}$  and  $\bar{\nu}_{OH}$ .
- (V) Study of static and dynamic field splitting of librational modes and their assignments in condensed systems.
- (VI) The quantitative determination of the nature of intermolecular coupling of the stretching and bending modes of water in crystals.
- (VII) Experimental estimation of force constants and their theoretical verification.